
Electronic Thesis and Dissertation Repository

3-8-2019 11:00 AM

Cell Recruitment and Differentiation in Wound Repair

John Walker, *The University of Western Ontario*

Supervisor: Hamilton, Douglas W., *The University of Western Ontario*

Co-Supervisor: Flynn, Lauren E., *The University of Western Ontario*

A thesis submitted in partial fulfillment of the requirements for the Doctor of Philosophy degree
in Anatomy and Cell Biology

© John Walker 2019

Follow this and additional works at: <https://ir.lib.uwo.ca/etd>



Part of the [Cell and Developmental Biology Commons](#)

Recommended Citation

Walker, John, "Cell Recruitment and Differentiation in Wound Repair" (2019). *Electronic Thesis and Dissertation Repository*. 6063.

<https://ir.lib.uwo.ca/etd/6063>

This Dissertation/Thesis is brought to you for free and open access by Scholarship@Western. It has been accepted for inclusion in Electronic Thesis and Dissertation Repository by an authorized administrator of Scholarship@Western. For more information, please contact wlsadmin@uwo.ca.

Abstract

Chronic wounds represent a major health problem primarily affecting patients with underlying pathologies including diabetes and vasculopathy. These wounds are characterized by an impaired transition from the inflammatory to the proliferative phase of healing. In this thesis, the complex relationship between cells and their microenvironment was explored in the context of wound healing by investigating how intrinsic differences in fibroblasts affect their response to external stimuli, and how extracellular matrix (ECM) proteins modify cellular responses during acute wound repair. First, it was hypothesized that different subpopulations of fibroblasts could be identified in cutaneous tissue based on divergent embryonic expression patterns of the transcription factor *Foxd1*, and that these subpopulations would play varying roles during wound repair. Next, it was hypothesized that wound repair could be modulated in animal models by altering components of the ECM. To explore cell-intrinsic differences in the skin, a lineage tracing approach was applied to observe a population of cells derived from embryonic *Foxd1*-expressing progenitors during embryonic development and into adulthood. These cells contributed to a subpopulation of fibroblasts in adult dorsal skin that were enriched with transcripts for matrix modifying genes during homeostasis and following wounding relative to fibroblasts not of this origin. Next, Galectin-3, a multifunctional matricellular protein with pro-angiogenic, pro-fibrotic, and immunomodulatory properties in models outside of skin, was investigated to assess the role of this cell-extrinsic factor during cutaneous healing in mice and in human chronic wounds. Using a genetic deletion strategy, it was determined that galectin-3 was

dispensable during acute repair in mice. Finally, pilot studies were performed to investigate an acute wound model in juvenile pigs for assessing foam biomaterials derived from the ECM as a strategy to modulate wound healing by targeting the cellular microenvironment. While modifying the matrix composition of the biomaterials did not alter healing in this model, the findings support that further exploration into relevant models of impaired healing is warranted. Overall, the studies in this thesis have helped to elucidate complex interactions between cells and their environment during wound repair, providing relevant information for the design of future therapeutics for chronic wounds.

Keywords

Adipose-Derived Stem/Stromal Cells, Biomaterials, CCN2, Decellularized adipose tissue (DAT), Extracellular Matrix (ECM), Fibroblasts, Foxd1, Galectin-3, Lineage Tracing, Matricellular Proteins, Myofibroblasts, Periostin, Skin, Tissue Repair, Wound Healing.

Co-Authorship Statement

Chapter 1

John Walker wrote the chapter. Lauren E. Flynn and Douglas W. Hamilton contributed to the design of the introduction and provided critical feedback during preparation of this chapter.

Chapter 2

John Walker performed the experiments, data analysis, and prepared the figures. Douglas W. Hamilton conceived the initial study models. Douglas W. Hamilton and Lauren E. Flynn contributed to the ongoing experimental design and direction of the study. Douglas W. Hamilton acquired ethical approval for animal work. John Walker wrote the chapter with Lauren E. Flynn and Douglas W. Hamilton providing critical feedback. This chapter is in preparation for manuscript submission.

Chapter 3

John Walker performed the experiments, data analysis, and prepared the figures. Douglas W. Hamilton contributed to the design and direction of the study. Douglas W. Hamilton acquired ethical approval for collection of human tissue and animal work. Christopher G. Elliott contributed to experimental design and provided technical assistance. Thomas L. Forbes provided access to human tissues. Douglas W. Hamilton, Christopher G. Elliott, and Thomas L. Forbes provided critical feedback during manuscript preparation. A version of this chapter has been published in the Journal of Investigative Dermatology: Walker JT, Elliott CG, Forbes TL, Hamilton DW; Genetic Deletion of Galectin-3 Does Not Impair Full-Thickness Excisional Skin Healing (2016).

Chapter 4

John Walker performed the experiments, data analysis, and prepared the figures. Both Douglas W. Hamilton (animal model and periostin/CCN2 scaffold) and Lauren E. Flynn (DAT scaffolds, ASC biology) contributed to the design and direction of the study. Douglas W. Hamilton acquired ethical approval for animal work. Lauren E. Flynn acquired ethical approval for collection of human tissues. John Walker wrote the chapter with Lauren E. Flynn and Douglas W. Hamilton providing critical feedback. This study is a continuation of previous work in the Hamilton lab published in Tissue Engineering Part A: Elliott CG, Wang J, Walker JT, Michelsons S, Dunmore-Buyze J, Drangonva M, Leask A, Hamilton DW; Periostin and CCN2 Containing Biomaterials Suppress Inflammation and Induce the Proliferative Phase of Skin Healing in Diabetic Mice (2019). This chapter is in preparation for manuscript submission.

Chapter 5

John Walker wrote the chapter. Lauren E. Flynn and Douglas W. Hamilton contributed to the design of the discussion and provided critical feedback during preparation of this chapter.

Acknowledgements

First, I would like to express my sincere gratitude to my co-supervisors, Dr. Douglas Hamilton and Dr. Lauren Flynn. Through their collaborative mentorship they have provided immense support and have challenged me to become a better scientist. I am grateful for the freedom and encouragement they have given me to explore areas that I found particularly interesting, and for their thoughtful and critical feedback to improve the quality of the research and to support my personal growth. I have benefited greatly from their expertise and the time that they have provided over the years.

I would also like to thank my advisory committee members, Dr. Lina Dagnino, Dr. Andrew Leask, and Dr. Paul Walton. Their input has provided direction and has kept my thesis on course and focused.

I am grateful for the clinical collaborators that supported this work including Dr. Thomas Forbes, Dr. Aaron Grant, Dr. Brian Evans, and Dr. Robert Richards.

Thank you to all of the animal care staff, veterinary technicians, and veterinarians who made all of the animal work possible.

This work was funded through the Canadian Institute of Health Research (CIHR), and the Natural Sciences and Engineering Research Council (NSERC). I am thankful for the support from NSERC through their graduate scholarship program for funding at the Master's and Doctoral level.

I am thankful for the technical training provided by Christopher Elliott upon entering the Hamilton lab. Thank you to Cody Brown for his support in learning novel techniques in the Flynn lab. I would also like to thank all of the technical and support staff that have gone out of their way to provide training and assistance over the course of my degree.

I am thankful for the continued advice and encouragement from my brother, Michael Walker. His input has made me think more critically about experimental design and statistical analyses in animal studies.

For all of my lab mates and friends that have welcomed me into their lives, I am grateful for all of the extracurricular activities that have made my time in London incredibly rewarding.

Finally, I would like to thank Kylen for her endless motivation and support during this degree. Through her tireless work ethic and perseverance, she is a wonderful inspiration.

Table of Contents

Abstract	ii
Keywords	iii
Co-Authorship Statement.....	iv
Chapter 1	iv
Chapter 2.....	iv
Chapter 3.....	iv
Chapter 4.....	v
Chapter 5.....	v
Acknowledgements.....	vi
Table of Contents.....	viii
List of Tables	xvi
List of Figures.....	xvii
List of Appendices	xx
List of abbreviations	xxi
Chapter 1: Rationale, Literature Review and Thesis Overview	1
1.1 Rationale, Hypothesis and Objectives	1
1.2 Wound healing.....	3

1.3 Chronic wounds	8
1.4 Wound healing from a cell intrinsic perspective	11
1.4.1 Skin development.....	13
1.4.2 Origins of myofibroblasts in tissue repair.....	17
1.4.3 Sources of myofibroblasts in wound repair and fibrosis	19
1.4.4 Foxd1 as a marker for myofibroblast progenitors.....	24
1.5 Matricellular proteins in wound repair	26
1.5.1 Galectin-3.....	30
1.5.2 Periostin	34
1.5.3 CCN2	36
1.6 Strategies for healing chronic wounds	38
1.6.1 Growth factor therapies.....	40
1.6.2 MMP inhibitors.....	40
1.6.3 Biomaterials for wound repair	41
1.6.4 Cell therapies for wound healing	45
1.7 Thesis Overview	47
1.8 References.....	49
 Chapter 2: Lineage tracing of Foxd1-expressing embryonic progenitors to assess the role of divergent embryonic lineages on adult dermal fibroblast function	 71
2.1 Abstract.....	71

2.2 Introduction.....	72
2.3 Materials and methods	75
2.3.1 Mice	75
2.3.2 Tamoxifen injections	79
2.3.3 Wound healing.....	80
2.3.4 Histology and immunofluorescence microscopy analyses	80
2.3.5 Dermal fibroblast isolation	81
2.3.6 Fluorescence activated cell sorting	82
2.3.7 Cell Culture.....	83
2.3.8 RNA isolation	83
2.3.9 RT-qPCR array	84
2.3.10 TaqMan® qPCR	84
2.3.11 Statistical methods	85
2.4 Results.....	86
2.4.1 Foxd1 was expressed during murine embryonic development.....	86
2.4.2 Foxd1-expressing cells are rare in postnatal tissue during homeostasis and following wounding.....	94
2.4.3 Foxd1 lineage-positive cells contributed to diverse populations in adult skin	97
2.4.4 Foxd1 lineage-positive populations contributed to myofibroblasts during wound repair	100

2.4.5 Foxd1 lineage-positive fibroblasts displayed divergent fibrosis-related gene expression patterns during homeostasis and wound repair	105
2.4.6 Fibroblast lineage specific differences were not maintained in culture.....	110
2.4.7 Foxd1 lineage-positive fibroblasts did not mimic expression patterns of previously defined lineages.....	110
2.4.8 High expression of integrins $\alpha 2$ and $\alpha 3$ was associated with the FLN population	115
2.5 Discussion.....	120
2.6 Conclusions.....	126
2.7 Acknowledgements.....	127
2.8 References.....	127
Chapter 3: The role of Galectin-3 in cell recruitment and differentiation during wound healing.....	132
3.1 Abstract:.....	132
3.2 Introduction:.....	133
3.3 Materials and Methods:.....	135
3.3.1 Mice	135
3.3.2 Excisional wounding experiments	136
3.3.3 Patient samples.....	137
3.3.4 Histology.....	137
3.3.5 Hydroxyproline assay	138

3.3.6 Human primary fibroblast culture and mouse primary fibroblast culture	138
3.3.7 Cytokine treatment.....	139
3.3.8 RNA isolation and real-time quantitative PCR.....	140
3.3.9 Protein isolation and western blot.....	141
3.3.10 In vitro scratch wound assay.....	141
3.3.11 Gel contraction assay	142
3.3.12 Statistical methods	142
3.4 Results:.....	143
3.4.1 Galectin-3 mRNA and protein were up-regulated after excisional wounding and peaked 1 day after wounding	143
3.4.2 Genetic deletion of Galectin-3 impaired re-epithelialization but did not alter wound closure kinetics during excisional healing in mice	144
3.4.3 Genetic deletion of Galectin-3 did not affect immune cell infiltration, myofibroblast recruitment, or vascular density during wound repair.....	148
3.4.4 Genetic deletion of Galectin-3 did not alter transcriptional regulation of genes associated with fibrotic repair or angiogenesis.....	151
3.4.5 Galectin-3 was not required for the transition of dermal fibroblasts to myofibroblasts in vitro.....	151
3.4.6 Galectin-3 mRNA and protein were decreased in human non-healing skin wound tissue.....	156

3.4.7 Galectin-3 expression in dermal fibroblasts from human wounds was modulated by TGF β 1 and tumor necrosis factor- α	158
3.5 Discussion:.....	161
3.6 Conclusions:.....	166
3.7 References:.....	166
Chapter 4: Profibrotic and pro-angiogenic biomaterials to induce cell recruitment and differentiation during skin healing.....	172
4.1 Abstract:.....	172
4.2 Introduction:.....	173
4.3 Materials and methods:.....	177
4.3.1 Synthesis of bovine type I collagen and DAT foams	177
4.3.2 db/db mouse model.....	178
4.3.3 Porcine wound model	179
4.3.4 Histological assessment	180
4.3.5 Hydroxyproline assay	181
4.3.6 Porcine ASC isolation and tri-lineage differentiation.....	181
4.3.7 ASC labelling and seeding.....	183
4.3.8 Statistical methods	183
4.4 Results:.....	184
4.4.1 DAT foams increased the rate of wound closure in db/db mice.....	184

4.4.2 Addition of foam biomaterials into 2 cm diameter wounds in the dorsal skin of pigs induced a delay to the rate of healing, but did not alter the time to complete closure.....	185
4.4.3 Foam biomaterials did not alter the contractile or fibrotic phenotypes of the wounds	192
4.4.4 Foam biomaterials did not alter the vascular density of the wounds.....	195
4.4.5 CD68- and CD163-positive cell infiltrate within the wound bed was not significantly altered by the addition of biomaterials.....	198
4.4.6 Porcine ASCs displayed tri-lineage differentiation potential	199
4.4.7 ASC seeding affected closure differentially depending on the biomaterial carrier	203
4.4.8 ASC delivery on foam biomaterials did not alter histological parameters or hydroxyproline content of the granulation tissue.....	203
4.5 Discussion.....	209
4.6 Conclusions.....	213
4.7 Acknowledgements.....	213
4.8 References.....	213
Chapter 5: Discussion	218
5.1 General Discussion	218
5.1.1 Lineage tracing of Foxd1-expressing embryonic progenitors to assess the role of divergent embryonic lineages on adult dermal fibroblast function	218

5.1.2 The role of Galectin-3 in cell recruitment and differentiation during wound healing.....	221
5.1.3 Profibrotic and pro-angiogenic biomaterials to induce cell recruitment and differentiation during skin healing.....	223
5.1.4 Conclusion	226
5.2 Future directions	227
5.2.1 Investigating the functional relevance of divergent gene expression in Foxd1 lineage-positive fibroblasts	227
5.2.2 Galectin-3 as a therapeutic for impaired wound healing	231
5.2.3 Assessment of biomaterial scaffolds in a porcine model of impaired wound healing.....	233
5.2.4 Exploring the interplay between cell-intrinsic and -extrinsic properties governing wound repair	236
5.3 Summary	238
5.4 References.....	238
Appendices:.....	244
Curriculum Vitae	269

List of Tables

Table 1.1 Wound healing specific phenotypes following genetic manipulation of matricellular proteins.	28
Table 2.1: Antibodies used for histological assessment	81
Table 2.2: Taqman® probes used to assess gene expression.....	86
Table 3.1: Primary antibodies used for immunohistochemistry and western blot.....	139
Table 3.2: Taqman® probe sets used for RT-qPCR.	141
Table 4.1: Antibodies for histological assessment.....	181
Table A–1: Normalized Gene expression data relative to housekeeping panel from Qiagen RT ² Profiler array for fibrosis related genes; unwounded tissue comparison.....	254
Table A–2: Normalized Gene expression data relative to housekeeping panel from Qiagen RT ² Profiler array for fibrosis related genes; wounded tissue comparison.....	256
Table A–3: Normalized Gene expression data relative to housekeeping panel from Qiagen RT ² Profiler array for fibrosis related genes; FLN lineage comparison.....	259
Table A–4: Normalized Gene expression data relative to housekeeping panel from Qiagen RT ² Profiler array for fibrosis related genes; FLP lineage comparison.	261
Table A–5: Information on patient cells examined in vitro.....	263
Table A–6: Information on patients used for histological analysis.	264
Table A–7: Information on patients included in direct RNA analysis.....	264

List of Figures

Figure 1.1: Structures within skin from murine, porcine, and human sources.	16
Figure 1.2 Temporal expression of matricellular proteins during dermal wound repair.	30
Figure 2.1: Schematics of Cre/Lox strategies used to track <i>Foxd1</i> lineage-positive populations.	78
Figure 2.2: <i>Foxd1</i> -positive progenitor cells in the developing embryos contributed to FLP cells within the developing dermis.	89
Figure 2.3: FLP cells were most abundant in the medial dorsal skin during development and were primarily localized to the dorsal skin of adult mice.	91
Figure 2.4: Dermal FLP progenitors expressed <i>Foxd1</i> from E7.5 to E11.5.	93
Figure 2.5: FLP populations in adult skin and granulation tissue were not derived from de novo <i>Foxd1</i> expression in postnatal tissue.	96
Figure 2.6: <i>Foxd1</i> -positive progenitors gave rise to fibroblast, perivascular, and arrector pili populations within the adult skin.	99
Figure 2.7: FLP cells contributed to the myofibroblast population during wound repair.	102
Figure 2.8: FLP cells within day-3 granulation tissue co-labelled with fibroblast markers.	103
Figure 2.9: FLP cells within day-10 granulation tissue co-labelled with fibroblast markers.	104
Figure 2.10: FLP fibroblasts and FLN fibroblasts contributed differentially to skin homeostasis and wound repair.	108
Figure 2.11: Gene expression was differentially regulated within cell lineage between wounded and unwounded tissue.	109
Figure 2.12: Gene expression in FLP and FLN fibroblasts was altered in vitro.	113
Figure 2.13: Stratification of fibroblasts by <i>Foxd1</i> lineage did not directly overlap with previously characterized dermal fibroblast lineages.	114
Figure 2.14: $\alpha 2$, $\alpha 3$, and αV integrin expression in FLP and FLN cells within the granulation tissue at day 10 post wounding.	116
Figure 2.15: Binary Thresholding of $\alpha 2$, $\alpha 3$, αV integrins.	117
Figure 2.16: $\beta 1$ and $\beta 6$ integrin expression in FLP and FLN cells within the granulation tissue at day 10 post wounding.	118

Figure 2.17: Binary Thresholding of $\beta 1$ and $\beta 6$ integrins.....	119
Figure 3.1: Electrophoresis following PCR of DNA isolated from <i>Galectin-3</i> KO, wild type and heterozygous mice.....	136
Figure 3.2: Location of tissue isolated for mRNA expression in mice.....	143
Figure 3.3: Galectin-3 expression peaked in the inflammatory phase and remained present into the proliferative phase, primarily expressed in arginase I-positive cells.....	145
Figure 3.4: Genetic deletion of Galectin-3 did not affect gross wound closure but did impair the rate of re-epithelialization by 7 days post wounding.....	147
Figure 3.5: Genetic deletion of Galectin-3 did not affect the immune cell infiltrate by 3 days post wounding.....	149
Figure 3.6: Genetic deletion of galectin-3 did not affect wound composition at 7 and 15 days post wounding.....	150
Figure 3.7: Transcript abundance of genes associated with fibrotic response and revascularization were unchanged by <i>Galectin-3</i> KO, 7 days post wounding.	153
Figure 3.8: <i>Galectin-3</i> KO mouse dermal fibroblasts did not have impaired function in vitro.....	154
Figure 3.9: WT and <i>Galectin-3</i> KO mouse dermal fibroblasts formed α SMA stress fibers following TGF β 1 treatment.	155
Figure 3.10: Galectin-3 expression was decreased in human chronic wound tissue and was negatively correlated with neutrophil elastase expression.....	157
Figure 3.11: Regulation of Galectin-3 expression in human non-involved and wound edge dermal fibroblasts by TGF β 1 and TNF α	160
Figure 4.1: DAT and BTC foams.	179
Figure 4.2: DAT foams improved healing in diabetic mice compared to untreated wounds and electrospun collagen scaffold control treatment.	187
Figure 4.3: Addition of foam biomaterials into excisional wounds in the dorsal skin of pigs decreased the rate of wound closure.	189
Figure 4.4: The rate of wound closure within the first week of healing was reduced in wounds treated with biomaterials.	191
Figure 4.5: Wound contraction and matrix production were not affected by treatment with the biomaterials.....	194

Figure 4.6: Treatment with foam biomaterials did not alter the vascular density of the wound bed.....	197
Figure 4.7: Foam biomaterials did not alter macrophage infiltration.	201
Figure 4.8: Porcine ASCs differentiated towards the adipogenic, osteogenic, and chondrogenic lineages.....	202
Figure 4.9: Closure kinetics of wounds treated with ASC-seeded biomaterials.....	205
Figure 4.10: PKH labelled porcine ASCs were detectable within the granulation tissue at 7 days post wounding.....	206
Figure 4.11: ASC-seeded biomaterials did not alter the histological parameters or hydroxyproline content of treated wounds.	208
Figure A-1: Negative staining controls for staining.....	245
Figure A-2: FLP cells contribute to populations within the heart, lungs, and kidney in mice at embryonic day 14.5.....	246
Figure A-3: High magnification images of porcine granulation tissue stained with Masson's trichrome stain.	247
Figure A-4: High magnification images of α SMA and vimentin stained porcine wound tissue at Day 7 and Day 28.	248
Figure A-5: High magnification images of CD146 stained porcine wound tissue at Day 7 and Day 28.....	249
Figure A-6: High magnification images of CD68 and CD163 stained porcine wound tissue at Day 7 and Day 28.	250
Figure A-7: High magnification images of wounds treated with ASC seeded biomaterials at 7 days.	252
Figure A-8: Individual wound size measurements used to complete the regression analyses highlighted in Figures 3.2 and 3.3.....	253

List of Appendices

Appendix A: Supplemental Figures and Tables	244
Appendix B: Human Ethics Approval	265
Appendix C: Animal Ethics Approval	267

List of abbreviations

ADAM	A disintegrin and metalloproteinase
AGE	Advanced glycation end-products
ASC	Adipose derived mesenchymal stem/stromal cell
BTC	Purified type I collagen from bovine tendon
bFGF	Basic fibroblast growth factor
BMP	Bone morphogenic protein
CCN2	CCN family member 2 (connective tissue growth factor)
CD	Cluster of differentiation
CRD	Carbohydrate recognition domain
DAMP	Damage associated molecular pattern
DAT	human decellularized adipose tissue
DPP4	Dipeptidyl peptidase-4 (CD26)
dpw	days post wounding
DT	<i>Diphtheria</i> Toxin
DTR	<i>Diphtheria</i> Toxin receptor
E	embryonic day
ECM	extracellular matrix
EGFR	Epidermal growth factor receptor
EMT	Epithelial to mesenchymal transition
ERK	Extracellular signal-regulated kinase 1
FACS	Fluorescence-activated cell sorting

FAK	Focal adhesion kinase
FBS	Fetal bovine serum
FDA	United States Food and Drug Administration
FLN	Foxd1 lineage-negative
FLP	Foxd1 lineage-positive
Foxd1	Forkhead box D1
GFP	green fluorescence protein
IBMX	3-isobutyl-1-methylxanthine
IGF	Insulin-like growth factor
IL	Interleukin
ISCT	International Society for Cellular Therapy
KO	knockout
LOX	Lysyl Oxidase
LTBP	Latent TGF β binding protein
lsl	Loxp-STOP-Loxp
Mgat5	α -1,6-mannosylglycoprotein 6-beta-N-acetylglucosaminyltransferase A
MMP	Matrix metalloproteinase
MSC	Mesenchymal stem/stromal cell
NOS2	Nitric oxide synthase 2
PBS	Phosphate buffered saline
PDGF	Platelet derived growth factor
PDGFR	Platelet derived growth factor receptor
PN	Periostin

PS	Penicillin/streptomycin
RTK	Receptor tyrosine kinase
SIS	Small intestine submucosa
SPARC	Secreted protein acidic and rich in cysteine
tdTomato	Tandem dimer Tomato red fluorescent protein variant
TGF β	Transforming growth factor beta
TGF β R	Transforming growth factor beta receptor
TIMP	Tissue inhibitor of metalloproteinase
TLR	Toll-like receptor
TNF α	Tumor necrosis factor alpha
TNX	Tenascin-X
TSP	Thrombospondin
UBM	Urinary bladder matrix
VEGF	Vascular endothelial growth factor
VEGFR	Vascular endothelial growth factor receptor
vWF	Von Willebrand Factor
WT	wild type
α SMA	Alpha- smooth muscle actin

Chapter 1: Rationale, Literature Review and Thesis Overview

1.1 Rationale, Hypothesis and Objectives

Full thickness wound repair in skin is a complex and multifaceted process which, at best, results in the formation of scar tissue. In more severe cases such as in wounds of patients with underlying comorbidities, including vascular disease or diabetes, chronic wounds can develop. A major difference between these two disparate outcomes is a transition from an inflammatory state into the proliferative phase of healing. Thus, a better understanding of the factors that mediate this transition in acute wounds may enable novel therapeutic approaches for the treatment of impaired healing. Transition from the inflammatory to the proliferative phase of healing is dependent on appropriate cell recruitment, differentiation, and function, which are themselves dependent on cell intrinsic properties and the properties of their microenvironment. In the present thesis, previous work from the Hamilton and Flynn laboratories was expanded upon to further the understanding of these cell intrinsic and extrinsic properties required for healing, with a focus on fibroblast activation and differentiation into myofibroblasts, for the purpose of guiding the development of future biomaterials.

This thesis explored the hypothesis that fibroblast activation and differentiation into myofibroblasts during an acute healing response rely on cell-intrinsic differences stemming from a population's embryonic lineage, and cell-extrinsic factors present within the extracellular matrix (ECM). Specifically, it was first hypothesized that

embryonic progenitors that express *Foxd1* would contribute to myofibroblast progenitors within the skin, and that binary expression of *Foxd1* could be used to stratify dermal fibroblasts to identify unexplored embryonic lineages of myofibroblast progenitors present within the adult dorsal dermis (Aim 1). Second, it was hypothesized that modifying the ECM by deletion of genes coding for ECM proteins normally expressed during wound healing would impair granulation tissue formation, while adding exogenous pro-fibrotic and pro-angiogenic ECM components would enhance granulation tissue formation and angiogenesis in models of acute cutaneous wound healing (Aims 2 and 3).

These were explored through the following three aims:

1. To assess *Foxd1* expression in cutaneous myofibroblast progenitor populations during development, and to determine how cells derived from *Foxd1*-expressing progenitors contribute to wound repair.
2. To identify the expression profile of Galectin-3 in murine skin during homeostasis and cutaneous wound healing and investigate the effect of genetic deletion of *Galectin-3* on cutaneous wound repair. Further, to characterize the expression of Galectin-3 in human chronic wound tissue.
3. To investigate a porcine acute wound healing model for assessing the effects of ECM-based foam biomaterials, as well as exploring the potential of the biomaterials as platforms for the delivery of exogenous porcine ASCs.

1.2 Wound healing

In healthy adults, wound healing is a multifaceted process that elicits a rapid repair response, culminating in a fibrotic scar that lacks both form and function (Eming et al. 2014; Martin and Nunan 2015). Wound healing is a temporal process that develops through a series of overlapping phases characterized by specific cell and molecular events within each phase (Singer and Clark 1999; Velnar et al. 2009). Initially, hemostasis occurs to limit blood loss and reduce the risk of systemic infection, with blood clotting also providing molecular signals that initiate tissue repair (Velnar et al. 2009). The inflammatory phase is characterized first by neutrophil infiltration, with a primary role in targeting infection through their innate immune function (Martin and Leibovich 2005; Velnar et al. 2009). Temporally, macrophages migrate into the wound, debriding damaged tissue, phagocytosing neutrophils, and stimulating transition into the proliferative phase through the release of growth factors such as transforming growth factor- β 1 (TGF β 1), platelet derived growth factor (PDGF), and vascular endothelial growth factor (VEGF) (Barrientos et al. 2008). During the proliferative phase, fibroblasts, which are the primary effectors of tissue repair, migrate into the wound, proliferate, and begin producing a temporary matrix called granulation tissue (Martin and Leibovich 2005; Velnar et al. 2009). Finally, in the remodeling phase, fibroblasts turn over the granulation tissue into a type I collagen rich scar (Velnar et al. 2009). Each of these phases will be discussed in more detail below.

Hemostasis is a rapid process, critical to limit blood loss, and at the same time necessary to initiate the wound repair response (Martin and Leibovich 2005; Velnar et al. 2009).

Upon disruption of the endothelial barrier, platelets are exposed to the underlying matrix,

binding to collagens through $\alpha 2\beta 1$ integrin- and von Willebrand factor (vWF)-mediated recognition, inducing their activation (Tomokiyo et al. 2005; Ruggeri 2009). Initially, this results in the aggregation of platelets, forming a physical barrier, which is then strengthened by a fibrin matrix, formed through the coagulation cascade (Golebiewska and Poole 2015). In addition to initiating the coagulation cascade, platelets also release factors which inhibit angiogenesis, including angiostatin, and platelets are themselves capable of sequestering growth factors including VEGF (Klement et al. 2009; Bodnar 2015). While this response is imperative to regain homeostasis, platelet activation and degranulation further supports activation of circulating neutrophils and monocytes through cytokine and growth factor release, inducing their presentation of adhesion molecules to promote cellular homing to the site of injury (Bodnar 2015; Golebiewska and Poole 2015; Kral et al. 2016). Moreover, many of the factors released by platelets have been reported to have direct antimicrobial effects (Tang et al. 2002).

The inflammatory response is further supported by resident macrophages and dendritic cells (Yates et al. 2012). In response to tissue damage and platelet degranulation, neutrophils are next to populate the wound bed, followed by the recruitment of circulating monocytes, which differentiate into macrophages (Velnar et al. 2009). Together, neutrophils and macrophages make up the bulk of the innate immune response through their release of inflammatory mediators and bactericidal factors, including reactive oxygen species (Yates et al. 2012). Moreover, neutrophils and macrophages are important for the debridement of the inflamed tissue through the release of proteases and through phagocytosis, removing bacteria and cellular debris from the damaged tissue (Singer and Clark 1999; Barrientos et al. 2008; Yates et al. 2012). Finally, neutrophils

and macrophages are a major source of growth factors that initiate and regulate angiogenesis, as well as fibroblast recruitment and activation, advancing the wound beyond the inflammatory phase (Barrientos et al. 2008). Although it is evident that neutrophils have a role in pathogen defense and growth factor secretion, it should be noted that they are not necessary for an effective wound healing response in wounds inflicted using sterile instruments and kept within a clean experimental environment (Dovi et al. 2003). In fact, using an excisional wound model in neutrophil depleted-wild type and -diabetic mice, Dovi *et al.* showed an increased rate of wound re-epithelialization in neutrophil depleted animals compared to controls. Conversely, temporal depletion of macrophages using a *diphtheria* toxin (DT)/ DT receptor (DTR) approach, suggested that they play important roles in both the inflammatory and proliferative phases of healing, but not in the remodeling phase (Lucas et al. 2010). Notably, Lucas *et al.* showed a decreased rate of closure, associated with decreased α SMA and CD31 content within the wounds, following early depletion of macrophages, suggesting impaired myofibroblast differentiation and reduced angiogenesis, respectively.

Throughout the healing process, keratinocytes play an active role beyond restoring the skin's barrier function through re-epithelialization. Upon injury, keratinocytes release antimicrobial peptides and other members of the alarmin family of proteins (including IL1 α), which act as damage associated molecular patterns (DAMPs), to further stimulate local inflammation through toll like receptor (TLR) signaling (Juránová et al. 2017). Furthermore, activated keratinocytes are a source of matrix metalloproteinases (MMPs),

which play critical roles in migration, remodeling and signaling during the wound repair process (Caley et al. 2015).

Following the inflammatory response, the proliferative phase begins, characterized by the infiltration of myofibroblasts and neovasculature (Singer and Clark 1999; Velnar et al. 2009; Reinke and Sorg 2012). Generally, fibroblasts migrate into the wound bed in response to chemotactic stimuli including PDGF and basic fibroblast growth factor (bFGF) and differentiate into myofibroblasts, primarily in response to TGF β 1 (Hinz 2007, 2016; Barrientos et al. 2008). Myofibroblasts are a contractile cell type often characterized by their incorporation of α SMA into stress fibers, enabling strong force generation (Hinz et al. 2001; Hinz 2007). Moreover, this population is the primary contributor of ECM during wound repair (Hinz 2016). Wound contraction initiates a positive feedback mechanism through which increased matrix stiffness enhances myofibroblast differentiation through both mechano-sensing and activation of latent TGF β 1 (Hinz 2015). Myofibroblasts are responsible for the production of type I and type III collagen, which further increases the stiffness of the ECM. However, the processes described in this simplified system are now known to be far more complex, with recent observations highlighting differential roles of fibroblast subsets during tissue repair (Dulauroy et al. 2012; Driskell et al. 2013; Rinkevich et al. 2015). Several studies have described fibroblasts as a heterogeneous population of cells that contribute differentially to tissue repair (Driskell and Watt 2015). This topic will be discussed further in section 1.4.

In conjunction with the proliferation and differentiation of fibroblasts, endothelial cells migrate into the wound in response to the release of pro-angiogenic stimuli, such as

VEGF and bFGF, released by keratinocytes, fibroblasts, and inflammatory cells (Barrientos et al. 2008). This response results in a rapid and extensive revascularization of the wound; however, the resultant vascular network is leaky, unstable, and poorly perfused (Bluff et al. 2006; Kim et al. 2009; Bolitho et al. 2010; Wietecha et al. 2013).

The remodeling phase of wound repair takes place from months to years following the initial injury (Velnar et al. 2009). During this phase, fibroblasts reorganize the randomly arranged collagen fibrils into parallel bundles, and many of the blood vessels and fibroblasts present in the wound undergo apoptosis (Xue and Jackson 2015). While the processes that lead to the expansion of endothelial cells and fibroblasts during earlier stages have been extensively studied, those which result in a regressive phenotype are less well characterized (Wietecha et al. 2013). There are several mechanisms that have been proposed to mediate vascular regression in wound healing, including changes in ECM composition, decreased pericyte coverage, low shear stress in poorly perfused vessels, and reduced availability of pro-angiogenic growth factors concomitant with an increase in anti-angiogenic proteins and peptide fragments (Wietecha et al. 2013). Similarly, myofibroblasts have been shown to undergo apoptosis following wound resolution (Desmoulière et al. 1995). The mechanisms through which this occurs are still under investigation, although potential contributing factors include: decreased growth factor stimulation, which decreases resistance to apoptosis; decreased mechanical stress on cells following ECM regeneration; and increased cell-cell contact (Hinz 2007; Hinz and Gabbiani 2010). Interestingly, recent data have highlighted an alternate pathway for fibroblast deactivation, in which they differentiate into subcutaneous adipocytes during wound resolution (Plikus et al. 2017).

In this manner, successful wound repair results in effective recovery of the skin's barrier function; however, the resultant scar does not completely recapitulate native skin (Eming et al. 2014; Martin and Nunan 2015). In humans, scar tissue lacks functional elements, including hair follicles and sweat glands (Li et al. 2017). Moreover, in a rat model, cutaneous scars recovered only about 80% of the tensile strength of unwounded skin (Levenson et al. 1965). While not perfect regeneration, formation of normal scar tissue has evolved as the mechanism of healing. Alternatively, an impaired healing response manifests as a reduction in ECM production, as in chronic wounds, or an excess of ECM production, as in hypertrophic and keloid scars (Martin and Nunan 2015).

1.3 Chronic wounds

Although the studies within this thesis focused primarily on understanding the mechanisms involved during acute wound healing, the long-term goal of this work is to apply these findings to chronic wounds to identify novel therapeutic strategies. As such, an overview of repair in a chronic wound setting follows, with an emphasis on the discrepancies between acute and chronic healing.

Chronic skin wounds are a complex clinical issue most prevalent in patients with underlying comorbidities, including diabetes, vasculopathy, impaired mobility and increased age (Demidova-Rice et al. 2012). Although the underlying susceptibility of patients to impaired healing might differ, chronic wounds of diverse etiology are similarly impaired, and are all characterized by excessive and prolonged inflammation (Demidova-Rice et al. 2012; Frykberg and Banks 2015). Despite remaining in an inflammatory state, chronic wounds are also characterized by persistent infections (Frykberg and Banks 2015). Prolonged inflammation is especially problematic for wound

repair due to the release of reactive oxygen species and proteolytic enzymes, which contribute to destruction of ECM, growth factors, and signaling molecules, creating a non-permissive microenvironment for tissue repair (Barrientos et al. 2008; Moor et al. 2009; Frykberg and Banks 2015). For example, levels of VEGF mRNA were found to be upregulated in human chronic wound tissue compared to uninjured tissue, but correlated with low protein content (Lauer et al. 2000). Moreover, in this study, chronic wound fluid, but not acute wound fluid, resulted in the proteolytic degradation of VEGF.

In addition to these extrinsic factors affecting closure, the cells themselves may have intrinsic differences that affect how they respond to available growth factors. For example, the surface receptor for TGF β 1, TGF β receptor II (TGF β RII), was found to be decreased in fibroblasts isolated from chronic wound tissue, which also displayed impaired TGF β 1-induced proliferation in comparison to fibroblasts isolated from unwounded tissue from the same patient (Kim et al. 2003). However, our group has previously observed no change in proliferative capacity of chronic wound edge fibroblasts compared to fibroblasts sourced from non-wounded tissue from the same patient (Elliott et al. 2015). Further, chronic wound fibroblasts displayed enhanced expression of *Acta2* (α SMA) mRNA in response to TGF β 1 relative to those from non-wounded tissue (Elliott et al. 2015). Thus, there is a possibility that, given a suitable environment, resident fibroblasts may be able to respond appropriately through activation and matrix deposition to contribute to tissue repair.

The relationship between cells and their microenvironment has also been investigated in chronic wounds (Peppas et al. 2009; Schultz and Wysocki 2009; Widgerow 2011). The dynamic reciprocity between cells and the ECM is critical for normal wound repair;

however, it is also evident that a modified ECM or altered cell phenotype, as described in chronic wounds, can disrupt this relationship (Schultz et al. 2011). As an example, impaired TGF β 1 signaling in chronic wounds is evident, alongside high expression of MMPs and reduced expression of tissue inhibitors of metalloproteinases (TIMPs). These altered signals all result in impaired matrix deposition. Additionally, it is established that activation of TGF β 1 from latent TGF binding protein (LTBP-1) requires force generation by the cell to the matrix-bound LTBP-1, a process mediated by integrin binding (Hinz 2015). However, without a sufficiently rigid matrix, such activation is impaired, increasing TGF β 1 deficiency, which results in impaired matrix production.

The pathophysiology of chronic wounds is further exacerbated, particularly in diabetes, by accumulation of advanced glycation end-products (AGEs) (Singh et al. 2014; Van Putte et al. 2016). AGEs are a heterogeneous group of compounds formed from non-enzymatic reactions between reducing sugars and free amino groups on proteins, which form at a rate limited by the concentration of the reducing sugar (Ahmed and Thornalley 2007). While diabetic patients can produce higher levels of endogenous AGEs due to higher levels of reducing sugars in tissues for prolonged periods of time, humans without diabetes are also susceptible to accumulation through diet, with both endogenous and exogenous sources accumulating over time (Luevano-Contreras and Chapman-Novakofski 2010; Singh et al. 2014). Importantly, data from our group has identified high levels of AGEs within chronic wounds, compared to uninjured tissue from the same patient (Pepe et al. 2014). In addition to roles in cell signaling pathways through AGE-receptors, AGE formation on proteins inhibits function and the ability to interact effectively with other molecules, and may make them more difficult to degrade (Ahmed

and Thornalley 2007; Peppas et al. 2009). Importantly, it has been shown in multiple studies that AGEs inhibit wound healing. Both ingestion (Zhu et al. 2011) and injection (Berlanger et al. 2005) of AGEs have led to altered, diabetes-like wound healing in rodents. Furthermore, a study performed by Liao *et al.* (2009) identified that placing a glycated, lyophilized collagen matrix into a pre-existing wound of healthy mice was sufficient to cause deleterious effects to the wound healing process similar to that seen with diabetes, including impaired rate of healing, reduced cell infiltration, and reduced fibroblast contractility (Liao et al. 2009).

Relative to acute wounds, chronic wounds are associated with a range of deficient signaling mechanisms (Demidova-Rice et al. 2012; Frykberg and Banks 2015). This is manifest in changes in both intercellular signaling and the interactions between cells and their environment (Barrientos et al. 2008; Schultz and Wysocki 2009; Demidova-Rice et al. 2012; Frykberg and Banks 2015). Although advances have been made to chronic wound therapies, many patients still do not respond to treatment (Santema et al. 2016; Norman et al. 2017), suggesting a need for novel therapeutics targeting specific pathological features.

1.4 Wound healing from a cell intrinsic perspective

In acute wounds, the bulk functionality of myofibroblast progenitors, including any cell that can differentiate into myofibroblasts, requires proliferation and migration into the granulation tissue, and differentiation into contractile myofibroblasts that secrete ECM proteins, especially collagens (Hinz 2007). The factors that induce myofibroblast

activation are cell extrinsic in nature, including matrix stiffness, signaling molecules such as TGF β 1, or ECM components such as matricellular proteins or the ED-A splice variant of fibronectin (Serini et al. 1998; Hinz 2007). In contrast to these extrinsic factors, recent observations have supported a more nuanced system in which myofibroblast progenitor-specific intrinsic differences alter how they respond to extrinsic stimuli (Driskell and Watt 2015; Hu et al. 2018). Thus, whereas extrinsic factors stimulate myofibroblast differentiation, intrinsic factors control the degree to which a myofibroblast progenitor responds and the downstream effect of that response. These differences reside within the cells themselves and can be tracked using lineage tracing strategies to monitor subpopulations that have or are derived from progenitors that had unique gene expression patterns. The findings from these studies support a level of role specification based on the intrinsic nature of the myofibroblast progenitor and will be the focus of this section. A better understanding of the specific roles of fibroblast subsets, and how these subsets interact, may be useful in the identification of novel therapeutic targets or strategies for the treatment of chronic wounds.

Lineage tracing technology has been used to identify several distinct myofibroblast progenitor populations that play a role in skin repair and fibrosis, including fibroblasts, perivascular cells, adipogenic lineages, and bone-marrow derived populations (Dulauroy et al. 2012; Driskell et al. 2013; Suga et al. 2014; Marangoni et al. 2015; Rinkevich et al. 2015). Of particular interest from these findings, fibroblasts, as described through positive selection using PDGFR α within dermal isolates, or by negative selection as dermal cells lacking epithelial, endothelial and circulating cell markers, have been described as having subsets with different functional roles during wound healing

(Driskell et al. 2013; Rinkevich et al. 2015). Specifically, the fibrogenic potential, the propensity to produce ECM, has been suggested to vary between fibroblast subsets. Thus, not only are multiple cell types capable of contributing to the myofibroblast population, but there may be further levels of specialization within those cell types. Importantly, these intrinsic differences within fibroblast populations have been reported to arise during embryonic development (Driskell et al. 2013; Rinkevich et al. 2015; Jiang et al. 2018). Therefore, in order to appreciate the heterogeneity in fibroblasts, skin development will be discussed, highlighting both when and where dermal fibroblast populations arise. This will be followed by a discussion of the current understanding of the contributions of diverse myofibroblast progenitor populations to tissue repair in the skin and other organs.

1.4.1 Skin development

In mice, gastrulation initiates around embryonic day 5(E5)-E6, and is complete around E7.5 (Tam and Behringer 1997). At this time the mesoderm has split into three regions, known as the paraxial mesoderm, intermediate mesoderm, and lateral plate mesoderm. The paraxial mesoderm divides into somites, creating a segmented body plan in a rostral to caudal direction (Gilbert 2000). These somites then undergo differentiation into the sclerotome and the dermatomyotome, which itself splits into the dermatomes and myotomes. Importantly, the somite-derived dermatomes are the source of dorsal fibroblasts, whereas the lateral plate mesoderm gives rise to the dermal cells in both lateral and ventral dermis (Gilbert 2000). However, it is noteworthy that the lateral and ventral populations are less studied in animal models, in which the investigation of dorsal skin and dorsal wound tissue are most common.

Within the dorsal region, a recently described myofibroblast precursor population with strong fibrogenic potential, defined as being derived from *engrailed-1*-positive progenitors, arises from two parallel tracks ventral to the developing neural tube, and migrates dorsally around E10.5 (Jiang et al. 2018). Interestingly, this population began migrating from the rostral regions first followed by the caudal regions, fitting with the sequence of somite differentiation. These cells were then described to move laterally from the medial dorsal skin, replacing the lineage-negative fibroblast population, characterized by a lesser fibrogenic potential, by maintaining a clonal advantage (Jiang et al. 2018). Currently, it is unknown where the original population of lineage-negative fibroblasts arises, whether it is coming from an earlier wave of migration from the somites, or another population altogether. Once the fibroblast progenitor cells migrate to the dermis, the initial multipotent progenitors undergo further specification (Driskell et al. 2013). One distinct population makes up the upper papillary dermis, including the papillary fibroblasts, dermal sheath and dermal papilla, as well as the arrector pili muscles, whereas another population derives the reticular dermis and both the preadipocytes and adipocytes of the subcutaneous adipose tissue (Driskell et al. 2013). To appreciate the structures of the skin, histological sections of adult murine, porcine, and human skin are shown in Figure 1.1.

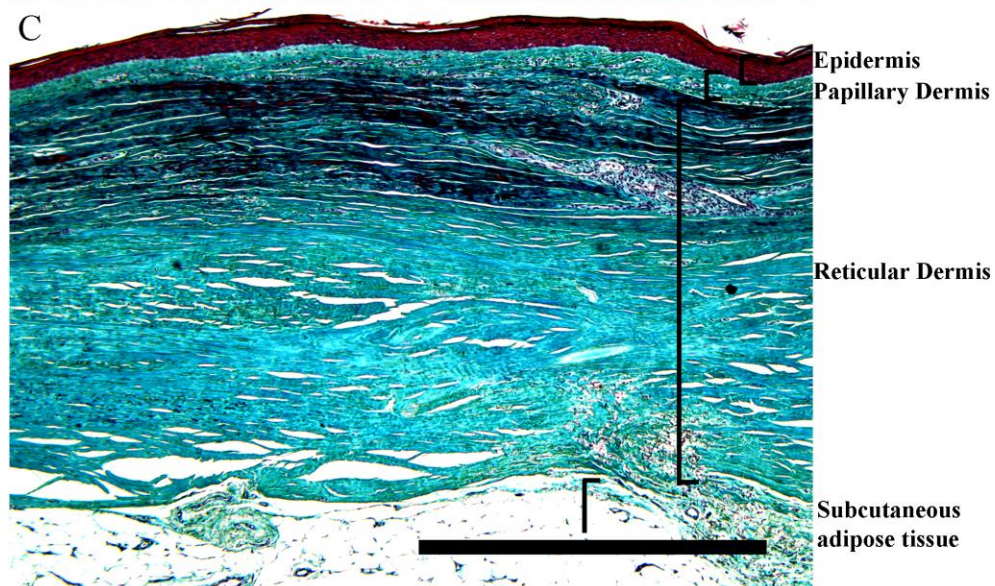
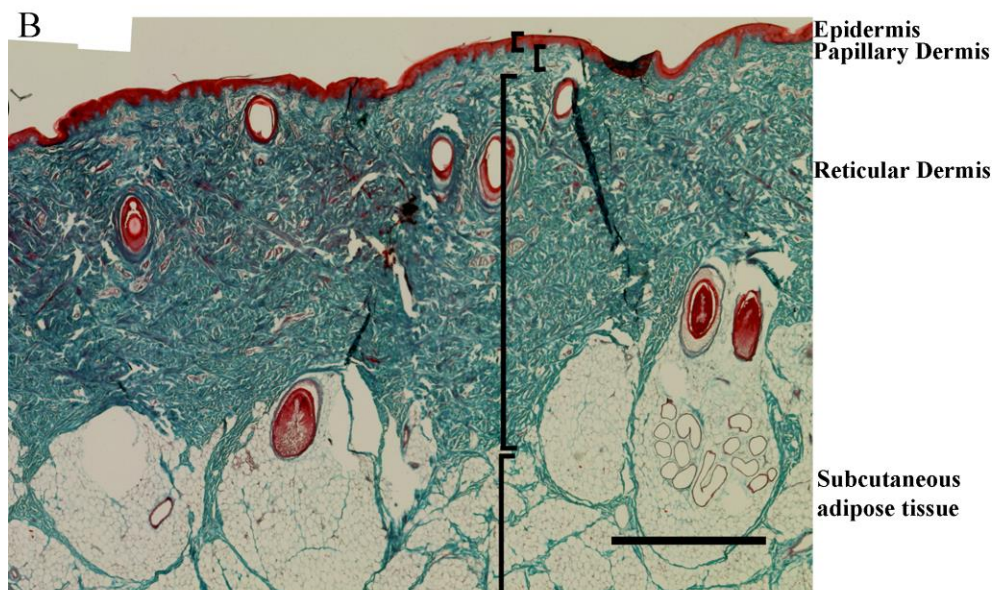
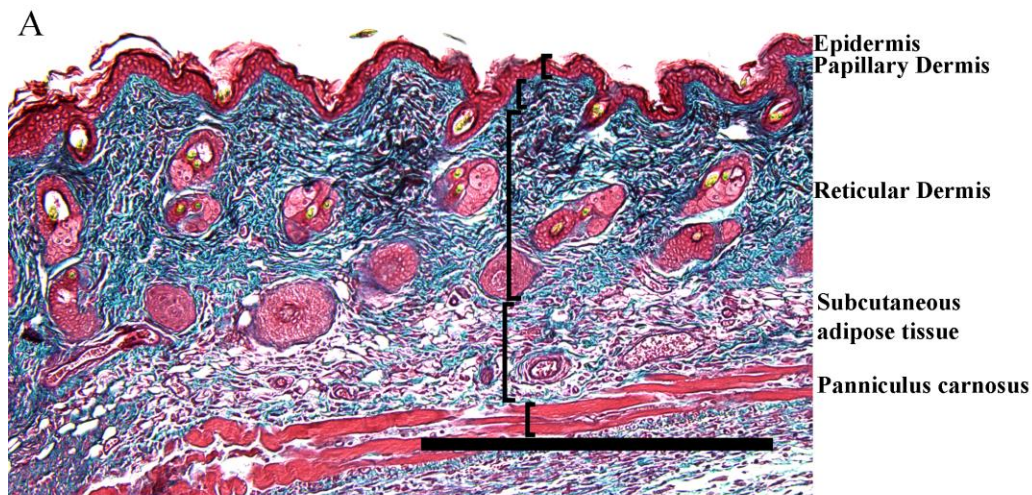


Figure 1.1: Structures within skin from murine, porcine, and human sources. Masson's trichrome stained sections of adult female mouse dorsal skin (A), juvenile male pig dorsal skin (B), and adult female human skin isolated from the lower limb (C). Scale bars are 500 μm for mouse skin and 1 mm for porcine and human skin. Cutaneous structures are highlighted including an approximation of the divide between the reticular dermis and papillary dermis. All species explored in this thesis possess the epidermis, papillary dermis, reticular dermis, and subcutaneous adipose tissue; however, only murine skin contains the panniculus carnosus muscle.

One notable change that occurs during development in mammals is a switch from nearly perfect dermal regeneration following wounding at early fetal stages, to scar formation at later stages; in mice, this switch occurs around E17.5 (Walmsley et al. 2015). Interestingly, this timeframe corresponds to a rapid increase in the cellular frequency of the more fibrogenic *engrailed-1* lineage of fibroblasts within the skin (Jiang et al. 2018), as well as a fate restriction between the cells of the upper papillary dermis and lower reticular dermis (Driskell et al. 2013). Additionally, it was recently reported that during this time, dermal fibroblasts undergo a critical change, switching from a proliferative phenotype to a synthetic phenotype (Rognoni et al. 2018). Prior to this proliferative switch, changes in tissue volume correlate with cell number, suggesting proliferation is primarily responsible for increased tissue mass. However, following this switch, ECM production becomes the major process, and proliferation is halted (Rognoni et al. 2018). It is noteworthy that these changes were described throughout the tissue, and not only in specific fibroblast subsets, suggesting independence of cell lineage. The ECM itself also undergoes a critical change during development in which an initially loose fibronectin-rich matrix changes to one rich in collagen I, providing greater tension (Jiang et al. 2018). From these important studies it is evident that the skin undergoes a remarkable shift during development that is related to changes in both cell intrinsic and cell extrinsic factors.

1.4.2 Origins of myofibroblasts in tissue repair

Myofibroblasts, characterized by their expression of α SMA, are the main source of ECM production following tissue injury (Hinz 2007). Numerous cell types can differentiate

into myofibroblasts in various fibrotic events, including wound healing (Hinz 2016). There has been a recent push towards identifying these precursor populations, predominantly using two different strategies for lineage tracing. First, bone marrow chimera models utilize a transplantation method in which genetically tagged hematopoietic stem cells from one animal are implanted into a non-genetically-tagged recipient that has undergone non-lethal irradiation to deplete endogenous hematopoietic lineages (Kretzschmar and Watt 2012; Hsu 2015). In this way, tagged cells will reconstitute the hematopoietic cell niche, and any hematopoietic populations to which those cells contribute will also be genetically tagged. The second method that has been widely used to track both hematopoietic and non-hematopoietic lineages is Cre/Lox based lineage tracing adapted from bacteriophage P1 (Kretzschmar and Watt 2012). This system is highly versatile, but for many applications a cell-type specific promoter is used to control the expression of Cre-recombinase, while a reporter sequence under control of a ubiquitous promoter is blocked by a transcriptional stop sequence that can be excised by recombinase activity (Kretzschmar and Watt 2012). In this way, the reporter sequence (fluorescent or enzymatic) is only expressed in cells that express Cre-recombinase, as well as the progeny of those cells. Utilizing these methods, several myofibroblast progenitor populations have been explored within the skin and other organs during fibrotic repair and will be discussed below. Identification of these key progenitor populations could have important implications for therapeutic strategies. For human chronic wounds, where matrix deposition is reduced, these findings could help to identify pro-fibrotic pathways for therapeutic activation or could identify specific surface markers to allow sourcing of pro-fibrotic cells from other sites for delivery into affected tissues.

1.4.3 Sources of myofibroblasts in wound repair and fibrosis

Due to the potential therapeutic benefits of identifying pro-fibrotic populations within the skin and other organs, several studies have employed lineage tracing strategies to investigate myofibroblast precursor populations. Within the dermis, it has long been assumed that resident fibroblasts in the neighboring tissue are the major source of myofibroblasts during dermal wound healing (Singer and Clark 1999). As an organ that is prone to injury from external sources, and one which maintains a large reservoir of potential myofibroblast progenitors, this seems intuitive; however, strong evidence for resident stromal cells as the major myofibroblast progenitor population has only been described more recently (Driskell et al. 2013; Marangoni et al. 2015; Rinkevich et al. 2015). Driskell *et al.* (2013) first documented different lineages of fibroblast populations in the dorsal dermis, which arise during development. During wound repair they showed that the lower lineage, consisting of fibroblasts in the reticular dermis and adipocyte precursors within the hypodermis, were the major contributors to granulation tissue synthesis. In contrast, the upper lineage of fibroblasts within the papillary dermis were recruited later, contributing only to the newly forming papillary dermis and required for regrowth of hair follicles (Driskell et al. 2013).

The idea that adipocyte precursors are sources of myofibroblasts was further supported by Marangoni *et al.* (2015) who made the observation that in human patients with skin fibrosis, and in animal models of induced skin fibrosis, the amount of adipose tissue in the hypodermis is decreased. To expand upon this initial observation, they demonstrated through lineage tracing that adiponectin-positive adipocytes differentiated into

myofibroblasts following bleomycin induced skin fibrosis in mice. More recently, Plikus *et al.* (2017), strengthened the relationship between adipocytes and myofibroblasts, showing that following wound repair, some of the myofibroblasts will differentiate into adipocytes (Plikus *et al.* 2017). A similar pattern of differentiation can also be seen during lung fibrosis in which lipogenic fibroblasts differentiate into myofibroblasts following a fibrogenic insult, and then dedifferentiate back into lipogenic fibroblasts during resolution (El Agha *et al.* 2017). Taken together, these findings suggest that there might be homology in the myofibroblast precursors of diverse tissues.

In another study, Rinkevich *et al.* (2015) used lineage tracing of *engrailed-1*, a protein expressed solely during development in a specific subset of dermal fibroblast precursors (Rinkevich *et al.* 2015). *Engrailed-1* lineage-derived fibroblasts begin to appear in the papillary dermis around embryonic day 12.5 (E12.5) and constitute only ~1% of the total fibroblast population. After this time, this population of cells expands into the reticular dermis, contributing to ~75% of dermal fibroblasts in adult mice. These cells are shown to be responsible for most of the ECM deposition during wound healing. Ablation of these cells resulted in an increase in the time required for healing, concomitant with a reduction in the amount of collagen deposition. These results would be expected given the high percentage of dermal fibroblasts that are derived from the *engrailed-1* lineage. As such, it is logical that matrix deposition and the rate of closure would be impaired when this population is ablated or inhibited. However, surprisingly, the overall tensile strength of healed wounds was similar for both control wounds and wounds in which the *engrailed-1* lineage was ablated (Rinkevich *et al.* 2015). Expanding on these findings, evidence was provided to show that the *engrailed-1* lineage fibroblasts were enriched for

CD26, a serine exopeptidase. Importantly, when wounds were treated with a small molecule inhibitor for CD26, scarring was reduced. Thus, using a relatively broad lineage tracing method, the authors identified a specific targetable and functionally relevant marker of myofibroblast progenitors within the skin.

Another population identified to have fibrogenic potential is perivascular cells. Dulauroy *et al.* (2012) showed that a population of perivascular cells within mouse ear dermis upregulated a disintegrin and metalloproteinase 12 (ADAM12) following chemically induced fibrosis (Dulauroy *et al.* 2012). Tracking of ADAM12 lineage-positive populations showed that through proliferation and differentiation into myofibroblasts, these cells were responsible for excessive matrix production, which could be decreased through their ablation (Dulauroy *et al.* 2012). It should be noted, however, that the stroma of the head and neck is derived from both the neural crest as well as the mesoderm (Santagati and Rijli 2003; Bhattacharjee *et al.* 2007). As such, the progenitor populations giving rise to myofibroblasts within the ear may not be the same as those within the dermis of more caudal regions, including the dorsum, where the stroma is derived primarily from the mesoderm (Ben-Yair 2003).

It has been shown that pericytes contribute to fibrotic repair in areas beyond those derived from the neural crest, including the tibialis anterior muscle (Dulauroy *et al.* 2012), kidney (Humphreys *et al.* 2010; Kramann *et al.* 2015), lung (Hung *et al.* 2013; Kramann *et al.* 2015), bone marrow (Schneider *et al.* 2017), heart (Kramann *et al.* 2015), and liver (Mederacke *et al.* 2013; Kramann *et al.* 2015). In contrast to these studies, other groups have provided evidence that pericytes are not a source of myofibroblasts. In a murine renal fibrosis model, LeBleu *et al.* (2013) used lineage tracing of the commonly

accepted pericyte markers PDGFR β and NG2 (LeBleu et al. 2013). Following injury, these cells expanded but contributed to only a small fraction of α SMA positive myofibroblasts. Moreover, ablation of proliferating PDGFR β^+ or NG2 $^+$ cells using a thymidine kinase/ ganciclovir strategy, did not alter matrix deposition following unilateral ureteral obstruction induced kidney fibrosis (LeBleu et al. 2013). In another study, a lineage tracing strategy using expression of the T-box 18 (Tbx18) transcription factor to label smooth muscle cells and pericytes throughout the mouse provided strong evidence that these cell types are not progenitors of myofibroblasts during muscle or cardiac fibrosis (Guimarães-Camboa et al. 2017).

The differences in these findings could potentially stem from the inherent heterogeneity in the perivascular cell population (Bodnar et al. 2016; Dias Moura Prazeres et al. 2017). Genetic lineage tracing strategies rely on differentiation via binary expression of single genes. However, finding a target that uniquely defines the entire population of interest during both homeostasis and following injury, may not be possible for many subpopulations. This may be true for pericytes, which originate from diverse embryonic precursor populations including the neural crest, mesoderm, and mesothelium (Dias Moura Prazeres et al. 2017). Additionally, a recent study identified that about one-quarter of pericytes within the rostral dorsal skin arise from a hematopoietic lineage, as defined by expression of the Vav-1 promoter (Yamazaki et al. 2017).

Another potential source of myofibroblasts that has been investigated is the circulating fibrocyte, a bone marrow derived cell that homes to injured tissues to aid in repair. However, the contribution of these cells to the myofibroblast population is often debated. Using both bone marrow chimera and parabiosis models, groups have shown that

circulating cells do not give rise to collagen-producing cells in injured skin (Higashiyama et al. 2011; Dulauroy et al. 2012; Rinkevich et al. 2015). However, using the same models, others have shown that circulating populations may give rise to a small subset of α -SMA negative, collagen-expressing circulating cells, which the authors attribute to collagen-producing macrophages based on morphology, co-labelling with Mac-3, and their temporal association with the inflammatory infiltrate (Barisic-Dujmovic et al. 2010). More recently, Suga *et al.* (2014) showed through lineage tracing that a population of hematopoietic-derived cells (based on expression of the Vav-1 promoter) contributed to the collagen and α SMA expressing myofibroblast population in a murine wound model (Suga et al. 2014). Although these cells represented approximately 10% of the cells within healthy dorsal dermis, following injury, these cells made up approximately 30% of cells within the granulation tissue, peaking in number at day 7 post wounding (Suga et al. 2014). Importantly, at this time point, 43% of these labelled cells expressed collagen I mRNA, and many also expressed α SMA, with the authors suggesting that these were hematopoietic-derived fibrocytes and that they contributed to the myofibroblast population. Tracking of vav-1 lineage cells over time indicated that they decreased after day 7 post wounding, down to basal levels by day 28 (Suga et al. 2014). Alternatively, it is possible that the Vav-1 lineage gives rise to mesenchymal populations during development, and it is these populations from which the myofibroblasts are derived upon wounding, not the circulating cells. This interpretation is supported by the findings of Yamazaki *et al.* (2017), who showed that Vav-1 derived populations could contribute to pericytes within the rostral dorsal dermis during embryonic development. Due to the different locations studied by Yamazaki *et al.* and Suga *et al.* (rostral dorsal dermis vs.

dorsal dermis, respectively) this alternative interpretation may not be accurate, yet it warrants further investigation. In combination, the evidence for the contribution of circulating cells is not strong, while several studies have provided evidence supporting the null hypothesis.

Overall, these studies suggest that resident cells are likely the major contributors of collagen producing cells within the wound healing response. Whether the populations that have been tracked to date overlap with each other, or whether they can be further divided into more specific populations is not currently known. While marker expression has, in the past, been used to stratify subpopulations of fibroblasts (Phipps et al. 1989), these more recent lineage tracing studies highlight that some of the heterogeneity exhibited by adult fibroblast populations arises from disparate embryonic lineages. The extent of fibroblast heterogeneity has recently been assessed in human dermal fibroblasts using single cell PCR (Philippeos et al. 2018; Tabib et al. 2018). However, whether the diversity characterized by single cell RNA-Sequencing studies results from different cell lineages, from different temporary states within a cell lineage, or combinations of these, is unknown. These findings support the need for additional lineage tracing models to identify different subsets of these fibroblast populations, which may help to identify distinct roles of varying subpopulations during tissue repair. Such findings would have important implications for therapies in the context of both impaired healing and fibrosis.

1.4.4 Foxd1 as a marker for myofibroblast progenitors

Foxd1 is a transcription factor of the forkhead box family (Quintero-Ronderos and Laissue 2018). The protein itself is coded by a single exon, and shares a high level of

homology within the DNA binding domain between mice and humans (Quintero-Ronderos and Laissue 2018). During development, *Foxd1* expression has been shown to be critical for development of the retina, optic chiasm, and kidney (Quintero-Ronderos and Laissue 2018). Within the kidneys, *Foxd1* was found to be expressed exclusively by the stromal populations, and not within the epithelium (Hatini et al. 1996). Global *Foxd1* knockout resulted in reduced kidney volume, fewer developed nephrons, and lethality shortly after birth (Hatini et al. 1996; Levinson 2005).

A recent study by Fetting *et al.* (2014) identified *Foxd1* as an important regulator of several ECM proteins including decorin and collagen IV (Fetting et al. 2014). Importantly, decorin has been shown to be a potent inhibitor of receptor tyrosine kinases (RTKs) and the TGF β superfamily pathways (Neill et al. 2012, 2015). In fact, during development, genetic deletion of *Foxd1* led to increased decorin expression resulting in impaired BMP7 signaling via the inhibition of SMAD signal transduction by decorin (Fetting et al. 2014). The authors showed that this results in an inability of stromal progenitor cells to differentiate, impairing proper kidney development. Thus, *Foxd1* expression is required for stromal progenitor populations to exhibit appropriate differentiation.

In addition to its critical roles during kidney development, cells derived from *Foxd1*-expressing progenitors have been shown to be myofibroblast precursors following tissue injury. Using a *Foxd1*-Cre knock-in mouse crossed with a *Rosa26-loxp-stop-loxp(lsl)-lacZ* reporter mouse, Humphreys *et al.* (2010) were able to provide strong evidence for a mesenchymal source of myofibroblasts during kidney fibrosis (Humphreys et al. 2010). Along with lineage tracing data showing that no renal epithelial cells contributed to the

myofibroblast population, this study provided strong evidence to refute the hypothesis that epithelial to mesenchymal transition (EMT) is a source of myofibroblasts in this process. Moreover, this group used this same model to support a resident mesenchymal contribution to myofibroblasts in bleomycin induced lung fibrosis (Hung et al. 2013).

As Fetting *et al.* (2014) describe, *Foxd1* expression is required to allow progenitor cells to differentiate during kidney development (Fetting et al. 2014). Similar to the kidney, TGF β signaling is also critical for the development of skin (Owens et al. 2008), and the stromal cells in both kidney and dorsal dermis are derived from the paraxial mesoderm during embryogenesis (Fomenou et al. 2005; Guillaume et al. 2009). Thus, there is a possibility that the progenitor cells that differentiate into the stromal populations in both the dorsal skin and the kidney follow a similar pattern of differentiation. However, whether this common pattern of differentiation includes transcriptional regulation by *Foxd1* is unknown. Moreover, if a *Foxd1*-positive progenitor derived population exists within the skin, it is unknown whether it would have similar profibrotic potential as the *Foxd1* lineage derived populations in the renal (Humphreys et al. 2010) and pulmonary (Hung et al. 2013) systems.

1.5 Matricellular proteins in wound repair

The cellular component of tissue exists within an extracellular framework, which together determine cell function. Importantly, changes to cell function result in changes to the ECM, which further modifies cell function, a process termed dynamic reciprocity (Thorne et al. 2015). This process is exemplified by the expression of matricellular

proteins, and their receptors, generally integrins, on the cell surface (Schultz et al. 2011). First defined by Bornstein (1995), matricellular proteins are a group of modular proteins that localize to the ECM, but do not necessarily provide structural support (Bornstein 1995). Instead, matricellular proteins interact with the ECM and cell surface receptors and have varied effects, which depend on the condition of the ECM, modifications made to the matricellular protein itself, and on the expression of receptors present on the cell membrane. In this way, matricellular proteins provide a direct link to transfer information on the state of the ECM to the cell. The rapid turnover and change in ECM composition during wound repair also involves changes in matricellular protein content, making it an important model to study their effects. Furthermore, as many of these proteins regulate processes in the inflammatory and proliferative phases of healing, modifying their activity may be a therapeutic strategy for impaired wound healing. In Table 1.1 below, the wound healing specific phenotypes observed following genetic manipulation of specific matricellular proteins are described, with their temporal expression patterns shown in Figure 1.2. The matricellular proteins focused on in this thesis, Galectin-3, Periostin, and CCN2, will be discussed in more detail below.

Table 1.1 Wound healing specific phenotypes following genetic manipulation of matricellular proteins. From Walker et al. Cell–matrix interactions governing skin repair: matricellular proteins as diverse modulators of cell function. Res Reports Biochem 2015;5:1–16

Matricellular Protein	Influence on excisional skin healing	References
CCN2	Fibroblast-specific deletion of CCN2 does not affect cutaneous wound healing of 4 mm wounds evident by no difference in collagen content, myofibroblast differentiation, and proliferation in CCN2-null and wild-type mice.	(Liu et al. 2014)
Galectin-7	Galectin-7-deficient mice displayed a reduced re-epithelialization potential compared with wild-type littermates during wound healing of superficial scratch along the length of the tail and this effect was attributed to a defect in cell migration.	(Gendronneau et al. 2008)
Hevin	Closure and maturity of cutaneous excisional 5 mm wounds were accelerated in hevin-null compared to wild-type mice.	(Sullivan et al. 2008)
Osteopontin	Osteopontin mutant mice resulted in disorganization of matrix and an alteration of collagen fibrillogenesis leading to smaller diameter collagen fibrils after incisional wound healing.	(Liaw et al. 1998)
Periostin	Excisional wound (3 mm) closure was delayed in Periostin-null mice coupled with a delay in re-epithelialization and reduced proliferation of keratinocytes. During excisional wound (6 mm) healing, Periostin-null mice had reduced level of myofibroblast differentiation compared to wild-type mice. The attenuated myofibroblast differentiation in Periostin-null mice was rescued by addition of recombinant Periostin containing scaffolds. Incisional wounding re-established embryonic pattern of Periostin deposition in adult skin.	(Nishiyama et al. 2011) (Elliott et al. 2012) (Zhou et al. 2010)

SPARC	<p>A significant delay in wound closure in 25 mm wounds in SPARC-null mice compared to wild type mice. A significant reduction in granulation tissue formation and ECM protein production in 6 mm wounds in SPARC-null mice compared to wild-type mice.</p> <p>A significant increase in the rate of wound closure in SPARC-null compared to wild-type mice at 4 and 7 days post-wounding in 5 mm excisional wounds.</p>	<p>(Basu et al. 2001)</p> <p>(Bradshaw et al. 2002)</p>
Tenascin-C	Healing of 6 mm excisional wounds was not significantly altered in tenascin-C deficient mice compared to wild-type mice.	(Forsberg et al. 1996)
Tenascin-X (TNX)	No differences between TNX-null and wild-type mice were noted in the rate of wound closure, or in expression of fibrillar collagen during excisional wound healing (8 mm).	(Egging et al. 2007)
Thrombospondin-1 (TSP1)	<p>Delayed wound closure (by 6 days) and impaired granulation tissue in transgenic mice overexpressing TSP1 in the skin compared to wild-type when 6 mm excisional wounds were created.</p> <p>TSP1-null and TSP1/TSP2-null mice demonstrated reduced vascularization and impaired inflammatory phase compared to wild-type mice while TSP2 null mice were similar to wild-type mice.</p>	<p>(Streit et al. 2000)</p> <p>(Agah et al. 2002)</p>
Thrombospondin-2 (TSP2)	<p>At 14 days post-wounding, the vascular density in wild-type, TSP1-null and TSP1/TSP2 double-null mice was the same, but TSP2-null wounds remained highly vascularized.</p> <p>At 14 days post-wounding 6 mm excisional wounds, TSP2-null mice showed greater neovascularization and MMP-2 compared to wild-type mice.</p> <p>The levels of MMP-2, MMP-9, TIMP-1, TIMP-2, and soluble VEGF were increased in 6 mm excisional wounds in TSP2-null mice compared to wild-type mice.</p>	<p>(Bornstein et al. 2004)</p> <p>(Agah et al. 2004)</p> <p>(MacLauchlan et al. 2009)</p>

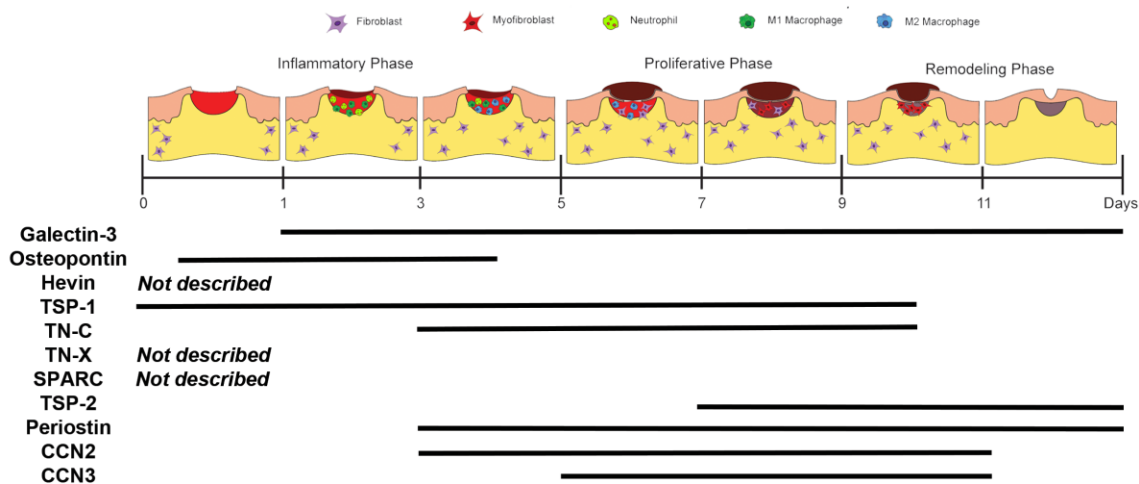


Figure 1.2 Temporal expression of matricellular proteins during dermal wound repair. From Walker et al. Cell–matrix interactions governing skin repair: matricellular proteins as diverse modulators of cell function. Res Reports Biochem 2015;5:1–16.

1.5.1 Galectin-3

Like all galectins, Galectin-3 contains a C-terminus carbohydrate recognition domain (CRD) that recognizes β -galactosides (Larsen et al. 2011); however, Galectin-3 is unique from the other proteins in the family in that it has an N-terminus glycine/proline rich tandem repeat region with similarity to collagen (Ahmad et al. 2004). The glycine/proline rich N-terminus was described to enable the protein to form a unique homo-pentamer (Ahmad et al. 2004), but can be cleaved from the carbohydrate recognition domain by MMP-9, which, interestingly, also increases the affinity of the carbohydrate recognition domain for glycans (Ochieng et al. 1998).

Galectin-3 was shown to localize in the nucleus, cytoplasm, and the ECM. It contains a nuclear localization signal (Nakahara et al. 2006), however it lacks a signal for extracellular transport and is suspected to traverse the plasma membrane through a novel

mechanism (Larsen et al. 2011). Notably, it was observed to be differentially expressed over the course of acute wound healing in rats (Gál et al. 2011). Within the wound, Galectin-3 was highly expressed during the inflammatory phase but decreased into the proliferative phase of healing. Similarly, in the epidermis, Galectin-3 was expressed at high levels normally and during the initial inflammation phase, but decreased subsequently (Gál et al. 2011).

Galectin-3 has been observed to play important roles in the innate immune system. Although Galectin-3 is not a chemoattractant for neutrophils, in models of lung and skin infection Galectin-3 was observed to contribute to neutrophil accumulation at the sites of infection (Nieminen et al. 2008; Bhaumik et al. 2013). One described mechanism for this is through Galectin-3-mediated cell adhesion between neutrophils and endothelial cells at the site of injury to promote extravasation at sites of inflammation (Sato et al. 2002). Furthermore, upon resolution of inflammatory processes, Galectin-3 has been described to participate in neutrophil clearance by mediating phagocytosis of apoptotic neutrophils by macrophages (Karlsson et al. 2009). Galectin-3 has also been linked to macrophage polarization into a pro-regenerative M2 phenotype (MacKinnon et al. 2008). Bone marrow derived macrophages from *Galectin-3* knockout and wild-type mice showed similar release of pro-inflammatory cytokines *in vitro*, but *Galectin-3* knockout animals displayed impaired differentiation into an M2 phenotype in response to interleukin-4 (IL4) and IL-13 stimulation (MacKinnon et al. 2008).

Galectin-3 has also been implicated in different roles in fibrosis, a process which, like cutaneous wounding, initiates with inflammation, but yields extensive matrix production, impairing organ function (Wynn and Ramalingam 2012). Genetic deletion of *Galectin-3*

has been explored in models of hepatic (Henderson et al. 2006; Jiang et al. 2012), renal (Henderson et al. 2008; Okamura et al. 2011), and pulmonary (MacKinnon et al. 2012) fibrosis. Importantly, in each of these studies, deletion of *Galectin-3* impaired myofibroblast differentiation. Whether a similar result would be observed during cutaneous wound healing has not been previously explored.

Galectin-3 is important for the re-epithelialization of both corneal (Cao et al. 2002) and skin wounds (Liu et al. 2012) in mice. During corneal wound healing, Galectin-3 was highly expressed at the leading edge of the migrating epithelium, and knockout mice were slower to re-epithelialize (Cao et al. 2002). This deficiency was shown to be independent of epithelial cell proliferation, leading the authors to suggest that there was a migratory defect. This migratory defect was replicated in *Galectin-3* knockout keratinocytes both *in vitro* and *in vivo* in a skin wound healing model (Liu et al. 2012). In this system, intracellular Galectin-3 was found to regulate trafficking of epidermal growth factor receptor (EGFR), enabling endocytosed receptor to be recycled back to the plasma membrane after stimulation and preventing its degradation within the lysosome. This process led to enhanced EGFR presentation at the cell surface and was linked to increased signal transduction through phosphorylated extracellular signal-regulated kinase 1 (pERK) compared to *Galectin-3* knockout keratinocytes (Liu et al. 2012).

Finally, Galectin-3 has been described as an inducer of angiogenesis (Nangia-Makker et al. 2000, 2010, Markowska et al. 2010, 2011). Galectin-3 was determined to mediate both bFGF- and VEGF-induced angiogenesis *in vitro* and *in vivo* (Markowska et al. 2010). Chromatography using HUVEC lysates run through Galectin-3 coated columns, followed by matrix-assisted laser desorption ionization time of flight mass spectrometry identified

both αv and $\beta 3$ integrin subunits as major binding partners of Galectin-3. Interestingly, both of these integrin subunits are known mediators of VEGF- and bFGF-induced angiogenesis (Brooks et al. 1994; Liu 2003). Galectin-3 was further found to induce clustering of $\alpha v\beta 3$ integrins in HUVECs through a mechanism that could be inhibited either by adding lactose (a ligand of the CRD of Galectin-3), but not sucrose, or by cleaving the glycine/proline rich N-terminus domain of Galectin-3 (Markowska et al. 2010).

These data suggest that Galectin-3 binds to integrin subunits αV and $\beta 3$ through its CRD, and tethers multiple integrins together through formation of homo-pentamers via its N-terminal domain. Moreover, it was determined that knockdown of α -1,6-mannosylglycoprotein 6-beta-N-acetylglucosaminyltransferase A (Mgat5), a protein involved in the synthesis of N-acetyllactosamine glycans (recognition sites of the CRD of Galectin-3), blocked Galectin-3 induced clustering of these integrins, suggesting that the appropriate glycan signal on $\alpha v\beta 3$ integrins must be present for this interaction. Importantly, the downstream effect of $\alpha v\beta 3$ integrin clustering was focal adhesion kinase (FAK) activation, which is an important downstream mediator of integrin-induced angiogenic signaling (Zhao and Guan 2011). Further supporting its role in angiogenesis, Galectin-3 was found to bind VEGFR-2 through a similar mechanism, reducing receptor internalization after stimulation by VEGF-A and effectively increasing surface expression of this important mediator of angiogenic signaling (Markowska et al. 2011).

From the studies highlighted above, it is evident that Galectin-3 may function in a wound healing response beyond what has been described in re-epithelialization (Liu et al. 2012), which was investigated in this thesis.

1.5.2 Periostin

Periostin is a matricellular protein comprised of several modular domains including an EMI domain with homology to the EMILIN protein family, four Fas-1 domains with homology to *drosophila* fascilin-1, and a C-terminal domain with binding sites for heparan sulfate proteoglycans (Kii and Ito 2017). Both the EMI and Fas-1 domains have been identified to interact with a range of different extracellular proteins including collagens, fibronectin, other matricellular proteins, integrins, and secreted enzymes including lysyl oxidase (LOX) (Kudo 2011; Kii and Ito 2017). The C-terminal domain can be alternatively spliced, potentially modifying how Periostin interacts with heparan sulfate proteoglycans in the ECM and on cell surfaces, although this requires further investigation (Hoersch and Andrade-Navarro 2010; Kii and Ito 2017).

During skin development in mice, Periostin was most highly expressed in subcutaneous tissue and the dermal-epidermal junction at E13.5, with lesser expression noted throughout the developing dermis (Zhou et al. 2010). This pattern of expression remained relatively consistent within neonatal mice, but expression began to appear surrounding hair follicles as these structures began to develop. In healthy adult skin, Periostin expression was noted primarily surrounding hair follicles. Conversely, upon wounding, Periostin expression within the neighboring skin more closely mimicked the patterns during development, where it was expressed throughout the dermis and within the dermal-epidermal junction (Zhou et al. 2010). Within the granulation tissue, Periostin protein was first detected at 3 days post wounding, peaking at 7 days post wounding (Jackson-Boeters et al. 2009), corresponding with the peak Periostin transcript level (Elliott et al. 2012). In contrast to acute wounding in mice, investigation into Periostin

transcript levels in human chronic wound tissue suggested that it was significantly downregulated within the wound tissue compared to unwounded tissue from the same patient (Elliott et al. 2015).

Genetic deletion of Periostin in mouse models resulted in impaired wound closure manifested during the proliferative phase of healing (Nishiyama et al. 2011; Elliott et al. 2012). As one possible mechanism for this impairment, Nishiyama *et al.* (2011) highlighted impaired keratinocyte proliferation resulting in delayed re-epithelialization. Further, Elliott *et al.* (2012) identified a role of Periostin in wound contraction, compounding the effects of delayed re-epithelialization on wound closure. Whereas wild-type mice displayed a strong induction of α SMA at the mRNA and protein levels by 7 days post wounding, this response was impaired in Periostin knockout mice (Elliott et al. 2012). Using culture models, it was determined that dermal fibroblasts isolated from knockout animals displayed impaired myofibroblast differentiation on soft surfaces (Elliott et al. 2012). In this model, exogenous Periostin was sufficient to recover a wild-type phenotype. Importantly, this recovery could be blocked by inhibition of FAK activation or through the delivery of antibodies to block β 1 integrin, suggesting that Periostin signals through β 1 integrins to promote FAK activation in order to promote myofibroblast differentiation (Elliott et al. 2012). Further, it was determined that the addition of exogenous Periostin to knockout animals following wounding was sufficient to recover a normal healing response (Ontsuka et al. 2012; Elliott et al. 2012).

Based on the findings from Periostin knockout mice and the evidence of low Periostin transcript levels in human chronic wound tissue, exogenous Periostin was explored previously by the Hamilton lab as a potential therapeutic for impaired healing (Elliott et

al. 2018). To investigate its therapeutic potential, exogenous Periostin was delivered into wounds in a type II diabetic mouse model (db/db) which displays impaired wound healing (Elliott et al. 2018). Critically, the rate of wound healing in this model was significantly enhanced following delivery of Periostin compared to control wounds and was similar to the rate of healing observed in wild-type mice. These findings supported the therapeutic potential of exogenous Periostin for impaired wound healing.

1.5.3 CCN2

CCN2, originally named connective tissue growth factor (CTGF), is one of six members of the CCN protein family, also including CCN1 (Cyr61), CCN3 (Nov), CCN4 (Wisp1), CCN5 (Wisp2), and CCN6 (Wisp3) (Brigstock et al. 2003; Perbal 2013). These proteins are characterized by a common set of four modular domains, including an insulin-like growth factor binding protein domain, a von Willibrand factor type-C repeat, a thrombospondin type-1 repeat, and a C-terminal cystine knot motif, with the exception of CCN5, which lacks the cystine knot motif (Holbourn et al. 2008). These modular domains allow these proteins to interact with a range of different ECM and cell membrane proteins including collagens, fibronectin, integrins, and TGF β family members. The versatility of CCN proteins is enhanced by protein cleavage, which can further modify their interactions (Holbourn et al. 2008). The overarching model for CCN proteins is one in which they alter signaling by controlling spatial relationships between ligands and their receptors, and create domains integrating multiple receptors to coordinate cellular responses (Perbal 2013).

During development, CCN2 was most highly expressed within the vasculature and in developing bone and cartilaginous tissues of mice (Friedrichsen et al. 2003). Following genetic ablation of CCN2, mouse embryos displayed severe skeletal defects leading to perinatal lethality (Ivkovic 2003). However, knockout animals did not display altered skin development, as assessed through blood vessel density, skin thickness, and matrix deposition (Liu and Leask 2011).

In rodent skin, CCN2 was expressed at low levels under homeostatic conditions, however, upon wounding or induction of fibrosis, CCN2 expression was greatly upregulated (Igarashi et al. 1993; Kapoor et al. 2008; Liu et al. 2010). CCN2 has been described to have an integral role in the development of bleomycin-induced skin fibrosis in mice (Liu et al. 2011). Using tamoxifen inducible Cre under the control of a *Colla2* promoter sequence, Liu *et al.* targeted genetic deletion of CCN2 in collagen producing fibroblasts. Following deletion, myofibroblast activation via treatment with bleomycin was ameliorated and the level of fibrosis was reduced as measured by dermal thickness and matrix deposition (Liu et al. 2011). Using the same system, it was further determined that CCN2 was dispensable during cutaneous wound healing, with CCN2 knockout animals displaying no deficits in the rate of closure or the composition of the granulation tissue (Liu et al. 2014). However, CCN2 is also expressed by keratinocytes during wound re-epithelialization (Kiwanuka et al. 2013); whether this could compensate for fibroblast-specific deletion is not known.

Previous investigations concluded that CCN2 transcript levels were not different in human chronic wound tissue compared to unaffected tissues from the same patient (Elliott et al. 2015), contrasting its upregulation in animal models of acute wound healing

(Igarashi et al. 1993; Kapoor et al. 2008). Conversely, its expression is strongly upregulated in fibrotic conditions in humans, and the level of expression correlates with the severity of fibrosis across organs (Leask et al. 2009), including skin where both blood plasma and interstitial levels of the N-terminal domain of CCN2 positively correlated with disease severity (Dziadzio et al. 2005). As such, previous work in the Hamilton lab investigated whether exogenous CCN2 could be used therapeutically to induce fibrotic processes, including angiogenesis and matrix deposition, in a db/db mouse model of impaired wound healing (Elliott et al. 2018). Similar to the results described for Periostin, treatment with exogenous CCN2 was sufficient to increase the rate of healing in db/db mice to a level that was similar to that observed in wild-type mice (Elliott et al. 2018). Moreover, micro-computed tomography imaging of the vasculature within treated wounds supported a pro-angiogenic response following CCN2 treatment (Elliott et al. 2018). Although genetic deletion of CCN2 within collagen I expressing cells was determined to be inconsequential for cutaneous wound healing (Liu et al. 2014), the positive effects of exogenous CCN2 on models of impaired healing warrant further investigation to probe its potential as a wound healing therapeutic.

1.6 Strategies for healing chronic wounds

The current standard of care for chronic wound patients targets the underlying pathophysiology and can differ depending on wound etiology. For example, in diabetic patients, controlling hyperglycemia and developing a nutritious diet are priorities (Frykberg and Banks 2015; Han and Ceilley 2017). Alternatively, in patients with vascular ulcers, strategies to improve blood flow are beneficial, including vascular surgeries and compression therapy (Frykberg and Banks 2015; Han and Ceilley 2017).

Hyperbaric oxygen therapy can also be included to increase oxygen tension within the wound if these primary strategies fail. Across wound etiologies, maintaining a moist wound environment that is free of infection is critical (Frykberg and Banks 2015; Han and Ceilley 2017). Upon detection of infection, wounds are treated aggressively with antimicrobial agents, including antibiotics and silver-based therapies. Debridement is also of particular importance across etiologies, as it allows healthier tissue to contribute to wound repair while removing the dead tissue, which can further aid in reducing the bacterial load (Frykberg and Banks 2015; Han and Ceilley 2017). Finally, negative pressure therapy has been widely supported as an effective strategy to enhance healing by stimulating granulation tissue formation and increasing wound contraction (Frykberg and Banks 2015; Han and Ceilley 2017). Although these different strategies constitute the standard of care, they are not adequate to facilitate closure in a large number of patients. For example, clinical studies that have investigated standard care as a control treatment in diabetic foot ulcers have reported approximately 30% complete closure within follow up periods of 6-16 weeks, and approximately 10% frequency of lower extremity amputation (Santema et al. 2016).

To complement standard care, many novel therapeutics have been approved by United States Food and Drug Administration (FDA) for the treatment of chronic wounds. However, these are generally chosen based on clinician preference and personal experience, and are not backed by quality clinical data (Snyder et al. 2012; Frykberg and Banks 2015). Some of these complementary strategies, as well as more exploratory approaches will be discussed in more detail below.

1.6.1 Growth factor therapies

Despite promise in animal models, with the exception of PDGF-BB, growth factor therapies have not been successfully translated to the clinic, potentially due in part to the proteolytic nature of chronic wounds (Barrientos et al. 2008; Han and Ceilley 2017). PDGF-BB has received approval from the FDA for use in chronic wounds, but has displayed only limited efficacy and is not widely used (Apelqvist et al. 2008; Papanas and Maltezos 2010). There has been speculation into the limited efficacy of growth factor therapies. Singer and Clark (1999) proposed that the use of single growth factors in such a complex, dysregulated microenvironment may not be adequate and suggested the use of combination therapies at specific intervals to promote wound healing (Singer and Clark 1999). However, to date there are no growth factor combination therapies approved for use.

1.6.2 MMP inhibitors

To reduce matrix degradation, MMP inhibitors have been explored for wound healing, but MMPs also possess a number of necessary functions that promote healing. For example, both MMP-9 knockout mice (Kyriakides et al. 2009) and rats treated with the broad spectrum MMP inhibitor BB-94 (Mirastschijski et al. 2010) showed significantly delayed wound healing. However, in a chronic wound setting, inhibition of MMPs remains a potential clinical target to improve healing (Caley et al. 2015). A strategy utilizing the collagenous ECM from sheep forestomach has, in limited clinical assessment, shown to be effective for treatment of chronic wounds (Bohn et al. 2016). This strategy relies on providing a large amount of substrate to inhibit endogenous proteases, while simultaneously sequestering growth factors and cytokines to prevent

their degradation (Negron et al. 2014; Bohn et al. 2016). In fact, this mechanism of overwhelming endogenous MMPs is likely a major factor in the reported efficacy of many collagen based wound dressings (Fleck and Simman 2010).

1.6.3 Biomaterials for wound repair

A wide range of biomaterials have been developed for wound healing applications, including both wound dressings and skin substitutes (Mir et al. 2018). Skin substitutes, which are the focus here, will be defined as materials designed for cellular infiltration, acting themselves as a biodegradable scaffold. This broad definition encompasses a wide range of materials including those designed from biological sources and synthetic polymer-based materials (Shahrokhi et al. 2014; Mir et al. 2018). Furthermore, these can be either acellular or combined with fibroblasts and/or keratinocytes. Based on this broad classification, numerous skin substitutes have been developed. In 2012, Snyder *et al.* compiled a comprehensive assessment identifying 57 skin substitutes for use in treatment of chronic wounds that have been approved by the FDA and are commercially available (Snyder et al. 2012). However, a recent Cochrane review investigating the use of skin grafts and skin substitutes for treatment of diabetic foot ulcers showed a moderate improvement with current therapeutics when combined with standard care (Santema et al. 2016). In this review, the combined data collected from clinical trials exploring the use of standard care plus skin grafts or skin substitutes including Dermagraft®, Apligraf®, OASIS®, and TheraSkin®, resulted in a frequency of complete closure of 42%, compared to 27% with standard care alone within a follow-up period of 6-16 weeks. The differences between therapeutics were inconclusive. Thus, while the current generation of

skin substitutes are improving the quality of life of a large number of people affected by chronic wounds, there is clearly a need for improved clinical outcomes.

1.6.3.1 Collagen-based biomaterials for wound healing

Collagens are the most abundant proteins in natural ECM, providing a structural network to support cells and a biologically active substrate that can interact directly with cell surface receptors and sequester secreted proteins to modulate bioavailability (Chattopadhyay and Raines 2014). Furthermore, collagens are naturally biodegradable and contain cryptic sequences that are released upon degradation, which can stimulate angiogenic or regenerative inflammatory pathways (Postlethwaite et al. 1978; Perumal et al. 2008; Ames et al. 2016). Depending on the processing conditions applied to extract the collagens, much of the antigenicity responsible for immune rejection can be lost, allowing xenogeneic-derived ECM to successfully integrate into host tissues (Ruszczak 2003; Badylak 2004). These properties have made collagens attractive structural components for medical applications (Chattopadhyay and Raines 2014). Type I collagen is the most abundant of the collagen proteins and has been widely used in the production of biomaterials (Chattopadhyay and Raines 2014). Several commercially available collagen-based materials have been developed for wound healing applications, such as SkinTemp®, Collatamp®, and Integra™ Matrix Wound Dressing (Ruszczak 2003).

Collagen-based biomaterials can be synthesized from purified collagen using different techniques depending on the target applications (Chattopadhyay and Raines 2014). Specific scaffold formats investigated to date include foams (sponge), membranes, and injectables, all of which can be further modified physically and/or biologically

(Chattopadhyay and Raines 2014). Examples of physical modifications include chemical cross-linking or inclusion of synthetic polymers, whereas biological modifications can include drug or cell delivery. Based on these possible modifications, a wide range of collagen-based materials have been synthesized and explored in wound healing environments. Foam synthesis, a focus in this thesis, will be discussed in more detail below.

Collagen foams can be synthesized by lyophilizing frozen solubilized collagen, with physical properties altered by manipulating the concentration of collagen and the rate of freezing (Doillon 1987; Chattopadhyay and Raines 2014). Early investigations into these materials highlighted their porous structure enabling cellular infiltration during a wound healing response (Doillon 1987). Investigating a foam made from type I collagen, chitosan, and chondroitin sulphate, Berthod *et al.* observed increased collagen synthesis by fibroblasts relative to tissue culture plastic or a collagen gel (Berthod *et al.* 1993). The authors attributed this to the porous nature of the foams, which allowed secreted collagen to be dispersed further from the cells. This is in contrast to the reduced collagen synthesis observed in fibroblasts cultured within collagen gels relative to tissue culture plastic, which the authors hypothesized relates to negative feedback by cells trapped in a collagen-rich environment with low porosity (Mauch *et al.* 1988; Berthod *et al.* 1993), but may also involve differences in matrix stiffness (Kanta 2015).

The structural properties of collagen foams also make them suitable carriers for exogenous cells and proteins. Using chemically cross-linked collagen foams, Marks *et al.* delivered allogeneic guinea pig fibroblasts or exogenous bFGF to wounds in a guinea pig model, both of which significantly increased the final tensile strength of the wounds over

treatment with collagen foams alone (Marks et al. 1991). The ability to easily modify physical properties, shape, and biological functionality of collagen-based foams makes them a highly versatile platform for the development of novel wound healing strategies.

1.6.3.2 Decellularized tissues for wound healing

Several biomaterials have been developed from decellularized tissues and are commercially available for wound healing applications including decellularized cadaveric skin (Alloderm™; GraftJacket®), decellularized porcine small intestinal submucosa (SIS; OASIS®), decellularized porcine urinary bladder matrix (UBM; Matristem®), and decellularized fetal bovine skin (PriMatrix™), highlighting the utility of decellularized tissues (Turner and Badylak 2015).

Decellularized tissues include a complex array of ECM proteins, including structural proteins, matricellular proteins, growth factors, and cytokines, more closely mimicking a native ECM than matrices derived from purified components (Badylak 2002). As an example of the complexity within decellularized tissues, a recent proteomics study from the Flynn lab investigated the protein composition of decellularized human adipose tissue and bone, identifying a total of 906 and 1478 unique proteins within the processed tissues, respectively (Kuljanin et al. 2017). These proteins included structural proteins, glycoproteins, proteoglycans, matricellular proteins, and signaling proteins (Kuljanin et al. 2017), all of which are important mediators of wound healing (Turner and Badylak 2015).

ECM can be sourced from human adipose tissue that is commonly discarded in medical procedures including abdominoplasties and panniculectomies (Flynn 2010). Decellularized adipose tissue (DAT) is an acellular, collagen-rich, multicomponent material containing intact collagen fibrils, and, similar to purified collagen, can be processed into foam biomaterials (Flynn 2010; Yu et al. 2013; Kuljanin et al. 2017). Subcutaneous implantation of DAT foams into an immune competent rat model yielded an early angiogenic response, and eventual tissue remodeling, characterized by an initial inflammatory response that subsided with time (Yu et al. 2013). Recent investigation using a bead foam synthesis method, designed for increased cellular infiltration, further supported the angiogenic potential of DAT (Morissette Martin et al. 2018). Purified collagen- and DAT-based bead foams were seeded with chronic wound edge dermal fibroblasts. Interestingly, cells cultured on DAT bead foams secreted higher levels of angiogenic factors, including VEGF, hepatocyte growth factor, stromal cell-derived factor 1, angiopoietin-1, and PDGF-BB. Furthermore, following subcutaneous implantation into athymic mice, wound edge dermal fibroblast seeded DAT bead foams demonstrated greater CD31⁺ cell infiltration compared to seeded collagen bead foams (Morissette Martin et al. 2018). Using a relevant cell type, these findings support the potential of DAT in a chronic wound environment, warranting further investigation into wound healing models.

1.6.4 Cell therapies for wound healing

Current commercially-available cell therapies for wound healing come in the form of living skin equivalents including a neonatal foreskin fibroblast seeded matrix

(Dermagraft®; Organogenesis) and a neonatal foreskin keratinocyte/fibroblast seeded matrix (Apligraf®; Organogenesis) (Snyder et al. 2012). These materials are considered advanced care options and are only recommended for use if alternative therapies have failed within a one-month (Apligraf®) or six-week (Dermagraft®) follow-up period, and only in cases where the wounds are not infected (Snyder et al. 2012). A recent Cochrane review supported their clinical use, identifying a 50% increase in the rate of complete closure for both of these products compared to standard care alone (Santema et al. 2016). However, it is important to note that roughly half of patients treated with Apligraf® and Dermagraft® still fail to exhibit appropriate healing (Santema et al. 2016). Whether alternative cell sources might result in better outcomes is not known.

Mesenchymal stem/stromal cells (MSCs) are multipotent progenitor populations that upon isolation are characterized by a set of minimal criteria outlined by the International Society for Cellular Therapy (ISCT). These include adherence to tissue culture plastic, positive surface marker expression of CD73, CD90, and CD105, negative surface marker expression of CD45, CD34, CD14, CD11b, CD79 α , CD19, and HLA-DR, and the capacity to differentiate into adipogenic, chondrogenic, and osteogenic lineages in culture (Dominici et al. 2006). Perivascular populations characterized by *in vivo* expression of CD146 were shown to exhibit MSC characteristics upon isolation and culturing, and could be isolated in abundance from the stromal vascular fraction of adipose tissue (Crisan et al. 2008). Importantly, for allogeneic applications, these adipose-derived MSCs (ASCs) can be isolated from normally discarded medical waste (Hassan et al. 2014).

The use of MSCs shows potential for wound healing applications by supporting endogenous fibroblast and keratinocyte activation, angiogenesis, and

modulation/resolution of the inflammatory phase (Lee et al. 2016). In a db/db mouse model of impaired healing, murine ASC treatment increased granulation thickness, angiogenesis and the rate of re-epithelialization (Nambu et al. 2009, 2011). Similar results were observed in streptozotocin-induced diabetic rats, which displayed an increased rate of healing associated with reduced CD45-positive cell infiltration, and increased cell proliferation and fibroblast activation at the wound edge (Kuo et al. 2016). Many of the beneficial effects of ASCs are thought to be attributed to their secretome, which includes angiogenic and pro-fibrotic factors, immune-modulating cytokines, as well as matrix modifying proteins including collagens, TIMPs, and MMPs (Park et al. 2008; Lee et al. 2010; Salgado et al. 2010; Dubey et al. 2018).

Limited clinical investigation of MSC delivery to patients with chronic wounds lasting greater than one year and not responding to conventional and advanced therapeutics, supported the use of MSCs in chronic wound patients (Falanga et al. 2007). These findings also suggested that the beneficial results are dose dependent, with greater cell delivery correlating with improved healing (Falanga et al. 2007). Thus, delivery strategies that can distribute high numbers of MSCs across the area of the granulation tissue could be supportive of better clinical outcomes.

1.7 Thesis Overview

With a focus on exploring intrinsic differences in the fibroblast populations during skin development and wound healing, the effect of embryonic lineage on fibroblast function was first explored in a murine model. A Cre/Lox lineage tracing method was used to

track *Foxd1* lineage-positive cells and explore whether resident myofibroblast progenitors within the skin shared *Foxd1* as a common developmental gene signature to those previously-described in lung (Hung et al. 2013) and kidneys (Humphreys et al. 2010). Further, the expression profile of this lineage was characterized in the skin during homeostasis and wound repair and compared to the non-*Foxd1*-lineage fibroblasts. Within this aim, it was hypothesized that the *Foxd1* lineage would contribute to skin development, and that these lineage-positive cells would be a major source of myofibroblasts during wound repair.

In the second chapter, the role of the matricellular protein Galectin-3 was investigated as a potential extrinsic factor mediating cutaneous repair in an acute wound model in knockout mice. Previous investigation has supported a role of Galectin-3 in wound re-epithelialization (Liu et al. 2012), however further investigation into how this protein functions within the granulation tissue was warranted. Furthermore, investigation into Galectin-3 regulation in human chronic wounds and chronic wound fibroblasts had not been previously performed and could provide insight into dysregulated mechanisms that may be targeted in future therapeutic development. Within this aim, it was hypothesized that genetic deletion of Galectin-3 would result in an unresolved inflammatory state, impaired angiogenesis, and reduced myofibroblast accumulation resulting in delayed wound closure relative to wild-type mice.

In the final experimental chapter, pilot studies were performed as a first step towards the development of novel therapeutic approaches with the potential to modulate both cell infiltration and the wound microenvironment to promote healing. More specifically, a porcine acute wound model was explored due to the reported anatomical similarities

between porcine and human skin (Sullivan et al. 2001). Within this model, a variety of ECM-derived foam biomaterials were tested, as they offer a versatile platform to combine proteins of interest, as well as for cell therapy. Type I collagen foams incorporating Periostin and CCN2 were tested, as these matricellular proteins were previously shown to improve wound closure when added exogenously in a *db/db* model of impaired wound healing (Elliott et al. 2018). Further, foams derived from the more complex ECM of human DAT were also assessed. Preliminary testing was also performed to assess the potential of the foams as a platform for therapeutic delivery of porcine ASCs. It was hypothesized that all of the foam biomaterials would improve the rate of wound closure and promote wound angiogenesis and myofibroblast differentiation relative to untreated controls. These studies represented important first steps in applying a more relevant pre-clinical large animal model, which is critically needed for the design of more effective biomaterials-based therapies for treating chronic wounds in humans.

1.8 References

- Agah A, Kyriakides TR, Lawler J, Bornstein P (2002) The lack of thrombospondin-1 (TSP1) dictates the course of wound healing in double-TSP1/TSP2-null mice. *Am J Pathol* 161:831–839. doi: 10.1016/S0002-9440(10)64243-5
- Agah A, Kyriakides TR, Letrondo N, et al (2004) Thrombospondin 2 levels are increased in aged mice: consequences for cutaneous wound healing and angiogenesis. *Matrix Biol* 22:539–547. doi: 10.1016/j.matbio.2003.10.006
- Ahmad N, Gabius HJ, André S, et al (2004) Galectin-3 Precipitates as a Pentamer with Synthetic Multivalent Carbohydrates and Forms Heterogeneous Cross-linked Complexes. *J Biol Chem* 279:10841–10847. doi: 10.1074/jbc.M312834200

- Ahmed N, Thornalley PJ (2007) Advanced glycation endproducts: What is their relevance to diabetic complications? *Diabetes, Obes Metab* 9:233–245. doi: 10.1111/j.1463-1326.2006.00595.x
- Ames JJ, Contois L, Caron JM, et al (2016) Identification of an endogenously generated cryptic collagen epitope (XL313) that may selectively regulate angiogenesis by an integrin yes-associated protein (YAP) mechano-transduction pathway. *J Biol Chem* 291:2731–2750. doi: 10.1074/jbc.M115.669614
- Apelqvist J, Bakker K, van Houtum WH, Schaper NC (2008) Practical guidelines on the management and prevention of the diabetic foot. *Diabetes Metab Res Rev* 24:S181–S187. doi: 10.1002/dmrr.848
- Badylak SF (2004) Xenogeneic extracellular matrix as a scaffold for tissue reconstruction. *Transpl Immunol* 12:367–377. doi: 10.1016/j.trim.2003.12.016
- Badylak SF (2002) The extracellular matrix as a scaffold for tissue reconstruction. *Semin Cell Dev Biol* 13:377–383
- Barisic-Dujmovic T, Boban I, Clark SH (2010) Fibroblasts/myofibroblasts that participate in cutaneous wound healing are not derived from circulating progenitor cells. *J Cell Physiol* 222:703–712. doi: 10.1002/jcp.21997
- Barrientos S, Stojadinovic O, Golinko MS, et al (2008) Growth factors and cytokines in wound healing. *Wound Repair Regen* 16:585–601. doi: 10.1111/j.1524-475X.2008.00410.x
- Basu A, Kligman LH, Samulewicz SJ, Howe CC (2001) Impaired wound healing in mice deficient in a matricellular protein SPARC (osteonectin, BM-40). *BMC Cell Biol* 2:15. doi: 10.1186/1471-2121-2-15
- Ben-Yair R (2003) Coherent development of dermomyotome and dermis from the entire mediolateral extent of the dorsal somite. *Development* 130:4325–4336. doi: 10.1242/dev.00667
- Berlanga J, Cibrian D, Guillen I, et al (2005) Methylglyoxal administration induces diabetes-like microvascular changes and perturbs the healing process of cutaneous

- wounds. *Clin Sci* 109:83–95. doi: 10.1042/CS20050026
- Berthod F, Hayek D, Damour O (1993) Collagen synthesis by fibroblasts cultured within a collagen sponge. *Biomaterials* 14:
- Bhattacharjee V, Mukhopadhyay P, Singh S, et al (2007) Neural crest and mesoderm lineage-dependent gene expression in orofacial development. *Differentiation* 75:463–477. doi: 10.1111/j.1432-0436.2006.00145.x
- Bhaumik P, St-Pierre G, Milot V, et al (2013) Galectin-3 Facilitates Neutrophil Recruitment as an Innate Immune Response to a Parasitic Protozoa Cutaneous Infection. *J Immunol* 190:630–640. doi: 10.4049/jimmunol.1103197
- Bluff JE, O’Ceallaigh S, O’Kane S, et al (2006) The microcirculation in acute murine cutaneous incisional wounds shows a spatial and temporal variation in the functionality of vessels. *Wound Repair Regen* 14:434–442. doi: 10.1111/j.1743-6109.2006.00142.x
- Bodnar RJ (2015) Chemokine Regulation of Angiogenesis During Wound Healing. *Adv Wound Care* 4:641–650. doi: 10.1089/wound.2014.0594
- Bodnar RJ, Satish L, Yates CC, Wells A (2016) Pericytes: A newly recognized player in wound healing. *Wound Repair Regen* 24:204–214. doi: 10.1111/wrr.12415
- Bohn G, Liden B, Schultz G, et al (2016) Ovine-Based Collagen Matrix Dressing: Next-Generation Collagen Dressing for Wound Care. *Adv Wound Care* 5:1–10. doi: 10.1089/wound.2015.0660
- Bolitho C, Xaymardan M, Lynch GW, Zoellner H (2010) Vascularity during wound maturation correlates with fragmentation of serum albumin but not ceruloplasmin, transferrin, or haptoglobin. *Wound Repair Regen* 18:211–222. doi: 10.1111/j.1524-475X.2010.00572.x
- Bornstein P (1995) Diversity of function is inherent in matricellular proteins: An appraisal of thrombospondin 1. *J Cell Biol* 130:503–506. doi: 10.1083/jcb.130.3.503
- Bornstein P, Agah A, Kyriakides TR (2004) The role of thrombospondins 1 and 2 in the

- regulation of cell-matrix interactions, collagen fibril formation, and the response to injury. *Int J Biochem Cell Biol* 36:1115–1125. doi: 10.1016/j.biocel.2004.01.012
- Bradshaw AD, Reed MJ, Sage EH (2002) SPARC-null mice exhibit accelerated cutaneous wound closure. *J Histochem Cytochem* 50:1–10. doi: 10.1177/002215540205000101
- Brigstock DR, Goldschmeding R, Katsube KI, et al (2003) Proposal for a unified CCN nomenclature. *J Clin Pathol - Mol Pathol* 56:127–128. doi: 10.1136/mp.56.2.127
- Brooks P, Clark R, Cheresch D (1994) Requirement of vascular integrin alpha v beta 3 for angiogenesis. *Science* (80-) 264:569–571. doi: 10.1126/science.7512751
- Caley MP, Martins VLC, O'Toole EA (2015) Metalloproteinases and Wound Healing. *Adv Wound Care* 4:225–234. doi: 10.1089/wound.2014.0581
- Cao Z, Said N, Amin S, et al (2002) Galectins-3 and -7, but not galectin-1, play a role in re-epithelialization of wounds. *J Biol Chem* 277:42299–42305. doi: 10.1074/jbc.M200981200
- Chattopadhyay S, Raines RT (2014) Review collagen-based biomaterials for wound healing. *Biopolymers* 101:821–833. doi: DOI 10.1002/bip.22486 ABSTRA
- Crisan M, Yap S, Casteilla L, et al (2008) A Perivascular Origin for Mesenchymal Stem Cells in Multiple Human Organs. *Cell Stem Cell* 3:301–313. doi: 10.1016/j.stem.2008.07.003
- Demidova-Rice TN, Hamblin MR, Herman IM (2012) nd Chronic Wounds: Biology, Causes, and Approaches to Care. 25:304–314. doi: 10.1097/01.ASW.0000416006.55218.d0.Acute
- Desmoulière A, Redard M, Darby I, Gabbiani G (1995) Apoptosis mediates the decrease in cellularity during the transition between granulation tissue and scar. *Am J Pathol* 146:56–66
- Dias Moura Prazeres PH, Sena IFG, Borges I da T, et al (2017) Pericytes are heterogeneous in their origin within the same tissue. *Dev Biol* 427:6–11. doi:

10.1016/j.ydbio.2017.05.001

Doillon CJ (1987) Porous Collagen Sponge Wound Dressings: In vivo and in vitro Studies. *J Biomater Appl* 2:562–578. doi: 10.1177/088532828700200404

Dominici M, Le Blanc K, Mueller I, et al (2006) Minimal criteria for defining multipotent mesenchymal stromal cells. The International Society for Cellular Therapy position statement. *Cytotherapy* 8:315–317. doi: 10.1080/14653240600855905

Dovi J V, He L, Dipietro L a (2003) Accelerated wound closure in neutrophil-depleted mice. *J Leukoc Biol* 73:448–455. doi: 10.1189/jlb.0802406.http

Driskell RR, Lichtenberger BM, Hoste E, et al (2013) Distinct fibroblast lineages determine dermal architecture in skin development and repair. *Nature* 504:277–281. doi: 10.1038/nature12783

Driskell RR, Watt FM (2015) Understanding fibroblast heterogeneity in the skin. *Trends Cell Biol* 25:92–99. doi: 10.1016/j.tcb.2014.10.001

Dubey NK, Mishra VK, Dubey R, et al (2018) Revisiting the advances in isolation, characterization and secretome of adipose-derived stromal/stem cells. *Int J Mol Sci* 19:1–23. doi: 10.3390/ijms19082200

Dulauroy S, Di Carlo SE, Langa F, et al (2012) Lineage tracing and genetic ablation of ADAM12 + perivascular cells identify a major source of profibrotic cells during acute tissue injury. *Nat Med* 18:1262–1270. doi: 10.1038/nm.2848

Dziadzio M, Usinger W, Leask A, et al (2005) N-terminal connective tissue growth factor is a marker of the fibrotic phenotype in scleroderma. *QJM - Mon J Assoc Physicians* 98:485–492. doi: 10.1093/qjmed/hci078

Egging D, van Vlijmen-Willems I, van Tongeren T, et al (2007) Wound healing in tenascin-X deficient mice suggests that tenascin-X is involved in matrix maturation rather than matrix deposition. *Connect Tissue Res* 48:93–98. doi: 10.1080/03008200601166160

- El Agha E, Moiseenko A, Kheirollahi V, et al (2017) Two-Way Conversion between Lipogenic and Myogenic Fibroblastic Phenotypes Marks the Progression and Resolution of Lung Fibrosis (Cell Stem Cell (2017) 20(2) (261–273) (S1934590916303447) (10.1016/j.stem.2016.10.004)). Cell Stem Cell 20:571. doi: 10.1016/j.stem.2017.03.011
- Elliott CG, Forbes TL, Leask A, Hamilton DW (2015) Inflammatory microenvironment and tumor necrosis factor alpha as modulators of periostin and CCN2 expression in human non-healing skin wounds and dermal fibroblasts. Matrix Biol 43:71–84. doi: 10.1016/j.matbio.2015.03.003
- Elliott CG, Wang J, Guo X, et al (2012) Periostin modulates myofibroblast differentiation during full-thickness cutaneous wound repair. J Cell Sci 125:121–132. doi: 10.1242/jcs.087841
- Elliott CG, Wang J, Walker JT, et al (2018) Periostin and CCN2 Scaffolds Promote the Wound Healing Response in the Skin of Diabetic Mice. Tissue Eng Part A 2018–0268.:Under review
- Eming SA, Martin P, Tomic-canic M, et al (2014) Wound repair and regeneration: mechanism, signaling and translation. Sci Transl Med 6:doi:10.1126/scitranslmed.3009337. doi: 10.1126/scitranslmed.3009337.Wound
- Falanga V, Iwamoto S, Chartier M, et al (2007) Autologous Bone Marrow–Derived Cultured Mesenchymal Stem Cells Delivered in a Fibrin Spray Accelerate Healing in Murine and Human Cutaneous Wounds. Tissue Eng 13:1299–1312. doi: 10.1089/ten.2006.0278
- Fetting JL, Guay JA, Karolak MJ, et al (2014) FOXD1 promotes nephron progenitor differentiation by repressing decorin in the embryonic kidney. Development 141:17–27. doi: 10.1242/dev.089078
- Fleck CA, Simman R (2010) Modern collagen wound dressings: Function and purpose. J Am Col Certif Wound Spec 2:50–54. doi: 10.1016/j.jcws.2010.12.003
- Flynn LE (2010) The use of decellularized adipose tissue to provide an inductive

- microenvironment for the adipogenic differentiation of human adipose-derived stem cells. *Biomaterials* 31:4715–4724. doi: 10.1016/j.biomaterials.2010.02.046
- Fomenou MD, Scaal M, Stockdale FE, et al (2005) Cells of all somitic compartments are determined with respect to segmental identity. *Dev Dyn* 233:1386–1393. doi: 10.1002/dvdy.20464
- Forsberg E, Hirsch E, Fröhlich L, et al (1996) Skin wounds and severed nerves heal normally in mice lacking tenascin-C. *Proc Natl Acad Sci U S A* 93:6594–6599. doi: 10.1073/pnas.93.13.6594
- Friedrichsen S, Heuer H, Christ S, et al (2003) CTGF expression during mouse embryonic development. *Cell Tissue Res* 312:175–188. doi: 10.1007/s00441-003-0712-6
- Frykberg RG, Banks J (2015) Challenges in the Treatment of Chronic Wounds. *Adv Wound Care* 4:560–582. doi: 10.1089/wound.2015.0635
- Gál P, Vasilenko T, Kostelníková M, et al (2011) Open Wound Healing In Vivo: Monitoring Binding and Presence of Adhesion/Growth-Regulatory Galectins in Rat Skin during the Course of Complete Re-Epithelialization. *Acta Histochem Cytochem* 44:191–199. doi: 10.1267/ahc.11014
- Gendronneau G, Sidhu SS, Delacour D, et al (2008) Galectin-7 in the control of epidermal homeostasis after injury. *Mol Biol Cell* 19:5541–9. doi: 10.1091/mbc.E08-02-0166
- Gilbert S (2000) Paraxial Mesoderm: The Somites and Their Derivatives. In: *Developmental Biology*, 6th edn. Sinauer Associates, Sunderland (MA)
- Golebiewska EM, Poole AW (2015) Platelet secretion: From haemostasis to wound healing and beyond. *Blood Rev* 29:153–162. doi: 10.1016/j.blre.2014.10.003
- Guillaume R, Bressan M, Herzlinger D (2009) Paraxial mesoderm contributes stromal cells to the developing kidney. *Dev Biol* 329:169–175. doi: 10.1016/j.ydbio.2009.02.034

- Guimarães-Camboa N, Cattaneo P, Sun Y, et al (2017) Pericytes of Multiple Organs Do Not Behave as Mesenchymal Stem Cells In Vivo. *Cell Stem Cell* 20:345–359.e5. doi: 10.1016/j.stem.2016.12.006
- Han G, Ceilley R (2017) Chronic Wound Healing: A Review of Current Management and Treatments. *Adv Ther* 34:599–610. doi: 10.1007/s12325-017-0478-y
- Hassan WU, Greiser U, Wang W (2014) Role of adipose-derived stem cells in wound healing. *Wound Repair Regen* 22:313–325. doi: 10.1111/wrr.12173
- Hatini V, Huh SO, Herzlinger D, et al (1996) Essential role of stromal mesenchyme in kidney morphogenesis revealed by targeted disruption of Winged Helix transcription factor BF-2. *Genes Dev* 10:1467–1478. doi: 10.1101/gad.10.12.1467
- Henderson NC, Mackinnon AC, Farnworth SL, et al (2006) Galectin-3 regulates myofibroblast activation and hepatic fibrosis. *Proc Natl Acad Sci* 103:5060–5065. doi: 10.1073/pnas.0511167103
- Henderson NC, Mackinnon AC, Farnworth SL, et al (2008) Galectin-3 expression and secretion links macrophages to the promotion of renal fibrosis. *Am J Pathol* 172:288–298. doi: 10.2353/ajpath.2008.070726
- Higashiyama R, Nakao S, Shibusawa Y, et al (2011) Differential contribution of dermal resident and bone marrow-derived cells to collagen production during wound healing and fibrogenesis in mice. *J Invest Dermatol* 131:529–536. doi: 10.1038/jid.2010.314
- Hinz B (2016) The role of myofibroblasts in wound healing. *Curr Res Transl Med* 64:171–177. doi: 10.1016/j.retram.2016.09.003
- Hinz B (2007) Formation and function of the myofibroblast during tissue repair. *J Invest Dermatol* 127:526–537. doi: 10.1038/sj.jid.5700613
- Hinz B (2015) The extracellular matrix and transforming growth factor- β 1: Tale of a strained relationship. *Matrix Biol* 47:54–65. doi: 10.1016/j.matbio.2015.05.006
- Hinz B, Celetta G, Tomasek JJ, et al (2001) Alpha-Smooth Muscle Actin Expression

- Upregulates Fibroblast Contractile Activity. *Mol Biol Cell* 12:2730–2741. doi: 10.1091/mbc.12.9.2730
- Hinz B, Gabbiani G (2010) Fibrosis: recent advances in myofibroblast biology and new therapeutic perspectives. *F1000 Biol Rep* 2:1–5. doi: 10.3410/B2-78
- Hoersch S, Andrade-Navarro MA (2010) Periostin shows increased evolutionary plasticity in its alternatively spliced region. *BMC Evol Biol* 10:. doi: 10.1186/1471-2148-10-30
- Holbourn KP, Acharya KR, Perbal B (2008) The CCN family of proteins: structure-function relationships. *Trends Biochem Sci* 33:461–473. doi: 10.1016/j.tibs.2008.07.006
- Hsu Y-C (2015) The Theory and Practice of Lineage Tracing. *Stem Cells* 33:3197–3204. doi: 10.1002/stem.2123.The
- Hu MS, Moore AL, Longaker MT (2018) A Fibroblast Is Not a Fibroblast Is Not a Fibroblast. *J Invest Dermatol* 138:729–730. doi: 10.1016/j.jid.2017.10.012
- Humphreys BD, Lin SL, Kobayashi A, et al (2010) Fate tracing reveals the pericyte and not epithelial origin of myofibroblasts in kidney fibrosis. *Am J Pathol* 176:85–97. doi: 10.2353/ajpath.2010.090517
- Hung C, Linn G, Chow YH, et al (2013) Role of lung Pericytes and resident fibroblasts in the pathogenesis of pulmonary fibrosis. *Am J Respir Crit Care Med* 188:820–830. doi: 10.1164/rccm.201212-2297OC
- Igarashi A, Okochi H, Bradham DM, Grotendorst GR (1993) Regulation of Connective Tissue Growth Factor Gene Expression in Human Skin Fibroblasts and During Wound Repair. *Mol Biol Cell* 4:637–645. doi: 10.1091/mbc.4.6.637
- Ivkovic S (2003) Connective tissue growth factor coordinates chondrogenesis and angiogenesis during skeletal development. *Development* 130:2779–2791. doi: 10.1242/dev.00505
- Jackson-Boeters L, Wen W, Hamilton DW (2009) Periostin localizes to cells in normal

- skin, but is associated with the extracellular matrix during wound repair. *J Cell Commun Signal* 3:125–133. doi: 10.1007/s12079-009-0057-3
- Jiang D, Correa-Gallegos D, Christ S, et al (2018) Two succeeding fibroblastic lineages drive dermal development and the transition from regeneration to scarring. *Nat Cell Biol* 20:422–431. doi: 10.1038/s41556-018-0073-8
- Jiang JX, Chen X, Hsu DK, et al (2012) Galectin-3 modulates phagocytosis-induced stellate cell activation and liver fibrosis in vivo. *AJP Gastrointest Liver Physiol* 302:G439–G446. doi: 10.1152/ajpgi.00257.2011
- Juráňová J, Franková J, Ulrichová J (2017) The role of keratinocytes in inflammation. *J Appl Biomed* 15:169–179. doi: 10.1016/j.jab.2017.05.003
- Kanta J (2015) Collagen matrix as a tool in studying fibroblastic cell behavior. *Cell Adhes Migr* 9:308–316. doi: 10.1080/19336918.2015.1005469
- Kapoor M, Liu S, Huh K, et al (2008) Connective tissue growth factor promoter activity in normal and wounded skin. *Fibrogenesis Tissue Repair* 1:3. doi: 10.1186/1755-1536-1-3; 10.1186/1755-1536-1-3
- Karlsson A, Christenson K, Matlak M, et al (2009) Galectin-3 functions as an opsonin and enhances the macrophage clearance of apoptotic neutrophils. *Glycobiology* 19:16–20. doi: 10.1093/glycob/cwn104
- Kii I, Ito H (2017) Periostin and its interacting proteins in the construction of extracellular architectures. *Cell Mol Life Sci* 74:4269–4277. doi: 10.1007/s00018-017-2644-4
- Kim BC, Kim HT, Park SH, et al (2003) Fibroblasts from chronic wounds show altered TGF- β -signaling and decreased TGF- β type II receptor expression. *J Cell Physiol* 195:331–336. doi: 10.1002/jcp.10301
- Kim M-H, Curry F-RE, Simon SI (2009) Dynamics of neutrophil extravasation and vascular permeability are uncoupled during aseptic cutaneous wounding. *Am J Physiol Cell Physiol* 296:C848-56. doi: 10.1152/ajpcell.00520.2008

- Kiwanuka E, Hackl F, Caterson EJ, et al (2013) CCN2 is transiently expressed by keratinocytes during re-epithelialization and regulates keratinocyte migration in vitro by the ras-MEK-ERK signaling pathway. *J Surg Res* 185:e109–e119. doi: 10.1016/j.jss.2013.05.065
- Klement GL, Yip TT, Cassiola F, et al (2009) Platelets actively sequester angiogenesis regulators. *Blood* 113:2835–2842. doi: 10.1182/blood-2008-06-159541
- Kral JB, Schrottmaier WC, Salzmann M, Assinger A (2016) Platelet Interaction with Innate Immune Cells. *Transfus Med Hemotherapy* 43:78–88. doi: 10.1159/000444807
- Kramann R, Schneider RK, Dirocco DP, et al (2015) Perivascular Gli1+ progenitors are key contributors to injury-induced organ fibrosis. *Cell Stem Cell* 16:51–66. doi: 10.1016/j.stem.2014.11.004
- Kretzschmar K, Watt FM (2012) Lineage tracing. *Cell* 148:33–45. doi: 10.1016/j.cell.2012.01.002
- Kudo A (2011) Periostin in fibrillogenesis for tissue regeneration: Periostin actions inside and outside the cell. *Cell Mol Life Sci* 68:3201–3207. doi: 10.1007/s00018-011-0784-5
- Kuljanin M, Brown CFC, Raleigh MJ, et al (2017) Collagenase treatment enhances proteomic coverage of low-abundance proteins in decellularized matrix bioscaffolds. *Biomaterials* 144:130–143. doi: 10.1016/j.biomaterials.2017.08.012
- Kuo Y-R, Wang C-T, Cheng J-T, et al (2016) Adipose-Derived Stem Cells Accelerate Diabetic Wound Healing through the Induction of Autocrine and Paracrine Effects. *Cell Transplant* 25:71–81. doi: 10.3727/096368915X687921
- Kyriakides TR, Wulsin D, Skokos EA, et al (2009) Mice that lack matrix metalloproteinase-9 display delayed wound healing associated with delayed reepithelialization and disordered collagen fibrillogenesis. *Matrix Biol* 28:65–73. doi: 10.1016/j.matbio.2009.01.001
- Larsen L, Chen HY, Saegusa J, Liu FT (2011) Galectin-3 and the skin. *J Dermatol Sci*

64:85–91. doi: 10.1016/j.jdermsci.2011.07.008

Lauer G, Sollberg S, Cole M, et al (2000) Expression and proteolysis of vascular endothelial growth factor is increased in chronic wounds. *J Invest Dermatol* 115:12–18. doi: 10.1046/j.1523-1747.2000.00036.x

Leask A, Parapuram SK, Shi-Wen X, Abraham DJ (2009) Connective tissue growth factor (CTGF, Ccn2) gene regulation: A potent clinical bio-marker of fibroproliferative disease? *J Cell Commun Signal* 3:89–94. doi: 10.1007/s12079-009-0037-7

LeBleu VS, Taduri G, O’Connell J, et al (2013) Origin and function of myofibroblasts in kidney fibrosis. *Nat Med* 19:1047–1053. doi: 10.1038/nm.3218

Lee DE, Ayoub N, Agrawal DK (2016) Mesenchymal stem cells and cutaneous wound healing: novel methods to increase cell delivery and therapeutic efficacy. *Stem Cell Res Ther* 7:37. doi: 10.1186/s13287-016-0303-6

Lee MJ, Kim J, Kim MY, et al (2010) Proteomic Analysis of Tumor Necrosis Factor- α -Induced Secretome of Human Adipose Tissue-Derived Mesenchymal Stem Cells research articles. *J Proteome Res* 9:1754–1762

Levenson SM, Geever EF, Crowley LV, et al (1965) the Healing of Rat Skin Wounds. *Ann Surg* 161:293–308. doi: 10.1097/00000658-196502000-00019

Levinson RS (2005) Foxd1-dependent signals control cellularity in the renal capsule, a structure required for normal renal development. *Development* 132:529–539. doi: 10.1242/dev.01604

Li Y, Zhang J, Yue J, et al (2017) Epidermal Stem Cells in Skin Wound Healing. *Adv Wound Care* 6:297–307. doi: 10.1089/wound.2017.0728

Liao H, Zakhaleva J, Chen W (2009) Cells and tissue interactions with glycated collagen and their relevance to delayed diabetic wound healing. *Biomaterials* 30:1689–1696. doi: 10.1016/j.biomaterials.2008.11.038

Liaw L, Birk DE, Ballas CB, et al (1998) Altered wound healing in mice lacking a

- functional osteopontin gene (spp1). *J Clin Invest* 101:1468–1478. doi: 10.1172/JCI2131
- Liu S, Leask A (2011) CCN2 is not required for skin development. *J Cell Commun Signal* 5:179–182. doi: 10.1007/s12079-011-0129-z
- Liu S, Shi-Wen X, Abraham DJ, Leask A (2011) CCN2 is required for bleomycin-induced skin fibrosis in mice. *Arthritis Rheum* 63:239–246. doi: 10.1002/art.30074
- Liu S, Taghavi R, Leask A (2010) Connective tissue growth factor is induced in bleomycin-induced skin scleroderma. *J Cell Commun Signal* 4:25–30. doi: 10.1007/s12079-009-0081-3
- Liu S, Thompson K, Leask A (2014) CCN2 expression by fibroblasts is not required for cutaneous tissue repair. *Wound Repair Regen* 22:119–124. doi: 10.1111/wrr.12131
- Liu W, Hsu DK, Chen HY, et al (2012) Galectin-3 regulates intracellular trafficking of EGFR through alix and promotes keratinocyte migration. *J Invest Dermatol* 132:2828–2837. doi: 10.1038/jid.2012.211
- Liu Z-J (2003) VEGF-A and V 3 integrin synergistically rescue angiogenesis via N-Ras and PI3-K signaling in human microvascular endothelial cells. *FASEB J* 17:1931–+. doi: 10.1096/fj.02-1171fje
- Lucas T, Waisman A, Ranjan R, et al (2010) Differential Roles of Macrophages in Diverse Phases of Skin Repair. *J Immunol* 184:3964–3977. doi: 10.4049/jimmunol.0903356
- Luevano-Contreras C, Chapman-Novakofski K (2010) Dietary advanced glycation end products and aging. *Nutrients* 2:1247–1265. doi: 10.3390/nu2121247
- MacKinnon AC, Farnworth SL, Hodgkinson PS, et al (2008) Regulation of Alternative Macrophage Activation by Galectin-3. *J Immunol* 180:2650–2658. doi: 10.4049/jimmunol.180.4.2650
- MacKinnon AC, Gibbons MA, Farnworth SL, et al (2012) Regulation of transforming growth factor- β 1-driven lung fibrosis by galectin-3. *Am J Respir Crit Care Med*

185:537–546. doi: 10.1164/rccm.201106-0965OC

MacLauchlan S, Skokos EA, Agah A, et al (2009) Enhanced angiogenesis and reduced contraction in thrombospondin-2 - Null wounds is associated with increased levels of matrix metalloproteinases-2 and -9, and soluble VEGF. *J Histochem Cytochem* 57:301–313. doi: 10.1369/jhc.2008.952689

Marangoni RG, Korman BD, Wei J, et al (2015) Myofibroblasts in murine cutaneous fibrosis originate from adiponectin-positive intradermal progenitors. *Arthritis Rheumatol* 67:1062–1073. doi: 10.1002/art.38990

Markowska AI, Jefferies KC, Panjwani N (2011) Galectin-3 protein modulates cell surface expression and activation of vascular endothelial Growth factor receptor 2 in human endothelial cells. *J Biol Chem* 286:29913–29921. doi: 10.1074/jbc.M111.226423

Markowska AI, Liu F-T, Panjwani N (2010) Galectin-3 is an important mediator of VEGF- and bFGF-mediated angiogenic response. *J Exp Med* 207:1981–1993. doi: 10.1084/jem.20090121

Marks MG, Doillon C, Silvert FH (1991) Effects of fibroblasts and basic fibroblast growth factor on facilitation of dermal wound healing by type I collagen matrices. *J Biomed Mater Res* 25:683–696. doi: 10.1002/jbm.820250510

Martin P, Leibovich SJ (2005) Inflammatory cells during wound repair: The good, the bad and the ugly. *Trends Cell Biol* 15:599–607. doi: 10.1016/j.tcb.2005.09.002

Martin P, Nunan R (2015) Cellular and molecular mechanisms of repair in acute and chronic wound healing. *Br J Dermatol* 173:370–378. doi: 10.1111/bjd.13954

Mauch C, Hatamochi A, Scharffetter K, Krieg T (1988) Regulation of collagen synthesis in fibroblasts within a three-dimensional collagen gel. *Exp Cell Res* 178:493–503. doi: 10.1016/0014-4827(88)90417-X

Mederacke I, Hsu CC, Troeger JS, et al (2013) Fate tracing reveals hepatic stellate cells as dominant contributors to liver fibrosis independent of its aetiology. *Nat Commun* 4:1–11. doi: 10.1038/ncomms3823

- Mir M, Ali MN, Barakullah A, et al (2018) Synthetic polymeric biomaterials for wound healing: a review. *Prog Biomater* 7:1–21. doi: 10.1007/s40204-018-0083-4
- Mirastschijski U, Schnabel R, Claes J, et al (2010) Matrix metalloproteinase inhibition delays wound healing and blocks the latent transforming growth factor- β 1-promoted myofibroblast formation and function. *Wound Repair Regen* 18:223–234. doi: 10.1111/j.1524-475X.2010.00574.x
- Moor AN, Vachon DJ, Gould LJ (2009) Proteolytic activity in wound fluids and tissues derived from chronic venous leg ulcers. *Wound Repair Regen* 17:832–839. doi: 10.1111/j.1524-475X.2009.00547.x
- Morissette Martin P, Grant A, Hamilton DW, Flynn LE (2018) Matrix composition in 3-D collagenous bioscaffolds modulates the survival and angiogenic phenotype of human chronic wound dermal fibroblasts. *Acta Biomater* 1–12. doi: 10.1016/j.actbio.2018.10.042
- Nakahara S, Hogan V, Inohara H, Raz A (2006) Importin-mediated nuclear translocation of Galectin-3. *J Biol Chem* 281:39649–39659. doi: 10.1074/jbc.M608069200
- Nambu M, Ishihara M, Kishimoto S, et al (2011) Stimulatory effect of autologous adipose tissue-derived stromal cells in an atelocollagen matrix on wound healing in diabetic db/db mice. *J Tissue Eng* 2:1–7. doi: 10.4061/2011/158105
- Nambu M, Kishimoto S, Nakamura S, et al (2009) Accelerated wound healing in healing-impaired db/db mice by autologous adipose tissue-derived stromal cells combined with atelocollagen matrix. *Ann Plast Surg* 62:317–321. doi: 10.1097/SAP.0b013e31817f01b6
- Nangia-Makker P, Honjo Y, Sarvis R, et al (2000) Galectin-3 induces endothelial cell morphogenesis and angiogenesis. *Am J Pathol* 156:899–909. doi: 10.1016/S0002-9440(10)64959-0
- Nangia-Makker P, Wang Y, Raz T, et al (2010) Cleavage of galectin-3 by matrix metalloproteases induces angiogenesis in breast cancer. *Int J Cancer* 127:2530–2541. doi: 10.1002/ijc.25254

- Negron L, Lun S, May BC (2014) Ovine forestomach matrix biomaterial is a broad spectrum inhibitor of matrix metalloproteinases and neutrophil elastase. *Int Wound J* 11:392–397. doi: 10.1111/j.1742-481X.2012.01106.x
- Neill T, Schaefer L, Iozzo R V. (2012) Decorin: A guardian from the matrix. *Am J Pathol* 181:380–387. doi: 10.1016/j.ajpath.2012.04.029
- Neill T, Schaefer L, Iozzo R V (2015) Oncosuppressive functions of decorin. *Mol Cell Oncol* 2:e975645. doi: 10.4161/23723556.2014.975645
- Nieminen J, St-Pierre C, Bhaumik P, et al (2008) Role of Galectin-3 in Leukocyte Recruitment in a Murine Model of Lung Infection by *Streptococcus pneumoniae*. *J Immunol* 180:2466–2473. doi: 10.4049/jimmunol.180.4.2466
- Nishiyama T, Kii I, Kashima TG, et al (2011) Delayed re-epithelialization in periostin-deficient mice during cutaneous wound healing. *PLoS One* 6:. doi: 10.1371/journal.pone.0018410
- Norman G, Westby M, Rithalia A, et al (2017) Dressings and topical agents for treating pressure ulcers (Review) Dressings and topical agents for treating pressure ulcers (Review). *Cochrane Database Syst Rev* Dr. doi: 10.1002/14651858.CD011947.pub2
- Ochieng J, Green B, Evans S, et al (1998) Modulation of the biological functions of galectin-3 by matrix metalloproteinases. *Biochim Biophys Acta - Gen Subj* 1379:97–106. doi: 10.1016/S0304-4165(97)00086-X
- Okamura DM, Pasichnyk K, Lopez-Guisa JM, et al (2011) Galectin-3 preserves renal tubules and modulates extracellular matrix remodeling in progressive fibrosis. *Am J Physiol Physiol* 300:F245–F253. doi: 10.1152/ajprenal.00326.2010
- Ontsuka K, Kotobuki Y, Shiraishi H, et al (2012) Periostin, a matricellular protein, accelerates cutaneous wound repair by activating dermal fibroblasts. *Exp Dermatol* 21:331–336. doi: 10.1111/j.1600-0625.2012.01454.x
- Owens P, Han G, Li AG, Wang XJ (2008) The role of Smads in skin development. *J Invest Dermatol* 128:783–790. doi: 10.1038/sj.jid.5700969

- Papanas N, Maltezos E (2010) Benefit-risk assessment of becaplermin in the treatment of diabetic foot ulcers. *Drug Saf* 33:455–461. doi: 10.2165/11534570-000000000-00000
- Park B-S, Jang K, Sung J-H, et al (2008) Adipose-Derived Stem Cells and Their Secretory Factors as a Promising Therapy for Skin Aging. *Dermatologic Surg* 34:1323–1326. doi: 10.1111/j.1524-4725.2008.34283.x
- Pepe D, Elliott CG, Forbes TL, Hamilton DW (2014) Detection of galectin-3 and localization of advanced glycation end products (AGE) in human chronic skin wounds. *Histol Histopathol* 29:251–258. doi: 10.14670/HH-29.251
- Peppas M, Stavroulakis P, Raptis SA (2009) Advanced glycoxidation products and impaired diabetic wound healing. *Wound Repair Regen* 17:461–472. doi: 10.1111/j.1524-475X.2009.00518.x
- Perbal B (2013) CCN proteins: A centralized communication network. *J Cell Commun Signal* 7:169–177. doi: 10.1007/s12079-013-0193-7
- Perumal S, Antipova O, Orgel JPRO (2008) Collagen fibril architecture, domain organization, and triple-helical conformation govern its proteolysis. *Proc Natl Acad Sci* 105:2824–2829. doi: 10.1073/pnas.0710588105
- Philippeos C, Telerman SB, Oulès B, et al (2018) Spatial and Single-Cell Transcriptional Profiling Identifies Functionally Distinct Human Dermal Fibroblast Subpopulations. *J Invest Dermatol* 138:811–825. doi: 10.1016/j.jid.2018.01.016
- Phipps RP, Penney DP, Keng P, et al (1989) Characterization of Two Major Populations of Lung Fibroblasts: Distinguishing Morphology and Discordant Display of Thy 1 and Class II MHC. *Am J Respir Cell Mol Biol* 1:65–74. doi: 10.1165/ajrcmb/1.1.65
- Plikus M V., Guerrero-Juarez CF, Ito M, et al (2017) Regeneration of fat cells from myofibroblasts during wound healing. *Science* (80-) 355:748–752. doi: 10.1126/science.aai8792
- Postlethwaite AE, Seyer JM, Kang AH (1978) Chemotactic attraction of human fibroblasts to type I, II, and III collagens and collagen-derived peptides. *Proc Natl*

Acad Sci 75:871–875

Quintero-Ronderos P, Laissue P (2018) The multisystemic functions of FOXD1 in development and disease. *J Mol Med* 96:725–739. doi: 10.1007/s00109-018-1665-2

Reinke JM, Sorg H (2012) Wound repair and regeneration. *Eur Surg Res* 49:35–43. doi: 10.1159/000339613

Rinkevich Y, Walmsley GG, Hu MS, et al (2015) Identification and isolation of a dermal lineage with intrinsic fibrogenic potential. *Science* (80-) 348:aaa2151. doi: 10.1126/science.aaa2151

Rognoni E, Pisco AO, Hiratsuka T, et al (2018) Fibroblast state switching orchestrates dermal maturation and wound healing. *Mol Syst Biol* 14:e8174. doi: 10.15252/msb.20178174

Ruggeri ZM (2009) Platelet adhesion under flow. *Microcirculation* 16:58–83. doi: 10.1080/10739680802651477

Ruszczak Z (2003) Effect of collagen matrices on dermal wound healing. *Adv Drug Deliv Rev* 55:1595–1611. doi: 10.1016/j.addr.2003.08.003

Salgado AJ, Reis RL, Sousa N, Gimble JM (2010) Adipose Tissue Derived Stem Cells Secretome: Soluble Factors and Their Roles in Regenerative Medicine. *Curr Stem Cell Res Ther* 5:103–110

Santagati F, Rijli FM (2003) Cranial neural crest and the building of the vertebrate head. *Nat Rev Neurosci* 4:806–818. doi: 10.1038/nrn1221

Santema TB, Poyck PPC, Ubbink DT (2016) Skin grafting and tissue replacement for treating foot ulcers in people with diabetes. *Cochrane Database Syst Rev* 2016:. doi: 10.1002/14651858.CD011255.pub2

Sato S, Ouellet N, Pelletier I, et al (2002) Role of Galectin-3 as an Adhesion Molecule for Neutrophil Extravasation During Streptococcal Pneumonia. *J Immunol* 168:1813–1822. doi: 10.4049/jimmunol.168.4.1813

Schneider RK, Mullally A, Dugourd A, et al (2017) Gli1+Mesenchymal Stromal Cells

Are a Key Driver of Bone Marrow Fibrosis and an Important Cellular Therapeutic Target. *Cell Stem Cell* 20:785–800.e8. doi: 10.1016/j.stem.2017.03.008

Schultz GS, Davidson JM, Kirsner RS, et al (2011) Dynamic reciprocity in the wound microenvironment. *Wound Repair Regen* 19:134–148. doi: 10.1111/j.1524-475X.2011.00673.x

Schultz GS, Wysocki A (2009) Interactions between extracellular matrix and growth factors in wound healing. *Wound Repair Regen* 17:153–162. doi: 10.1111/j.1524-475X.2009.00466.x

Serini G, Ropraz P, Geinoz A, et al (1998) The Fibronectin Domain ED-A Is Crucial for Myofibroblastic Phenotype Induction by Transforming Growth Factor-beta 1. *J Biol Chem* 273:873–881

Shahrokhi S, Arno AI, Jeschke MG (2014) The use of dermal substitutes in burn surgery: Acute phase. *Dermatol Surg* 40:193–210. doi: 10.1007/978-3-7091-1586-2_16

Singer AJ, Clark R (1999) Mechanisms of Disease - Cutaneous Wound Healing. *N Engl J Med* 341:738–746

Singh VP, Bali A, Singh N, Jaggi AS (2014) Advanced glycation end products and diabetic complications. *Korean J Physiol Pharmacol* 18:1–14. doi: 10.4196/kjpp.2014.18.1.1

Snyder DL, Sullivan N, Schoelles KM (2012) Skin Substitutes for Treating Chronic Wounds - Technology Assessment. *Agency Healthc Res Qual* 89

Streit M, Velasco P, Riccardi L, et al (2000) Thrombospondin-1 suppresses wound healing and granulation tissue formation in the skin of transgenic mice. *EMBO J* 19:3272–3282. doi: 10.1093/emboj/19.13.3272

Suga H, Rennert RC, Rodrigues M, et al (2014) Tracking the elusive fibrocyte: Identification and characterization of collagen-producing hematopoietic lineage cells during murine wound healing. *Stem Cells* 32:1347–1360. doi: 10.1002/stem.1648

- Sullivan MM, Puolakkainen PA, Barker TH, et al (2008) Altered tissue repair in hevin-null mice: Inhibition of fibroblast migration by a matricellular SPARC homolog. *Wound Repair Regen* 16:310–319. doi: 10.1111/j.1524-475X.2008.00370.x
- Sullivan TP, Eaglstein WH, Davis SC, Mertz P (2001) The pig as a model for human wound healing. *Wound Repair Regen* 9:66–76. doi: 10.1046/j.1524-475x.2001.00066.x
- Tabib T, Morse C, Wang T, et al (2018) SFRP2/DPP4 and FMO1/LSP1 define major fibroblast populations in human skin. *J Invest Dermatol* 138:1–9. doi: 10.1016/j.jid.2017.09.045
- Tam PPL, Behringer RR (1997) Mouse gastrulation: The formation of a mammalian body plan. *Mech Dev* 68:3–25. doi: 10.1016/S0925-4773(97)00123-8
- Tang Y-Q, Yeaman MR, Selsted ME (2002) Antimicrobial peptides from human platelets. *Infect Immun* 70:6524–33. doi: 10.1128/IAI.70.12.6524
- Thorne JT, Segal TR, Chang S, et al (2015) Dynamic Reciprocity Between Cells and Their Microenvironment in Reproduction¹. *Biol Reprod* 92:1–10. doi: 10.1095/biolreprod.114.121368
- Tomokiyo K, Kamikubo Y, Hanada T, et al (2005) Von Willebrand factor accelerates platelet adhesion and thrombus formation on a collagen surface in platelet-reduced blood under flow conditions. *Blood* 105:1078–1084. doi: 10.1182/blood-2004-05-1827
- Turner NJ, Badylak SF (2015) The Use of Biologic Scaffolds in the Treatment of Chronic Nonhealing Wounds. *Adv Wound Care* 4:490–500. doi: 10.1089/wound.2014.0604
- Van Putte L, De Schrijver S, Moortgat P (2016) The effects of advanced glycation end products (AGEs) on dermal wound healing and scar formation: a systematic review. *Scars, Burn Heal* 2:205951311667682. doi: 10.1177/2059513116676828
- Velnar T, Bailey T, Smrkolj V (2009) The Wound Healing Process: An Overview of the Cellular and Molecular Mechanisms. *J Int Med Res* 37:1528–1542. doi:

10.1177/147323000903700531

- Walker JT, Kim SS, Michelsons S, et al (2015) Cell–matrix interactions governing skin repair: matricellular proteins as diverse modulators of cell function. *Res Reports Biochem* 5:1–16. doi: 10.2147/RRBC.S57407
- Walmsley GG, Hu MS, Xing Hong W, et al (2015) A Mouse Fetal Skin Model of Scarless Wound Repair. *J Vis Exp* 522973791–52297. doi: 10.3791/52297
- Widgerow AD (2011) Chronic wound fluid-thinking outside the box. *Wound Repair Regen* 19:287–291. doi: 10.1111/j.1524-475X.2011.00683.x
- Wietecha MS, Cerny WL, Dipietro LA (2013) Mechanisms of vessel regression: Toward an understanding of the resolution of angiogenesis. In: Heber-Katz E, Stocum DL (eds) *Current Topics in Microbiology and Immunology*. Springer Berlin Heidelberg, Berlin, Heidelberg, pp 3–32
- Wynn TA, Ramalingam TR (2012) Mechanisms of fibrosis: Therapeutic translation for fibrotic disease. *Nat Med* 18:1028–1040. doi: 10.1038/nm.2807
- Xue M, Jackson CJ (2015) Extracellular Matrix Reorganization During Wound Healing and Its Impact on Abnormal Scarring. *Adv Wound Care* 4:119–136. doi: 10.1089/wound.2013.0485
- Yamazaki T, Nalbandian A, Uchida Y, et al (2017) Tissue Myeloid Progenitors Differentiate into Pericytes through TGF- β Signaling in Developing Skin Vasculature. *Cell Rep* 18:2991–3004. doi: 10.1016/j.celrep.2017.02.069
- Yates CC, Hebda P, Wells A (2012) Skin Wound Healing and Scarring: Fetal Wounds and Regenerative Restitution. *Birth Defects Res Part C - Embryo Today Rev* 96:325–333. doi: 10.1002/bdrc.21024
- Yu C, Bianco J, Brown C, et al (2013) Porous decellularized adipose tissue foams for soft tissue regeneration. *Biomaterials* 34:3290–3302. doi: 10.1016/j.biomaterials.2013.01.056
- Zhao X, Guan JL (2011) Focal adhesion kinase and its signaling pathways in cell

migration and angiogenesis. *Adv Drug Deliv Rev* 63:610–615. doi: 10.1016/j.addr.2010.11.001

Zhou HM, Wang J, Elliott C, et al (2010) Spatiotemporal expression of periostin during skin development and incisional wound healing: Lessons for human fibrotic scar formation. *J Cell Commun Signal* 4:99–107. doi: 10.1007/s12079-010-0090-2

Zhu Y, Lan F, Wei J, et al (2011) Influence of Dietary Advanced Glycation End Products on Wound Healing in Nondiabetic Mice. *J Food Sci* 76:T5–T10. doi: 10.1111/j.1750-3841.2010.01889.x

Chapter 2: Lineage tracing of *Foxd1*-expressing embryonic progenitors to assess the role of divergent embryonic lineages on adult dermal fibroblast function

2.1 Abstract

Recent studies have highlighted the functional diversity of dermal fibroblast populations in health and disease, with part of this diversity linked to fibroblast lineage and embryonic origin. In particular, fibroblast lineage has become an important predictor for determining fibroblast function during skin development, as well as during homeostasis and repair in adult skin. Single-cell transcriptional profiling studies have been pivotal in determining the extent of diversity in fibroblast populations localized in skin. However, whether this diversity is derived from different discrete cell states within fibroblasts of the same lineage, or is defined by different lineages, is not known. Additionally, it is unclear whether common expression signatures in disparate embryonic progenitor populations can lead to similar functional properties in their fibroblast progeny across organs. Fibroblasts derived from *Foxd1*-expressing progenitors contribute to the myofibroblast populations present in lung and kidney fibrosis in mice. Here, it was hypothesized that dermal fibroblast progenitors would express *Foxd1*, and that the fibroblast progeny of these cells would contribute to granulation tissue formation during cutaneous wound repair. Using a Cre/Lox system to genetically track populations derived

from *Foxd1*-expressing progenitors, lineage-positive fibroblasts were identified as a subset of the dermal fibroblast population. At embryonic day 9.5 (E9.5), lineage-positive cells were evident within the most dorsal embryonic tissues, contributing to the developing dermal fibroblast population, and remaining in this niche into adulthood. Using real-time PCR array analysis of fluorescence activated cell sorting (FACS)-enriched fibroblasts isolated from adult tissues at 10 days post-wounding demonstrated that the *Foxd1* lineage-positive dermal fibroblasts were enriched with transcripts associated with matrix synthesis relative to their *Foxd1* lineage-negative counterparts. Specifically, within fibroblasts isolated from the wound tissue, transcripts for the extracellular matrix constituents type III collagen, decorin, CCN2, and thrombospondin 2 were enriched in *Foxd1* lineage-positive fibroblasts. Conversely, in *Foxd1* lineage-negative fibroblasts, there was an enrichment in transcripts for cell surface receptors including several integrins, and soluble signaling factors including tumor necrosis factor-alpha ($TNF\alpha$), platelet derived growth factor-A (PDGF-A) and PDGF-B. This work provides a foundation for the future assessment of functional differences between fibroblasts of *Foxd1*-positive and -negative lineages and characterization of markers of differentiation for translational research outside of a lineage tracing context.

2.2 Introduction

Within the skin, resident fibroblasts have long been proposed as the source of myofibroblasts during cutaneous wound repair (Singer and Clark 1999). Recent evidence from lineage tracing studies in mice has supported this hypothesis (Driskell et al. 2013; Rinkevich et al. 2015), while other research has demonstrated complementary myofibroblast contribution from perivascular cells, adipocytes, and bone marrow-derived

populations in skin fibrosis and wound healing (Dulauroy et al. 2012; Suga et al. 2014; Marangoni et al. 2015). Myofibroblasts, characterized by the expression of alpha smooth muscle actin (α SMA), are the main source of extracellular matrix (ECM) production during tissue injury (Gabbiani 2003; Hinz 2007). As such, investigation into the progenitors from which these myofibroblast populations originate within the skin during health and disease could provide insight into novel strategies to improve wound healing and treat skin fibrosis (Driskell and Watt 2015; Hu et al. 2018).

An important finding from lineage tracing studies is that there is previously unrecognized heterogeneity within the fibroblast subpopulation of myofibroblast progenitors, and that this heterogeneity is correlated with specific gene expression signatures in embryonic precursor populations (Driskell et al. 2013; Driskell and Watt 2015; Rinkevich et al. 2015; Hu et al. 2018). During development, the most dorsal fibroblast population, characterized by the expression of *Blimp1* and *Lrig1*, gives rise to the papillary dermal fibroblasts of post-natal mice (Driskell et al. 2013). In contrast, the more ventral population, expressing *Dlk1*, contributes to the reticular dermal fibroblasts and underlying adipogenic population (Driskell et al. 2013). Furthermore, lineage tracing analysis of these populations identified unique contributions to dermal wound repair in adult mice. While the *dlk1*-traced lower dermis contributed to early granulation tissue formation, the upper *blimp1*-traced population migrated into the wound during re-epithelialization, and contributed primarily to hair follicle regeneration (Driskell et al. 2013).

Further investigation of embryonic lineages identified that there are different fibroblast subsets with distinct specialization contributing to granulation tissue formation

(Rinkevich et al. 2015). Tracing a population of fibroblasts characterized by embryonic expression of *Engrailed-1*, Rinkevich *et al.* identified a subset of fibroblasts with greater fibrogenic potential relative to fibroblasts derived from precursors not expressing *Engrailed-1*. More importantly, in this study, the cell surface marker and enzyme CD26 (Dipeptidyl peptidase-4; Dpp4) was enriched on adult mouse fibroblasts of the fibrogenic *Engrailed-1* lineage. In adult mice, wounds treated with a chemical inhibitor of Dpp4 healed more slowly but had a significant reduction in scar size, highlighting the translational potential of this research (Rinkevich et al. 2015).

The level of heterogeneity within dermal fibroblasts has recently been assessed in human skin using single-cell qPCR analysis (Philippeos et al. 2018; Tabib et al. 2018). These studies have identified approximately five subpopulations of fibroblasts based on cluster analysis of gene expression profiles. Whether these populations are fixed, and predetermined based on developmental lineage, or if cells from one discrete sub-type can transition to another, are critical questions arising from these studies with important clinical implications. Lineage tracing studies in mice represent a promising tool to begin to explore these important questions.

In fibrotic processes including dermal wound healing and organ fibrosis, myofibroblasts are implicated as the effector cell of uncontrolled matrix deposition across organs, regardless of the available pool of myofibroblast precursors in that organ (Hinz et al. 2012; El Agha et al. 2017). Recent lineage tracing studies have also demonstrated that unique embryonic gene signatures within dermal fibroblast precursors are predictive of unique myofibroblast functions during dermal wound repair in adulthood (Driskell et al. 2013; Rinkevich et al. 2015). Consequently, it was hypothesized that specific common

embryonic gene signatures between myofibroblast progenitors of different organs would be predictive of common myofibroblast functions. Binary expression of *Foxd1* during embryogenesis presented a potential candidate as a common gene expression signature. *Foxd1* is a transcription factor expressed primarily during development, and is required for appropriate renal stromal cell differentiation from progenitors during embryogenesis (Levinson 2005; Fetting et al. 2014). Additionally, as a lineage tracing marker, resident *Foxd1* lineage-derived populations in the kidney and lung contributed to the myofibroblast populations in induced renal fibrosis following unilateral ureteral obstruction and ischemia reperfusion injury, as well as bleomycin induced lung fibrosis, respectively (Humphreys et al. 2010; Hung et al. 2013). In the present study, using a Cre/Lox lineage tracing system in mice, the *Foxd1* lineage of stromal cells was investigated in dorsal skin development, homeostasis, and wound healing. It was hypothesized that binary expression of *Foxd1* during embryogenesis would be a useful marker to identify a distinct stromal cell progenitor population and that the progeny of this population would contribute to dermal fibroblasts in adult skin and myofibroblasts upon cutaneous wounding.

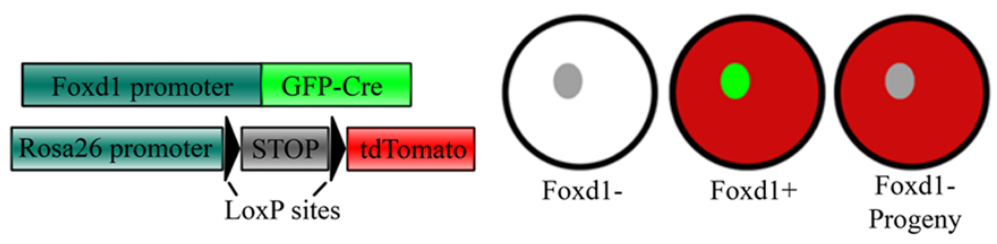
2.3 Materials and methods

2.3.1 Mice

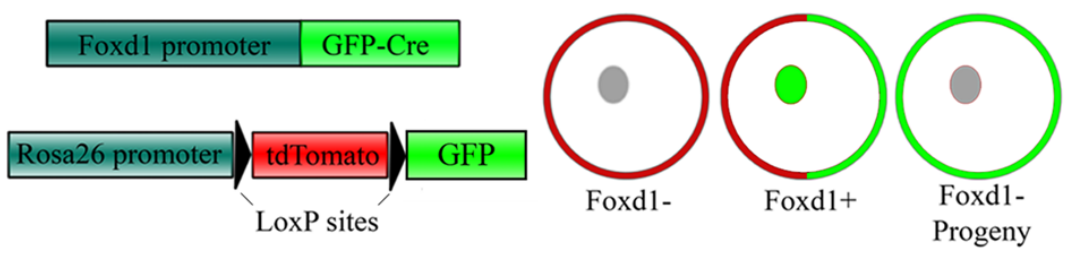
All animal procedures were in compliance with protocols approved by the University Council on Animal Care at Western University (Animal use protocol # 2016-085). *Foxd1*^{GC} (*Foxd1*^{tm1(GFP/Cre)Amc/J}), *Foxd1*^{GCE} (*B6;129S4-Foxd1*^{tm2(GFP/Cre/ERT2)Amc/J}), *Ai14* (*B6.Cg-Gt(ROSA)26Sor*^{tm14(CAG-tdTomato)Hze/J}), and *mTmG* (*B6.129(Cg)-Gt(ROSA)26Sor*^{tm4(ACTB-tdTomato,-EGFP)Luo/J}) mice were purchased from The Jackson

Laboratory (Farmington, CT). Schematics and brief descriptions of each of the Cre/Lox models used in this study are provided in Figure 2.1. Mice were genotyped as per The Jackson Laboratory's instructions. Mice that were heterozygous for the alleles of interest were used for all experiments. For timed pregnancy, females were monitored for vaginal plugs and the day following was considered embryonic day 0.5 (E0.5). Embryos were isolated from pregnant females at E9.5, E10.5, E11.5, E14.5, and E17.5 as specified for each experiment. For all time-points, at least 3 embryos were analyzed from at least 2 independent litters.

A Foxd1GC/Ai14



B Foxd1GC/mTmG



C Foxd1GCE/Ai14

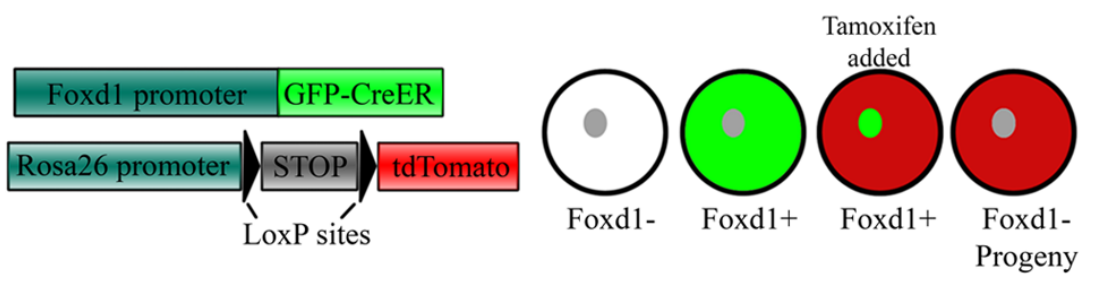


Figure 2.1: Schematics of Cre/Lox strategies used to track *Foxd1* lineage-positive populations. (A) A cross between *Foxd1*^{IGC} and *Ai14* mice yields tdTomato positive populations in cells derived from *Foxd1*-expressing progenitors. (B) A cross between *Foxd1*^{IGC} and *mTmG* results in membrane-targeted tdTomato expression in all *Foxd1* lineage-negative populations and membrane-bound eGFP in all *Foxd1* lineage-positive populations. (C) A cross between *Foxd1*^{IGCE} and *Ai14* mice is similar to the cross in (A), however the modified human estrogen receptor (ER) fragment attached to the Cre-recombinase impedes translocation into the nucleus preventing recombination in the absence of the synthetic ER ligand, tamoxifen (Metzger and Chambon 2001).

2.3.2 Tamoxifen injections

To temporally control Cre-mediated recombination, mice carrying a tamoxifen-inducible Cre variant, CreER^{T2}, were crossed to *Ai14* reporter mice (Figure 2.1C) (Metzger and Chambon 2001; Feil et al. 2009). Using this strategy, injection of tamoxifen was used to determine the temporal expression of *Foxd1* in both embryonic and adult tissues. Timed pregnancies were used for the embryo isolations as above. In these animals, tamoxifen was injected intraperitoneally into pregnant females twice on 2 consecutive days at a dose of 0.6 mg per day. For all studies, a solution of 10 mg/mL tamoxifen in 90% corn oil (Sigma) and 10% ethanol was administered. A minimum of 3 embryos from one or more litters were analyzed at all time-points.

Tamoxifen injection in postnatal mice was performed on mice heterozygous for both *Foxd1*GCE and *Ai14* alleles (Figure 2.1C). At 1 month of age, mice were injected with 1 mg of tamoxifen each day for 3 consecutive days. At 2 months of age, wounding experiments were performed using a non-splinted wound model as previously described (Elliott et al. 2012). Briefly, the dorsal skin of mice was shaved, and hair was removed with depilating cream (Nair®). Two full-thickness dorsal wounds were made with a 6 mm biopsy punch (Integra™ Miltex™). Wounds were left to heal without bandaging. Pain was managed using 0.05 mg/Kg buprenorphine administered intraperitoneally prior to surgery and again 6-8 hours following surgery. Directly following wounding, mice were subjected to a second tamoxifen regimen of 1 mg each day for 3 consecutive days. After 7 days post wounding, the animals were euthanized, and tissues were collected for histological analyses. Postnatal tamoxifen injection and wounding was performed on 6 animals. Tissues from these animals were compared to unwounded adult skin, and

granulation tissue at 7 days post wounding (non-splinted) from constitutively active *Foxd1GC/Ai14* mice (Figure 2.1A).

2.3.3 Wound healing

With the exception of mice wounded and injected with tamoxifen as described above, all excisional wounds were splinted and wrapped as described previously (Dunn et al. 2013). The dorsal skin was shaved, and the remaining hair was removed with depilating cream (Nair®). The 6 mm wounds were created with a biopsy punch and wounds were splinted open with silicone splints (Grace Bio labs), which were held in place with a cyanoacrylate adhesive and 6-0 nylon sutures. Wounds were then covered with an adhesive contact layer (Mepitel® One; Mölnlycke) and a semi-occlusive dressing (OPSITE®; Smith & Nephew), prior to being wrapped in a self-adherent bandage and cloth tape. Following surgery, pain was controlled using 0.05 mg/Kg buprenorphine delivered intraperitoneally prior to surgery and 6-8 hours following surgery. Dressings were changed every 3-4 days. For the 21-day time point, bandages and splints were removed after 14 days.

2.3.4 Histology and immunofluorescence microscopy analyses

Isolated embryos, skin, and wound tissue were fixed in 10% neutral buffered formalin for 24 hours at 4°C. These tissue samples were then dehydrated in a sucrose gradient prior to embedding in frozen section compound (Leica). Samples were frozen on dry ice and were stored at -20°C. Cryosections were cut to 8 µm thickness. Unstained sections to investigate only endogenous fluorescent proteins, were washed in phosphate buffered saline (PBS) and directly mounted with VectaShield mounting media with DAPI (Vector Labs). For antibody labelling, slides were first washed with 1% sodium dodecyl sulfate

for 5 minutes, rinsed three times in PBS, and incubated for 30 minutes in 10% horse serum in PBS for blocking. Sections were then incubated with primary antibodies as outlined in Table 2.1 in 10% horse serum. Following staining, slides were stained with VectaShield mounting media with DAPI (Vector Labs). No-primary controls were used for negative controls for antibody labelling (shown in Appendix Figure A1).

Table 2.1: Antibodies used for histological assessment

Target	Tissue investigated	Antibody ID	Dilution
α SMA	Adult	Ab5694 (Abcam)	1:100
CD26	Adult	AF954 (R&D systems)	1:50
GFP	Embryonic/Adult	Ab6673 (Abcam)	1:200
PDGFR α	Adult	AF1062 (R&D systems)	1:100
PDGFR β	Adult	AF1042 (R&D systems)	1:50
CD31	Adult	Ab28364 (Abcam)	1:200
Vimentin	Adult	Ab92547 (Abcam)	1:500
α 2 Integrin	Adult	AF1740 (R&D systems)	1:50
α 3 Integrin	Adult	AB1920 (EMD Millipore)	1:200
α V Integrin	Adult	AF1219 (R&D systems)	1:50
β 1 Integrin	Adult	AF2405 (R&D systems)	1:50
β 6 Integrin	Adult	AF2389 (R&D systems)	1:50

2.3.5 Dermal fibroblast isolation

To isolate dermal fibroblasts from wounded and subject-matched healthy tissue, skin was excised from mice 10 days post wounding using an 8 mm biopsy punch centered on the middle of the wound, or excised from unwounded, depilated dorsal skin outside of the

wounded area. For isolation of naïve healthy fibroblasts for culture studies, unwounded mice were depilated, and the dorsal skin was removed immediately. In all cases, subcutaneous fat was mechanically removed from the skin. The full, excised dorsal skin was then incubated in 0.25% trypsin with 100 µg/mL dispase for 30 minutes at 37°C. The epidermis was then removed mechanically by scraping the surface with a scalpel blade, and the remaining dermis was minced with a scalpel. The minced tissue was incubated in a digest solution of 4 mg/mL collagenase IV (Gibco) in DMEM/Ham's F-12 media for 2 hours, at 37°C on a shaker set to 100 rpm. The resultant cell suspension was filtered through 100 µm and 40 µm nylon filters and prepared for FACS. Individual samples were processed independently from wounded and unwounded tissue. For isolation of naïve healthy fibroblasts, cells from 4-6 mice were pooled.

2.3.6 Fluorescence activated cell sorting

Cell suspensions were stained with LIVE/DEAD fixable aqua stain (Life technologies), as per the manufacturer's instructions. Cells were then incubated on ice for 25 minutes with APC-labelled antibodies for CD31 (BD Pharmingen; 551262), CD45 (BD Pharmingen; 559864), and EpCAM (BD Pharmingen; 563478) each diluted 1:25 in PBS with 5% FBS, to negatively select for endothelial, bone marrow derived, and epithelial populations, respectively. Cells were then sorted on a FACSAria III cell sorter as follows. Forward- and side-scatter were first used to select individual cells. Using a 405 nm laser with a 510/50 filter, cells negative for the LIVE/DEAD fixable aqua stain were selected. Next, using a 633 nm laser with 660/20 filter, cells negative for APC were selected. Finally, the remaining fibroblast populations were sorted into the *Foxd1* lineage-positive

(FLP) and *Foxd1* lineage-negative (FLN) subpopulations based on expression of tdTomato using a 561 nm laser with 610/20 filter.

2.3.7 Cell Culture

To assess isolated cells in culture, free-floating soft collagen gels were used as a 3-dimensional culture substrate. For these studies, 2 mg/mL collagen gels were synthesized by neutralizing 6 mg/mL collagen (Nutragen; Advanced Biomatrix) with HEPES (final concentration 0.02 M). This solution was then combined with FACS-sorted fibroblasts in culture media. For each 500 μ L collagen gel, 70,000 cells were seeded using a 24-well suspension culture plate as a mold. The samples were incubated for 30 minutes at 37°C to allow gelation and then detached from the well plate with a pipette tip. Samples were cultured in DMEM/Ham's F-12 media supplemented with penicillin/streptomycin and 10% FBS. To induce a myofibroblast phenotype, one set of samples was treated with 5 ng/mL mouse TGF β 1 (R&D Systems) whereas the other was left untreated. Depending on the cell yield, 1-3 collagen gels were synthesized per treatment group for each cell lineage. After 16 hours, the cells were cultured in DMEM/Ham's F-12 media supplemented with 5% FBS, with fresh TGF β 1 added daily, for a total of 7 days. On day 7, the gels were digested in 4 mg/mL collagenase type IV (Gibco) in DMEM/Ham's F-12 media for RNA isolation. Multiple gels from the same group were pooled. These cell culture experiments were performed on isolated cells from a total of 6 independent digestions, each combining the pooled fibroblasts from 4-6 mice.

2.3.8 RNA isolation

RNA was isolated from freshly-sorted FLP and FLN fibroblast populations and from cells cultured in collagen gels. For all samples, RNA was isolated with TRIzol reagent

(Life Technologies) and purified using RNeasy micro kits (Qiagen, Valencia, CA), including DNase digestion. Isolated RNA was stored at -20°C for short-term storage prior to quantitation.

2.3.9 RT-qPCR array

To assess cell intrinsic differences between FACS-sorted FLP and FLN fibroblasts during homeostasis and wound healing, a RT² profiler array for genes associated with fibrosis (Qiagen; PAMM-120Z) was used to measure gene expression. Samples were collected independently from 8 mice and were divided into 4 groups each (FLP wound, FLN wound, FLP unwounded, FLN unwounded). Isolated RNA was converted to cDNA with a RT² first strand kit (Qiagen), and pre-amplified with array specific primers. Genes that were not consistently amplified in any group were removed from further analysis. Expression was normalized to a panel of housekeeping genes. Outliers in the $2^{-\Delta Ct}$ values were calculated using the ROUT method (Q = 1.0%) (Motulsky and Brown 2006) in GraphPad Prism. Two groups of the 32 total groups were deemed to have a high number of outliers and were completely removed from further analysis. In the remaining data set, 23 data points were removed as outliers, of the 2,220 total data points remaining (~1%). $2^{-\Delta Ct}$ values were then compared with multiple t-tests and adjusted for multiple comparisons with a false discovery rate correction set to 10%.

2.3.10 TaqMan® qPCR

Gene expression in freshly-sorted FLP and FLN fibroblast populations from unwounded mouse skin, along with the two populations cultured in collagen gels for 7 days as described in Section 2.3.7, were assessed with TaqMan® probe sets (ThermoFisher Scientific) using iTaq Universal 1-step master mix (Bio-rad) as per the manufacturer's

instructions. Samples were run in triplicate. Threshold cycles were compared to a standard curve generated from serial dilutions of unsorted dermal isolates for relative quantitation. The resultant relative quantities were then normalized to endogenous 18S rRNA. The TaqMan® probe sets used in this study are listed in Table 2.2. Isolated cells from a total of 6 independent digestions, each combining the pooled fibroblasts from 4-6 mice, were assessed.

2.3.11 Statistical methods

With the exception of the analysis performed on the array data as described above, statistical analyses were performed using R statistics software (R core team 2017) using the “nlme” package for linear and nonlinear mixed effects models (Pinheiro et al. 2014), and the “multcomp” package for simultaneous inference in general parametric models (Hothorn et al. 2008). GraphPad Prism software version 6 (GraphPad, La Jolla, CA) was used to produce graphs. Statistical analyses were performed using linear mixed effects models. Data were compared, correcting for multiple comparisons as described by Hothorn *et al.* (2008). Corrected p-values <0.05 were considered to be statistically significant.

Table 2.2: Taqman® probes used to assess gene expression

Target	Probe ID
<i>Acta2</i>	Mm01546133_m1
<i>Coll1a1</i>	Mm00801666_g1
<i>Col3a1</i>	Mm01254476_m1
<i>Ctgf</i>	Mm01192933_g1
<i>Itga2</i>	Mm00434371_m1
<i>Itgb8</i>	Mm00623991_m1
<i>Lox</i>	Mm00495386_m1
<i>Mmp3</i>	Mm00440295_m1
<i>Dlk1</i>	Mm00494477_m1
<i>Dpp4</i>	Mm00494548_m1
<i>Pdgfra</i>	Mm00440701_m1
<i>Thy1</i>	Mm00493681_m1
<i>Eukaryotic 18S</i>	4332641

2.4 Results

2.4.1 *Foxd1* was expressed during murine embryonic development

Using a lineage tracing strategy to track *Foxd1* derived populations (schematic shown in Figure 2.1A), contribution of this lineage to dermal populations during early development was observed (Figure 2.2). *Foxd1* expression was assessed in embryos from embryonic day (E)9.5-E17.5. Within this time frame, *Foxd1* was expressed from E9.5-E11.5 within the head and in the dorsal region of the embryo, where it was expressed in proximity to the neural tube, both ventrally and laterally. At E14.5, expression was primarily confined

to the head, with reduced expression moving posteriorly. No *Foxd1* expression was detected at E17.5.

Notably, at E9.5, the earliest stage examined, FLP cells that were negative for *Foxd1* were present within the dorsal tissue of the embryo, suggesting they were derived from a population that expressed *Foxd1* prior to E9.5. By E14.5 and up to the final stage examined of E17.5, it was observed that FLP cells contributed to the cell populations within the dermis (Figure 2.2). FLP cells were also evident in several internal organs throughout the embryo, including, but not limited to, the kidney, lungs, and with a low frequency in the heart (Appendix Figure A2). Within the developing dermis, FLP cells were distributed primarily along the midline, dorsal to the neural tube, however, the frequency of these cells was decreased in the lateral dermis (Figure 2.3; shown in an *mTmG* reporter as described in Figure 2.1B). Within adult mice, the ventral dermis was only sparsely populated by FLP cells, although they remain abundant within the dorsal dermis (Figure 2.3C).

To further define when dermal FLP progenitors express *Foxd1* developmentally, a tamoxifen-inducible system was utilized to induce recombination at specific intervals and investigate down-stream evidence of recombination within the dorsal skin (Figure 2.4A). With the exception of tamoxifen injection from E5.5 to E6.5, injection at all other intervals yielded tdTomato positive FLP cells within the dorsal dermis at E14.5. A difference in the populations labelled between earlier (E7.5-8.5) and late (E10.5-11.5) tamoxifen injection was observed. More specifically, while recombined cells were identified throughout the developing dermis following earlier injection, later injection primarily labelled the most ventral cells in the developing dorsal dermis (Figure 2.4B).

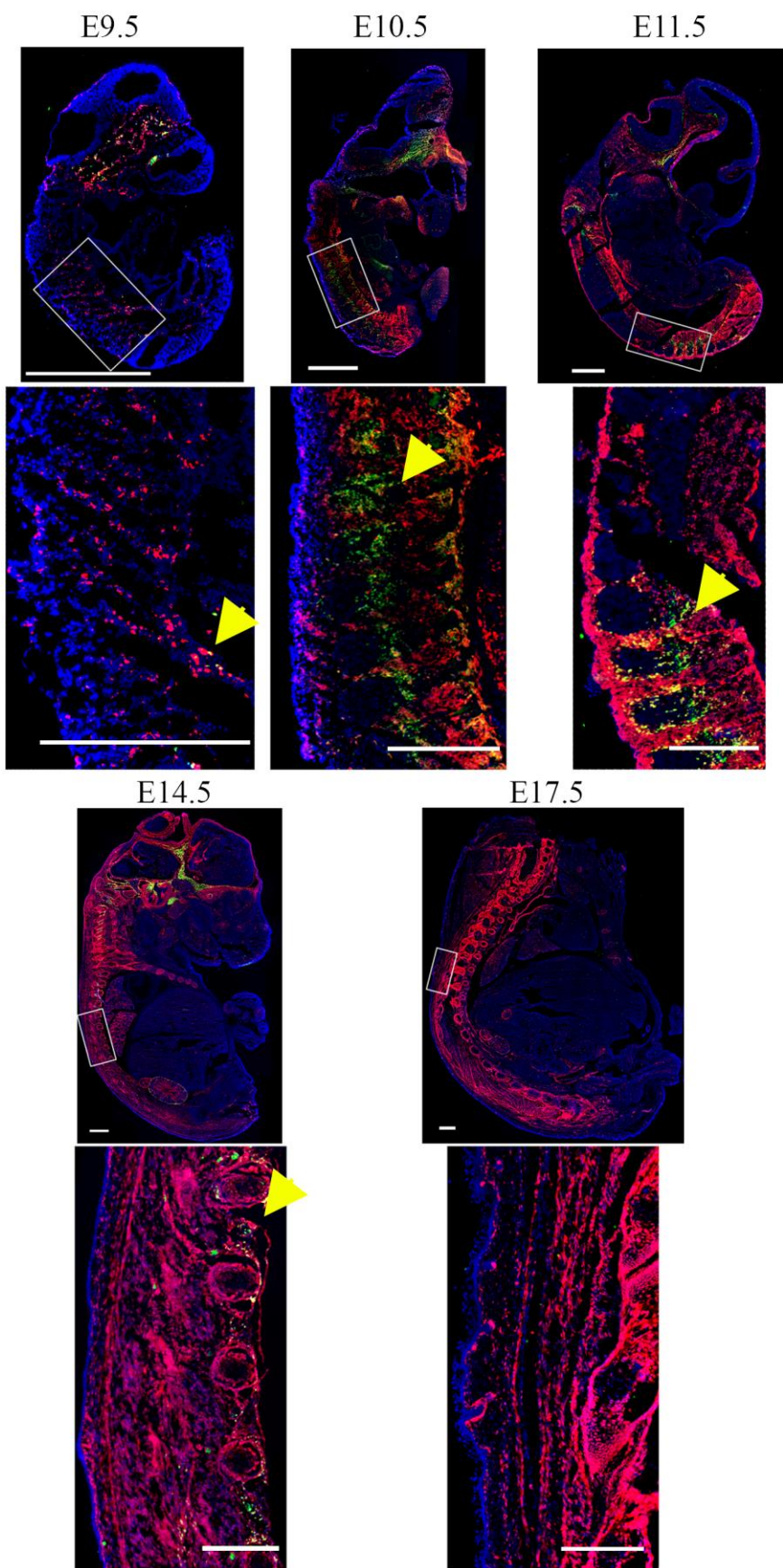


Figure 2.2: *Foxd1*-positive progenitor cells in the developing embryos contributed to FLP cells within the developing dermis. During development, *Foxd1-GFP-Cre* (green) was most highly expressed within the head and in the dorsal region, in proximity to the neural tube. FLP cells (red) contribute to a range of tissues within the embryo, including the dermis. Scale is 1 mm (full embryos). The indicated regions of interest are shown below. Yellow arrows indicate examples of GFP positive cells. Scale bar is 500 μ m.

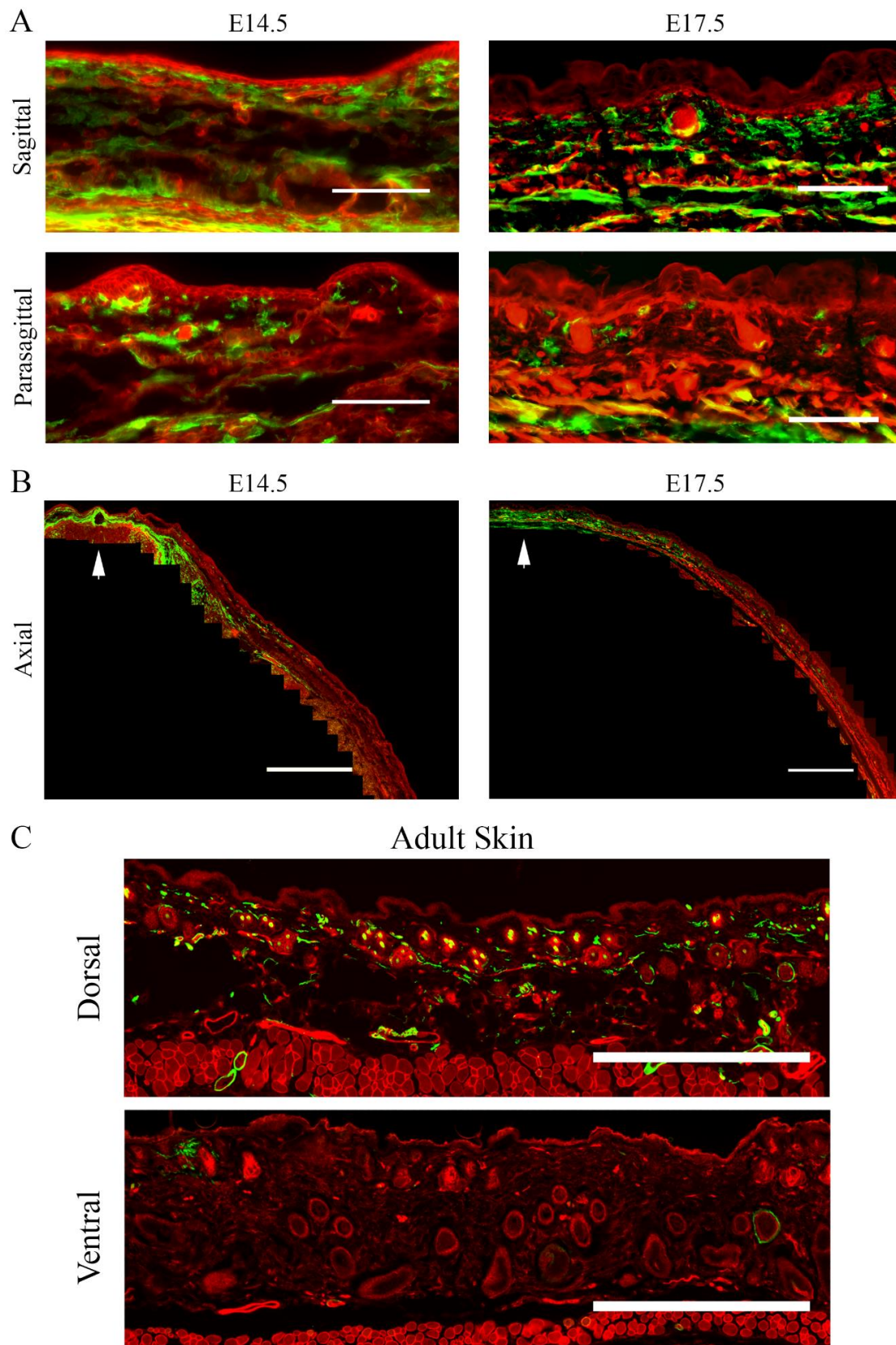


Figure 2.3: FLP cells were most abundant in the medial dorsal skin during development and were primarily localized to the dorsal skin of adult mice. *Foxd1^GC* mice were crossed with an *mTmG* reporter (model in Figure 2.1B) to investigate FLP (Green) and FLN (Red) contributions to skin during embryonic development and adulthood. (A) Sections taken along the sagittal plane were imaged, and those that contained the neural tube were stratified as sagittal sections, whereas those that did not were considered parasagittal. Scale bars are 200 μm . (B) Axial sections at E14.5 and E17.5 showing the dorsolateral quarter of the embryos highlight the contribution of FLP cells to the medial dorsal skin, with fewer cells dispersed laterally. The dorsal midline of the axial images is indicated by the arrow. Scale bar is 1 mm. (C) Isolated skin from adult mice shows minimal contribution of FLP cells to the ventral skin, although they remain abundant in dorsal skin. Scale is 1 mm. Representative images from 5 embryos are shown for sagittal sections, from 3 embryos for axial sections, and from 3 adult mice for the dorsal and ventral sections.

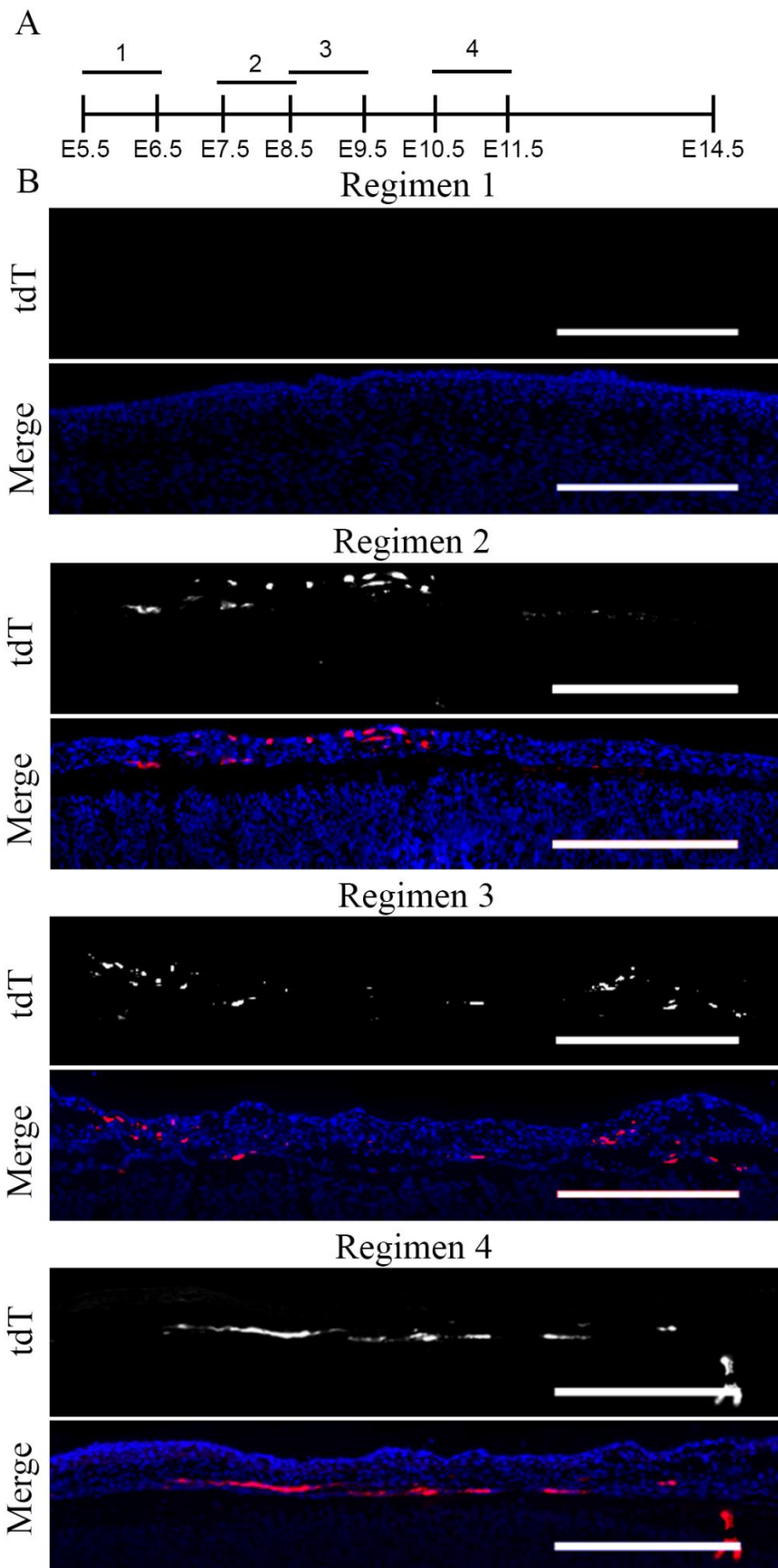


Figure 2.4: Dermal FLP progenitors expressed *Foxd1* from E7.5 to E11.5. (A) Using a *Foxd1*GCE/*Ai14* cross (Figure 2.1C), tamoxifen was injected at different intervals to determine when dermal FLP progenitors expressed *Foxd1* during development. (B) Injection at intervals ranging from E7.5 to E11.5 resulted in recombination, evident by the tdTomato positive cells present at E14.5. Scale bars are 500 μ m. A minimum of 3 embryos were observed for each injection regimen.

2.4.2 Foxd1-expressing cells are rare in postnatal tissue during homeostasis and following wounding

In adult skin, FLP cells were present throughout the dermis and hypodermis, and following wounding were observed in the granulation tissue (Figure 2.5A). To determine if postnatal expression of *Foxd1* was contributing to the FLP populations observed in these tissues, recombination in a tamoxifen inducible Cre model was investigated by crossing the *Foxd1^{GCE}* line with the *Ai14* reporter (Figure 2.1C). Using this system, tamoxifen was delivered to postnatal mice before and after wounding and a histological assessment of recombination was performed (Figure 2.5B). Low numbers of cells in the skin and granulation tissue expressed tdTomato (<0.1%, n=6). This was further supported using flow cytometry to detect GFP-Cre positive fibroblasts in healthy adult skin of *Foxd1^{GCE}/Ai14* mice, in which a mean frequency of 0.091% ($\pm 0.054\%$; n=7) of GFP positive fibroblasts was measured. Combined with the expression patterns observed during embryogenesis, these data suggest that the FLP cells present within the dermis were primarily derived from embryonic precursors that expressed *Foxd1*, and that *de novo* expression of *Foxd1* in postnatal dermis during homeostasis and wound healing was minimal.

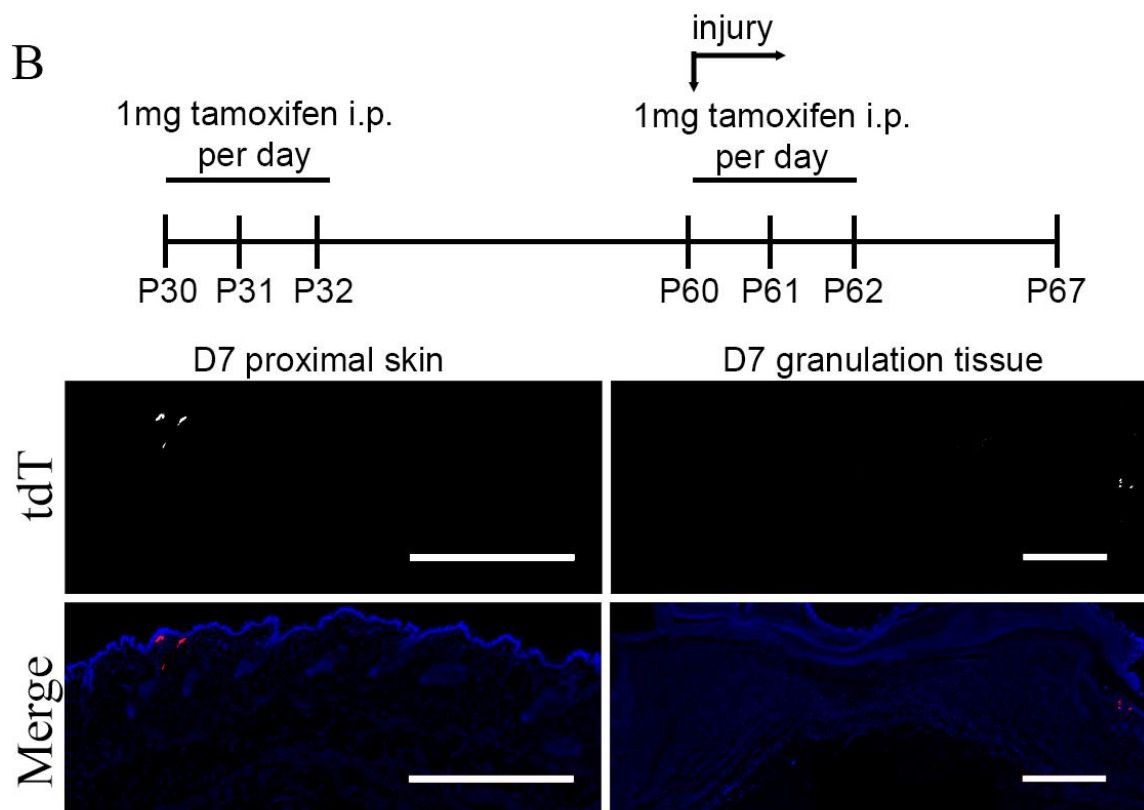
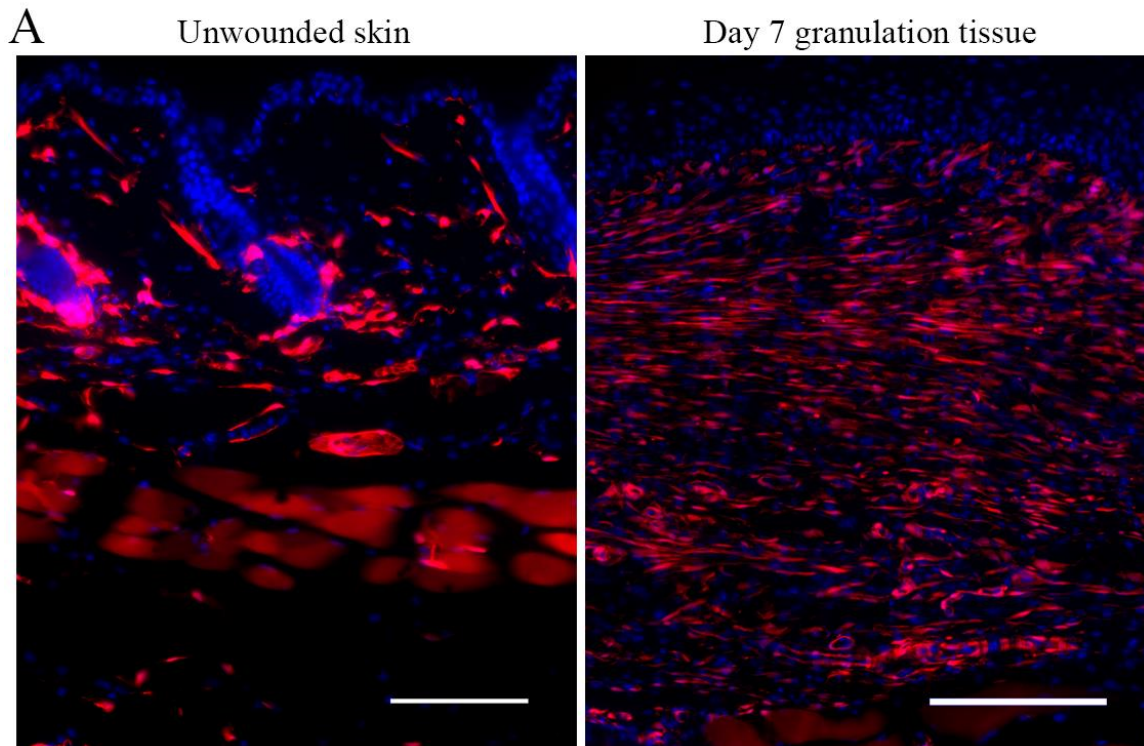


Figure 2.5: FLP populations in adult skin and granulation tissue were not derived from de novo *Foxd1* expression in postnatal tissue. (A) In constitutively active *Foxd1^GC/Ai14* mice, FLP cells (tdTomato positive) are observed throughout the skin and granulation tissue. (B) In a tamoxifen inducible model utilizing the *Foxd1^GCE/Ai14* cross, tamoxifen injection into postnatal tissue resulted in a low level of recombination, resulting in few tdTomato positive cells. (Scale bars are 1 mm). Postnatal injection of tamoxifen was performed in 6 mice.

2.4.3 Foxd1 lineage-positive cells contributed to diverse populations in adult skin

To characterize the differentiated populations represented by the *Foxd1* lineage, the constitutively active *Foxd1*IGC line crossed to the *Ail4* reporter was assessed (schematic shown in Figure 2.1A). Within the dorsal skin, it was evident from histological examination that *Foxd1* derived populations were present throughout the dermis and even within the panniculus carnosus muscle (Figure 2.5A). To determine more specifically which populations these cells were contributing to within the dermis, adult mouse skin was labeled with several markers expressed in fibroblasts (vimentin, PDGFR α , PDGFR β , and CD26), the endothelial marker CD31, and the smooth muscle and myofibroblast marker α SMA. All of the fibroblast markers explored overlapped with tdTomato expression, however tdTomato negative populations were also noted to label for these markers (Figure 2.6). Minimal overlap between tdTomato and CD31 was observed, suggesting that FLP cells were not a major contributor to the endothelial population. Co-labelling with α SMA highlighted the contribution of FLP cells to arrector pili muscles as well as some of the perivascular α SMA-expressing populations. Furthermore, FLP cells were observed in the dermal sheath population surrounding hair follicles (Figure 2.6, yellow arrows).

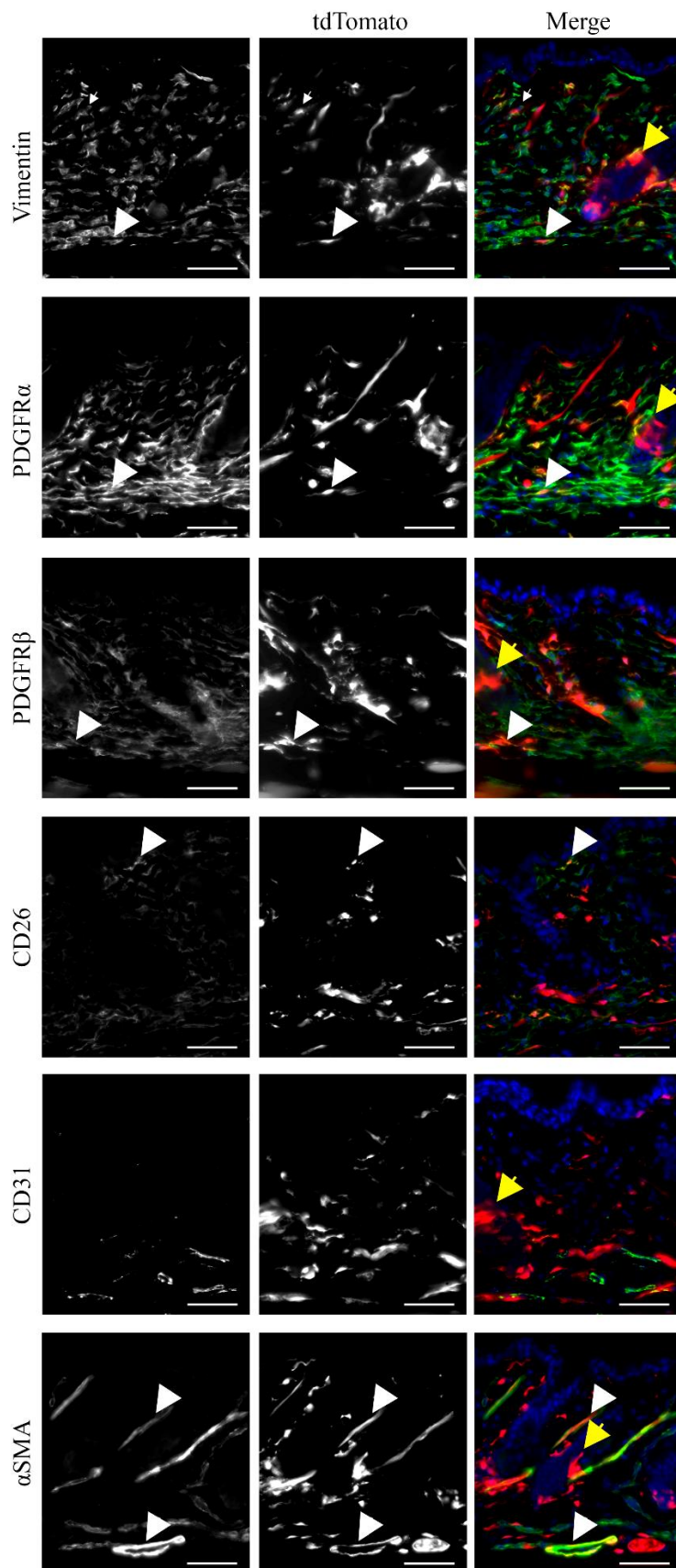


Figure 2.6: *Foxd1*-positive progenitors gave rise to fibroblast, perivascular, and arrector pili populations within the adult skin. Unwounded tissue was isolated from mice expressing *Foxd1^{IGC}* and *Ai14* alleles. Merged images show tdTomato (FLP) in red and nuclei are labelled with DAPI in blue. Scale is 100 μ m. Representative images are shown from 3 mice. White arrows indicate representative cells with dual labeling; yellow arrows highlight FLP populations associated with hair follicles.

2.4.4 Foxd1 lineage-positive populations contributed to myofibroblasts during wound repair

Next, the contribution of FLP cells to wound healing was investigated using a splinted wound model in constitutively active *Foxd1^{IGC}/Ai14* mice (Schematic in Figure 2.1A). At 3 days post wounding, sparse FLP cells were evident throughout the wound bed, with a qualitatively higher density observed at the wound edges (Figure 2.7). The density of FLP cells within the wound qualitatively increased by 7 days post wounding and again at 10 days post wounding, remaining relatively consistent up to the final time point of 21 days post wounding. The FLP cells within the wound tissue contributed to the stromal population, as shown by overlap with vimentin, PDGFR α , PDGFR β , and CD26, as well as contributing to the α SMA positive myofibroblast population at day 3 and 10 post wounding (Figure 2.8 for day 3; Figure 2.9 for day 10). However, it was evident that the FLP population only gave rise to a subset of these populations, with FLN cells also contributing. Again, overlap with CD31 was minimal, supporting that this lineage was not a major contributor to endothelial cells in the dermis.

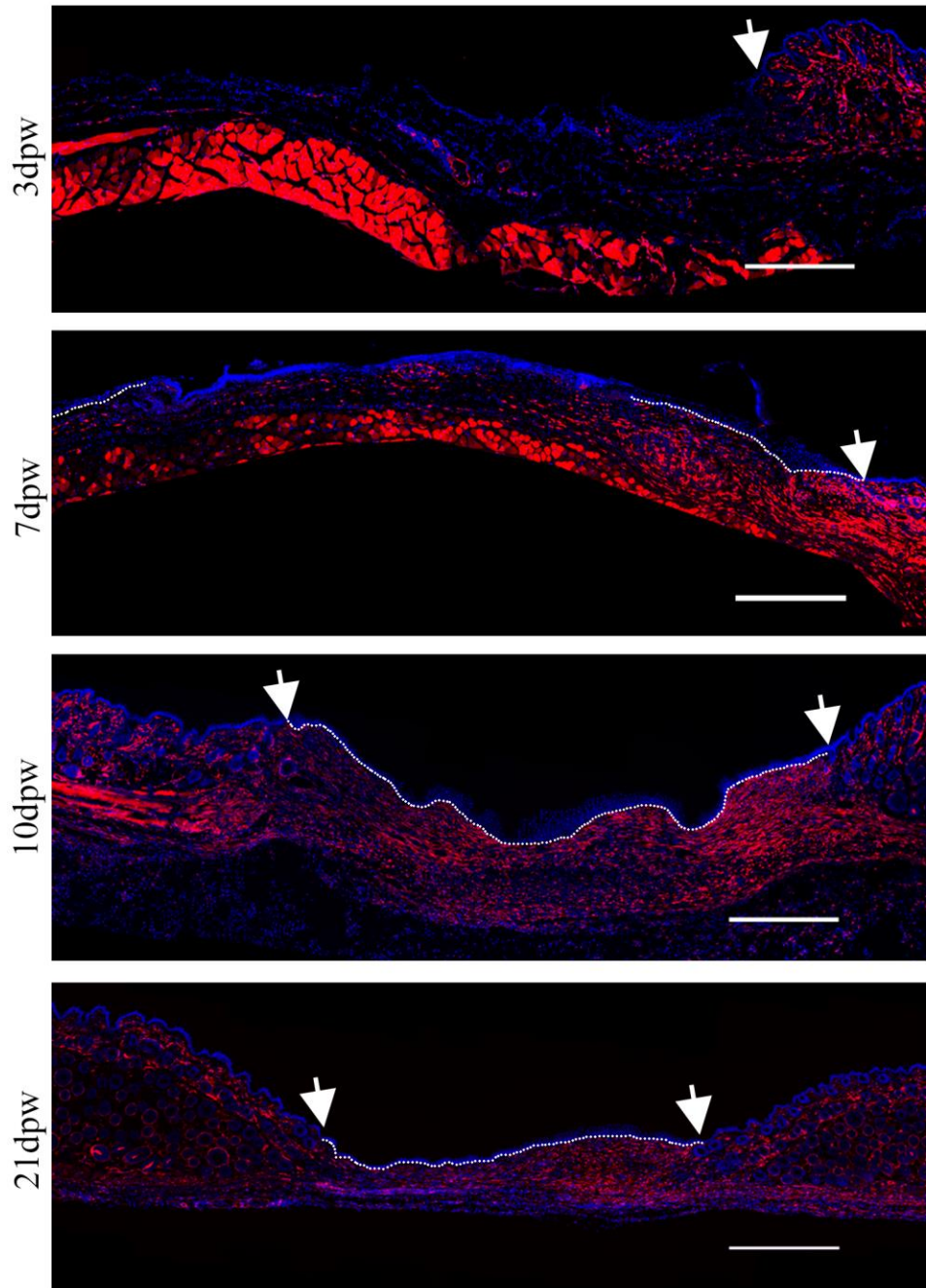


Figure 2.7:FLP cells contributed to the myofibroblast population during wound repair. FLP cells (tdTomato positive) began to appear at 3 days post wounding (dpw) at the wound edge (indicated with arrows) and increase in density over time to 10 days post wounding, remaining up to 21 days post wounding. Lines indicate the granulation tissue-epidermal junction. scale bar is 1 mm; n=3-4 mice per time point.

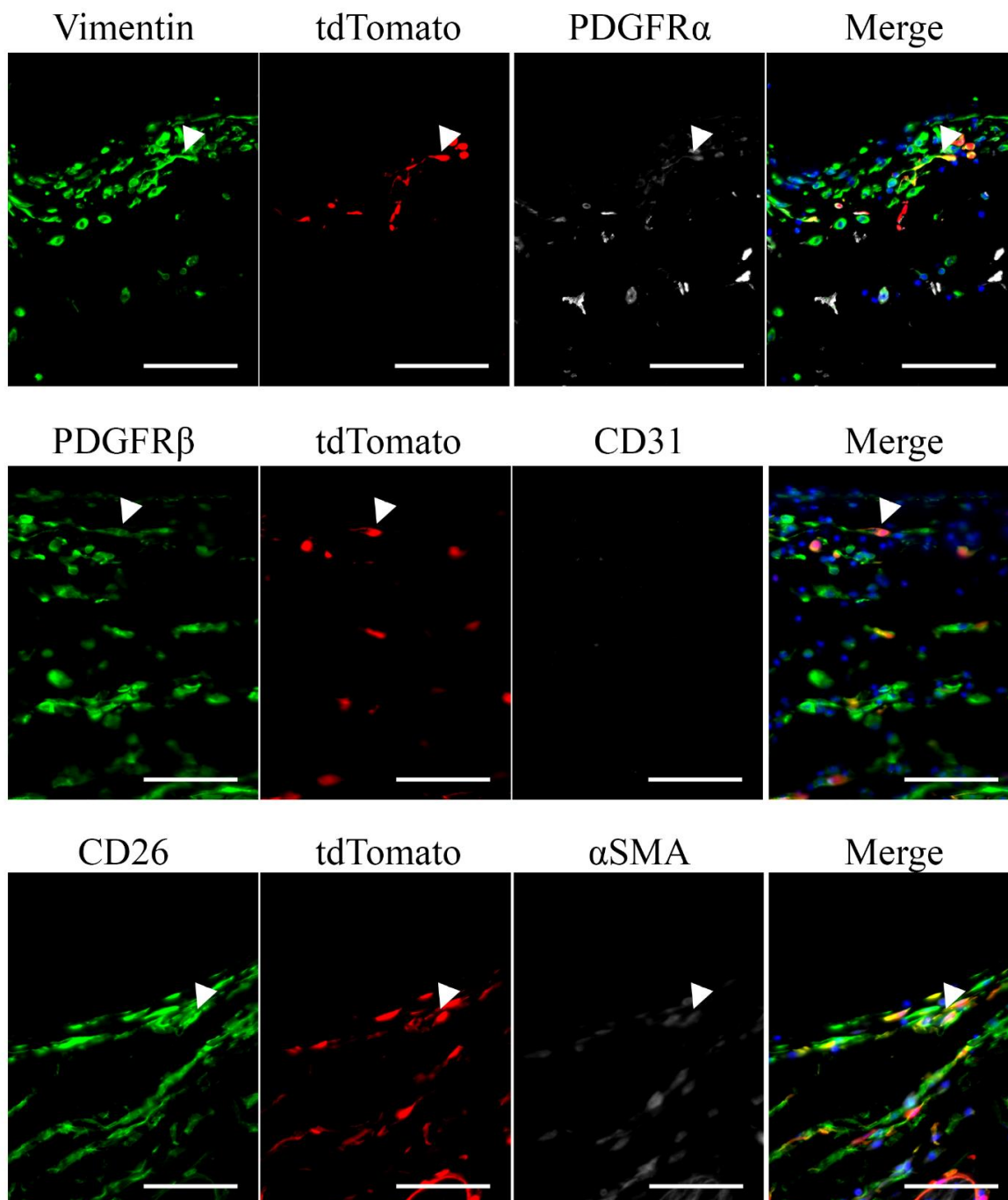


Figure 2.8: FLP cells within day-3 granulation tissue co-labelled with fibroblast markers. Arrows indicate points of interest, highlighting overlap with fibroblast markers and FLP cells (tdTomato positive). CD31 positive endothelial cells were not present beyond the edges of the wound at this time. Nuclei are stained with DAPI (blue). Scale bars are 100 μ m. Representative images are shown from a sample of 3 mice.

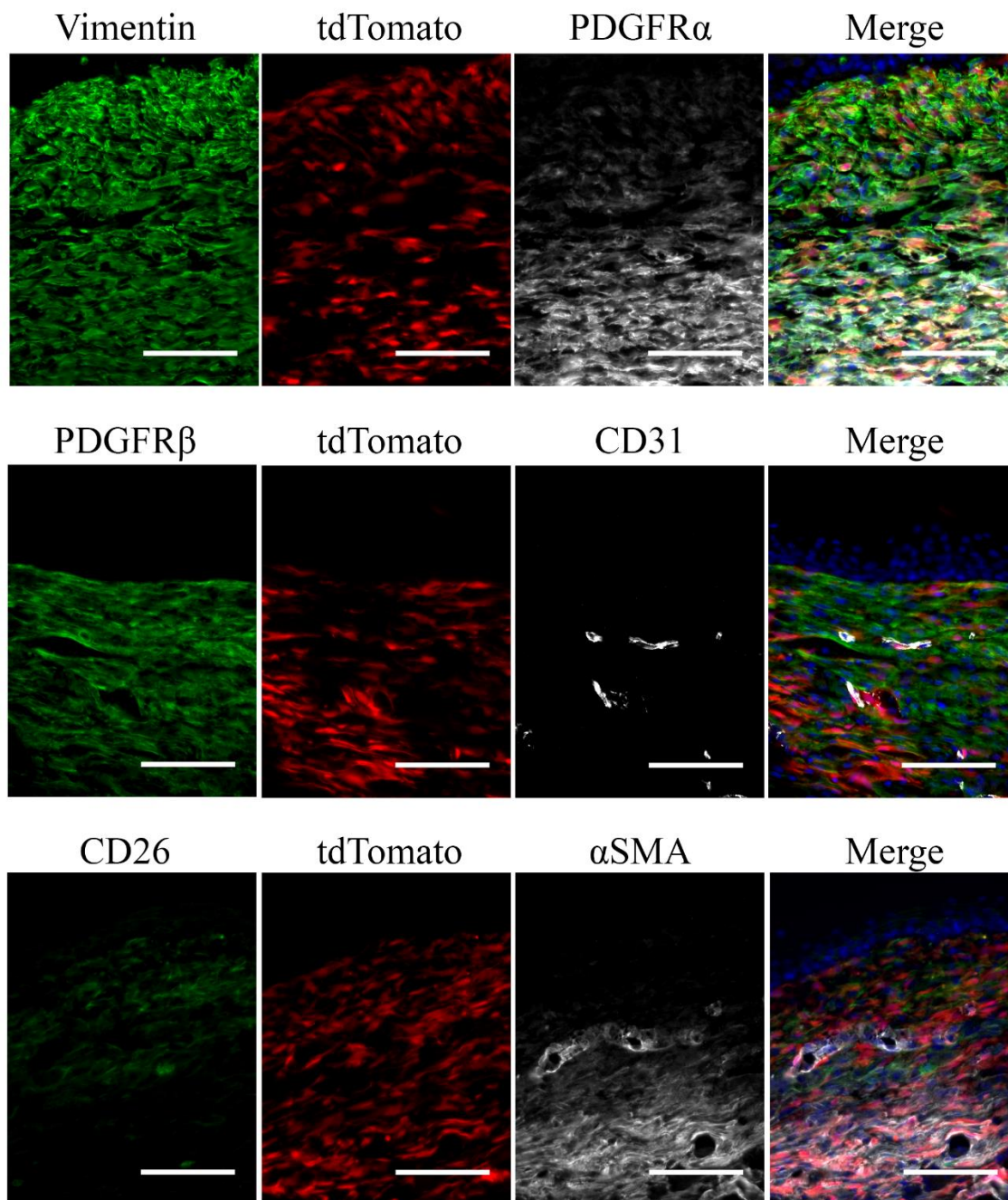


Figure 2.9: FLP cells within day-10 granulation tissue co-labelled with fibroblast markers. FLP cells (tdTomato positive) overlap with staining for fibroblast (vimentin, PDGFR α , PDGFR β , CD26) and myofibroblast (α SMA) markers within the granulation tissue. Nuclei are stained with DAPI (blue). Scale bars are 100 μ m. Representative images are shown from a sample of 4 mice.

2.4.5 Foxd1 lineage-positive fibroblasts displayed divergent fibrosis-related gene expression patterns during homeostasis and wound repair

Next, whether the *Foxd1* lineage was associated with functional differences within the fibroblast population during homeostasis and following wounding was explored using gene expression arrays. Wound tissue and unwounded skin surrounding the wound was isolated from constitutively active *Foxd1*^{G/C}/*Ai14* mice 10 days following wounding. Using FACS, a negative selection approach was taken, removing cells positive for EpCAM, CD45, or CD31, thereby enriching for the fibroblast population (Figure 2.10A). Notably, some of the cells excluded using this strategy did express tdTomato and thus could represent epithelial or endothelial populations that were not frequently observed histologically. Alternatively, these could represent bone marrow derived populations. The fibroblast enriched populations were then sorted into FLP and FLN populations based on their expression of tdTomato. No differences in distribution of FLP fibroblasts were evident between wounded and unwounded populations (60.0±9.7 vs. 54.1±8.5% FLP positive in wounded and unwounded, respectively; $p > 0.05$). However, a modest increase in FLP fibroblast number was observed in the wounded tissue when compared to naïve healthy dorsal skin (60.0±9.7% vs. 49.6±6.8; $p < 0.05$).

From these populations, the RNA was isolated and gene expression was assessed using a PCR array for a pre-selected set of fibrosis related genes. The following genes were not consistently detected in any group and were removed from further analysis: *Ccl12*, *Ccr2*, *Fasl*, *Ifng*, *Il13*, *Il4*, *Il5*, *Inhbe*, *Plg*, and *Serpina1a*. Gene expression data was compared between lineages within tissue status (i.e. FLP wounded vs. FLN wounded) and between tissue status within lineages (i.e. FLP wounded vs FLP unwounded) and differentially

expressed genes were selected using a false discovery rate of 10% (Figure 2.10C-D, Figure 2.11). For a complete list of comparisons see Appendix Table A1-A4. Interestingly, a difference in transcripts enriched in the FLP fibroblasts versus those enriched in FLN fibroblasts was noted. More specifically, transcripts associated with matrix production and remodeling, including *lox*, *serpinh1*, *col3a1*, *dcn*, *mmp3*, and *mmp14* were enriched in the FLP population. In contrast, the FLN population was enriched in transcripts associated with cell signaling, and matrix interaction including several integrins, surface receptors, and cytokines.

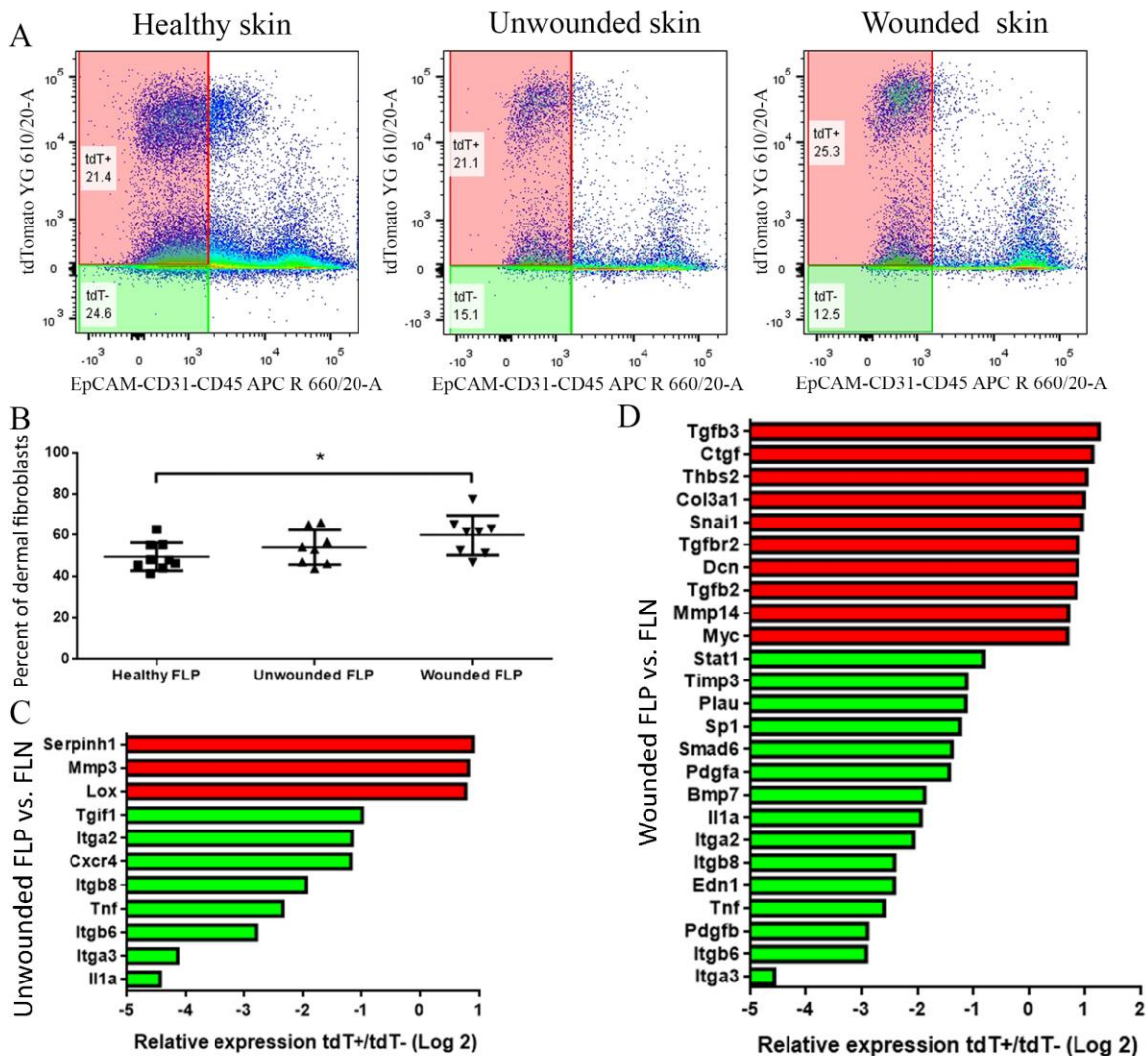


Figure 2.10: FLP fibroblasts and FLN fibroblasts contributed differentially to skin homeostasis and wound repair. (A) Fibroblasts were isolated from dorsal wounded and unwounded skin from mice 10 days post wounding (n= 8 mice) and from healthy naïve skin (n= 9 isolations; 4-6 mice per isolation) and enriched by FACS. Data were analyzed with linear mixed effects models; *p<0.05. (B) The frequency of FLP fibroblast populations within wounded and unwounded tissue was compared to that of fibroblasts isolated from naïve unwounded animals. (C and D) Isolated RNA from wounded and unwounded dermal fibroblasts was compared using a Qiagen RT² Profiler array, and transcripts significantly enriched in either FLP or FLN populations are shown. Red bars represent transcripts enriched in the tdTomato-positive FLP population, and green bars represent those enriched in the tdTomato-negative FLN population. Data were analyzed by multiple t-tests and were controlled for multiple comparisons using a false discovery rate correction of 10%.

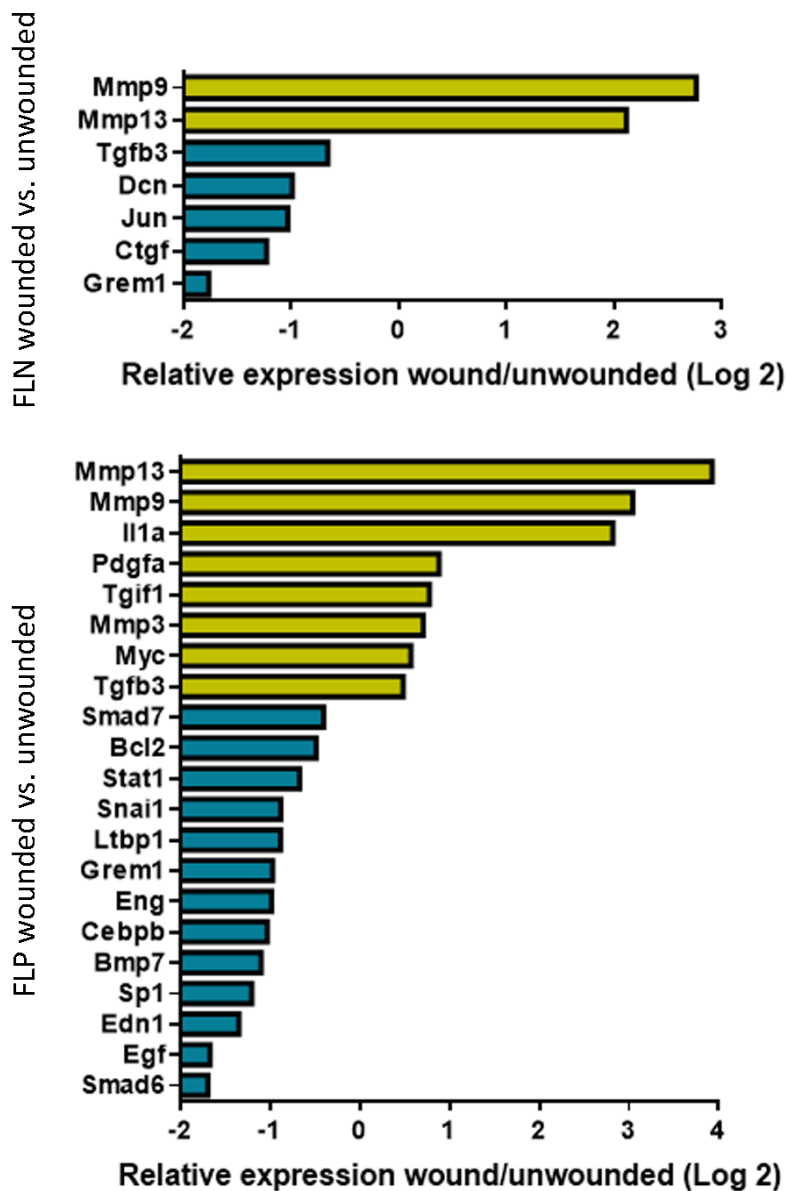


Figure 2.11: Gene expression was differentially regulated within cell lineage between wounded and unwounded tissue. Isolated RNA from FLP (tdTomato-positive) and FLN (tdTomato-negative) dermal fibroblasts was compared using a Qiagen RT² Profiler array, and transcripts significantly enriched in either wounded or unwounded populations are shown. Yellow bars represent transcripts enriched in the wound population, and blue bars represent those enriched in the unwounded population. Data were analyzed by multiple t-tests and were controlled for multiple comparisons using a false discovery rate correction of 10%.

2.4.6 Fibroblast lineage specific differences were not maintained in culture

To determine whether these populations could be further investigated in a controlled culture environment, the effect of culturing on gene expression patterns in cells derived from healthy, naïve dermis was explored. Using a type I collagen gel as a compliant 3-dimensional culture substrate, mRNA levels of a selection of candidate genes identified on the array were assessed in FACS-sorted naïve, healthy dorsal dermal fibroblasts directly following isolation, and again after 1 week in culture in the presence or absence of TGF β 1 (Figure 2.12). The data were analyzed using a linear mixed effects model to assess the significance of cell lineage (FLP vs. FLN) and treatment (freshly isolated; cultured without TGF β 1; cultured with TGF β 1) as predictors of gene expression. Importantly, in this model, cell lineage was determined to be a significant factor in the expression of *colla1*, *itga2*, and *itgb8* in the freshly-isolated cell populations ($p < 0.05$), whereas cell treatment was a significant factor for the expression of all genes. Notably, relative expression differences were smaller in these naïve fibroblasts versus those isolated from the wound and unwounded tissues. Moreover, for the markers explored, no differences were noted between the FLP and FLN lineages following 1 week of culture under the conditions in the current study.

2.4.7 Foxd1 lineage-positive fibroblasts did not mimic expression patterns of previously defined lineages

In addition to assessing these genes above, the expression of a set of markers that have been previously shown to define subsets of fibroblasts within the skin was measured. Driskell *et al.* (2013) defined subsets of fibroblasts based on their position within the skin, using differential protein expression of Dlk1 and CD26 (gene: *Dpp4*) (Driskell *et al.*

2013). It has since been confirmed by Philippeos *et al.* (2018), that the gene expression of these markers correlates with their protein expression (Philippeos *et al.* 2018). Furthermore, the *Engrailed-1* positive progenitor derived population defined by Rinkevich *et al.* (2015), was enriched in CD26 protein. In humans, expression of *DPP4* was observed to be a defining characteristic of one of two major subsets of dermal fibroblasts by single-cell RNA sequencing analysis (Tabib *et al.* 2018). PDGFR α and CD90 (Thy1), have been reported to be widely expressed in dermal fibroblast populations, and not differentially expressed in previously-investigated dermal fibroblast lineages (Driskell *et al.* 2013; Rinkevich *et al.* 2015; Philippeos *et al.* 2018). To determine how FLP and FLN cells related to these predefined fibroblast subsets, these genes were assessed in FLP and FLN fibroblast populations (Figure 2.13). Notably, cell lineage did not affect the expression of any of these genes in freshly isolated dermal fibroblasts or following 7 days in culture, but as with the functional markers assessed above, all of these genes were significantly affected by cell culture. Specifically, *Dlk1*, *Pdgfra*, and *Thy1* expression were increased in culture, whereas *Dpp4* expression was decreased.

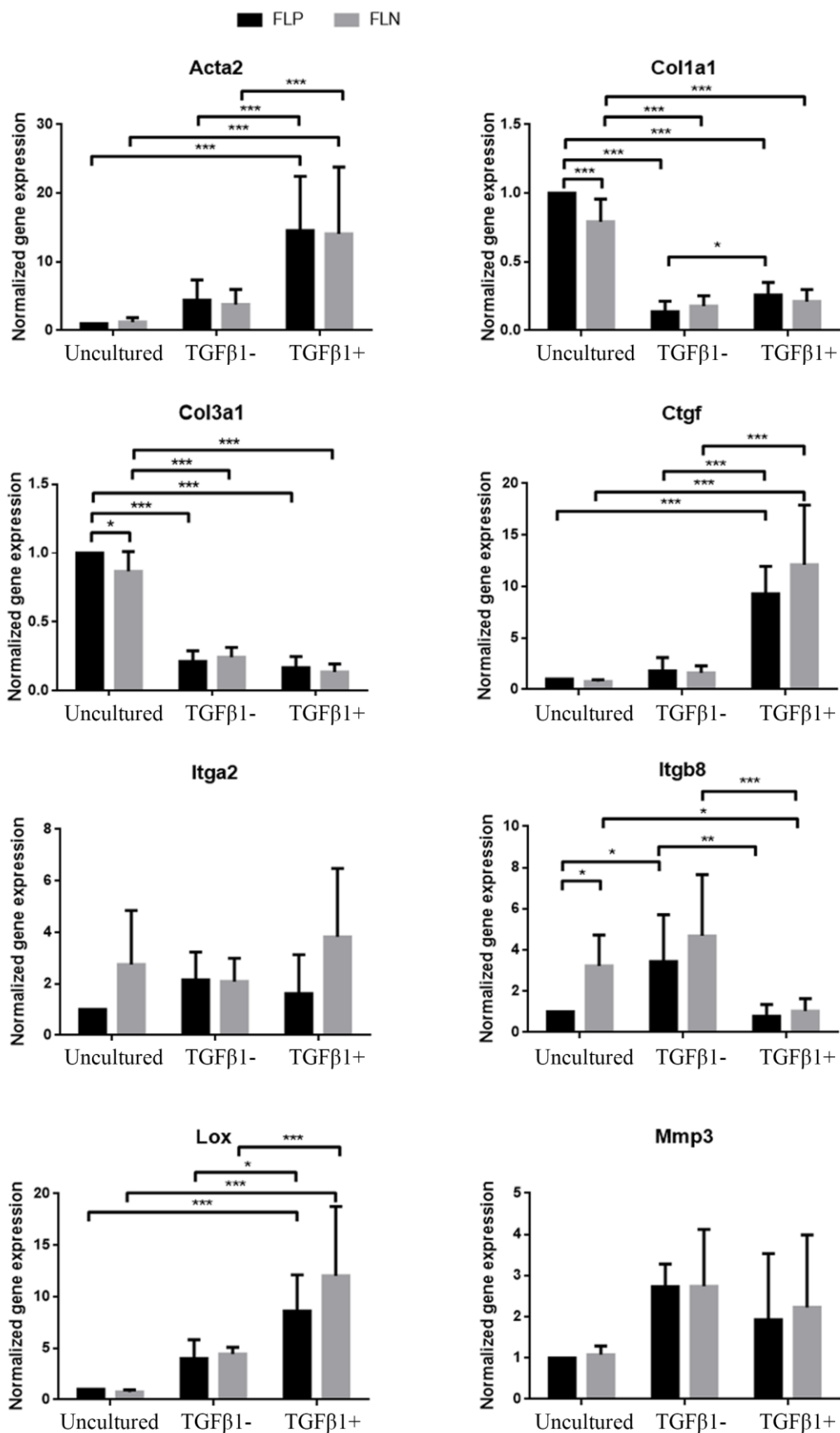


Figure 2.12: Gene expression in FLP and FLN fibroblasts was altered in vitro.

Quantitative PCR was used to assess gene expression in FLP and FLN fibroblasts isolated from naïve healthy dorsal skin and following culture on 2 mg/mL type I collagen gels with or without treatment with 5 ng/mL TGF β 1 for 1 week. 18S rRNA was used as a control. Dorsal skin was pooled from 4-6 mice for each isolation; n=6 independent cell isolations. Data were analyzed with linear mixed effects models; * p <0.05; ** p <0.01; *** p<0.001.

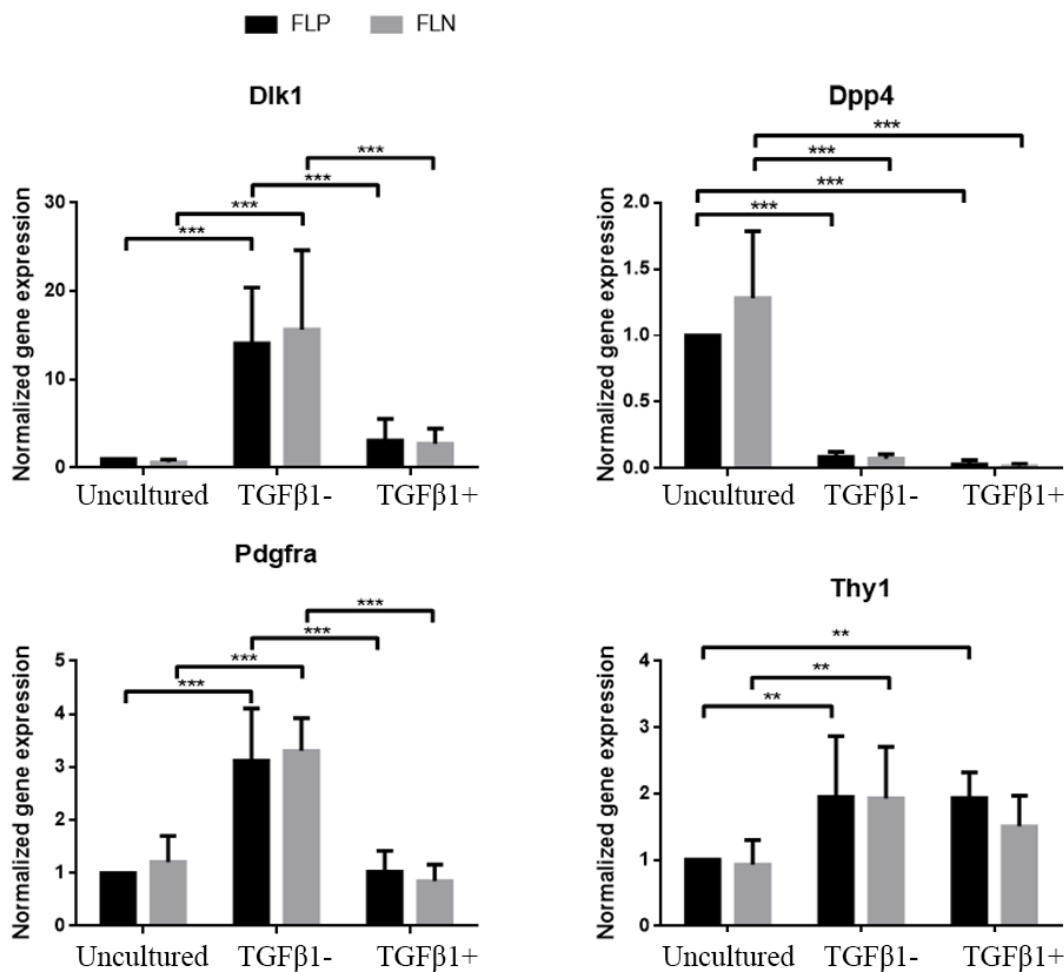


Figure 2.13: Stratification of fibroblasts by *Foxd1* lineage did not directly overlap with previously characterized dermal fibroblast lineages. Quantitative PCR was used to assess gene expression in FLP and FLN fibroblasts isolated from naïve healthy dorsal skin and following culture on 2 mg/mL type I collagen gels with or without treatment with 5 ng/mL TGFβ1. 18S rRNA was used as a control. Dorsal skin was pooled from 4-6 mice for each isolation; n=6 independent cell isolations. Data were analyzed with linear mixed effects models; ** p < 0.01; *** p < 0.001.

2.4.8 High expression of integrins $\alpha 2$ and $\alpha 3$ was associated with the FLN population

Although many of the differentially expressed genes code for secreted proteins, several integrins were expressed at higher levels in the FLN fibroblasts. As these proteins are important mediators of cell-matrix interactions (Koivisto et al. 2014), it was hypothesized that differential expression may be at the forefront of lineage differences during homeostasis and wound repair. To assess whether these proteins would be useful markers and could provide a potential mechanism for the functional diversity of these two lineages, their distribution was explored histologically in excisional wounds at 10 days after wounding. To visualize both the FLP and FLN populations, a cross between *Foxd1^GC* and *mTmG* reporter mice was assessed (schematic shown in Figure 2.1B). Labelling for integrins $\alpha 2$, $\alpha 3$, αV , $\beta 1$, and $\beta 6$ showed that they were widely distributed throughout the granulation tissue and expressed in both FLP and FLN cells (Figure 2.14 and 2.16). Using these images, a binary threshold to show only the highest level of staining within the stromal tissue was set (Figure 2.15 and 2.17). Interestingly with this gating, low levels of overlap between FLP (GFP⁺) cells and high $\alpha 2$, $\alpha 3$ and $\beta 6$ integrin expression were noted, whereas overlap was more prominent for $\beta 1$, and αV integrin. However, it should be noted that the antibody used to detect $\beta 6$ integrin has been described to have cross-reactivity with murine $\beta 1$, $\beta 2$, and $\beta 3$ integrins. Therefore, the observed immuno-labelling may not be specific to $\beta 6$ integrin, requiring further exploration.

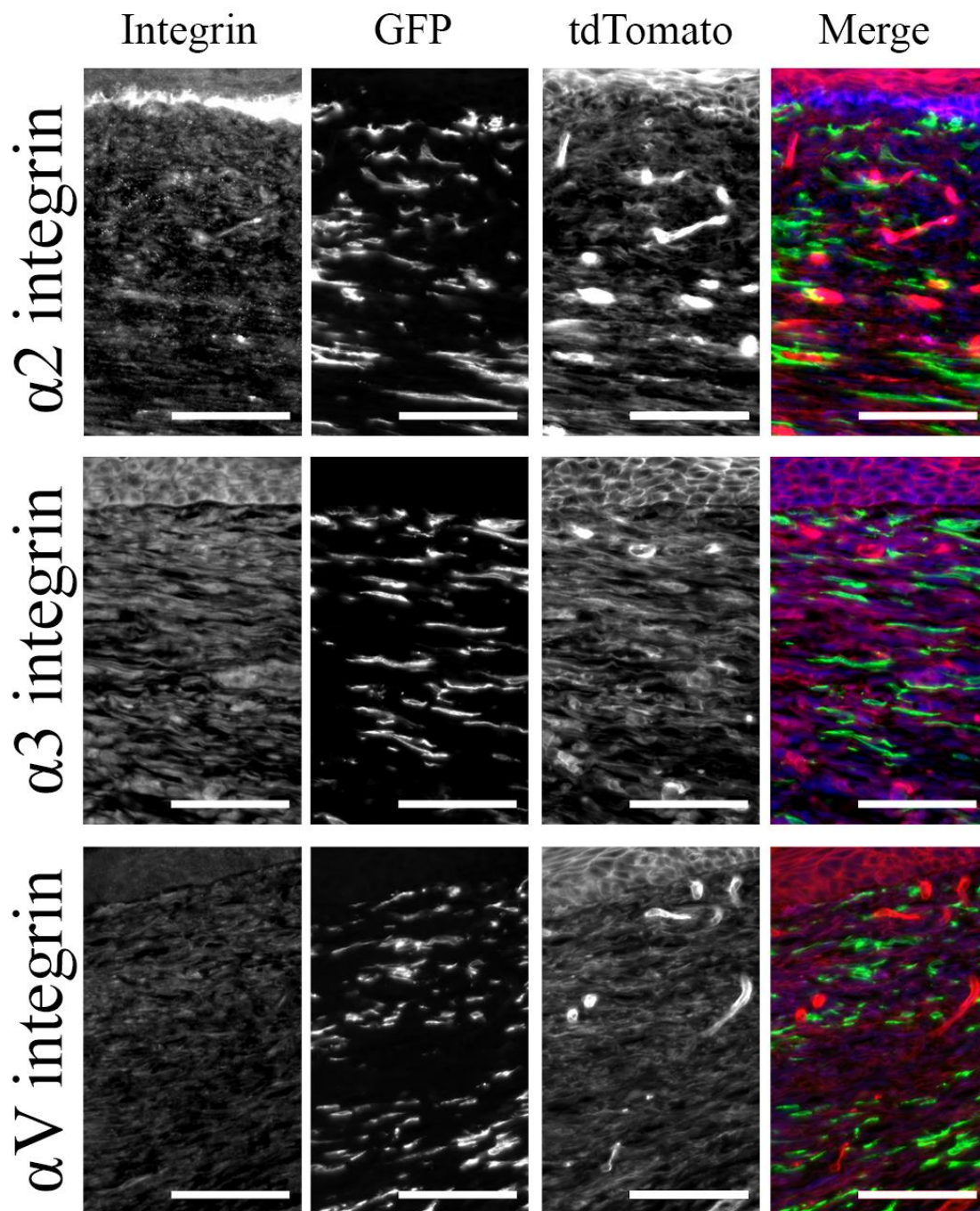


Figure 2.14: $\alpha 2$, $\alpha 3$, and αV integrin expression in FLP and FLN cells within the granulation tissue at day 10 post wounding. Isolated wound tissue from *Foxd1GC/mTmG* mice was cryopreserved and sectioned to 8 μm thickness. Samples were fluorescently labelled for integrins (blue) and compared to endogenous fluorescent proteins in FLP (green) and FLN (red) populations. Scale bar is 100 μm .

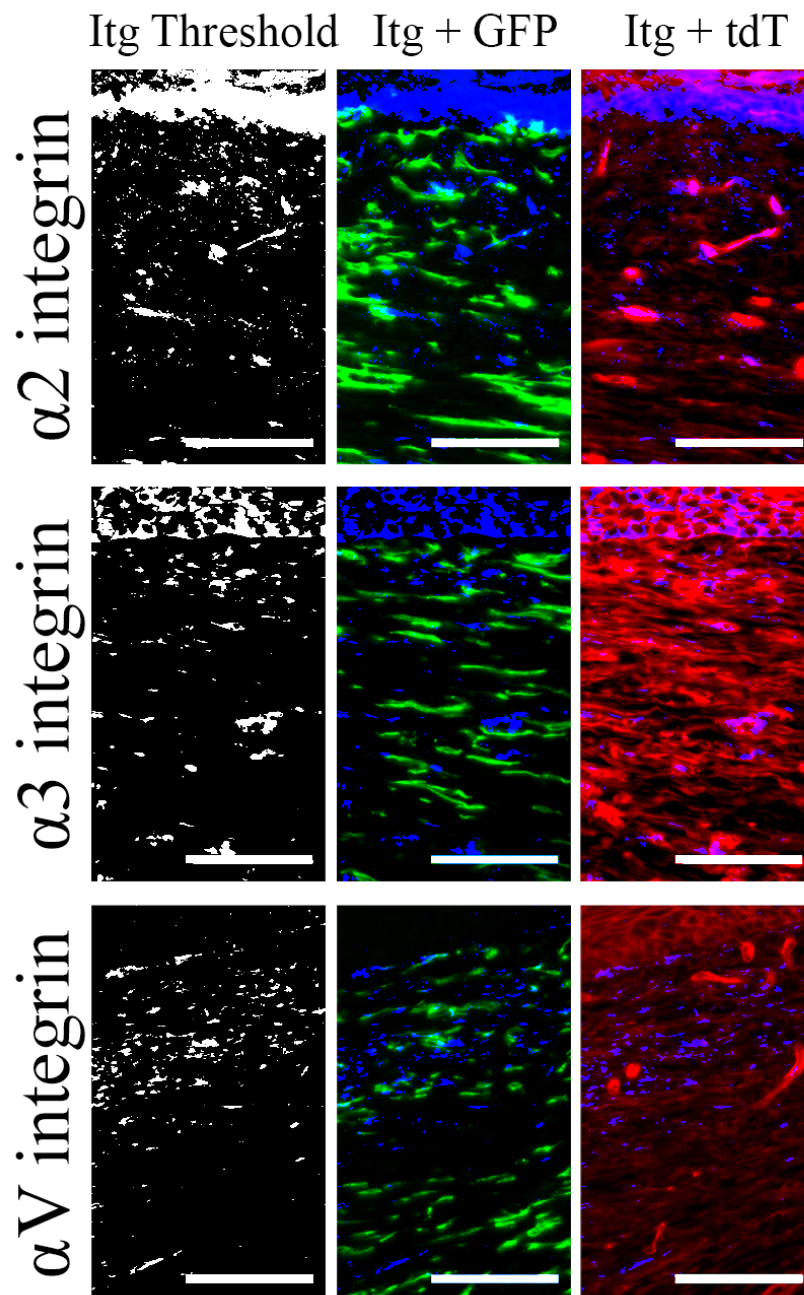


Figure 2.15: Binary Thresholding of $\alpha 2$, $\alpha 3$, αV integrins. High expression of alpha-integrins was observed by setting a binary threshold on staining in Figure 2.14 to select for pixels with the highest intensity within the granulation tissue. Thresholding of these integrins (blue) resulted in qualitatively low levels of overlap between integrins $\alpha 2$ or $\alpha 3$ and FLP cells (green). FLN cells are shown in red. Representative images are shown from a sample of 6 mice. Scale bar is 100 μm .

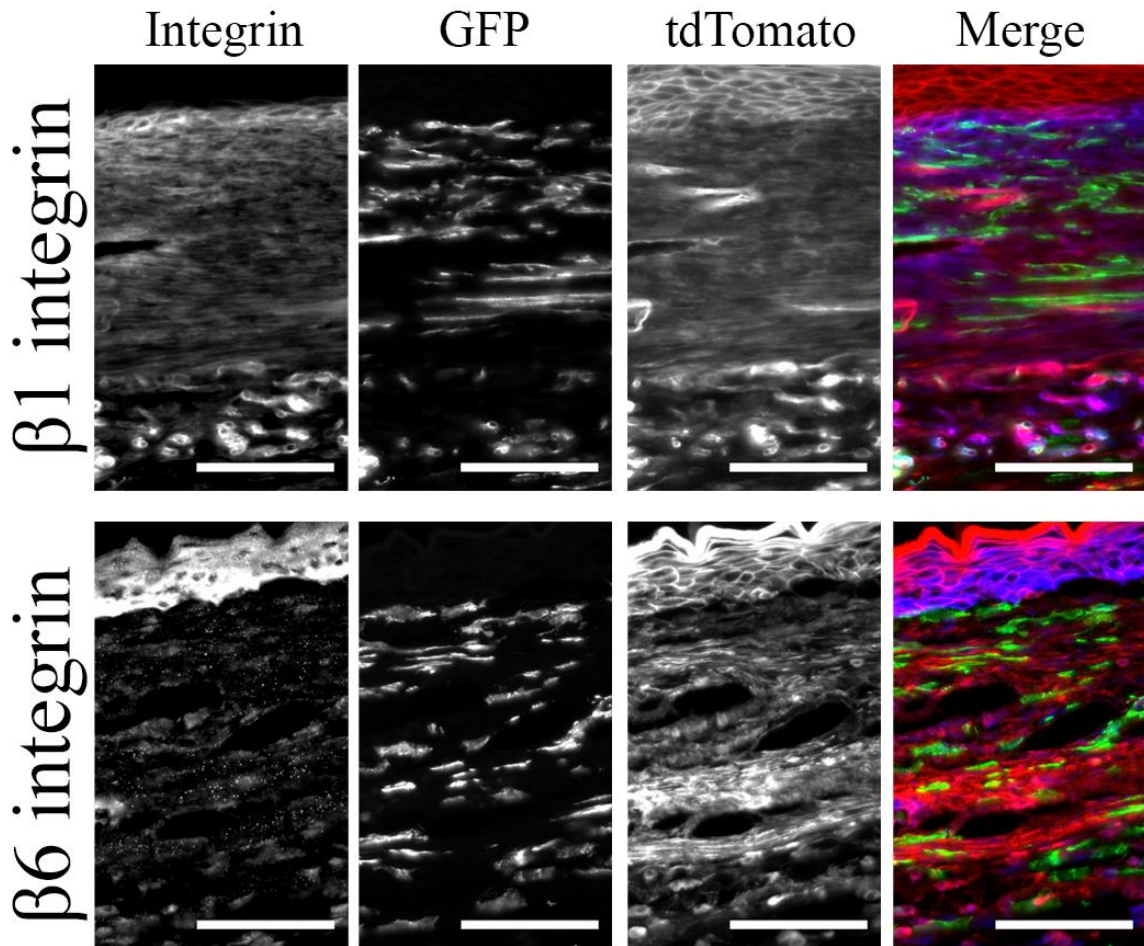


Figure 2.16: $\beta 1$ and $\beta 6$ integrin expression in FLP and FLN cells within the granulation tissue at day 10 post wounding. Isolated wound tissue from *Foxd1GC/mTmG* mice was cryopreserved and sectioned to 8 μm thickness. Samples were fluorescently labelled for integrins (blue) and compared to endogenous fluorescent proteins in FLP (green) and FLN (red) populations. Scale bar is 100 μm .

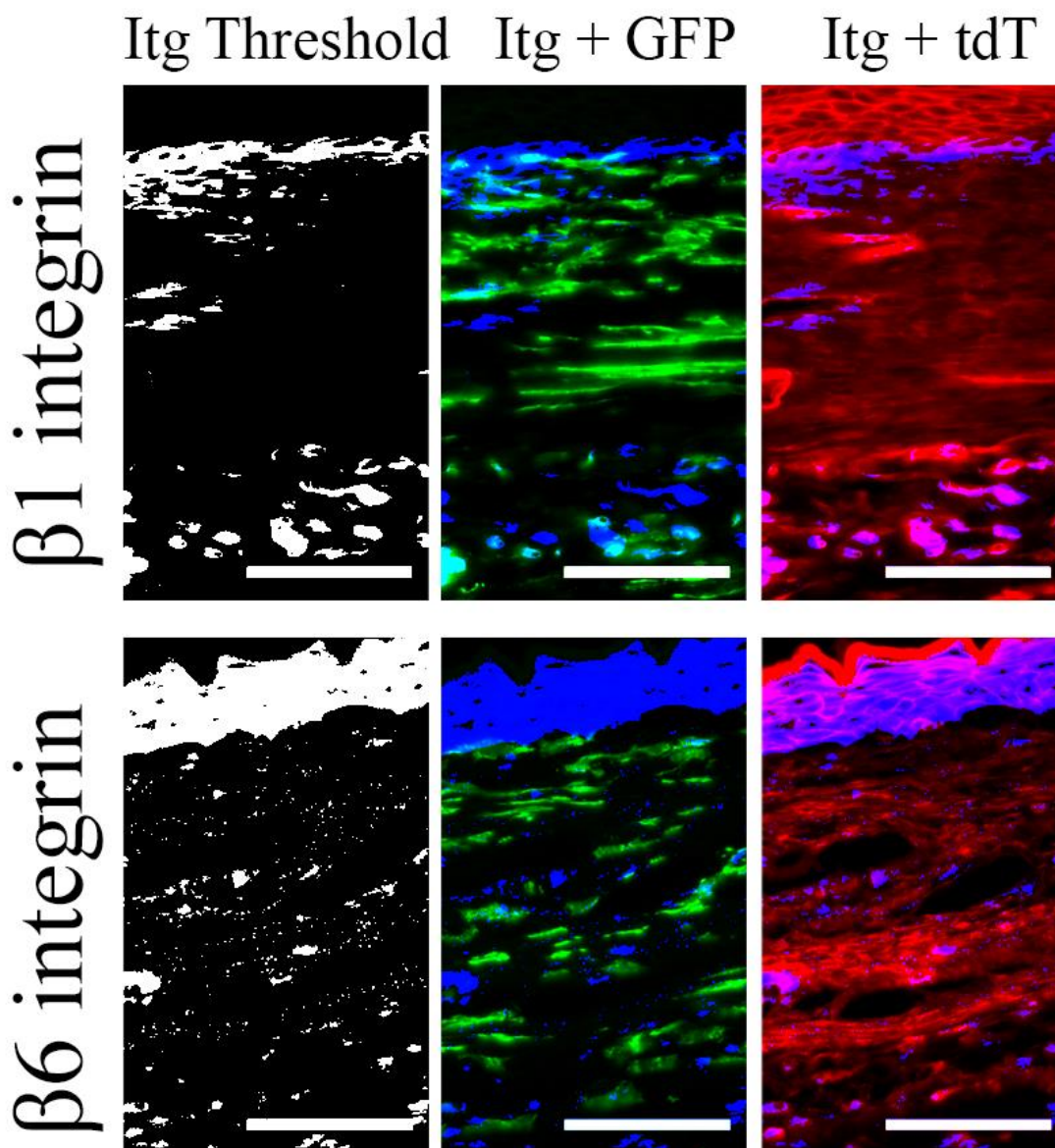


Figure 2.17: Binary Thresholding of $\beta 1$ and $\beta 6$ integrins. High expression of beta-integrins was observed by setting a binary threshold on staining in Figure 2.16 to select for pixels with the highest intensity within the granulation tissue. Thresholding of these integrins (blue) resulted in qualitatively low levels of overlap between integrin $\beta 6$ and FLP cells (green). FLN cells are shown in red. Representative images are shown from a sample of 6 mice. Scale bar is 100 μm .

2.5 Discussion

Using a lineage tracing approach, embryonic progenitors that differentially expressed *Foxd1* were investigated and found to give rise to fibroblasts in adult tissue that maintained differences. Although the hypothesis that fibroblasts differentiate into stable populations with divergent functions has been previously described (Phipps et al. 1989; McIntosh et al. 1994), these data support more recent studies showing that these different populations arise from unique expression patterns during development (Driskell et al. 2013; Rinkevich et al. 2015).

The FLP population described here does not appear to directly overlap with previously-described embryonic lineages. The *Engrailed-1* lineage described in adult mice by Rinkevich *et al.* (2015) and during development by Jiang *et al.* (2018), has some similarities with the *Foxd1* lineage, but also exhibits differences. Similar to what was observed in the *Foxd1* lineage, Jiang *et al.* described a developmental migratory pattern in which progenitors located ventral and lateral to the neural tube migrated into the medial dorsal dermis around E10.5, and then began to spread laterally (Jiang et al. 2018). However, the *Foxd1* lineage represented only ~50% of the dermal fibroblasts in unwounded tissue, in comparison to ~70% described by Rinkevich *et al.* (2015). Further, differential gene expression of *dpp4* was not detected in the *Foxd1* lineage, which was upregulated at the protein level in the *Engrailed-1* lineage. Regardless, both *Foxd1* and *Engrailed-1* derived populations display an enhanced fibrogenic potential compared to their lineage-negative counterparts, and thus likely share a common subset of cells specialized in matrix production.

The populations described by Driskell *et al.* (2013) showed distinct spatial localization during development and early post-natal growth, which was not identified in the *Foxd1* lineage. Moreover, differential gene expression of *Dlk1* and *Dpp4*, which correspond with the reticular and papillary dermal fibroblast populations, respectively, was not evident in the populations sorted based on the *Foxd1* lineage. Interestingly, the differentiation of multipotent progenitors into upper and lower dermal lineages described by Driskell *et al.* occurs around E12.5, which is much later than the patterns observed for the *Foxd1* lineage. Further, in the inducible Cre model described here, later tamoxifen injection from E10.5 to E11.5 yielded recombination primarily in the deep fibroblast population by E14.5, whereas earlier injection resulted in a more widely distributed population of recombined cells, spread between deep and superficial populations. Thus, it is proposed that as cells migrated dorsally into the dermis during development, they ceased to express *Foxd1*.

In this proposed model, the cells that migrate earlier in development would stop expressing *Foxd1* earlier and become the most dorsal fibroblasts in the skin, whereas those migrating later would have more sustained *Foxd1* expression and contribute more ventrally within the dermis. The significance of this is that the multipotent progenitors described at E12.5 by Driskell *et al.* could already be predetermined upper or lower dermal populations based on positional cues that arise from a temporal switch related to their initial migration into the developing dermis. Moreover, the observed stratification of the labelled population based on the timing of tamoxifen injection, when combined with the work of Driskell *et al.*, suggests that a sub-lineage of FLP fibroblasts are reticular FLP fibroblasts, which may be distinct from papillary FLP fibroblasts. As the reticular

population was shown to be the primary contributor to granulation tissue formation and matrix deposition (Driskell et al. 2013), it would be expected that a reticular FLP lineage may be a more specific fibrogenic population of interest. Unfortunately, due to complications with tamoxifen injection into pregnant females, a dose that yielded high levels of recombination and resulted in live births was not identified, and thus this was not pursued further. However, it is speculated based on the tissue architecture during early repair, as well as from the findings of Driskell *et al.*, that the FLP fibroblasts that migrated into the wound were coming from the lower dermis, and thus the repair process was selecting for this reticular sub-population.

Using histological and gene expression analyses, expression of α -SMA was consistent in both cell lineages within the wound, suggesting that myofibroblast activation was similar in both groups. Conversely, the differential gene expression patterns suggest that while both groups can differentiate into a contractile myofibroblast phenotype, their complementary functional specification may be diverse. Importantly, unique expression signatures were noted suggesting that the expression of genes associated with matrix synthesis and remodeling was enhanced in FLP fibroblasts, while the expression of genes associated with cell signaling was enhanced in FLN fibroblasts. In general, it is notable that the gene expression changes, especially those upregulated in the FLP subset, were subtle, with both populations producing transcripts for ECM synthesis and remodeling. Nevertheless, assuming that gene expression would correlate directly with protein expression, the 2-fold increase of *Col3a1* mRNA detected in the FLP fibroblasts (60% of wound fibroblasts) relative to FLN fibroblasts (40% of wound fibroblasts) within the wound tissue, would indicate that 75% of the fibroblast-produced type III collagen was

generated by the FLP lineage. However, whether a depletion of this population would result in reduced collagen production, or whether FLN cells could compensate for this loss, would require further investigation. Studies of the greater fibrogenic *Engrailed-1* lineage using diphtheria toxin induced depletion or selective cell transplantation, have shown that a reduction of this population reduced scar formation, while enrichment enhanced scar formation (Rinkevich et al. 2015; Jiang et al. 2018). Consequently, it would be interesting to explore the *Foxd1* lineage in these model systems, as it would be postulated to have similar functional effects.

Due to the enrichment of transcripts for cell receptors and signaling molecules present in the FLN population, it was proposed that these cells may act as regulators of FLP function. However, in order to systematically explore the interactions between the two populations, a robust *in vitro* model system would be required. It is well established that culture on stiff substrates results in myofibroblast activation, which can be avoided on soft matrices (Hinz 2007; Balestrini et al. 2012). Conversely, culture in 3D matrices yields a quiescent, non-proliferative cell state that more closely mimics that of native tissue (Erler and Weaver 2009; Rognoni et al. 2018). To first determine if gene expression could be maintained *in vitro*, a compliant collagen gel was used as a culture substrate and TGF β 1 was used to selectively stimulate myofibroblast activation. Naïve fibroblasts were used rather than the unwounded and wounded populations due to the cell yield required. Notably, the gene expression differences in the naïve healthy population appeared to be diminished relative to their potentially more activated counterparts isolated from unwounded tissue from mice 10 days post wounding that was included in the array analysis. Regardless, expression of *colla1*, α 2 and β 8 integrins was determined

to be significantly affected by cell lineage in this freshly-isolated population, similar to the array findings.

Using the collagen gel culture system, *Coll1a1*, *Col3a1*, and *Itgb8*, all of which were expressed at higher levels in freshly isolated FLP fibroblasts compared to FLN fibroblasts, were expressed similarly between the groups after culturing. It is well established that culture on collagen gels reduces collagen synthesis (Gillery et al. 1992; Eckes et al. 1993), which occurs through $\alpha1\beta1$ integrin stimulation (Langholz et al. 1995). However, treatment with TGF β 1 was still sufficient to upregulate *coll1a1* expression in FLP fibroblasts, albeit to a level below that of freshly isolated fibroblasts. Thus, the cell culture method explored here resulted in a significant change in the gene expression patterns of these populations, inducing a reversion towards a common phenotype. In partial contrast to these findings, after culturing human papillary and reticular dermal fibroblasts on tissue culture plastic, Philippeos *et al.* found that while the populations did not retain their native differential expression of Wnt-signaling related genes, they maintained differences in the expression of inflammatory mediators and ECM-related genes including *coll1a1*, and *coll1a2* (Philippeos et al. 2018). These cells also retained functional differences when stimulated with IFN γ . Moreover, in an organotypic culture system comprised of decellularized human skin seeded with a keratinocyte layer and cultured human fibroblasts from either the papillary or reticular dermal populations, both fibroblast populations maintained functional differences (Philippeos et al. 2018). While the papillary population migrated physically closer to the keratinocyte layer, and induced the formation of rete ridges and a thicker keratinocyte layer, the reticular population did not show preferential migration to the keratinocyte

layer or induce these structural changes (Philippeos et al. 2018). Thus, even though gene expression was altered in the culture system investigated, functional differences may be retained. Potentially, use of an organotypic culture system as employed by Philippeos *et al.* could be useful to study cell function in a more biologically relevant model.

Finally, in this study the differential expression of several integrins between cell lineages was observed. As these proteins are pivotal for the interaction between cells and the ECM (Koivisto et al. 2014), they are interesting candidates for future exploration that may represent an integral cell intrinsic difference that mediates cell phenotype. Transcripts for *Itga2*, *Itga3*, *Itgb6*, and *Itgb8* were all significantly enriched in the FLN fibroblasts in both wounded and unwounded tissue. Integrin $\alpha2\beta1$ is a collagen I- and III-binding integrin which supports collagen fibril formation and is involved in collagen gel contraction (Eckes et al. 2006; Koivisto et al. 2014). Integrin $\alpha3\beta1$, is a laminin-binding integrin. Interestingly, in alveolar epithelial cells $\alpha3\beta1$ integrin was shown to mediate non-canonical TGF $\beta1$ signaling via Smad-2 phosphorylation of β -catenin, a process that the authors linked to epithelial to mesenchymal transition (EMT) (Kim et al. 2009). Importantly, lineage tracing studies have suggested that resident stromal cells are the major contributors to myofibroblasts in lung fibrosis, while support for EMT as a source of myofibroblasts is not as strong (Rock et al. 2011; Bartis et al. 2014). Whether a similar mechanism resulting in integrin $\alpha3\beta1$ -mediated non-canonical TGF $\beta1$ signaling takes place in the stromal population within the skin would be of interest. Both integrin $\beta6$ and $\beta8$ dimerize with integrin αV and are strongly linked to activation of TGF $\beta1$ signaling (Hinz 2015). Depletion of integrin αV in PDGFR β -expressing cells protected against fibrosis in models of hepatic, renal, and pulmonary fibrosis (Henderson et al. 2013). It

was, however, surprising to observe expression changes in integrin $\beta 6$, as it has primarily been reported in epidermal cells (Koivisto et al. 2014). This finding could indicate that there were contaminating keratinocytes within the sorted population, a potential limitation associated with using a negative selection-based approach for cell sorting. Although histological analysis supported that integrin $\beta 6$ was expressed within the stromal population in the skin, this labelling could be associated with the described cross-reactivity of the antibody with other integrins, including $\beta 1$, $\beta 2$, and $\beta 3$ integrins. As such, the current findings regarding the expression of $\beta 6$ integrin within the dermis are inconclusive. Alternatively, this may suggest that $\beta 6$ integrin has previously unrecognized roles within the dermal fibroblast population, but this requires further exploration.

Interestingly, as highlighted above many of the reported functions of these integrins support that they can modulate myofibroblast activation and function. Thus, a potential model for the interaction of FLP and FLN populations is one in which the FLP cells specialize as a matrix secreting population, whereas the FLN cells play a more supportive role, regulating the FLP population through growth factor secretion and activation. Future studies should focus on the further analysis of these integrins with techniques such as flow cytometry to confirm the integrin expression patterns and levels.

2.6 Conclusions

Using a Cre/Lox-based lineage tracing approach, an embryologically distinct fibroblast lineage, arising from *Foxd1*-expressing progenitors was characterized. This population migrated into the dermis during early development and contributed to the stromal population in adult skin. In adult skin, gene expression analysis suggested that these FLP

cells specialize in matrix synthesis and remodeling during homeostasis and wound repair. In contrast, gene expression patterns in *Foxd1* lineage-negative populations suggests these cells may play a more supportive role associated with increased gene expression of cell surface receptors, integrins, and cytokines. Overall, the gene expression differences in the FLP and FLN populations support a functional heterogeneity between these populations during homeostasis and tissue repair within the skin. Further functional characterization of FLP and FLN fibroblasts and their interactions could provide insight into novel mechanisms through which to modulate wound repair in cases of impaired healing, such as in chronic wounds or excessive scarring.

2.7 Acknowledgements

I would like to thank Dr. Kristin Chadwick at the London Regional Flow Cytometry Facility for her technical expertise with the FACS experiments.

2.8 References

- Balestrini JL, Chaudhry S, Sarrazy V, et al (2012) The mechanical memory of lung myofibroblasts. *Integr Biol* 4:410–421. doi: 10.1039/c2ib00149g
- Bartis D, Mise N, Mahida RY, et al (2014) Epithelial-mesenchymal transition in lung development and disease: Does it exist and is it important? *Thorax* 69:760–765. doi: 10.1136/thoraxjnl-2013-204608
- Driskell RR, Lichtenberger BM, Hoste E, et al (2013) Distinct fibroblast lineages determine dermal architecture in skin development and repair. *Nature* 504:277–281. doi: 10.1038/nature12783
- Driskell RR, Watt FM (2015) Understanding fibroblast heterogeneity in the skin. *Trends Cell Biol* 25:92–99. doi: 10.1016/j.tcb.2014.10.001

- Dulauroy S, Di Carlo SE, Langa F, et al (2012) Lineage tracing and genetic ablation of ADAM12 + perivascular cells identify a major source of profibrotic cells during acute tissue injury. *Nat Med* 18:1262–1270. doi: 10.1038/nm.2848
- Dunn L, Prosser HCG, Tan JTM, et al (2013) Murine Model of Wound Healing. *J Vis Exp* e50265. doi: 10.3791/50265
- Eckes B, Mauch C, Hüppe G, Krieg T (1993) Downregulation of collagen synthesis in fibroblasts within three-dimensional collagen lattices involves transcriptional and posttranscriptional mechanisms. *FEBS Lett* 318:129–133. doi: 10.1016/0014-5793(93)80006-G
- Eckes B, Zweers MC, Zhang ZG, et al (2006) Mechanical tension and integrin $\alpha 2\beta 1$ regulate fibroblast functions. *J Investig Dermatol Symp Proc* 11:66–72. doi: 10.1038/sj.jidsymp.5650003
- El Agha E, Kramann R, Schneider RK, et al (2017) Mesenchymal Stem Cells in Fibrotic Disease. *Cell Stem Cell* 21:166–177. doi: 10.1016/j.stem.2017.07.011
- Elliott CG, Wang J, Guo X, et al (2012) Periostin modulates myofibroblast differentiation during full-thickness cutaneous wound repair. *J Cell Sci* 125:121–132. doi: 10.1242/jcs.087841
- Erler JT, Weaver VM (2009) Three-dimensional context regulation of metastasis. *Clin Exp Metastasis* 26:35–49. doi: 10.1007/s10585-008-9209-8
- Feil S, Valtcheva N, Feil R (2009) Inducible Cre Mice. In: Wurst W, Kühn R (eds) *Gene Knockout Protocols: Second Edition*. Humana Press, Totowa, NJ, pp 343–363
- Fetting JL, Guay JA, Karolak MJ, et al (2014) FOXD1 promotes nephron progenitor differentiation by repressing decorin in the embryonic kidney. *Development* 141:17–27. doi: 10.1242/dev.089078
- Gabbiani G (2003) The myofibroblast in wound healing and fibrocontractive diseases. *J Pathol* 200:500–503. doi: 10.1002/path.1427
- Gillery P, Leperre A, Coustry F, et al (1992) Different regulation of collagen I gene transcription in three-dimensional lattice cultures. *FEBS Lett* 296:297–9.
- Henderson NC, Arnold TD, Katamura Y, et al (2013) Targeting of α v integrin identifies a core molecular pathway that regulates fibrosis in several organs. *Nat Med* 19:1617–1624. doi: 10.1038/nm.3282

- Hinz B (2007) Formation and function of the myofibroblast during tissue repair. *J Invest Dermatol* 127:526–537. doi: 10.1038/sj.jid.5700613
- Hinz B (2015) The extracellular matrix and transforming growth factor- β 1: Tale of a strained relationship. *Matrix Biol* 47:54–65. doi: 10.1016/j.matbio.2015.05.006
- Hinz B, Phan SH, Thannickal VJ, et al (2012) Recent developments in myofibroblast biology: Paradigms for connective tissue remodeling. *Am J Pathol* 180:1340–1355. doi: 10.1016/j.ajpath.2012.02.004
- Hothorn T, Bretz F, Westfall P (2008) Simultaneous inference in general parametric models. *Biometrical J* 50:346–363. doi: 10.1002/bimj.200810425
- Hu MS, Moore AL, Longaker MT (2018) A Fibroblast Is Not a Fibroblast Is Not a Fibroblast. *J Invest Dermatol* 138:729–730. doi: 10.1016/j.jid.2017.10.012
- Humphreys BD, Lin SL, Kobayashi A, et al (2010) Fate tracing reveals the pericyte and not epithelial origin of myofibroblasts in kidney fibrosis. *Am J Pathol* 176:85–97. doi: 10.2353/ajpath.2010.090517
- Hung C, Linn G, Chow YH, et al (2013) Role of lung Pericytes and resident fibroblasts in the pathogenesis of pulmonary fibrosis. *Am J Respir Crit Care Med* 188:820–830. doi: 10.1164/rccm.201212-2297OC
- Jiang D, Correa-Gallegos D, Christ S, et al (2018) Two succeeding fibroblastic lineages drive dermal development and the transition from regeneration to scarring. *Nat Cell Biol* 20:422–431. doi: 10.1038/s41556-018-0073-8
- Kim Y, Kugler MC, Wei Y, et al (2009) Integrin α 3 β 1 - dependent β -catenin phosphorylation links epithelial smad signaling to cell contacts. *J Cell Biol* 184:309–322. doi: 10.1083/jcb.200806067
- Koivisto L, Heino J, Häkkinen L, Larjava H (2014) Integrins in Wound Healing. *Adv Wound Care* 3:762–783. doi: 10.1089/wound.2013.0436
- Langholz O, Rockel D, Mauch C, et al (1995) Collagen and collagenase gene expression in three-dimensional collagen lattices are differentially regulated by α 1b1 and α 2b1 integrins. *JCell Biol* 131:1903–1915
- Levinson RS (2005) Foxd1-dependent signals control cellularity in the renal capsule, a structure required for normal renal development. *Development* 132:529–539. doi: 10.1242/dev.01604

- Marangoni RG, Korman BD, Wei J, et al (2015) Myofibroblasts in murine cutaneous fibrosis originate from adiponectin-positive intradermal progenitors. *Arthritis Rheumatol* 67:1062–1073. doi: 10.1002/art.38990
- McIntosh JC, Hagood JS, Richardson TL, Simecka JW (1994) Thy1 (+) and (-) lung fibrosis subpopulations in LEW and F344 rats. *Eur Respir J* 7:2131–2138. doi: 10.1183/09031936.94.07122131
- Metzger D, Chambon P (2001) Site- and time-specific gene targeting in the mouse. *Methods* 24:71–80. doi: 10.1006/meth.2001.1159
- Motulsky HJ, Brown RE (2006) Detecting outliers when fitting data with nonlinear regression - A new method based on robust nonlinear regression and the false discovery rate. *BMC Bioinformatics* 7:1–20. doi: 10.1186/1471-2105-7-123
- Philippeos C, Telerman SB, Oulès B, et al (2018) Spatial and Single-Cell Transcriptional Profiling Identifies Functionally Distinct Human Dermal Fibroblast Subpopulations. *J Invest Dermatol* 138:811–825. doi: 10.1016/j.jid.2018.01.016
- Phipps RP, Penney DP, Keng P, et al (1989) Characterization of Two Major Populations of Lung Fibroblasts: Distinguishing Morphology and Discordant Display of Thy 1 and Class II MHC. *Am J Respir Cell Mol Biol* 1:65–74. doi: 10.1165/ajrcmb/1.1.65
- Pinheiro J, Bates D, R-core (2014) Linear and Nonlinear Mixed Effects Models
- R core team (2017) R: A language and environment for statistical computing. R Found. Stat. Comput. Vienna, Austria.
- Rinkevich Y, Walmsley GG, Hu MS, et al (2015) Identification and isolation of a dermal lineage with intrinsic fibrogenic potential. *Science* (80-) 348:aaa2151. doi: 10.1126/science.aaa2151
- Rock JR, Barkauskas CE, Cronic MJ, et al (2011) Multiple stromal populations contribute to pulmonary fibrosis without evidence for epithelial to mesenchymal transition. *Proc Natl Acad Sci* 108:E1475–E1483. doi: 10.1073/pnas.1117988108
- Rognoni E, Pisco AO, Hiratsuka T, et al (2018) Fibroblast state switching orchestrates dermal maturation and wound healing. *Mol Syst Biol* 14:e8174. doi: 10.15252/msb.20178174
- Singer AJ, Clark R (1999) Mechanisms of Disease - Cutaneous Wound Healing. *N Engl J Med* 341:738–746

- Suga H, Rennert RC, Rodrigues M, et al (2014) Tracking the elusive fibrocyte: Identification and characterization of collagen-producing hematopoietic lineage cells during murine wound healing. *Stem Cells* 32:1347–1360. doi: 10.1002/stem.1648
- Tabib T, Morse C, Wang T, et al (2018) SFRP2/DPP4 and FMO1/LSP1 define major fibroblast populations in human skin. *J Invest Dermatol* 138:1–9. doi: 10.1016/j.jid.2017.09.045

Chapter 3: The role of Galectin-3 in cell recruitment and differentiation during wound healing

A version of this chapter has been published:

Walker, J.T., Elliott, C.G., Forbes, T.L., Hamilton, D.W. (2016) The role of Galectin-3 in cell recruitment and differentiation during wound healing. J Invest Dermatol. 136 (5): 1042-1050

3.1 Abstract:

Galectin-3 has been linked to the regulation of several molecular processes essential for acute cutaneous wound healing, but a comprehensive study of the role of Galectin-3 in skin healing has not previously been performed. With described roles in macrophage polarization, myofibroblast differentiation, re-epithelialization, and angiogenesis, it was hypothesized that genetic deletion of Galectin-3 would significantly impair healing of excisional skin wounds in mice. In wild-type mice, Galectin-3 expression correlated temporally with the inflammatory phase of healing. Genetic deletion of Galectin-3 did not alter gross wound healing kinetics even though delayed re-epithelialization was evident. Neither inflammatory nor mesenchymal cell infiltration or cell phenotype were altered up to 15 days post-wounding in knockout mice in comparison with healing in wild type mice, and isolated dermal fibroblast function *in vitro* was unchanged. The expression of Galectin-3 was further explored spatially in human chronic wound tissue in

relation to the immune cell infiltrate. Decreased mRNA expression and protein immunoreactivity in the wound edge tissue was observed, whereas markers of neutrophils, M1 and M2 macrophages were expressed abundantly. Both transforming growth factor- β 1 and tumor necrosis factor- α decreased Galectin-3 at the transcript level in human chronic wound edge dermal fibroblasts *in vitro*, providing a potential mechanism for this reduced expression in chronic wounds.

3.2 Introduction:

Impaired skin healing represents a clinically significant problem associated with vascular insufficiency, diabetes, and increasing age (Nelson and Bradley 2007; Sen et al. 2009). Although the underlying etiology of non-healing skin wounds is complex, it is established that the tissue remains in a proinflammatory state (Schultz and Wysocki 2009; Widgerow 2011; Demidova-Rice et al. 2012). Gaining an understanding of the molecular mechanisms involved in the persistence of the inflammatory state and of the associated paracrine effects of prolonged inflammation on the resident cell populations will be central to strategies to stimulate wound closure.

Implicated in several cellular processes associated with the inflammatory and proliferative phases of wound healing, Galectin-3 is a multifunctional lectin, consisting of a carbohydrate recognition domain, with a unique N-terminal repeat region in comparison to other galectins (Barondes et al. 1994). Galectin-3 has been implicated in initiating macrophage polarization into the anti-inflammatory wound healing related M2 phenotype (MacKinnon et al. 2008). In addition, it has been demonstrated to function as a chemotactic molecule for the recruitment of M2 macrophages in mouse tumors (Jia et al.

2013). Galectin-3 is highly expressed in M2 macrophages (Novak et al. 2012) and has been shown to play a major role in phagocytosis of opsonized cells (Sano et al. 2003; Karlsson et al. 2009), including neutrophils. This process is critical for terminating inflammation, preventing further tissue destruction (Karlsson et al. 2009). As chronic wounds are enriched with proteases and proinflammatory cytokines (Wiegand et al. 2010), an improved understanding of proteins involved in regulating these responses, including Galectin-3, would be of significance.

Temporally overlapping with the inflammatory phase, skin wounds progress into the proliferative phase of healing, where mesenchymal cells infiltrate and secrete extracellular matrix (Singer and Clark 1999). Several studies have implicated Galectin-3 in fibrotic processes, including hepatic (Henderson et al. 2006; Jiang et al. 2012), renal (Henderson et al. 2008), and pulmonary (MacKinnon et al. 2012) fibrosis, suggesting that it may play a role in the pro-fibrotic proliferative phase of wound healing as well. Interestingly, pulmonary fibroblasts isolated from Galectin-3 knockout (KO) mice display impaired myofibroblast differentiation and reduced type I collagen synthesis *in vitro* (MacKinnon et al. 2012). In addition to its role in modulating the myofibroblast phenotype, Galectin-3 has been linked to angiogenesis, a critical process during skin healing (Reinke and Sorg 2012). Exogenous Galectin-3 has been shown to enhance endothelial cell tube formation *in vitro*, and a Galectin-3 null breast cancer cell line was only able to induce angiogenesis *in vivo* if the cells were transfected with Galectin-3 cDNA (Nangia-Makker et al. 2000). Additionally, Galectin-3 loaded microbeads implanted into mouse corneas induced an angiogenic response (Markowska et al. 2010),

further demonstrating the potential role of Galectin-3 during the processes underlying the proliferative phase of healing.

One study that explored the influence of Galectin-3 deletion on skin healing showed delayed re-epithelialization due to impaired epidermal growth factor receptor trafficking upon activation (Liu et al. 2012). However, evidence clearly suggests that Galectin-3 may play significant roles in skin repair, beyond re-epithelialization. It was hypothesized that alterations in the inflammatory and proliferative phases of skin healing would manifest in *Galectin-3* KO mice. Secondly, Galectin-3 expression was assessed in human non-healing skin wounds and compared to the inflammatory cell infiltrate using markers of neutrophils and macrophages.

3.3 Materials and Methods:

3.3.1 Mice

All animal procedures were in compliance with protocols approved by the University Council on Animal Care at Western University (protocol number 2008-097). *Galectin-3* KO (*B6.Cg-Lgals3^{tm1Poi/J}*; 006338) mice were purchased from The Jackson Laboratory (Farmington, CT). These mice were crossed once with wild type (WT) *C57BL/6J* mice, also from The Jackson Laboratory (000664), to produce heterozygous offspring. Heterozygotes were set up into breeding pairs to generate homozygous *Galectin-3* KO and sex-matched WT littermates. Mice were genotyped per The Jackson Laboratory's instructions (Figure 3.1).

3.3.2 Excisional wounding experiments

For all *in vivo* experiments, 6-mm full-thickness excisional wounds were created as previously described (Elliott et al. 2012). Mice were euthanized, and tissue was isolated at 1, 3, 5, and 7 days after wounding. For closure kinetics, wounds were photographed with a digital camera at baseline, and days 3, 5, and 7 after wounding, using a ruler to standardize the image dimensions. ImageJ software (Schneider et al. 2012) was used to calculate the wounded area.

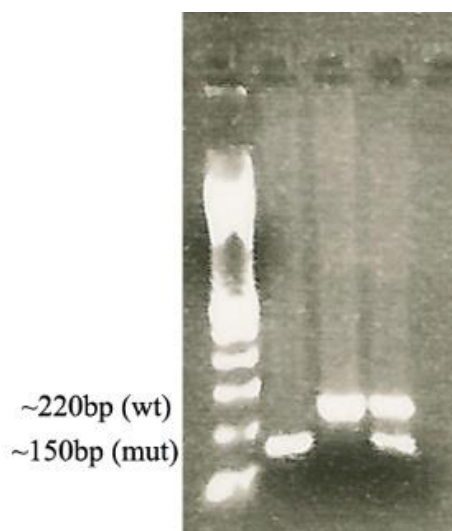


Figure 3.1: Electrophoresis following PCR of DNA isolated from *Galectin-3* KO, wild type and heterozygous mice. Lanes from left to right: TrackIt™ 1Kb Plus DNA ladder (Thermo Scientific); *Galectin-3* KO DNA, wild type DNA, heterozygous DNA.

3.3.3 Patient samples

All tissues were collected with written, informed consent from patients under protocols approved by the Western University Review Board for Health Sciences Research Involving Human Subjects (HREB #16245E). Isolation and experimental use of dermal fibroblasts from human tissue were approved by the Western University Review Board for Health Sciences Research Involving Human Subjects and are in accordance with the 1964 Declaration of Helsinki. Direct RNA analysis of Galectin-3 was performed on 15 patients. Histological analysis was performed in 9 patients, and *in vitro* cell experiments were performed on cells isolated from 4 patients (see Appendix Tables A5, A6, and A7 for relevant information).

3.3.4 Histology

Human and mouse tissues were fixed in 10% neutral buffered formalin and either processed to paraffin or into Frozen Section Compound (VWR, Mississauga, ON, Canada). Sections 5 µm thick were cut from paraffin blocks or 8 µm from frozen blocks. Colorimetric staining was performed using ImmPress HRP anti-mouse and anti-rabbit detection kits (Vectorlabs, Burlingame, CA), and a 3,3'-diaminobenzidine peroxidase substrate kit (Vectorlabs). In all cases, a minimum of three mice were used from each genotype. Nine human wounds were assessed for immune cell infiltration and fibrotic response. Blood vessel and immune cell quantification in mice were performed using ImageJ software (Schneider et al. 2012). Histological wound measurements were performed on Masson's trichrome-stained sections from 9 WT and 8 *Galectin-3* KO mice. Wound diameter was measured as the distance between the unwounded dermis in sections taken from the center of the wounds. Epithelial tongue length was measured as

the distance from the tip of the epithelial tongue to the unwounded dermis. Average epithelial tongue thickness was approximated by the equation: $\frac{\text{area of epithelial tongue}}{\text{length of epithelial tongue}}$. For a list of antibodies used for these experiments, see Table 3.1.

3.3.5 Hydroxyproline assay

Mouse skin tissue was isolated from the wound bed 15 days after wounding using a biopsy punch, and hydroxyproline content was measured using the Hydroxyproline Assay Kit (Sigma-Aldrich, Oakville, ON, Canada) following protocol instructions. Tissue was pooled from two wounds from each animal.

3.3.6 Human primary fibroblast culture and mouse primary fibroblast culture

Dermal fibroblasts were isolated from humans and mice using the explant culture technique previously described (Rittié and Fisher 2005). Cells were grown in DMEM (Thermo Fisher Scientific, Burlington, ON, Canada) supplemented with 10% fetal bovine serum. Fibroblasts were used from passage 1 (human cells) or at passage 3 (mouse cells) for experiments.

Table 3.1: Primary antibodies used for immunohistochemistry and western blot.

Staining	Antibody used	Supplier	Dilution
Galectin-3 (human)	SC-374253	Santa Cruz Biotechnology, Dallas, TX	1:400
Galectin-3 (mouse; colorimetric)	SC-20157	Santa Cruz Biotechnology, Dallas, TX	1:500
Galectin-3 (mouse; fluorescence)	eBioM3/38	eBioscience, San Diego, CA	1:50
Mannose Receptor	Ab64693	Abcam, Cambridge, MA	1:1000
Indolamine 2,3-dioxygenase	Ab55305	Abcam, Cambridge, MA	3:1000
Neutrophil elastase	Ab68672	Abcam, Cambridge, MA	1:2000
α SMA (mouse)	Ab5694	Abcam, Cambridge, MA	1:100
Vimentin	Ab92547	Abcam, Cambridge, MA	1:500
CD146	Ab75769	Abcam, Cambridge, MA	1:200
NOS2	Ab3523	Abcam, Cambridge, MA	1:50
Arginase I	SC-18354	Santa Cruz Biotechnology, Dallas, TX	1:100
GAPDH (western blot)	MAB374	Millipore, Billerica, MA	1:1000
α SMA (western blot)	A5228	Sigma Aldrich, Oakville, ON	1:1000

3.3.7 Cytokine treatment

Isolated fibroblasts were seeded into a six-well plate in DMEM containing 10% fetal bovine serum at a density of 100,000 (human) or 50,000 (mouse) cells per well in a 6-well plate. After 24 hours, cells were transferred into serum-free DMEM for an additional

24 hours. Then to the respective wells 5 ng/mL transforming growth factor β 1 (TGF β 1) (R&D Systems, Minneapolis, MN) and 1 ng/mL TNF α (R&D Systems) were added and samples were incubated for 24 hours (RNA analysis) or 48 hours (protein analysis). Untreated controls were cultured in serum-free DMEM without cytokine treatment. All experiments were run in triplicate. A dose response to TGF β 1 was performed in the presence of 0-5 ng/mL TGF β 1 with or without the ALK5 inhibitor SB431542 (10 μ M).

3.3.8 RNA isolation and real-time quantitative PCR

RNA was isolated with TRIzol reagent (Thermo Fisher Scientific) and purified using RNeasy mini kits (Qiagen, Valencia, CA). Taqman real-time PCR was performed using qSCRIPT XLT one-step real-time quantitative PCR ToughMix (Quanta Biosciences, Gaithersburg, MD) per the manufacturer's instructions. All samples were run in triplicate and relative quantity measurements were determined from a standard curve. mRNA quantity was normalized to endogenous 18S rRNA (Thermo Fisher Scientific). See Table 3.2 for a list of probes used. Location of non-involved, proximate, wound edge, and wound bed tissues in mice are demonstrated in Figure 3.2.

Table 3.2: Taqman® probe sets used for RT-qPCR.

Transcript	Probe identification
<i>LGALS3</i> (Human)	Hs00173587_m1
<i>Lgals3</i> (Mouse)	Mm00802901_m1
<i>Acta2</i>	Mm00725412_s1
<i>Colla2</i>	Mm00483888_m1
<i>Kdr</i>	Mm01222421_m1
<i>Lgals1</i>	Mm00839408_g1
<i>Lgals7</i>	Mm00456135_m1
18S rRNA	4352930E

3.3.9 Protein isolation and western blot

Protein isolation and western blots were performed as previously described (Elliott et al. 2012). Primary antibodies were applied to the membrane overnight in 5% milk tris buffered saline with 0.05% tween 20. Membranes were incubated in Alexafluor 680 conjugated goat anti-mouse (Thermo Fisher Scientific) and visualized with an Odyssey infrared imager (LI-COR, Lincoln, NE).

3.3.10 In vitro scratch wound assay

Isolated mouse fibroblasts were seeded into a six-well plate at a density of 150,000 cells per well in DMEM with 10% fetal bovine serum. Cells were allowed to adhere for 24 hours before being scratched with a sterile pipette tip. Images were taken every 20

minutes until the scratches closed. The average distance traveled by the cell front was calculated every 200 minutes. All experiments were run in triplicate.

3.3.11 Gel contraction assay

Isolated mouse fibroblasts were seeded into 20% collagen type I solution at a density of 50,000 cells/mL. Then 1 mL of this solution was placed into each well of a 24-well culture plate. After 45 minutes, a pipette tip was used to separate the polymerized gel from the culture plastic, and DMEM with 0.5% fetal bovine serum was added to each well with or without 5 ng/mL TGF β 1. After an additional 24 hours, the gels were removed, dabbed dry, and weighed to assess the extent of gel contraction. Each sample was run in triplicate.

3.3.12 Statistical methods

Statistical analyses were performed using R statistics software (R core team 2017), the “nlme” package for linear and nonlinear mixed effects models (Pinheiro et al. 2014), and the “multcomp” package for simultaneous inference in general parametric models (Hothorn et al. 2008) were used. GraphPad Prism software version 5 (GraphPad, La Jolla, CA) was used to produce graphs. Statistical analyses were performed using a t-test or linear mixed effects models as appropriate. As necessary, a Tukey post hoc test was used.

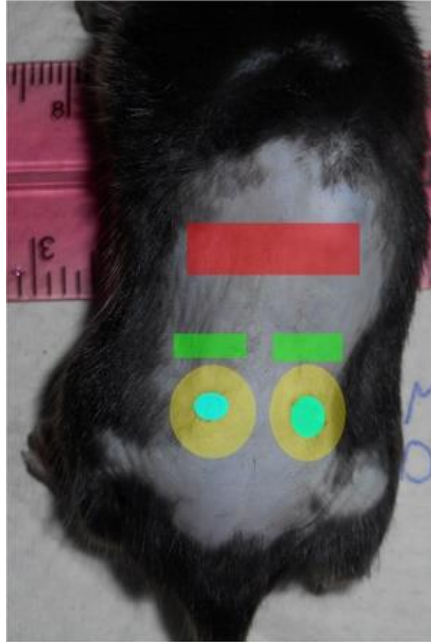


Figure 3.2: Location of tissue isolated for mRNA expression in mice. Red- Non-involved, green- proximate, yellow- wound edge, blue- wound bed.

3.4 Results:

3.4.1 Galectin-3 mRNA and protein were up-regulated after excisional wounding and peaked 1 day after wounding

Analysis of Galectin-3 expression profiles during cutaneous wound healing in wild-type (WT) mice showed *Lgals3* (gene coding Galectin-3) mRNA levels were significantly greater in the wound bed compared to non-involved tissue at day 1 ($p = 0.020$), but no significant differences were evident 3 or 7 days after wounding (Figure 3.3a). Histological examination of Galectin-3 protein showed expression in both the epidermis and dermis of unwounded skin, and within the wound bed up to 7 days after wounding (Figure 3.3b). Immunohistochemical labeling at days 3 and 7 (Figure 3.3c and 3.3d,

respectively) displayed that at 3 days, Galectin-3 showed a high degree of overlap with arginase I -positive cells (M2 macrophage marker), many of which were also positive for NOS2 (M1 macrophage marker). However, NOS2-positive cells that were negative for arginase I did not co-express Galectin-3. At day 3, α -smooth muscle actin (α SMA) and CD146 (expressed in endothelial cells and pericytes (Li et al. 2003)) were primarily confined to blood vessels in the deep wound bed and edges, and little overlap with Galectin-3 labeling was observed. In contrast, vimentin was expressed throughout the wound bed and showed some overlap with Galectin-3 (Figure 3.3c). The trends at day 7 were similar (Figure 3.3d). Galectin-3 was present primarily in arginase I-positive cells with lesser overlap with vimentin and α SMA noted.

3.4.2 Genetic deletion of Galectin-3 impaired re-epithelialization but did not alter wound closure kinetics during excisional healing in mice

To assess differences in the rate of wound closure between *Galectin-3* KO and WT mice, wound size based on gross appearance was assessed up to 7 days after wounding, at which time the tissue was analyzed histologically. No difference in gross closure kinetics was evident between genotypes ($p = 0.92$; Figure 3.4a), nor was there a difference in wound diameter in day 7 wounds measured histologically ($p = 0.068$; Figure 3.4c). However, *Galectin-3* KO mice displayed an impaired length of epithelial tongue ($p = 0.023$; Figure 3.4b and 3.4d) and a decreased percent of re-epithelialization ($p = 0.0018$; Figure 3.4e), without any change in epithelial thickness by 7 days after wounding ($p = 0.38$; Figure 3.4f).

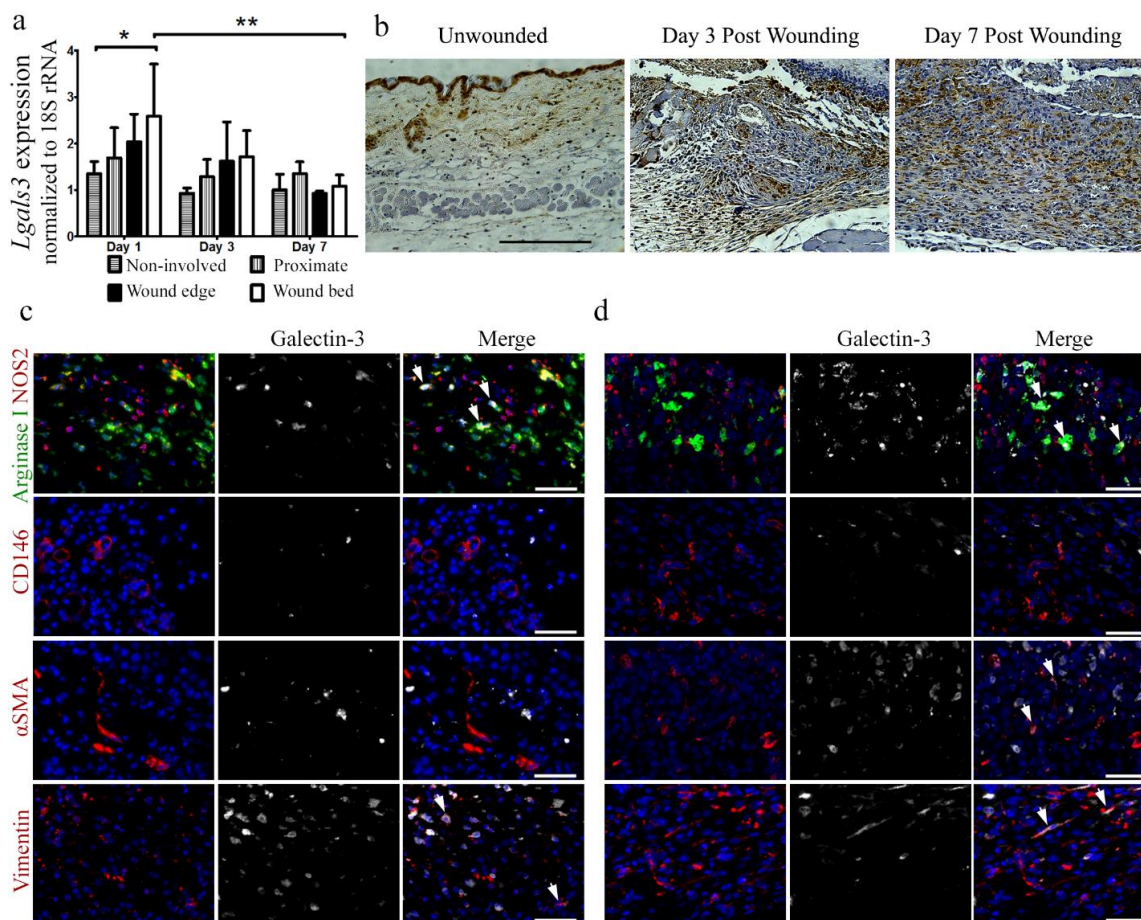


Figure 3.3: Galectin-3 expression peaked in the inflammatory phase and remained present into the proliferative phase, primarily expressed in arginase I-positive cells. 6-mm, full-thickness skin wounds were inflicted into the backs of WT and *Galectin-3* KO mice. (a) *Lgals3* expression was quantified in tissue from 1 to 7 days post wounding using quantitative PCR. Values are given as mean \pm standard deviation. Four mice per time point. * $p < 0.05$; ** $p < 0.01$. (b) Tissue isolated from unwounded skin and at 3 and 7 days post wounding was subjected to histological analysis of Galectin-3 expression. Bar = 200 μ m. WB, wound bed; WE, wound edge. Co-staining of tissue isolated at (c) day 3 and (d) day 7 after wounding shows overlap of Galectin-3 primarily in arginase I-positive cells and in cells expressing vimentin. Bar = 50 μ m.

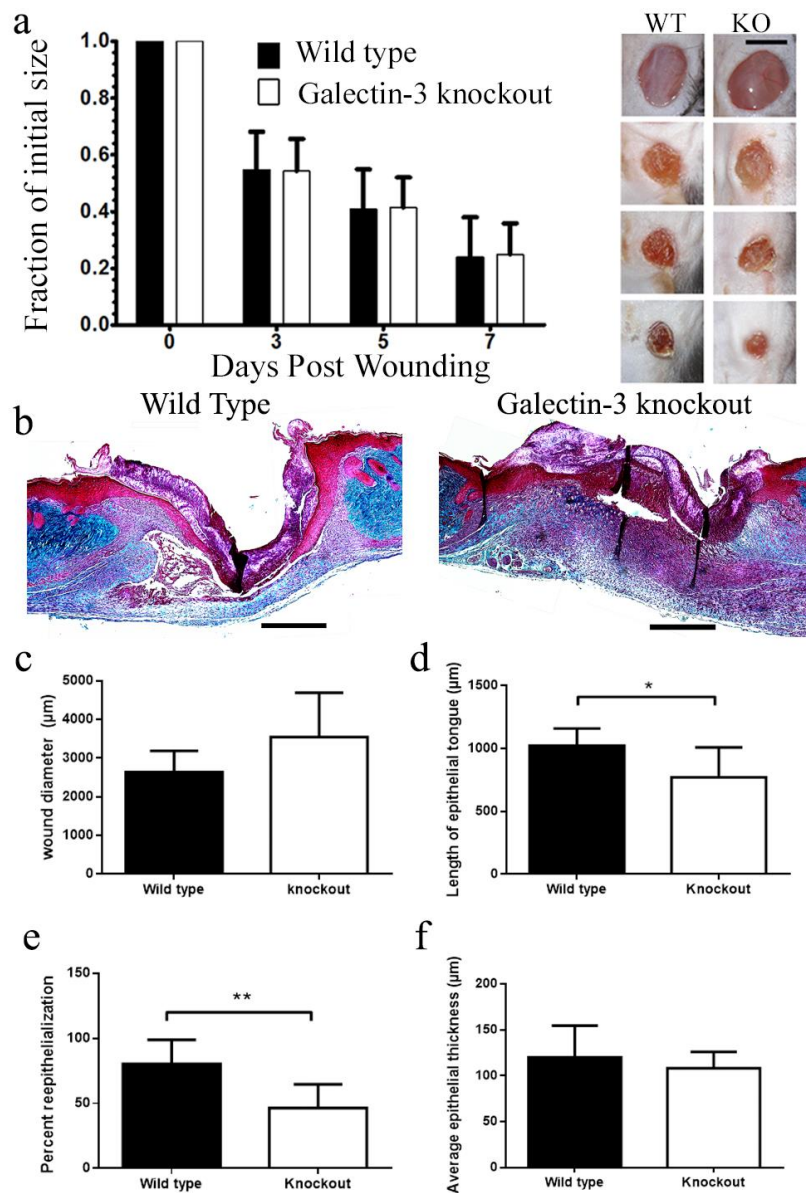


Figure 3.4: Genetic deletion of Galectin-3 did not affect gross wound closure but did impair the rate of re-epithelialization by 7 days post wounding. (a) Wound size was measured up to 7 days post wounding in 6-mm wounds from 13 knockout (KO) and 12 sex-matched wild-type (WT) littermates. Representative wounds are shown in the side panel in a KO mouse and its sex-matched littermate pair at 0, 3, 5, and 7 days post wounding (top to bottom). Bar = 5 mm. Data are expressed as mean \pm standard deviation. (b) Masson trichrome-stained sections were examined for the epithelial tongue length and thickness, and wound size (bar is 1 mm). (c) KO mice displayed a similar granulation tissue diameter to WT mice ($P=0.068$). (d) KO mice displayed impaired length of the epithelial tongue and (e) an impaired percent of re-epithelialization at 7 days post wounding, but no change in the epithelial thickness was noted (f). Eight KO and nine WT mice were quantified from histological sections. Data are expressed as mean \pm standard deviation. * $p < 0.05$; ** $p < 0.01$.

3.4.3 Genetic deletion of Galectin-3 did not affect immune cell infiltration, myofibroblast recruitment, or vascular density during wound repair

As impaired re-epithelialization in *Galectin-3* KO mice has been previously described (Liu et al. 2012), whether Galectin-3 deletion influenced inflammation, fibrosis, or angiogenesis was explored. Using antibodies specific for NOS2 (M1 polarization), arginase I (M2 polarization), and neutrophil elastase (neutrophils), no significant differences in macrophage abundance or phenotype or in neutrophil number within the wound bed were evident between genotypes at day 3 (Figure 3.5). Histological analysis of day 7 wounds demonstrated that both genotypes showed a similar expression pattern for α SMA (Figure 3.6a). Using CD146 expression as a marker for neovasculature, no differences in vessel density or vessel size were observed (Figure 3.6a). Analysis of granulation tissue with Masson's trichrome or Van Gieson stains at day 7 showed dense collagen within the unwounded tissue (Figure 3.6b, arrows) and areas of collagen deposition in the wound bed of both WT and KO animals. Analysis of tissue composition at day 15 showed that collagen content and α SMA levels were similar in KO and WT mice (Figure 3.5d). Hydroxyproline assays at 15 days after wounding confirmed similar levels of collagen in the wounds in both genotypes (Figure 3.6c).

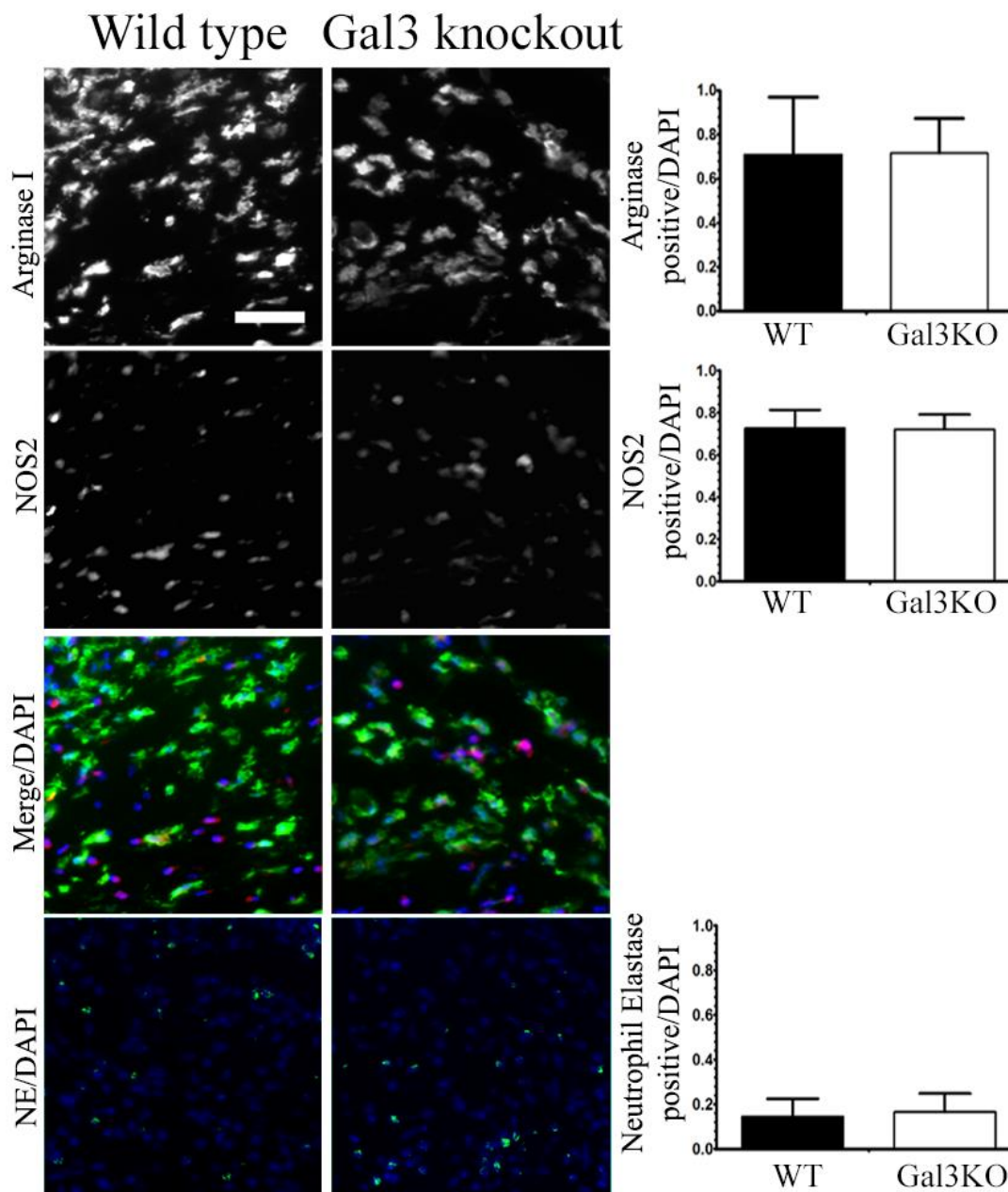


Figure 3.5: Genetic deletion of Galectin-3 did not affect the immune cell infiltrate by 3 days post wounding. Arginase I, NOS2, and neutrophil elastase (NE) were examined histologically from whole wounds, 3 days post wounding and quantified. Bar = 50 μ m. Five wild-type (WT)/Galectin-3 knockout (Gal3KO) sex-matched littermate pairs were analyzed.

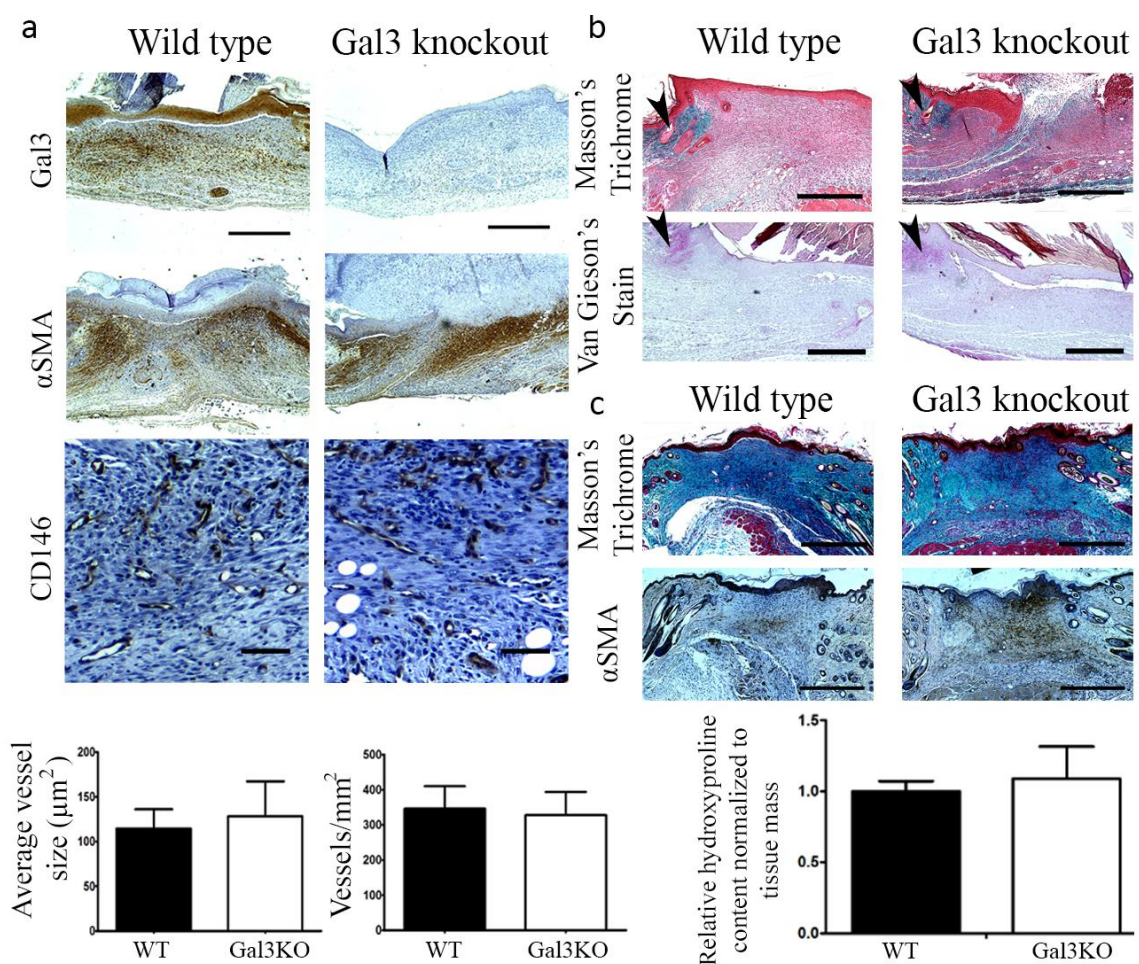


Figure 3.6: Genetic deletion of galectin-3 did not affect wound composition at 7 and 15 days post wounding. (a) Histological staining of Galectin-3 confirmed deletion of Galectin-3 in KO mice, whereas there was no change in α SMA staining. Bar = 500 μm . The density and average size of CD146-labeled blood vessels were quantified in seven KO and five WT mice. Bar = 50 μm . (b) Masson's trichrome- and Van Gieson-stained sections of day 7 wounds. Arrows show the edge of the wounds. Bar = 500 μm . (c) Masson's trichrome and α SMA staining of day 15 wounds and relative hydroxyproline content measured in day 15 wounds. Bar = 500 μm . Hydroxyproline content was measured in three sex-/age-matched WT/Gal3KO pairs.

3.4.4 Genetic deletion of Galectin-3 did not alter transcriptional regulation of genes associated with fibrotic repair or angiogenesis

Next, quantitative PCR was performed on RNA isolated from non-involved, proximate, wound edge and wound bed tissues in mice 7 days after wounding (Figure 3.7a-f). Expression of *Lgals3* was significantly lower in wound edge tissue compared to the proximate tissue in WT mice ($p < 0.001$; Figure 3.7a). *Acta2* expression was up-regulated in the wound bed compared to all other tissues in both WT ($p < 0.001$) and KO ($p < 0.001$) mice (Figure 3.7b). *Colla2* was not differentially expressed between genotypes, nor was its expression different between tissue locations (Figure 3.7c). Expression of *Kdr*, the gene for vascular endothelial growth factor receptor 2 as a marker of angiogenesis (Shih et al. 2002), was differentially expressed in the various tissue locations but was not different between genotypes (Figure 3.7d). Next, whether other galectin family members were upregulated to compensate for Galectin-3 deletion was assessed. Neither galectin-1, which shares functions with Galectin-3 (D'Haene et al. 2013; Jin Lim et al. 2014), nor galectin-7, which is linked to wound re-epithelialization (Cao et al. 2002), were significantly altered between genotypes in wound tissue 7 days after wounding (Figure 3.7e and f).

3.4.5 Galectin-3 was not required for the transition of dermal fibroblasts to myofibroblasts in vitro

Whether Galectin-3 expression in mouse dermal fibroblasts is required for myofibroblast differentiation was assessed. Addition of 5 ng/mL TGF β 1 caused down-regulation of Galectin-3 in WT cells ($p < 0.001$; Figure 3.8a) but up-regulation of *Acta2* in both WT ($p < 0.001$) and *Galectin-3* KO ($p < 0.001$) dermal fibroblasts. No significant differences

between genotypes was evident ($p = 0.74$; Figure 3.8b). Both *Galectin-3* KO and WT dermal fibroblasts contracted collagen gels after TGF β 1 treatment (Figure 3.8c), with α SMA stress fibers present in KO and WT cells (Figure 3.9). *In vitro* scratch wound assays identified no significant difference in migration rates between WT and *Galectin-3* KO fibroblasts ($p = 0.66$; Figure 3.8d).

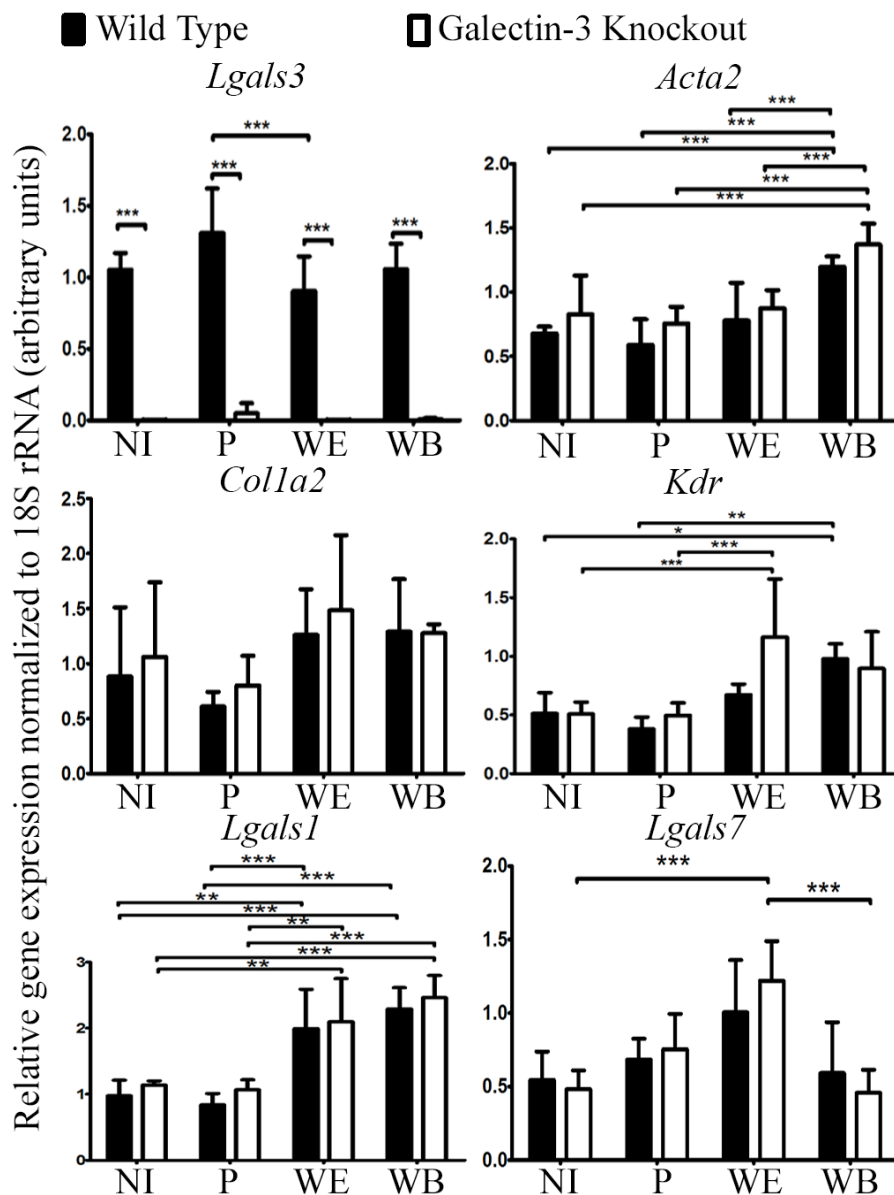


Figure 3.7: Transcript abundance of genes associated with fibrotic response and revascularization were unchanged by *Galectin-3* KO, 7 days post wounding. RNA was isolated from non-involved (NI), proximate (P), wound edge (WE), and wound bed (WB) tissues, 7 days post wounding, and quantified using quantitative PCR. Transcripts for fibrotic response genes *Acta2* and *Colla2*, and the vascular gene *Kdr*, were measured alongside *Lgals3* and its related family members *Lgals1* and *Lgals7*. Tissues were isolated from four sex-matched KO/WT pairs. Data are expressed as mean \pm standard deviation. *p < 0.05; **p < 0.01; ***p < 0.001.

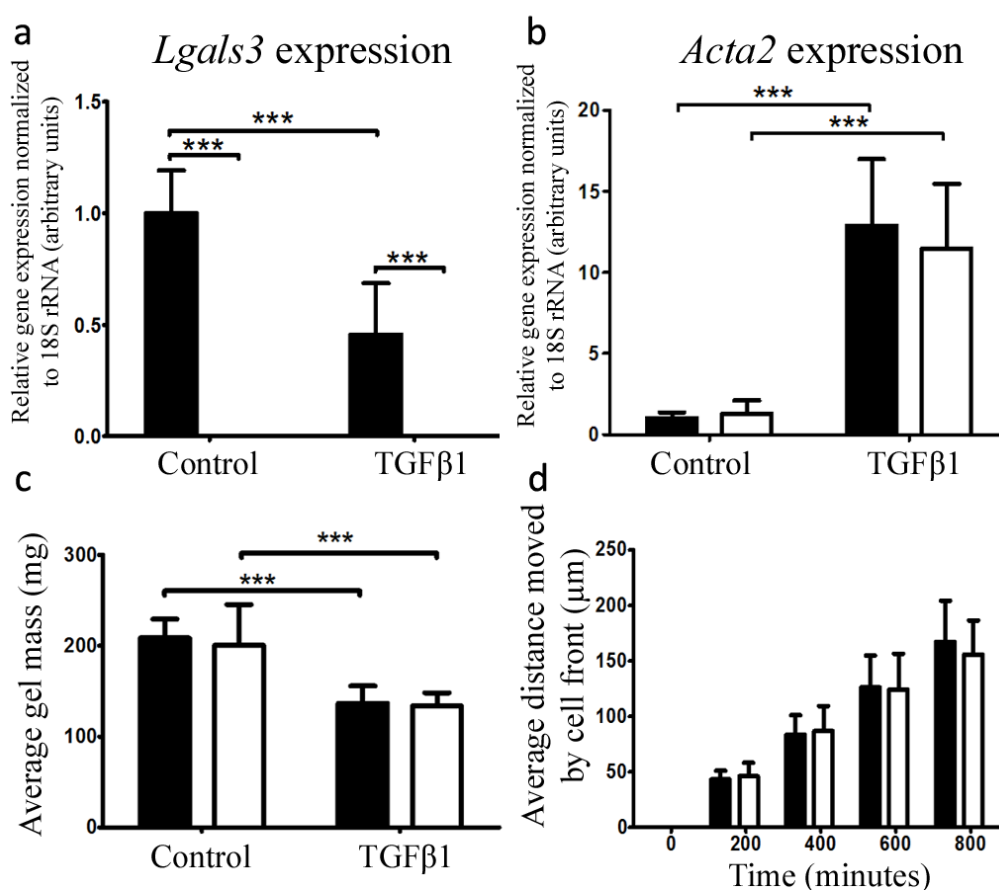


Figure 3.8: *Galectin-3* KO mouse dermal fibroblasts did not have impaired function *in vitro*. Cells from 4 independent fibroblast isolations from WT mice and their sex-matched *Galectin-3* KO littermates were treated with 5 ng/mL TGFβ1 for 24 hours prior to RNA isolation for RT-qPCR analysis of *Lgals3* (a), and *Acta2* (b). (c) A free collagen gel contraction assay in fibroblasts isolated from 4 wild type and 4 *Galectin-3* KO mice was conducted with or without the addition of 5 ng/mL TGFβ1. (d) An *in vitro* scratch wound assay was set up using dermal fibroblasts isolated from 5 WT and 4 *Galectin-3* KO mice and the average distance travelled by the cell front was measured. Values represented as mean ± SD. ***p<0.001. Black bars indicate WT dermal fibroblasts, white bars indicate *Galectin-3* KO dermal fibroblasts.

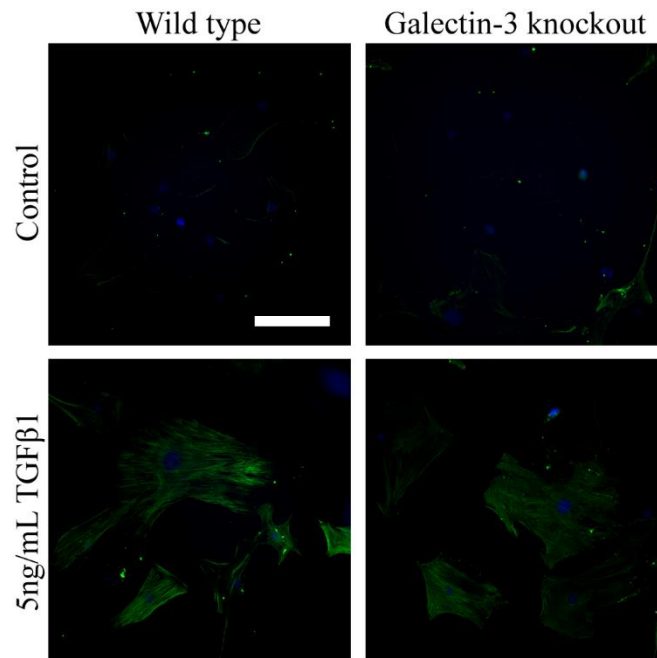


Figure 3.9: WT and *Galectin-3* KO mouse dermal fibroblasts formed α SMA stress fibers following TGF β 1 treatment. WT and *Galectin-3* KO mouse fibroblasts were treated with 5ng/mL TGF β 1 and stained for α SMA protein (green). Nuclei were labelled with DAPI (blue). Scale bar is 100 μ m.

3.4.6 Galectin-3 mRNA and protein were decreased in human non-healing skin wound tissue

As human chronic wounds remain in a prolonged inflammatory state, the subsequent studies focused on assessing Galectin-3 expression in human nonhealing wounds (Figure 3.10). Galectin-3 protein was observed in the epithelium in non-involved skin, but immunoreactivity decreased in tissue approaching the wound bed, with a lesser, variable immunoreactivity evident in the wound bed, as reported previously by our group (Pepe et al. 2014). In areas where Galectin-3 expression was low, large numbers of neutrophils were observed. Conversely, M1 macrophages (indolamine 2,3-dioxygenase positive cells) (Taylor and Feng 1991; Jaguin et al. 2013) and M2 macrophages (mannose receptor-positive cells) (Martinez et al. 2006; Madsen et al. 2013) were present in both areas of high and low Galectin-3 expression (Figure 3.10a and 3.10b). Transcript levels of Galectin-3 were significantly lower in the wound edge and proximate tissues than in non-involved tissues (30.9% of non-involved, $p < 0.001$, and 59.7% of non-involved, $p = 0.0027$, respectively; Figure 3.9c), and expression in the wound edge was significantly lower than the proximate tissue ($p = 0.048$).

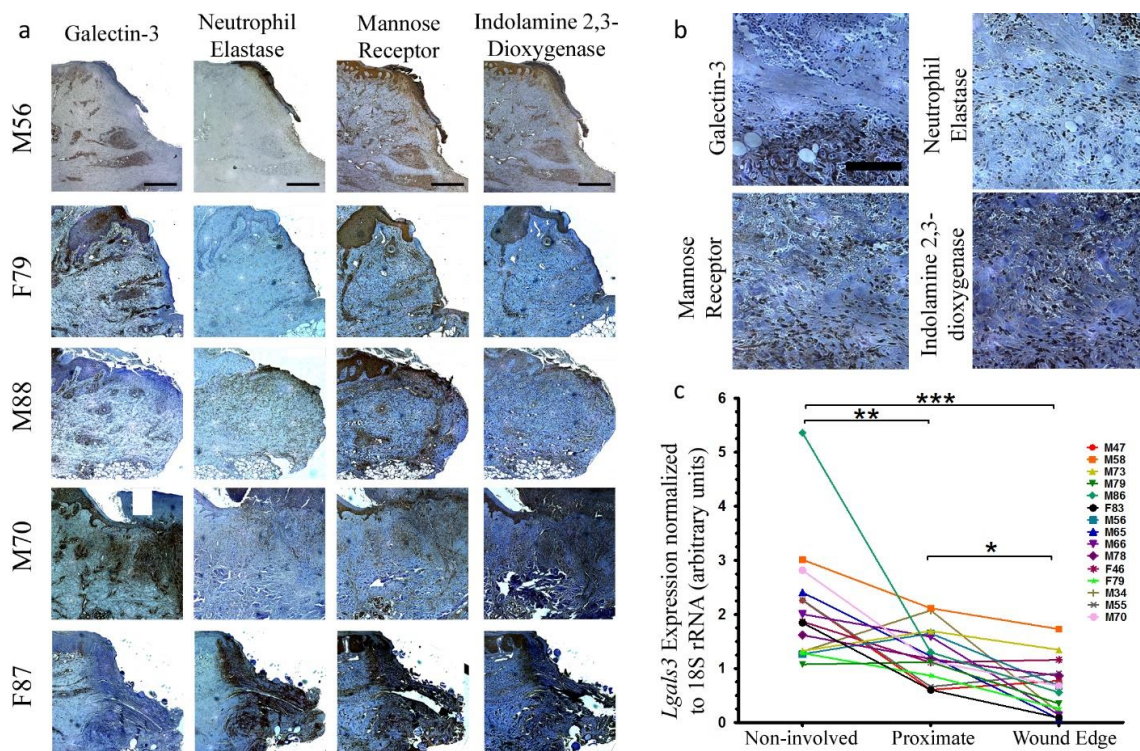


Figure 3.10: Galectin-3 expression was decreased in human chronic wound tissue and was negatively correlated with neutrophil elastase expression. (a) Histological analysis of Galectin-3, neutrophil elastase, mannose receptor, and indolamine 2,3-dioxygenase in the wound edge of human chronic wounds shown for 5 of 9 total patients examined. Bars = 1 mm. (b) High-magnification images of staining in the wound bed of patient M56. Bar = 100 μ m. (c) Quantification of *LGALS3* gene expression in 15 patients after lower extremity amputation in non-involved, proximate, and wound edge tissues. * $p < 0.05$; ** $p < 0.01$; *** $p < 0.001$. See Tables A6 and A7 for relevant patient information.

3.4.7 Galectin-3 expression in dermal fibroblasts from human wounds was modulated by TGFβ1 and tumor necrosis factor-α

The human dermal fibroblast response to the M1 and M2 cytokines, tumor necrosis factor (TNF)-α, and TGFβ1, respectively, was subsequently investigated (Figure 3.11). Addition of TGFβ1 significantly decreased *LGALS3* expression in chronic wound edge human dermal fibroblasts ($p < 0.001$) but did not significantly decrease expression in the non-involved fibroblasts of the same patients ($p = 0.63$). Similarly, TNFα only reduced *LGALS3* expression in the wound edge fibroblasts ($p = 0.032$) but not in the non-involved fibroblasts ($p = 0.996$). A combination of both cytokines had a similar effect to TNFα alone ($p = 0.016$ wound edge; $p = 1.00$ non-involved). Importantly, there was also a trend toward an interaction effect between the tissue of origin and the treatment variables ($p = 0.051$), suggesting fibroblasts from the wound edge responded differently to these cytokines than cells from non-involved tissue.

The strong inhibitory effect of TGFβ1 on *LGALS3* expression in wound edge fibroblasts was inhibited with the ALK5 inhibitor SB431542, and there was a significant interaction effect between the inhibitor and cytokine treatment variables ($p = 0.016$). To confirm that changes in *LGALS3* transcript levels translated into decreased protein expression, western blot analysis for Galectin-3 protein levels showed a decrease in the presence of TGFβ1 ($p < 0.001$), TNFα ($p = 0.0015$), and a combination of both ($p = 0.0045$) at 48 hours after treatment. Since the change in αSMA expression of dermal fibroblasts in response to TGFβ1 and TNFα has been well described (Goldberg et al. 2007), its expression was explored to determine whether wound edge fibroblasts shared this response. As expected,

TGF β 1 significantly increased α SMA expression ($p < 0.001$), which could be blocked with the addition of TNF α ($p = 0.020$).

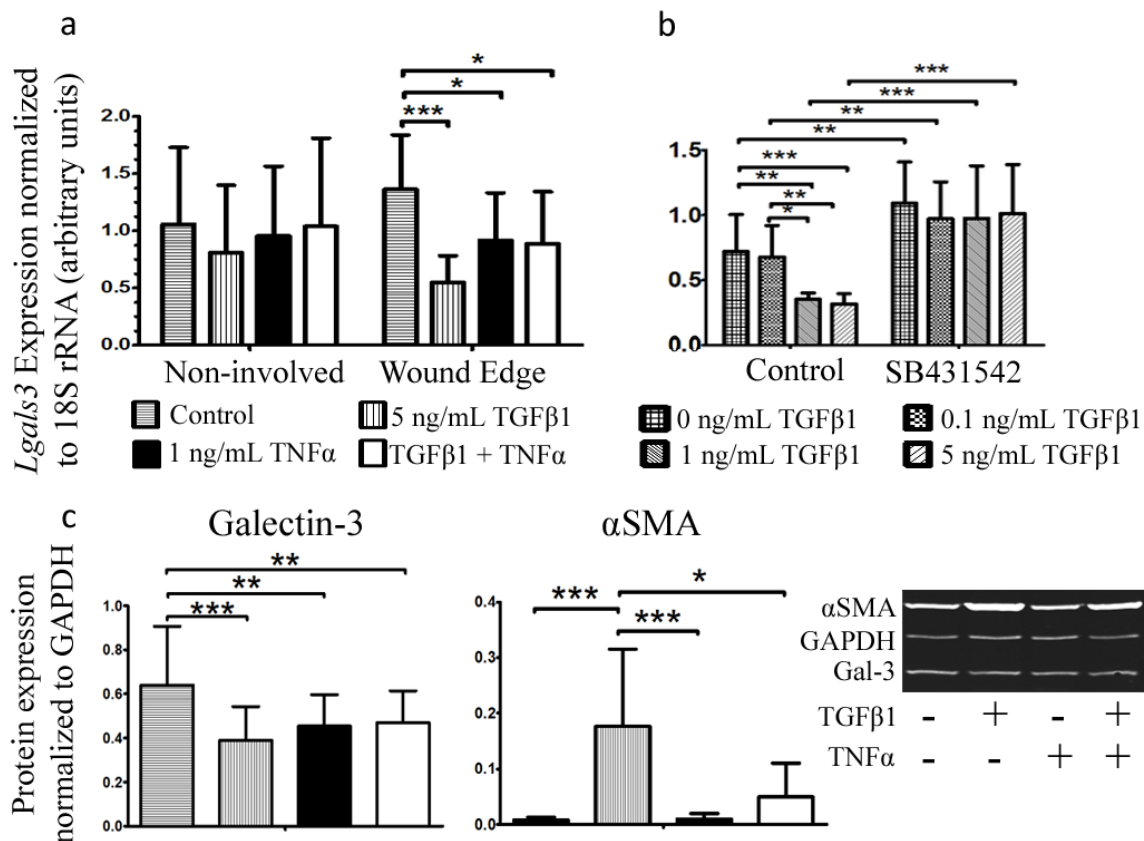


Figure 3.11: Regulation of Galectin-3 expression in human non-involved and wound edge dermal fibroblasts by TGFβ1 and TNFα. (a) Fibroblasts isolated from non-involved and wound edge tissues from patients with chronic wounds were subjected to combinations of 5 ng/mL TGFβ1 and 1 ng/mL TNFα for 24 hours. Cells isolated from four patients were used. (b) Dose response of wound edge dermal fibroblasts was performed from 0-5 ng/mL with or without addition of 10 μM of the ALK5 receptor inhibitor SB431542 for 24 hours. Cells isolated from five patients were used. (c) Effect of TGFβ1 and TNFα on Galectin-3 and αSMA protein content within wound edge fibroblasts was measured by western blot after 48 hours of stimulation. Cells isolated from four patients were used. Data are expressed as mean ± standard deviation. *p < 0.05; **p < 0.01; ***p < 0.001.

3.5 Discussion:

In this study, *Galectin-3* KO mice displayed impaired re-epithelialization 7 days after wounding, supporting previous work in dermal (Liu et al. 2012) and corneal healing (Cao et al. 2002). However, this was not concomitant with a significantly impaired rate of wound closure determined by gross examination. Wound closure in mice is heavily influenced by contraction and less so by re-epithelialization (Wong et al. 2011); thus, inhibition of re-epithelialization is possibly not great enough to manifest in significantly delayed closure in this model.

As impaired re-epithelialization in *Galectin-3* KO mice was previously characterized, roles of Galectin-3 in inflammation, granulation tissue synthesis, angiogenesis and wound contraction were investigated. In WT mice *Lgals3* expression was up-regulated during inflammation peaking at day 1, similar to previous findings in rats (Gál et al. 2011). Galectin-3 was expressed primarily in arginase I-positive cells and has previously been linked to phagocytosis of neutrophils by macrophages (Sano et al. 2003; Karlsson et al. 2009), M2 macrophage polarization (MacKinnon et al. 2008), and macrophage infiltration (Jia et al. 2013). As such, a decrease in M2 macrophage abundance in KO animals was expected, with increased neutrophil presence. However, similar numbers of arginase I-positive cells were observed within *Galectin-3* KO mice compared to WT mice, suggesting that while Galectin-3 may help promote M2 macrophage polarization *in vitro* (MacKinnon et al. 2008), it is not necessary for M2 polarization *in vivo* during acute healing. It has also been suggested that macrophage polarization *in vivo* is more complex than findings described *in vitro* (Sica and Mantovani 2012), as supported by the current

data showing inflammatory cells simultaneously expressing NOS2 and arginase I in both WT and KO animals.

It is possible that other proteins compensated for loss of Galectin-3, although assessment of galectin-1 and galectin-7 showed neither gene was significantly up-regulated in the absence of Galectin-3. However, basal expression of the proteins may be sufficient for compensation. Alternatively, non-family member proteins may compensate for its deletion. Since wound healing requires aspects associated with fibrosis (Wynn 2008; Johnson and Di Pietro 2013), the milder phenotype evident in *Galectin-3* KO mice during renal (Henderson et al. 2008), hepatic (Henderson et al. 2006), or lung (MacKinnon et al. 2012) fibrosis suggested *Galectin-3* KO mice would display impaired fibrotic responses after wounding. However, no differences in collagen deposition nor changes in α SMA gene or protein expression *in vivo* in *Galectin-3* KO mice were measured. Significantly, *in vitro*, the KO dermal fibroblasts treated with TGF β 1 showed no differences in α SMA gene expression, ability to contract a collagen gel, or incorporation of α SMA into stress fibers compared to WT cells. This is in contrast to *Galectin-3* KO pulmonary fibroblasts, which showed impaired myofibroblast differentiation and decreased collagen expression in response to TGF β 1 (MacKinnon et al. 2012). These findings suggest that there are intrinsic differences between these two fibroblast populations. This interpretation is corroborated by the *in vitro* findings showing decreased Galectin-3 expression in response to TGF β 1 in WT dermal fibroblasts, again opposing results with pulmonary fibroblasts (MacKinnon et al. 2012). Therefore, the profibrotic role of Galectin-3 appears highly tissue and cell specific, which is also evident with respect to its proangiogenic properties (Markowska et al. 2010, 2011; Nangia-Makker et al. 2010).

Previous studies have shown that Galectin-3 increases the surface expression of vascular endothelial growth factor receptor 2 (VEGFR2) (Markowska et al. 2011) and levels of vascular endothelial growth factor (VEGF) in macrophages (Machado et al. 2014), stimulating angiogenesis. However, no differences were observed in gene expression for *Kdr* between the mouse genotypes included in the current study, although *Kdr* was up-regulated in the wound bed and wound edge tissues at 7 days post wounding compared to unwounded skin. Furthermore, no significant differences in vessel density or average vessel size were noted within the granulation tissue at 7 days post wounding.

Although Galectin-3 expression is involved in the development of pulmonary, renal, and hepatic fibrosis in mouse models (Henderson et al. 2006, 2008; Jiang et al. 2012; MacKinnon et al. 2012), loss of expression did not impair the pro-fibrotic proliferative phase of dermal wound healing. While all of these processes involve the accumulation and activation of myofibroblasts from their respective myofibroblast progenitor pools (Hinz et al. 2012), it is evident that the mechanism through which these myofibroblast progenitors perceive environmental signals is different. This is exemplified by the differences between mouse primary pulmonary fibroblast observed by MacKinnon *et al.* (2012), and mouse primary dermal fibroblasts observed here. Cultured *Galectin-3* KO pulmonary fibroblasts were unable to upregulate α SMA or type I collagen in response to TGF β 1 *in vitro* as was observed for WT pulmonary fibroblasts, and genetic deletion of Galectin-3 was protective against bleomycin induced pulmonary fibrosis (MacKinnon et al. 2012). Conversely, dermal fibroblasts upregulated α SMA gene expression to the same extent as WT fibroblasts in response to TGF β 1 in culture and incorporated α SMA into stress fibers. Moreover, hydroxyproline content of the wound tissue at 15 days post

wounding was not different between WT and *Galectin-3* KO mice. Thus, while both lung and dermal fibroblasts can differentiate into myofibroblasts, subtle intrinsic differences exist in the mechanism through which this differentiation occurs, highlighting a level of heterogeneity between these two distinct myofibroblast progenitor populations.

Since human chronic wounds remain in a state of inflammation, the decrease in Galectin-3 expression within the wound bed compared to non-involved tissue was unexpected, opposing what was observed in WT mice during initial inflammation. Importantly, in human chronic wound tissue, expression of M1 and M2 macrophage markers appeared to be independent of Galectin-3 expression, whereas neutrophil elastase was negatively correlated with Galectin-3 expression. Although neutrophils provide an effective response to eliminate invading pathogens, they are not required for cutaneous healing and even delay wound re-epithelialization (Dovi et al. 2003). Given that Galectin-3 mediates phagocytosis of neutrophils by macrophages after neutrophil apoptosis (Karlsson et al. 2009), there may be a link between decreased Galectin-3 expression and impaired re-epithelialization in chronic wounds. Although *Galectin-3* KO mice displayed impaired re-epithelialization, no difference was measured in neutrophil abundance. Despite the fact that genetic deletion of Galectin-3 did not affect wound closure in mice, human chronic wounds tend to develop both in the elderly (patients ≥ 65 years account for 72% of pressure ulcers) (Sen et al. 2009) and in diabetic patients (accounting for approximately two-thirds of lower limb amputations) (Sen et al. 2009). Thus, in presence of underlying co-morbidities, it is possible that low Galectin-3 expression in the wound bed may be one part of the complex etiology leading to the persistence of chronic wounds in humans.

With respect to the regulation of Galectin-3 expression in fibroblasts, both TGF β 1 and TNF α were shown to reduce Galectin-3 expression in human dermal fibroblasts isolated from the wound edge of human chronic wounds, but not the non-involved fibroblasts. This fits with trends that our group has reported previously (Elliott et al. 2015), suggesting that chronic wound fibroblasts, although not able to function appropriately *in vivo*, respond strongly to certain stimuli *in vitro*. Since many fibrotic diseases correlate with high Galectin-3 levels (Henderson et al. 2008; Jiang et al. 2012; MacKinnon et al. 2012) and TGF β 1 is a potent inducer of a fibrotic phenotype in fibroblasts (Desmouliere et al. 1993), reduced Galectin-3 expression in response to TGF β 1 was unexpected. The current findings confirmed that chronic wound fibroblasts still respond appropriately to TGF β 1, as evidenced through their up-regulation of α SMA. Moreover, the same response was demonstrated in WT mouse dermal fibroblasts, supporting that the response was not species or disease-state specific.

Overall, the data show that the peak level of Galectin-3 mRNA associates with acute inflammation and that expression may be decreased after injury by the combined effects of TNF α and TGF β 1. It must also be mentioned that Galectin-3 is involved in the degradation of advanced glycation end products (AGEs) in human tissue, which is particularly important in diabetic individuals (Pugliese et al. 2014). Previous studies by our group showed that AGEs are inversely correlated with Galectin-3 expression in human chronic wounds (Pepe et al. 2014). Therefore, Galectin-3 expression may also be regulated differentially in these tissues through alternative mechanisms associated with advanced glycation end products.

3.6 Conclusions:

Through analysis of gene expression and histological parameters, no detectable wound healing specific phenotype was observed in the *Galectin-3* KO mice other than a reduced rate of re-epithelialization, as previously reported (Liu et al. 2012). Consistent with these findings, *Galectin-3* KO fibroblasts showed no notable deficits in the *in vitro* assays performed in the current study as compared to their WT counterparts.

In contrast to the increased expression of Galectin-3 during the inflammatory phase of healing relative to uninjured tissue in mice, human chronic wounds under-expressed Galectin-3 relative to patient-matched uninjured tissue, even though chronic wounds remain in a prolonged inflammatory state (Demidova-Rice et al. 2012). In isolated human chronic wound fibroblasts, Galectin-3 was down-regulated by both TGF β 1 and TNF α , both of which are expressed within human chronic wound tissue (Elliott et al. 2015), providing a potential mechanism for this difference. While the effects of genetic deletion of Galectin-3 in an acute wound model were mild, further investigation in an impaired model of healing, such as a diabetic mouse, could elucidate unrealized roles of this protein during wound repair.

3.7 References:

- Barondes SH, Cooper DNW, Gitt MA, Leffler H (1994) Galectins. Structure and function of a large family of animal lectins. *J Biol Chem* 269:20807–20810. doi: 10.1016/j.celrep.2015.02.012
- Cao Z, Said N, Amin S, et al (2002) Galectins-3 and -7, but not galectin-1, play a role in

- re-epithelialization of wounds. *J Biol Chem* 277:42299–42305. doi: 10.1074/jbc.M200981200
- D’Haene N, Sauvage S, Maris C, et al (2013) VEGFR1 and VEGFR2 Involvement in Extracellular Galectin-1- and Galectin-3-Induced Angiogenesis. *PLoS One* 8:e67029–e67029. doi: 10.1371/journal.pone.0067029
- Demidova-Rice TN, Hamblin MR, Herman IM (2012) nd Chronic Wounds: Biology, Causes, and Approaches to Care. 25:304–314. doi: 10.1097/01.ASW.0000416006.55218.d0.Acute
- Desmouliere A, Geinoz A, Gabbiani F, Gabbiani G (1993) Transforming growth factor- β 1 induces α -smooth muscle actin expression in granulation tissue myofibroblasts and in quiescent and growing cultured fibroblasts. *J Cell Biol* 122:103–111. doi: 10.1083/jcb.122.1.103
- Dovi J V, He L, Dipietro L a (2003) Accelerated wound closure in neutrophil-depleted mice. *J Leukoc Biol* 73:448–455. doi: 10.1189/jlb.0802406.http
- Elliott CG, Forbes TL, Leask A, Hamilton DW (2015) Inflammatory microenvironment and tumor necrosis factor alpha as modulators of periostin and CCN2 expression in human non-healing skin wounds and dermal fibroblasts. *Matrix Biol* 43:71–84. doi: 10.1016/j.matbio.2015.03.003
- Elliott CG, Wang J, Guo X, et al (2012) Periostin modulates myofibroblast differentiation during full-thickness cutaneous wound repair. *J Cell Sci* 125:121–132. doi: 10.1242/jcs.087841
- Gál P, Vasilenko T, Kostelníková M, et al (2011) Open Wound Healing In Vivo: Monitoring Binding and Presence of Adhesion/Growth-Regulatory Galectins in Rat Skin during the Course of Complete Re-Epithelialization. *Acta Histochem Cytochem* 44:191–199. doi: 10.1267/ahc.11014
- Goldberg MT, Han YP, Yan C, et al (2007) TNF- α suppresses α -smooth muscle actin expression in human dermal fibroblasts: An implication for abnormal wound healing. *J Invest Dermatol* 127:2645–2655. doi: 10.1038/sj.jid.5700890
- Henderson NC, Mackinnon AC, Farnworth SL, et al (2006) Galectin-3 regulates myofibroblast activation and hepatic fibrosis. *Proc Natl Acad Sci* 103:5060–5065. doi: 10.1073/pnas.0511167103

- Henderson NC, Mackinnon AC, Farnworth SL, et al (2008) Galectin-3 expression and secretion links macrophages to the promotion of renal fibrosis. *Am J Pathol* 172:288–298. doi: 10.2353/ajpath.2008.070726
- Hinz B, Phan SH, Thannickal VJ, et al (2012) Recent developments in myofibroblast biology: Paradigms for connective tissue remodeling. *Am J Pathol* 180:1340–1355. doi: 10.1016/j.ajpath.2012.02.004
- Hothorn T, Bretz F, Westfall P (2008) Simultaneous inference in general parametric models. *Biometrical J* 50:346–363. doi: 10.1002/bimj.200810425
- Jaguin M, Houlbert N, Fardel O, Lecureur V (2013) Polarization profiles of human M-CSF-generated macrophages and comparison of M1-markers in classically activated macrophages from GM-CSF and M-CSF origin. *Cell Immunol* 281:51–61. doi: 10.1016/j.cellimm.2013.01.010
- Jia W, Kidoya H, Yamakawa D, et al (2013) Galectin-3 accelerates M2 macrophage infiltration and angiogenesis in tumors. *Am J Pathol* 182:1821–1831. doi: 10.1016/j.ajpath.2013.01.017
- Jiang JX, Chen X, Hsu DK, et al (2012) Galectin-3 modulates phagocytosis-induced stellate cell activation and liver fibrosis in vivo. *AJP Gastrointest Liver Physiol* 302:G439–G446. doi: 10.1152/ajpgi.00257.2011
- Jin Lim M, Ahn J, Youn Yi J, et al (2014) Induction of galectin-1 by TGF- β 1 accelerates fibrosis through enhancing nuclear retention of Smad2. *Exp Cell Res* 326:125–135. doi: 10.1016/j.yexcr.2014.06.001
- Johnson A, Di Pietro LA (2013) Apoptosis and angiogenesis: An evolving mechanism for fibrosis. *FASEB J* 27:3893–3901. doi: 10.1096/fj.12-214189
- Karlsson A, Christenson K, Matlak M, et al (2009) Galectin-3 functions as an opsonin and enhances the macrophage clearance of apoptotic neutrophils. *Glycobiology* 19:16–20. doi: 10.1093/glycob/cwn104
- Li Q, Yu Y, Bischoff J, et al (2003) Differential expression of CD146 in tissues and endothelial cells derived from infantile haemangioma and normal human skin. *J Pathol* 201:296–302. doi: 10.1002/path.1443
- Liu W, Hsu DK, Chen HY, et al (2012) Galectin-3 regulates intracellular trafficking of EGFR through alix and promotes keratinocyte migration. *J Invest Dermatol*

- 132:2828–2837. doi: 10.1038/jid.2012.211
- Machado CM ari. L, Andrade LN ogueir. S, Teixeira VR, et al (2014) Galectin-3 disruption impaired tumoral angiogenesis by reducing VEGF secretion from TGFβ1-induced macrophages. *Cancer Med* 3:201–214. doi: 10.1002/cam4.173
- MacKinnon AC, Farnworth SL, Hodgkinson PS, et al (2008) Regulation of Alternative Macrophage Activation by Galectin-3. *J Immunol* 180:2650–2658. doi: 10.4049/jimmunol.180.4.2650
- MacKinnon AC, Gibbons MA, Farnworth SL, et al (2012) Regulation of transforming growth factor-β1-driven lung fibrosis by Galectin-3. *Am J Respir Crit Care Med* 185:537–546. doi: 10.1164/rccm.201106-0965OC
- Madsen DH, Leonard D, Masedunskas A, et al (2013) M2-like macrophages are responsible for collagen degradation through a mannose receptor-mediated pathway. *J Cell Biol* 202:951–966. doi: 10.1083/jcb.201301081
- Markowska AI, Jefferies KC, Panjwani N (2011) Galectin-3 protein modulates cell surface expression and activation of vascular endothelial Growth factor receptor 2 in human endothelial cells. *J Biol Chem* 286:29913–29921. doi: 10.1074/jbc.M111.226423
- Markowska AI, Liu F-T, Panjwani N (2010) Galectin-3 is an important mediator of VEGF- and bFGF-mediated angiogenic response. *J Exp Med* 207:1981–1993. doi: 10.1084/jem.20090121
- Martinez FO, Gordon S, Locati M, Mantovani A (2006) Transcriptional Profiling of the Human Monocyte-to-Macrophage Differentiation and Polarization: New Molecules and Patterns of Gene Expression. *J Immunol* 177:7303–7311. doi: 10.4049/jimmunol.177.10.7303
- Nangia-Makker P, Honjo Y, Sarvis R, et al (2000) Galectin-3 induces endothelial cell morphogenesis and angiogenesis. *Am J Pathol* 156:899–909. doi: 10.1016/S0002-9440(10)64959-0
- Nangia-Makker P, Wang Y, Raz T, et al (2010) Cleavage of Galectin-3 by matrix metalloproteases induces angiogenesis in breast cancer. *Int J Cancer* 127:2530–2541. doi: 10.1002/ijc.25254
- Nelson E, Bradley M (2007) Dressings and topical agents for arterial leg ulcers.

Cochrane Database Syst Rev

- Novak R, Dabelic S, Dumic J (2012) Galectin-1 and Galectin-3 expression profiles in classically and alternatively activated human macrophages. *Biochim Biophys Acta - Gen Subj* 1820:1383–1390. doi: 10.1016/j.bbagen.2011.11.014
- Pepe D, Elliott CG, Forbes TL, Hamilton DW (2014) Detection of Galectin-3 and localization of advanced glycation end products (AGE) in human chronic skin wounds. *Histol Histopathol* 29:251–258. doi: 10.14670/HH-29.251
- Pinheiro J, Bates D, R-core (2014) Linear and Nonlinear Mixed Effects Models
- Pugliese G, Iacobini C, Ricci C, et al (2014) Galectin-3 in diabetic patients. *Clin Chem Lab Med* 52:1413–1423. doi: 10.1515/cclm-2014-0187
- R core team (2017) R: A language and environment for statistical computing. R Found. Stat. Comput. Vienna, Austria.
- Reinke JM, Sorg H (2012) Wound repair and regeneration. *Eur Surg Res* 49:35–43. doi: 10.1159/000339613
- Rittié L, Fisher GJ (2005) Isolation and Culture of Skin Fibroblasts. *Fibros Res* 117:83–98. doi: 10.1385/1-59259-940-0:083
- Sano H, Hsu DK, Apgar JR, et al (2003) Critical role of Galectin-3 in phagocytosis by macrophages. *J Clin Invest* 112:389–397. doi: 10.1172/JCI200317592
- Schneider CA, Rasband WS, Eliceiri KW (2012) NIH Image to ImageJ: 25 years of image analysis. *Nat Methods* 9:671–675. doi: 10.1038/nmeth.2089
- Schultz GS, Wysocki A (2009) Interactions between extracellular matrix and growth factors in wound healing. *Wound Repair Regen* 17:153–162. doi: 10.1111/j.1524-475X.2009.00466.x
- Sen CK, Gordillo GM, Roy S, et al (2009) Human skin wounds: A major and snowballing threat to public health and the economy: PERSPECTIVE ARTICLE. *Wound Repair Regen* 17:763–771. doi: 10.1111/j.1524-475X.2009.00543.x
- Shih SC, Robinson GS, Perruzzi CA, et al (2002) Molecular profiling of angiogenesis markers. *Am J Pathol* 161:35–41. doi: 10.1016/S0002-9440(10)64154-5
- Sica A, Mantovani A (2012) Macrophage plasticity and polarization: In vivo veritas. *J Clin Invest* 122:787–795. doi: 10.1172/JCI59643
- Singer AJ, Clark R (1999) Mechanisms of Disease - Cutaneous Wound Healing. *N Engl J*

Med 341:738–746

Taylor MW, Feng GS (1991) Relationship between interferon-gamma, indoleamine 2,3-dioxygenase, and tryptophan catabolism. *FASEB J* 5:2516–22. doi: 10.1096/FASEBJ.5.11.1907934

Widgerow AD (2011) Chronic wound fluid-thinking outside the box. *Wound Repair Regen* 19:287–291. doi: 10.1111/j.1524-475X.2011.00683.x

Wiegand C, Schönfelder U, Abel M, et al (2010) Protease and pro-inflammatory cytokine concentrations are elevated in chronic compared to acute wounds and can be modulated by collagen type i in vitro. *Arch Dermatol Res* 302:419–428. doi: 10.1007/s00403-009-1011-1

Wong VW, Sorkin M, Glotzbach JP, et al (2011) Surgical Approaches to Create Murine Models of Human Wound Healing. *J Biomed Biotechnol* 2011:1–8. doi: 10.1155/2011/969618

Wynn T (2008) Cellular and molecular mechanisms of fibrosis. *J Pathol* 220:114–125. doi: 10.1002/path

Chapter 4: Profibrotic and pro-angiogenic biomaterials to induce cell recruitment and differentiation during skin healing

4.1 Abstract:

Chronic wounds place a major burden on the health care system and have severe consequences for those affected. While current advanced therapy options, including skin grafts and engineered skin/dermal substitutes, improve healing over standard care alone, they do not lead to complete healing in over half of patients treated. There is a desperate clinical need to improve upon existing therapeutics for the treatment of chronic wounds. The extracellular matrix provides not only mechanical support for cells but also contains many biological signals that regulate cell function. Understanding and utilizing these biological signals will be an important step in advancing wound care therapeutics. Previous experiments in the Hamilton lab identified a positive effect of biomaterials containing the matricellular proteins Periostin and CCN2 on wound closure in a diabetic mouse model; moreover, preliminary work presented here identified a similarly positive effect of decellularized adipose tissue-derived biomaterials on healing of wounds in diabetic mice. In the present study, porous foams fabricated from bovine type I collagen both with and without Periostin and CCN2 were investigated using an acute wound model in healthy pigs in comparison to similar scaffolds fabricated using human decellularized adipose tissue as the source material. A subset of each scaffold type was

also seeded with allogeneic porcine adipose-derived stem/stromal cells to assess the potential of the scaffolds as a cell delivery platform for wound healing. Scaffolds synthesized for this study could be easily customized in terms of size and shape, were easy to handle, and integrated well into the granulation tissue. Assessment of wound closure kinetics highlighted a modest delay in wounds treated with any foam biomaterial relative to untreated wounds, but did not alter the total time to heal. Histological parameters including inflammatory, mesenchymal, and vascular cell infiltration were not substantially altered by treatment with biomaterials in this model system. This study provides important baseline data for future investigation into models of impaired porcine wound healing.

4.2 Introduction:

Chronic wounds are classified based on their underlying etiology, and include pressure sores, venous ulcers, arterial ulcers, and diabetic ulcers (Demidova-Rice et al. 2012b; Frykberg and Banks 2015). Despite arising from disparate underlying pathologies, chronic wounds share common pathophysiological features, including a prolonged and excessive immune response, persistent infections, vascular insufficiency, and an inability to regenerate dermal and epidermal tissue (Armstrong et al. 1998; Valencia et al. 2001; Demidova-Rice et al. 2012b; Frykberg and Banks 2015). Combined, chronic wounds are a serious problem both clinically and economically (Sen et al. 2009; Frykberg and Banks 2015). In Canada, in 2011, diabetic foot ulcers alone affected 25,597 patients, costing \$547 M to treat (Hopkins et al. 2015).

Chronic wounds are commonly secondary to vascular insufficiency at both the macro- and micro-vascular level (Li et al. 2017). Macrovascular surgeries and therapeutic

compression remain common practices to improve macrocirculation in affected limbs (Demidova-Rice et al. 2012b; Baltzis et al. 2014). Microvascular complications which can arise from ischemia-reperfusion injury and diabetes related complications, are more difficult to treat, but a highly vascularized granulation tissue is an important clinical target for chronic wound treatment (Mustoe et al. 2006; Demidova-Rice et al. 2012a; Powers et al. 2016; Li et al. 2017; Valencia and Florez 2017). In addition to poor microvascular circulation, human chronic wounds are also associated with a prolonged inflammatory state, with decreased fibroblast migration and proliferation impairing transition into an appropriate proliferative phase (Baltzis et al. 2014). Therefore, it is hypothesized that therapeutics that can improve wound microcirculation, as well as increasing fibroblast proliferation and activation, would be beneficial for transitioning from the inflammatory phase to the proliferative phase of healing.

Previous studies in our laboratories have investigated two different approaches to creating biomaterials to improve the angiogenic and fibrogenic properties during tissue regeneration. First, biomaterials synthesized from bovine type I collagen, both with and without recombinant human matricellular proteins, Periostin and connective tissue growth factor (CCN2), were investigated. Periostin is a key regulator of myofibroblast differentiation (Elliott et al. 2012; Walker et al. 2016), and CCN2 has pro-fibrotic and pro-angiogenic effects (Hall-Glenn and Lyons 2011). Both proteins are upregulated during the fibrotic phase of acute wound repair in humans and mice, but are repressed in human chronic wounds (Elliott et al. 2015) and in wounds of diabetic mice (Elliott et al. 2018). Previous work by our group showed that the delivery of Periostin or CCN2 significantly increased the angiogenic and profibrotic responses during wound healing in

a diabetic mouse model of impaired healing (Elliott et al. 2018). While these studies were performed on materials synthesized through electrospinning, the present work investigated a foam biomaterial approach. This method enabled the fabrication of highly porous scaffolds designed for enhanced stability and better integration, which could be easily customized for shape and size, and did not require chemical cross-linking to maintain the biomaterial structure.

As a comparison to the collagen-based foams, compositionally more complex porous foams synthesized from the extracellular matrix isolated from human adipose tissue were also investigated. These decellularized adipose tissue (DAT)-derived foams were previously found to be pro-angiogenic following subcutaneous implantation in immune-competent rats (Yu et al. 2013). A recent proteomics study by our group has identified a massive array of structural and non-structural proteins present within DAT, including collagens, matricellular proteins, proteoglycans, glycoproteins and signaling molecules (Kuljanin et al. 2017). While collagen-based materials with incorporated Periostin and CCN2, and DAT-based scaffolds are compositionally distinct, they both hold potential as pro-regenerative biological wound dressings based on previous studies.

Although the mouse is the most widely-used model to study dermal healing, the structure and physiology of murine skin differs significantly from human skin (Wong et al. 2011; Zomer and Trentin 2018). More specifically, mouse skin is thinner and more compliant, has an additional muscle layer (the panniculus carnosus), lacks rete ridges, and is affected by changes in the hair growth cycle. Unfortunately, these differences have impacted the translation of therapeutics from mice into humans (Sullivan et al. 2001). In contrast, porcine skin is more structurally similar to that of humans and studies have suggested that

it may be more translationally relevant (Sullivan et al. 2001). More specifically, a review investigating more than 180 studies across 25 different wound therapeutics showed that only 53% of wound healing studies in small mammals correlated with those in humans in terms of their effects on the rate of wound closure, whereas porcine models showed a stronger correlation of 78% (Sullivan et al. 2001).

As an exploratory study to assess safety and compatibility, acute dorsal wounds in healthy juvenile pigs were treated with the biomaterials described above and the tissue response was assessed during the early proliferative stage at 7 days post-wounding, and during the remodelling phase at 28 days post-wounding. In addition to their potential as off-the-shelf pro-regenerative biological wound dressings, the foam biomaterials tested could be applied as carriers for cell therapies. In particular, mesenchymal stem/stromal cell (MSC) treatment is a promising therapeutic strategy for the treatment of human wounds (Falanga et al. 2007). Adipose-derived MSCs (ASCs) are an abundant population that can be harvested from tissues that would otherwise be discarded as medical waste. Supporting the selection of ASCs, novel lineage tracing data has suggested that adipogenic fibroblast lineages contribute to myofibroblast populations that play a role during wound healing, and in fibrotic disease (Driskell et al. 2013; Marangoni et al. 2015; El Agha et al. 2017). Furthermore, perivascular populations, a major source of MSCs across organs (Crisan et al. 2008), have been shown to naturally contribute to myofibroblasts during fibrotic injury in many organs including kidney, liver, lungs, heart, and bone marrow (Kramann et al. 2015; Schneider et al. 2017). Whether exogenous ASCs would contribute to wound closure through differentiation into myofibroblasts is unknown; however, much of the promise of ASCs lies in their paracrine capacity

including the potential to modulate the immune response towards a more pro-regenerative state, and induce angiogenesis (Nuschke 2014; Bateman et al. 2018). Within the context of this study, ASCs can be obtained in abundance from pigs (Williams et al. 2011), allowing for a clinically relevant allogeneic transplant model. As such, the potential of the foam biomaterials as an allogeneic cell delivery platform was probed at 7 days post-wounding.

The biomaterials investigated in this study have been reported to display pro-angiogenic and pro-fibrotic potential during tissue regeneration. In this study, we hypothesized that treatment with these biomaterials would improve the rate of wound closure and correspond with increased myofibroblast activation and enhanced angiogenesis within the granulation tissue compared to untreated wounds. Furthermore, we hypothesized that seeding these biomaterials with ASCs would be an effective strategy to deliver cells into the granulation tissue.

4.3 Materials and methods:

4.3.1 Synthesis of bovine type I collagen and DAT foams

Bovine type I collagen, purified from tendon (BTC) was purchased from Advanced Biomatrix and was minced in-house prior to further processing. Human decellularized adipose tissue was isolated from discarded tissue samples collected with informed consent from elective lipo-reduction procedures (HREB #105426) and pooled from 5 donors, as previously described (Flynn 2010). Lyophilized forms of these materials were rehydrated, treated with α -amylase to improve solubility and suspended in acetic acid, as

previously described (Yu et al. 2013). Foams used for the mouse pilot study were synthesized using 200 μL of 25 mg/mL suspended DAT or BTC loaded into a 48-well plate. For foams used in the porcine study, 1.5 mL of 15 mg/mL suspended DAT or BTC was transferred into a circular mold of 2 cm diameter. Loaded molds were frozen at -20°C prior to lyophilization. Representative images of the final rehydrated foams used in the porcine study are shown below in Figure 4.1. For the addition of Periostin and CCN2, following rehydration, BTC foams were soaked in a solution of 500 μL phosphate buffered saline (PBS) containing 2.6 $\mu\text{g}/\text{mL}$ of Periostin (Human; R&D Systems) and 2.6 $\mu\text{g}/\text{mL}$ CCN2 (Human; R&D Systems) overnight at 4°C . For treatment, foams were warmed prior to implantation.

4.3.2 *db/db mouse model*

As DAT foams had not previously been tested in a wound application, an initial pilot study was designed to explore their potential efficacy and physical suitability in a *db/db* mouse model of type II diabetes. All animal work was performed in accordance with protocols approved by the University Council on Animal Care at the University of Western Ontario, following the guidelines of the Canadian Council on Animal Care (protocol # 2016-085). The dorsal skin of 8 *db/db* mice (B6.BKS(D)Leprdb/J, 000697, JAX) was wounded using a 6 mm biopsy punch. Wounds were filled with electrospun collagen scaffolds, DAT foams (cut to an 8 mm diameter) or were left untreated. Closure was monitored over time and wound size was measured from photographs using ImageJ software (Schneider et al. 2012). Four of the animals were euthanized at 3 days post wounding, and the remaining 4 euthanized at 7 days post wounding.

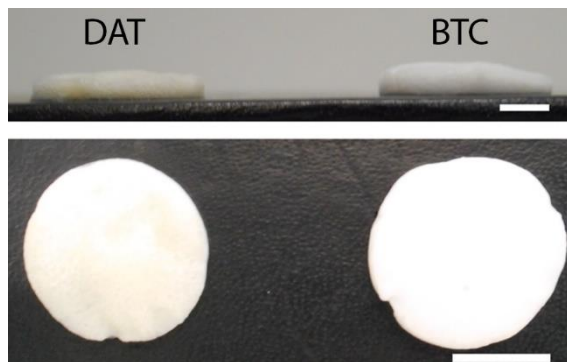


Figure 4.1: DAT and BTC foams. Scale bar in the top frame is 5 mm; scale bar in the bottom frame is 1 cm.

4.3.3 Porcine wound model

Nine 3-month-old male farm pigs (Landrace and Yorkshire backgrounds) from two different cohorts, were observed up to either 7 days post wounding (n=3) or 28 days post wounding (n=6), at which time the animals were euthanized, and the tissue collected for analysis (animal use protocol # 2017-082). Eight (day 7 cohort), or five (day 28 cohort) 2 cm diameter, circular full thickness excisional wounds were made in the dorsal skin using a custom punch biopsy. These wounds were either left untreated (2 untreated controls in the 28-day cohort), or treated with 2 stacked 2 cm diameter foam biomaterials from each treatment group: (i) purified type I collagen isolated from bovine tendon (BTC), (ii) BTC loaded with Periostin and CCN2 (PN/CCN2), or (iii) human DAT. The four remaining wounds in the 7-day cohort were used to assess porcine ASC-seeded BTC, BTC+PN/CCN2, and DAT foams relative to an additional untreated control. Only five of the six pigs in the 28-day cohort were treated with BTC+PN/CCN2 foams; all six pigs received each other treatment. Wounds were covered in a semi-occlusive dressing (Tegaderm™; 3M) and bandaged. Bandages were replaced as required. For the 7-day cohort, wounds were photographed starting at day 3, whereas those in the 28-day cohort

were first photographed for assessment of closure on day 7-12. Wound size was normalized to a ruler and measured using ImageJ software (Schneider et al. 2012).

4.3.4 Histological assessment

Immediately after euthanasia, tissue samples were collected. One quarter of the wound was frozen on dry ice for assessment of hydroxyproline content, and the remaining tissue was fixed in neutral buffered formalin. Tissues were dehydrated for cryopreservation using a sucrose gradient and embedded in Frozen Section Compound (Leica). Cryosections were cut to a thickness of 8 μm . Antigen retrieval was performed in all samples using 1% SDS in PBS for 5 minutes. Blocking was performed with horse serum and primary antibodies used are shown with dilutions in Table 4.1. Coverslips were mounted with VectaShield mounting media with DAPI (Vectorlabs).

For all measurements, only the viable granulation tissue was quantified, and not the eschar or the undegraded biomaterials. Quantification of staining was performed using macros in ImageJ software. For fluorescence quantification, 2-5 full depth vertical regions of interest with a width of one field of view ($\sim 1.4\text{ mm}$) were measured for each wound. For blood vessel quantification, a minimum size threshold was set to 100 pixels ($\sim 100\ \mu\text{m}^2$) to prevent quantitation of non-vascular structures. CD68 and CD163 staining were each thresholded for a minimum size of 10 pixels and a maximum size of 500 pixels ($\sim 10\text{-}500\ \mu\text{m}^2$). Cross-sectional wound diameter was measured from the junction of the unwounded dermis, the hypodermis, and the granulation tissue as a clear landmark. For all staining performed large vertical regions of interest are shown in the body of this chapter. For higher magnification images of each staining performed, please see Appendix Figure A3-A7.

Table 4.1: Antibodies for histological assessment

Target	Antibody	Dilution
CD146	Ab75769 (Abcam)	1:500
α SMA	A5228 (Sigma-Aldrich)	1:1000
Vimentin	Ab92547 (Abcam)	1:500
CD68	Ab125212 (Abcam)	1:100
CD163	MCA2311GA (Bio-rad)	1:100

4.3.5 Hydroxyproline assay

From each frozen wound and unwounded tissue sample, a section of tissue spanning the entire depth of the wound was removed (20-70 mg wet weight). These pieces were lyophilized prior to acid hydrolysis in 6 M HCl at 120°C for 3 hours. Measurement of hydroxyproline content was performed using the Hydroxyproline Assay Kit (Sigma-Aldrich) following the protocol instructions. Measured hydroxyproline content was normalized to tissue wet weight.

4.3.6 Porcine ASC isolation and tri-lineage differentiation

Dorsal, subcutaneous adipose tissue was harvested from four male donor pigs at ~3 months of age. The tissue was minced in a sterile environment, and then digested with 2 mg/mL collagenase type I (Sigma). The digested suspension was filtered through a 250 μ m pore size stainless steel mesh and allowed to gravity settle to allow removal of the floating adipocyte layer through aspiration. Red blood cells were removed using an ammonium chloride lysis buffer. The resultant cell population was seeded onto culture flasks and cultured at 39°C, 5% CO₂, in DMEM/Ham's F-12 media (Sigma) with 10% fetal bovine serum (FBS; VWR) and 1% penicillin/streptomycin (PS; Gibco). Media was

changed every 2-3 days, and cells were cultured for 3 passages at which time they were frozen and stored in liquid nitrogen. Assessment of tri-lineage differentiation and scaffold seeding was performed using passage 4 cells. For differentiation, control populations were cultured in non-inductive proliferation media consisting of the base media plus 10% FBS and 1% PS. In all cases, cells were cultured at 39°C with 5% CO₂.

Adipogenic differentiation was carried with slight modifications to that described by Hauner *et al.* and as previously published by Dr. Flynn (Hauner et al. 2001; Flynn 2010). Cells seeded at a density of 50,000 cells/cm² were treated with DMEM/Ham's F-12 media with 3% FBS, supplemented with 33 μM biotin, 17 μM pantothenate, 66 nM human insulin, 1 nM triiodothyronine, 10 μg/mL transferrin, 100 nM hydrocortisone, 1 μg/mL Troglitazone, 250 μM 3-isobutyl-1-methylxanthine (IBMX), and 1% PS. After 3 days, the troglitazone and IBMX were excluded from the formulation. Cells were cultured for 14 days, with media changes every 2 days. Staining with oil red O dye was used to assess the formation of intracellular lipid droplets at 14 days.

Chondrogenic differentiation was carried out on 250,000 cells, pelleted by centrifugation (5 minutes; 400 g) in the bottom of 15 mL conical tubes. These pellets were cultured in DMEM (Gibco), supplemented with 10% FBS, 50 μg/mL ascorbate-2-phosphate, 10 ng/mL TGFβ1, 6.25 μg/mL insulin, 100 nM dexamethasone and 1% PS. Media was changed every 2 days, and differentiation was assessed after 28 days. Cell pellets were frozen, cryosectioned, and collagen types I and II were observed by immunofluorescence (Ab90395, Ab34712; Abcam).

Osteogenic differentiation was carried out at a seeding density of 20,000 cells/cm² using αMEM (Gibco) supplemented with 10% FBS, 50 μM ascorbate-2-phosphate, 10 mM β-

glycerophosphate, 10 nM dexamethasone, and 1% PS. Matrix mineralization was assessed with von Kossa staining at 28 days.

4.3.7 ASC labelling and seeding

Passage 4 ASCs were labelled with PKH26 (Sigma-Aldrich) as per the manufacturer's instructions. Hydrated, sterilized 2 cm diameter foam biomaterials were placed individually into a 50 mL vented conical tube (Corning), and seeded with 1.5×10^6 ASCs in 3 mL DMEM/Ham's F-12 culture media with 10% FBS, and 1% PS at 39°C with 5% CO₂. The tubes were angled at 20-30° and placed on a rotating table set at 100 rpm, for 16 hours at 39°C. The scaffolds were then removed and placed in a 12-well plate for static culture for 2 additional days of static culture. All scaffolds were then transferred into DMEM/Ham's F-12 with 1% FBS on the evening prior to implantation. Matricellular proteins were added, at the concentrations described above, to seeded scaffolds in this final solution, to allow infiltration into the scaffold overnight. The following day, the seeded foam biomaterials were implanted into wounds, 2 scaffolds per wound as described for the unseeded scaffolds. Untreated wounds were left empty, and did not receive biomaterials or ASCs.

4.3.8 Statistical methods

Statistical analyses were performed using R statistics software (R core team 2017). *Db/db* mouse wound closure, all histological analyses, and hydroxyproline content were assessed using linear mixed effects models with the “nlme” (Pinheiro et al. 2014), and the “multcomp” package for simultaneous inference in general parametric models (Hothorn et al. 2008). Statistical comparisons were made within each treatment group between day

7 and day 28, and at both the 7- and 28-day time points, comparisons were made between each treatment group and the untreated control as the standard of care but were not made between different biomaterials groups due to the limited sample size. The values for the unwounded tissue were plotted for comparative purposes but were excluded from statistical analyses. Wound size measurements were estimated linearly at non-measured intervals for each pig, and this complete data set was used to fit the data to a regression model. Specifically, a basis spline function was used to fit the data to a regression curve, allowing estimation of wound size and variability between measured data. This was performed in R using the Companion to Applied Regression, “car” (Fox and Weisberg 2011), and Functional Data Analysis in R, “fda” (Ramsay et al. 2017) packages. Comparisons of these data were made with a 2-way ANOVA, and multiple comparisons were assessed using Dunnett’s test comparing to untreated wounds as the control. The raw size measurements used in the regression analysis are included in Appendix Figure A8.

4.4 Results:

4.4.1 DAT foams increased the rate of wound closure in db/db mice

Initial testing of the DAT foams was performed in a pilot study investigating wound closure up to 7 days post-wounding in a *db/db* mouse model of impaired wound healing. Treatment with 25 mg/mL DAT foams resulted in improved wound closure in comparison to untreated wounds, as well as those treated with electrospun bovine type I collagen scaffolds (Figure 4.2). Importantly, further investigation in wild-type mice revealed that the DAT foams fabricated at this concentration could be excluded from the

wounds over time by the cellular infiltrate. To address this issue, more porous 15 mg/mL foams were selected for future testing in the porcine model, following confirmation of improved integration through pilot testing in wild-type mice.

4.4.2 Addition of foam biomaterials into 2 cm diameter wounds in the dorsal skin of pigs induced a delay to the rate of healing, but did not alter the time to complete closure

Following the pilot study in mice, influence of each biomaterials on wound closure was assessed in a porcine model. The treatment of a wound with any biomaterial significantly delayed wound closure relative to untreated wounds (Figure 4.3). Notably, in the 7-day cohort, where wound size was measured more frequently within the first week compared to the 28-day cohort, the wound size was similar between days 3 and 7 in the wounds treated with each of the biomaterials (Figure 4.4). In contrast, the untreated wounds showed a more linear pattern of wound closure, with a significant reduction in size from day 3 to 7 ($p < 0.05$). However, the total time to heal did not change, with all wounds being completely closed by the day 28 end-point (Figure 4.3B).

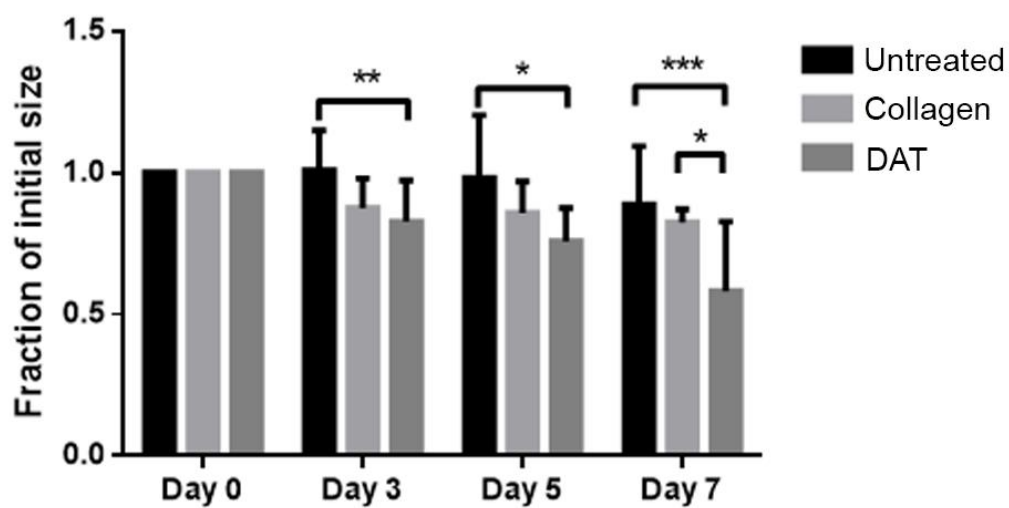
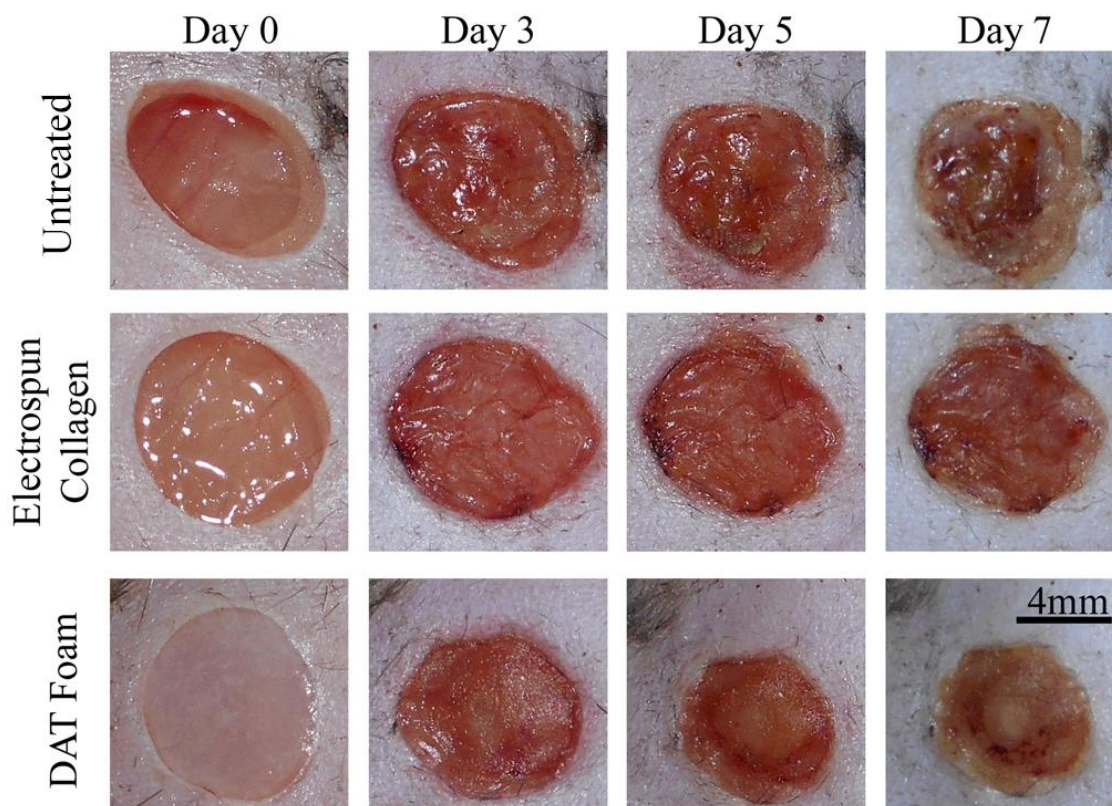


Figure 4.2: DAT foams improved healing in diabetic mice compared to untreated wounds and electrospun collagen scaffold control treatment. 6 mm diameter punch biopsies were taken from the dorsal skin of *db/db* mice. Photographs were taken to monitor wound size over time and measured using ImageJ software. (n=8, days 0 & 3; n=4, days 5 & 7); data were analyzed with linear mixed effects models; * p<0.05; ** p<0.01, *** p<0.001.

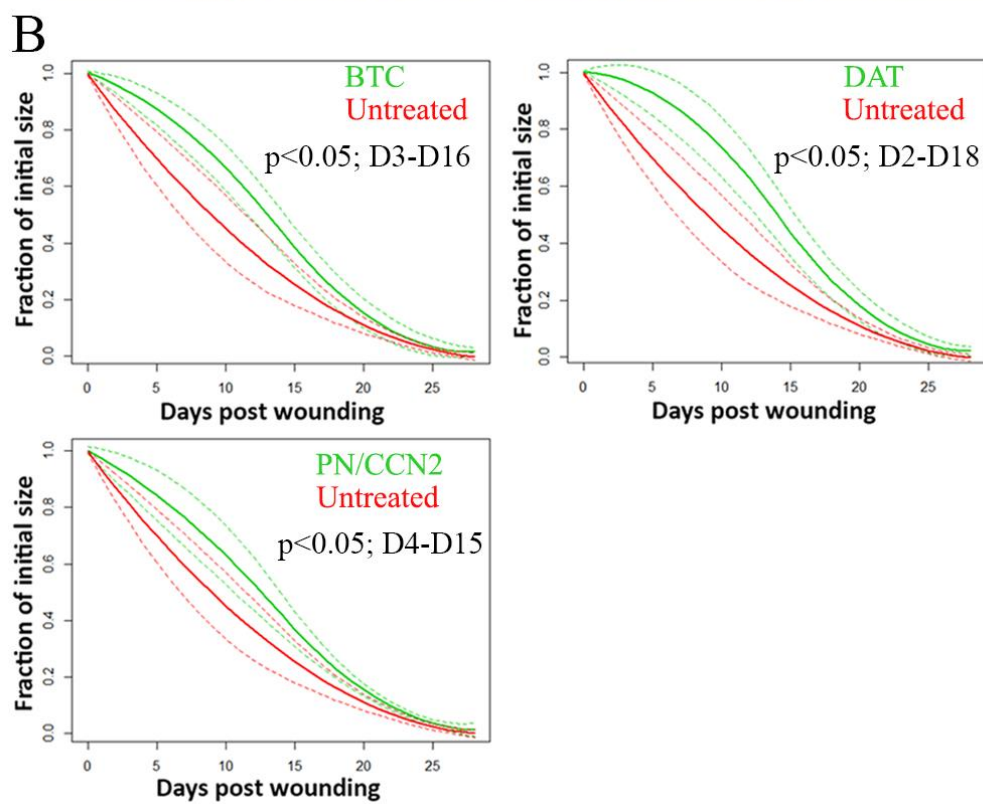
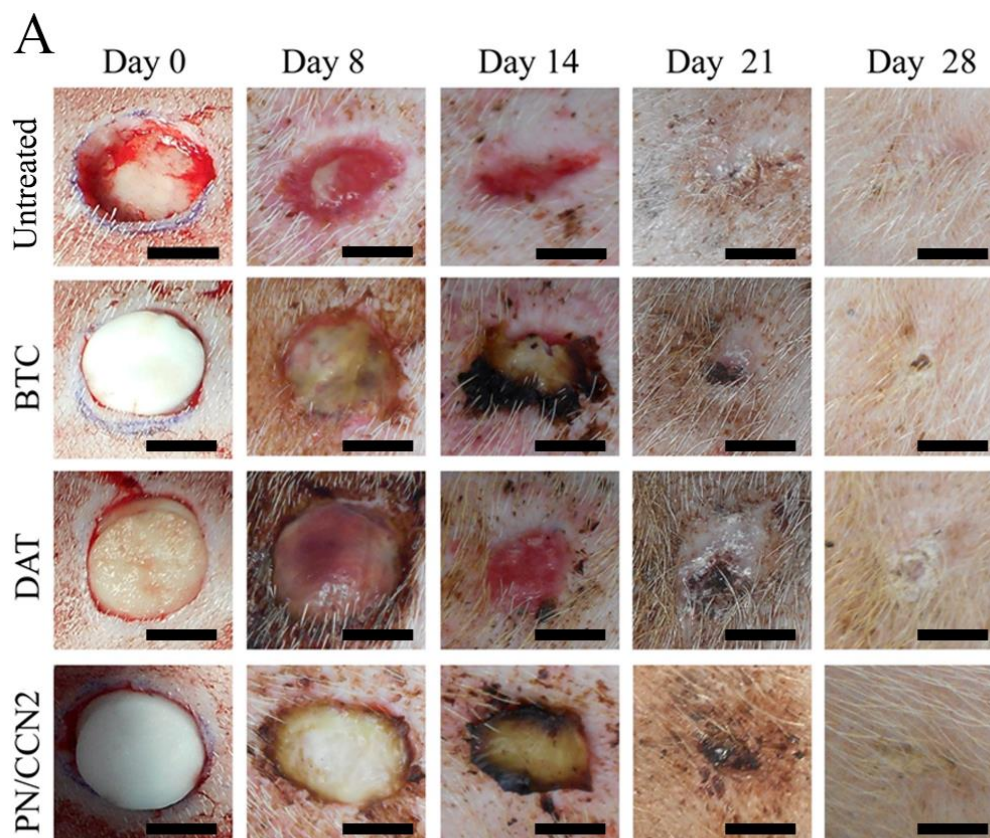


Figure 4.3: Addition of foam biomaterials into excisional wounds in the dorsal skin of pigs decreased the rate of wound closure. Foam biomaterials were added to fill 2 cm diameter excisional wounds in the dorsal skin for each treatment group (1 wound per treatment per pig; n=5-6 pigs for each treatment group) or were left untreated (untreated; 2 wounds per pig; n=6 pigs). (A) Photographs were taken over the course of the healing process. Scale bar is 1 cm. (B) Wound size was measured and then fit using a basis-spline function to compare closure kinetics of each treatment group to that of untreated wounds (solid lines indicate means; dashed lines indicate standard deviation; n=4 pigs for PN/CCN2 treated wounds; n=5 for all other groups). The range in which each treatment significantly differed from the untreated group was determined with a two-way ANOVA using the fitted data and each treatment group was compared to the untreated control group with a Dunnett's post hoc test.

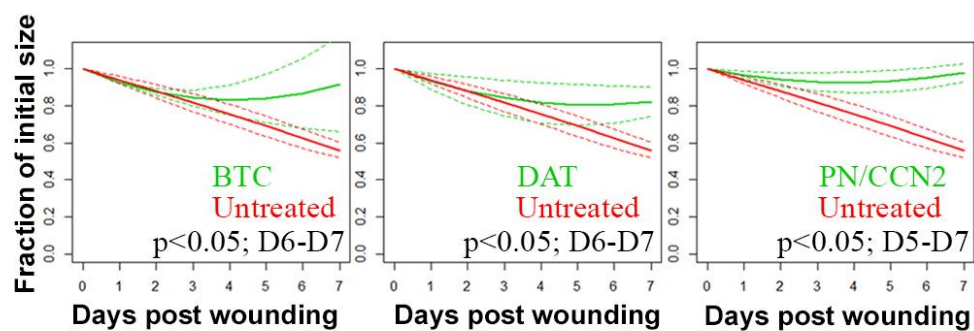
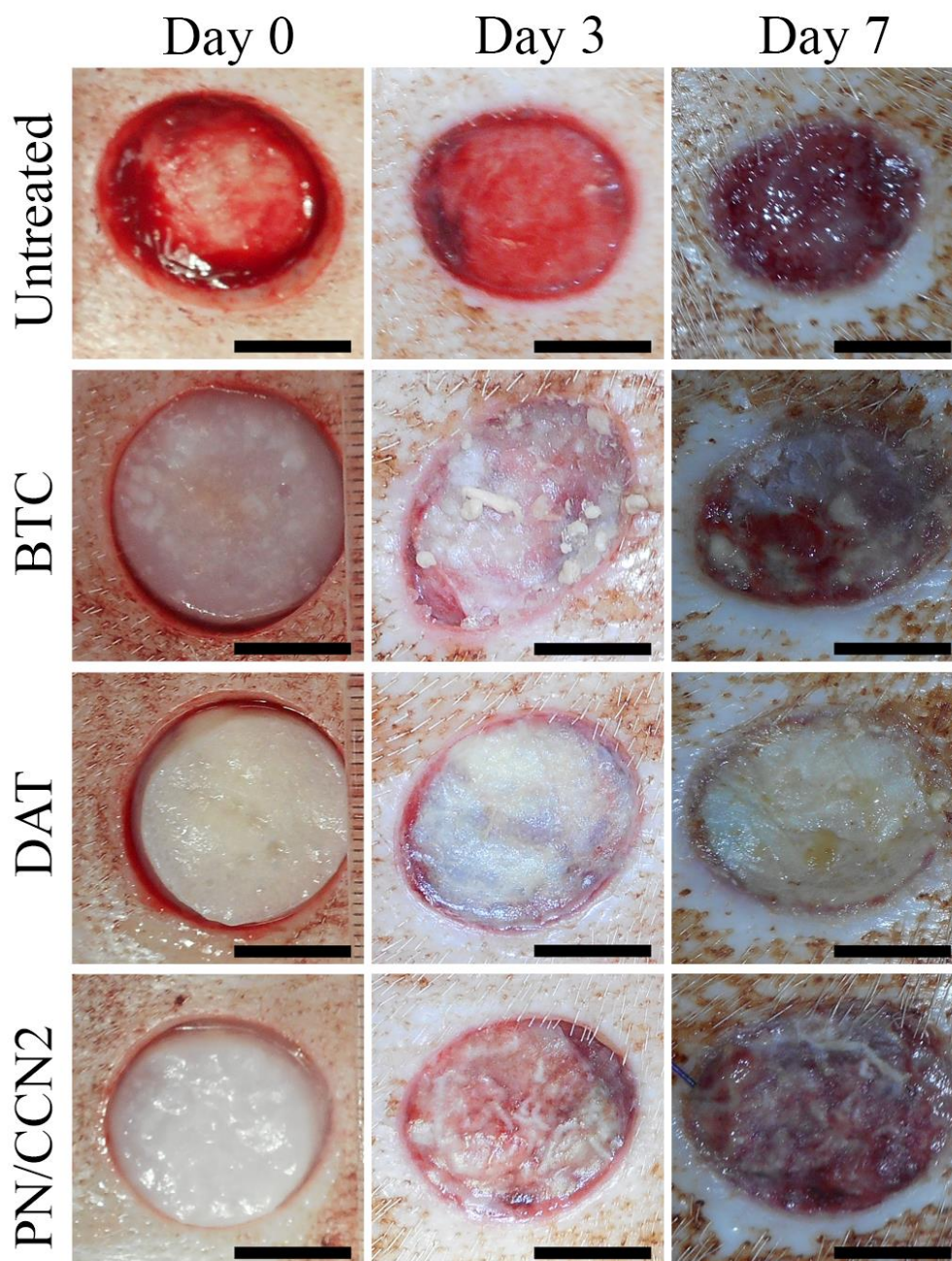


Figure 4.4: The rate of wound closure within the first week of healing was reduced in wounds treated with biomaterials. Wound size was measured and then fit using a basis-spline function to compare closure kinetics of each treatment group to that of untreated wounds (solid lines indicate means; dashed lines indicate standard deviation; n=3 pigs). Scale bar is 1 cm. The range in which each treatment significantly differed from the untreated group was determined with a two-way ANOVA using the fitted data and each treatment group was compared to the untreated control group with a Dunnett's post hoc test.

4.4.3 Foam biomaterials did not alter the contractile or fibrotic phenotypes of the wounds

To assess whether the delayed closure of the wounds treated with biomaterials resulted in decreased wound contraction, the wound diameter was measured in histological cross-sections in the middle of the wounds after 7 and 28 days (Figure 4.5A). All wounds, regardless of treatment, contracted to approximately 60% of their 2 cm original diameter by 28 days without any differences noted between treatment groups and untreated controls. Furthermore, the collagen content in the granulation tissue was similar as assessed through measurement of hydroxyproline content (Figure 4.5B) and visualized with Masson's trichrome staining in histological sections at 7 days (Figure 4.5C) and 28 days (Figure 4.5D; Appendix Figure A3).

It is noteworthy that the foam biomaterials remained within the wound throughout the experiment, and were infiltrated by cells; however, by day 7 variable amounts of scaffold remained intact and were not incorporated into the viable granulation tissue, likely to be removed with the eschar. Conversely, there was no evidence of the biomaterials coming out of the wound, and thus the scaffold materials not present in the eschar were assumed to have been remodeled with the granulation tissue at day 7. Staining of vimentin and α SMA by day 7 showed there was already an abundant infiltration of stromal cells and differentiated myofibroblasts within the wound at this time (Figure 4.5E; Appendix Figure A4). α SMA staining was highly variable, even across different areas of the same wound, notably detected more strongly at the base of the granulation tissue at day 7, but more uniformly expressed by day 28. Vimentin expressing cells were abundant

throughout the wound at both 7- and 28-days post wounding (Appendix Figure A4). No consistent differences were noted between treatment groups.

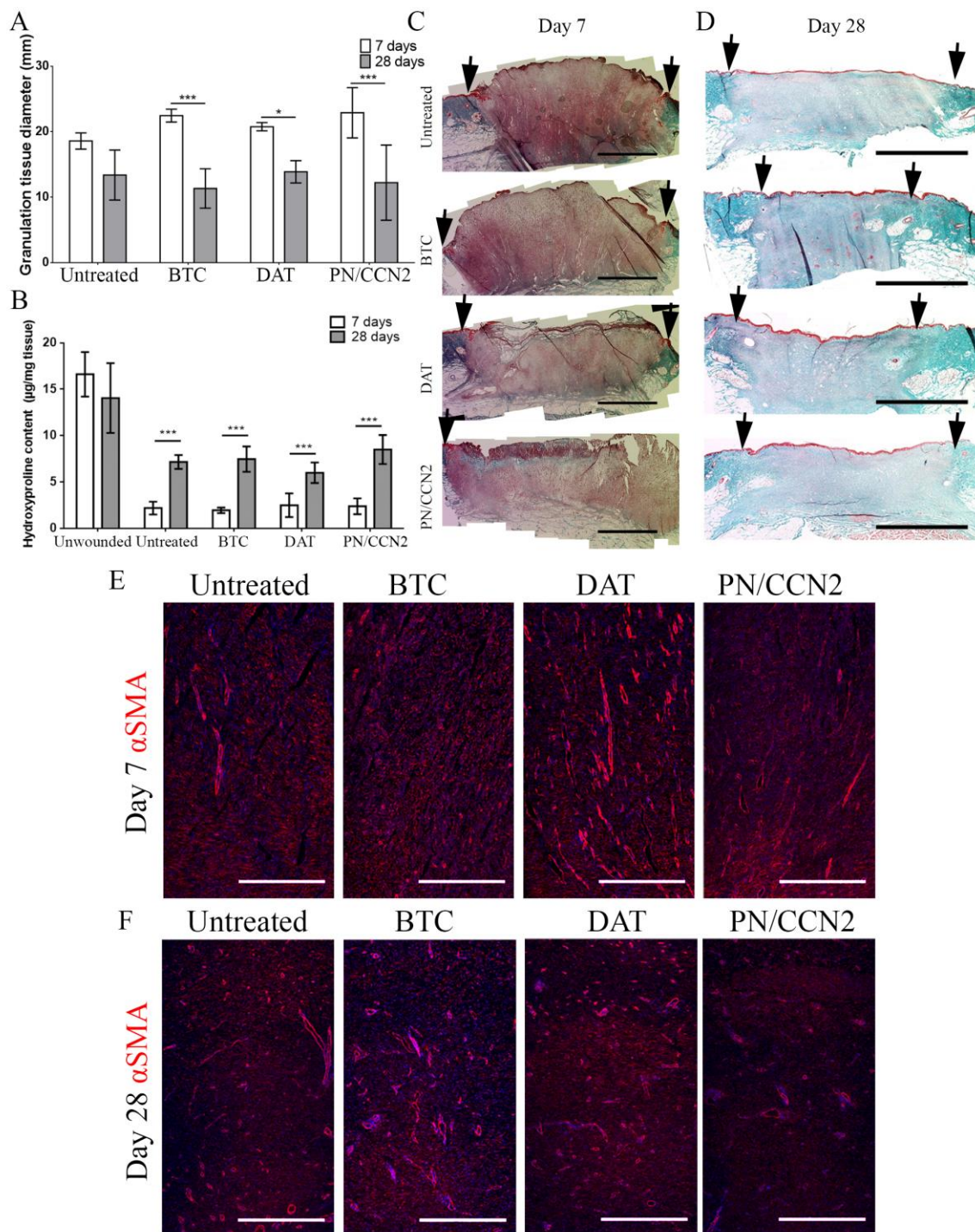


Figure 4.5: Wound contraction and matrix production were not affected by treatment with the biomaterials. (A) Full thickness skin samples, isolated from wounded and unwounded tissue, were sectioned along the midline of the wound and the granulation tissue diameter was measured in these cross sections (measurements taken from 2 cross sections per wound; n= 5-6 pigs at day 28; n= 3 pigs at day 7). (B) Hydroxyproline content was measured in fresh frozen samples from the wound (measured once per wound; n= 5-6 pigs at day 28; n= 3 pigs at day 7). Masson's trichrome staining of histological sections was used to qualitatively assess matrix deposition at day 7 (C) and day 28 (D); arrows indicate wound edge; performed twice per wound; n=5-6 pigs at day 28; n= 3 pigs at day 7. Scale is 5 mm. (E, F) α SMA staining of day 7 (n= 3) and day 28 (n=5-6) wound tissue. Nuclei are stained with DAPI. For co-staining with vimentin, see Appendix Figure A4. Scale bar is 1 mm. Data were analyzed using a linear mixed effects model; * p < 0.05; *** p < 0.001.

4.4.4 Foam biomaterials did not alter the vascular density of the wounds

Histological sections were stained for CD146 to assess the vascular density and average vessel size (Figure 4.6; Appendix Figure A5). CD146 is widely expressed on endothelial cells as well as perivascular cells, labelling similar structures as CD31 (Li et al. 2003). Quantification of the staining showed a significant decrease in vessel density between day 7 and 28 post wounding in all treatment groups, as expected through vascular regression; however, no differences were noted between treatment groups and the untreated control (Figure 4.6B). The average cross-sectional projection of vascular structures was also not different between treatment groups and the untreated control.

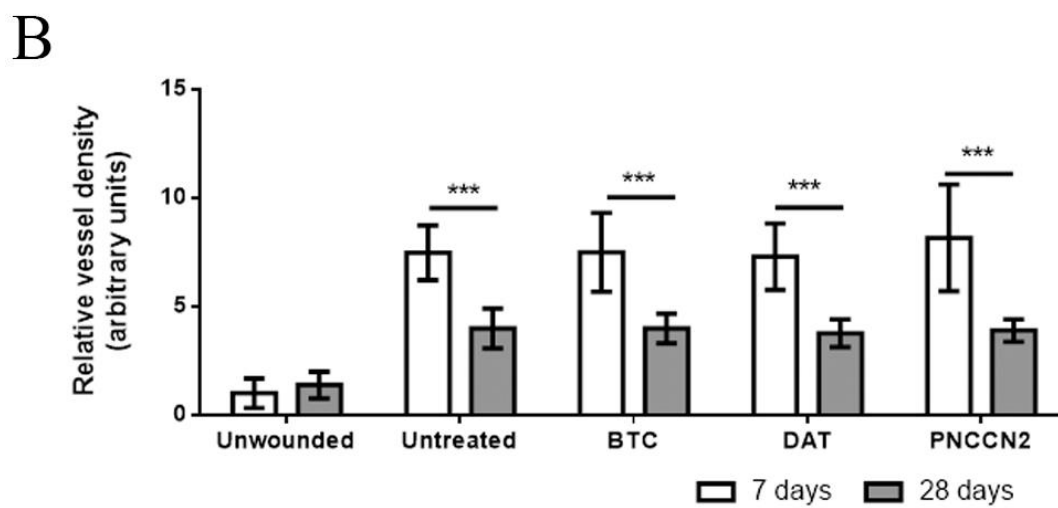
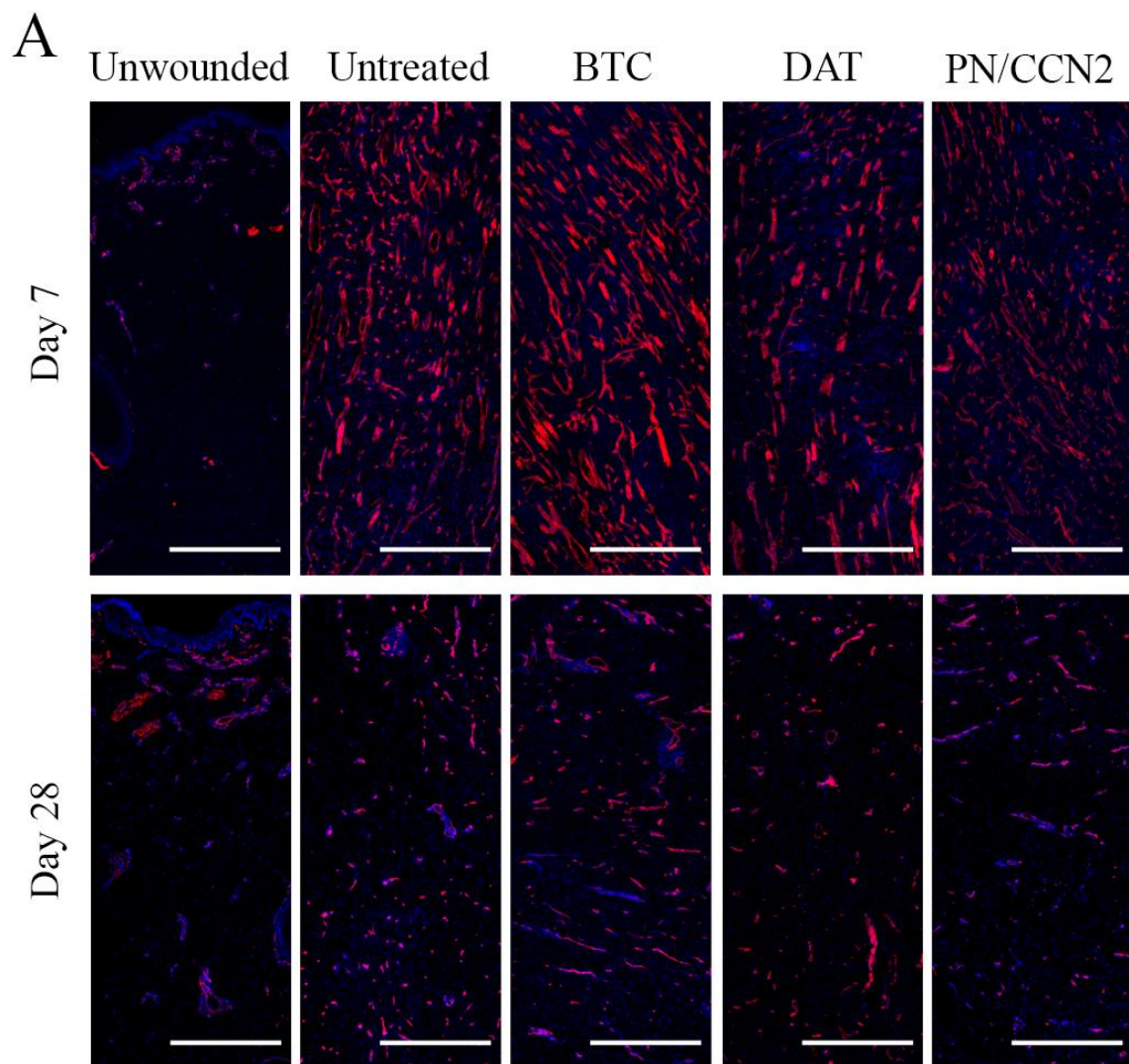


Figure 4.6: Treatment with foam biomaterials did not alter the vascular density of the wound bed. (A) Histological assessment of CD146 positive (red; shown at 28 days) vasculature showed that there were no differences in vessel density between treatment groups and the untreated control (B; n= 3 pigs at 7 days; n= 5-6 pigs at 28 days; 2-5 full depth vertical regions of interest were quantified per wound). Nuclei are stained with DAPI. Scale bar is 1 mm. Data were analyzed with a linear mixed effects model; *** p <0.001.

4.4.5 CD68- and CD163-positive cell infiltrate within the wound bed was not significantly altered by the addition of biomaterials

Histological sections were stained for macrophages with the markers CD68 and CD163 (Figure 4.7A; Appendix Figure A6). CD68 is often considered to label both inflammatory M1, and regenerative M2 macrophages, whereas CD163 has been linked towards M2 polarization (Buechler et al. 2000; Hesketh et al. 2017). CD68 has also been detected in cultured, non-myeloid lineages including endothelial cells and fibroblasts, although with a lower measured mean fluorescence intensity (Gottfried et al. 2008). Compared to the α SMA and vimentin staining performed here, it is evident that CD68 is not labelling the bulk fibroblast population, yet smaller subsets of CD68⁺ fibroblasts may be present. Conversely some staining is evident in and around vascular structures, identified by tight clusters of cell nuclei labelled with DAPI (examples can be seen in day 28 images of Appendix Figure A6). However, it is not clear whether this is extravasating CD68⁺ macrophages or endothelial cells. Interestingly, we noted similar staining in apparent vascular structures within unwounded tissue, but the extent of this was greater in tissue isolated at 7 days post wounding as compared to 28 days post wounding. These findings suggest that the inflammatory response in the unwounded tissues may be altered to some extent due to their proximity to the wounds. However, the reduction by day 28 suggests that the detected signal was not primarily due to the vasculature, which is similarly abundant in the unwounded tissues between the two time points. Within the porcine tissue assessed here, no difference in total CD68⁺ or CD163⁺ cell density was measured at either day 7 or day 28. However, a significant increase in dual-labelled CD68⁺CD163⁺ cells was noted at day 7 between the DAT and untreated groups. (Figure 4.7).

4.4.6 Porcine ASCs displayed tri-lineage differentiation potential

As a first step in the pilot study to assess the potential of the foams as cell delivery platforms for ASCs, the tri-lineage differentiation capacity of the isolated porcine ASCs was verified through histological analysis (Figure 4.8). Control cells cultured in non-inductive proliferation media, did not display markers of differentiation.

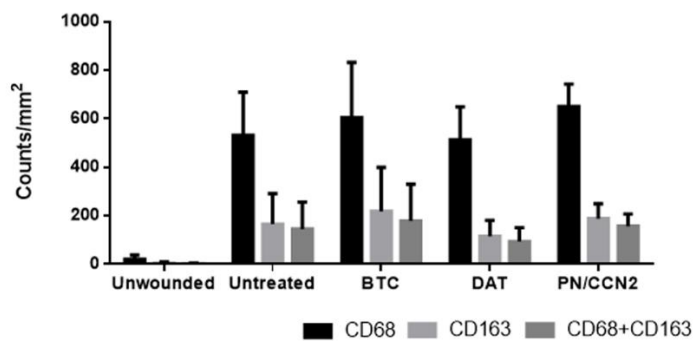
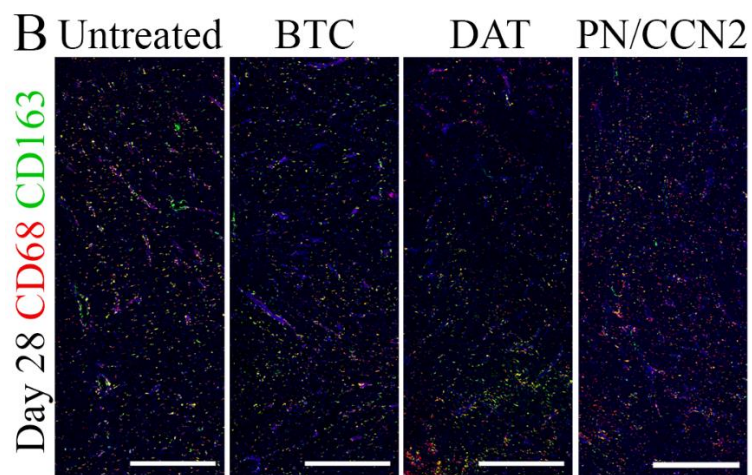
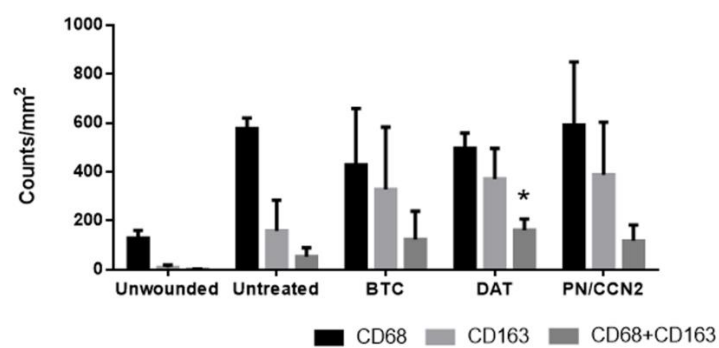
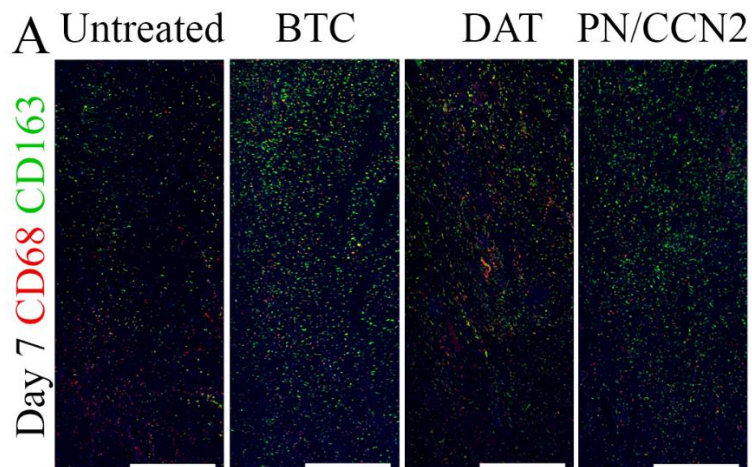


Figure 4.7: Foam biomaterials did not alter macrophage infiltration. Day 7 (A) and day 28 (B) wound tissue was stained for CD68 (red) and CD163 (green); nuclei are stained with DAPI (blue). Quantification was performed on each marker independently, as well as on dual labelled cells. n= 3 pigs at 7 days; n= 5-6 pigs at 28 days; 2-5 full depth vertical regions of interest were quantified per wound. Scale bar is 1 mm. Data were analyzed with linear mixed effects models; * $p < 0.05$ compared to the untreated control.

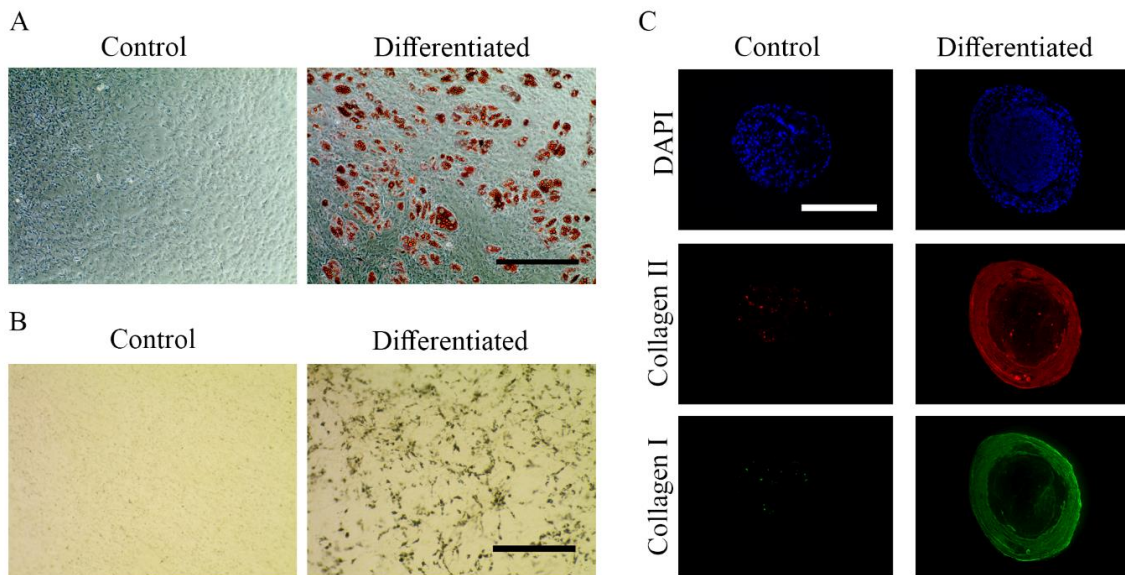


Figure 4.8: Porcine ASCs differentiated towards the adipogenic, osteogenic, and chondrogenic lineages. Adipogenic differentiation yielded cells with large fat vacuoles after 14 days of differentiation, as visualized with oil red O staining (A). Osteogenic differentiation resulted in calcium deposits, visualized with von Kossa staining, at 28 days of differentiation (B). Differentiation towards the chondrogenic lineage resulted in increased expression of both type I and type II collagens in ASC cell pellets by 28 days of differentiation (C). Scale bars are 500 μm .

4.4.7 ASC seeding affected closure differentially depending on the biomaterial carrier

To investigate ASC delivery, PKH26 labelled ASCs were seeded onto foam biomaterials and implanted into dorsal wounds in the porcine model. Seeding scaffolds with porcine ASCs resulted in the qualitative contraction of the scaffolds prior to implantation, which was noted to a greater extent in the type I collagen-based foams and occurring to a lesser extent in the DAT foams. Assessment of gross wound closure showed a significantly increased wound size in both DAT and PN/CCN2 containing groups as compared to the untreated wounds, but not in the BTC group (Figure 4.9). PKH26 positive cells were detected within the viable granulation tissue of all wounds treated with ASCs (Figure 4.10).

4.4.8 ASC delivery on foam biomaterials did not alter histological parameters or hydroxyproline content of the granulation tissue

Wound closure in wounds treated with ASC-seeded biomaterials was further assessed histologically, as previously performed in the unseeded scaffolds (Figure 4.11). Both seeded BTC and PN/CCN2 treatments resulted in a larger cross-sectional granulation tissue diameter compared to the untreated wounds, although none of the other parameters measured were different between the treatment groups and untreated wounds.

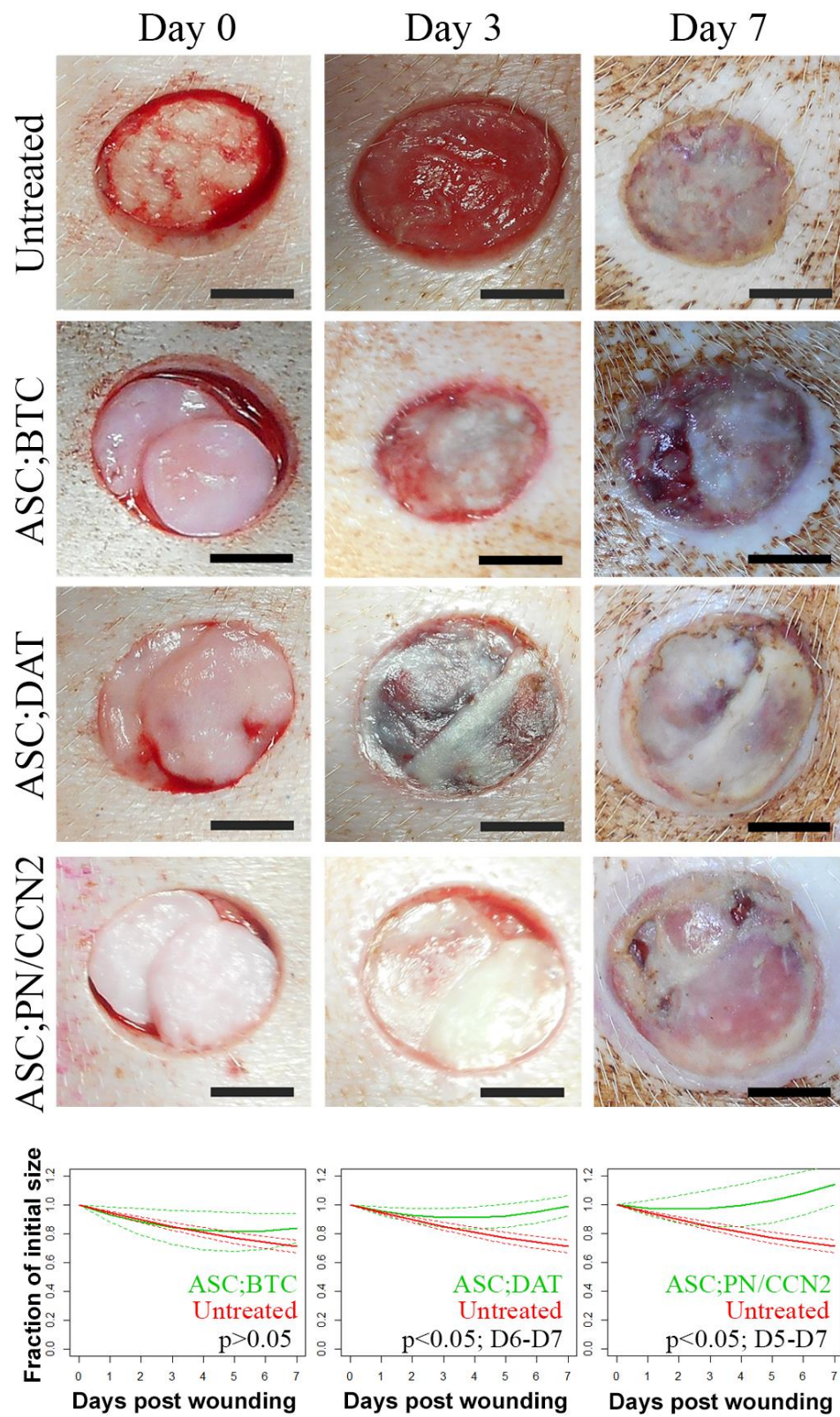


Figure 4.9: Closure kinetics of wounds treated with ASC-seeded biomaterials.

Wound size was measured, and closure kinetics were fit using a basis-spline function to compare each treatment group to untreated wounds (solid lines indicate means; dashed lines indicate standard deviation; n=3 pigs). Scale bar is 1 cm. The range in which each treatment significantly differed from the untreated group was determined with a two-way ANOVA using the fitted data and each treatment group was compared to the untreated control group with a Dunnett's post hoc test. Seeded BTC foams were not significantly different in size than untreated wounds.

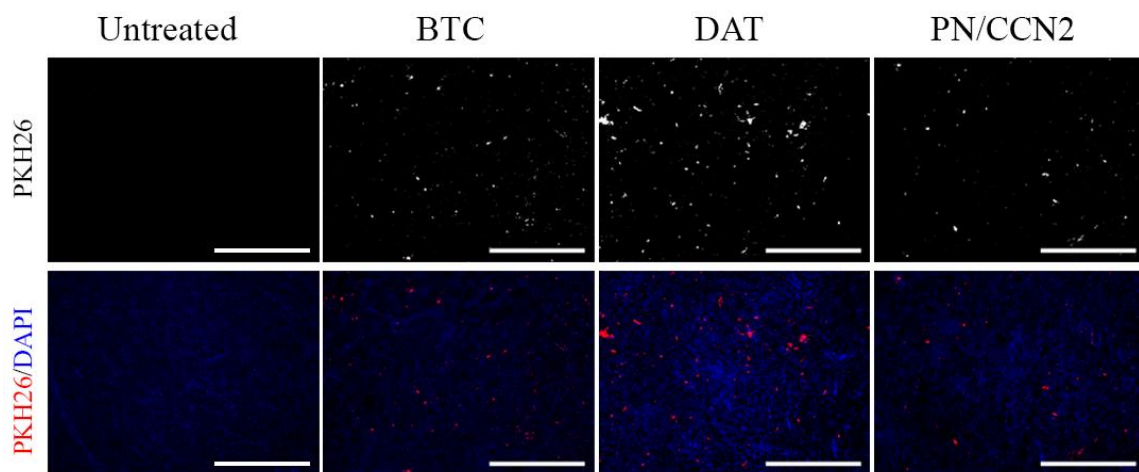


Figure 4.10: PKH labelled porcine ASCs were detectable within the granulation tissue at 7 days post wounding. PKH26 was detected within the granulation tissue of treated wounds. Nuclei are labelled with DAPI. Scale is 500 μ m.

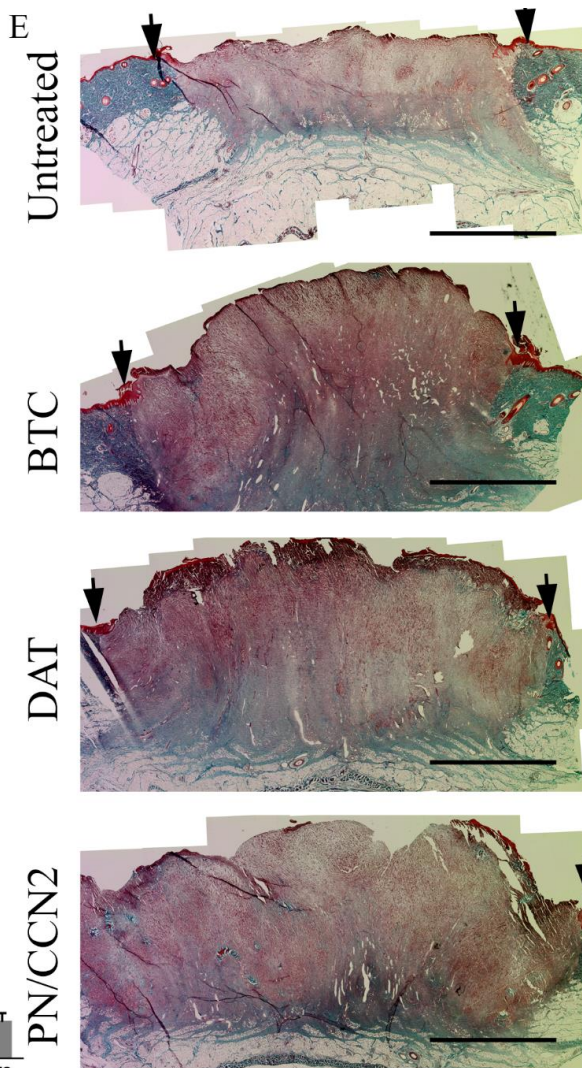
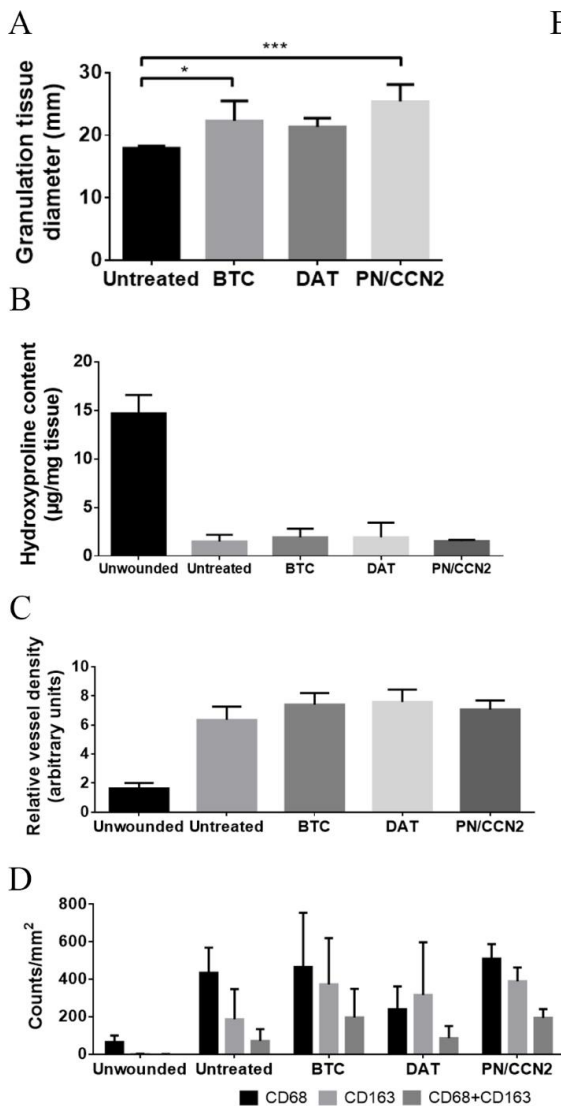


Figure 4.11: ASC-seeded biomaterials did not alter the histological parameters or hydroxyproline content of treated wounds. (A) Granulation tissue diameter was measured from wound cross-sections processed with Masson's trichrome stain (shown in E; measured twice per wound; * $p < 0.05$; *** $p < 0.001$). (B) Hydroxyproline content was measured in fresh frozen samples from the wound (measured once per wound). Relative vessel density was determined through immunofluorescence of CD146 (C), and macrophage counts were measured through quantification of CD68 and CD163 (D). Wounds from 3 pigs were assessed in all analyses; for C and D 3-5 full depth vertical regions of interest were quantified. (E) Masson's trichrome stain the full wound diameter. Arrows indicate wound edges; scale bar is 5 mm. For high magnification images of the staining performed see Appendix Figure A3 and A7. Data were analyzed using linear mixed effects models.

4.5 Discussion

Using a porcine acute wound model, treatment with either Periostin and CCN2 containing type I collagen foam biomaterials, or decellularized adipose tissue foam biomaterials, was shown to have relatively minor effects on wound healing parameters compared to wounds that were left untreated at both 7 and 28 days. Importantly, relative to untreated wounds, treatment with any biomaterial resulted in a delay in the gross wound closure rate. This difference was evident in early repair, but diminished over time, resulting in the same total time to heal in all groups. Based on the timing and normal appearance of the granulation tissue, it is postulated that the delayed wound closure is the result of the biomaterials providing mechanical resistance to contraction, rather than an alteration in the wound biology. It is hypothesized that the resistance provided by the foams would be less consequential in chronic wounds of the extremities, where skin is tightly anchored, and wound contraction has a smaller role in healing (Levinson 2013). This is supported by the improved rate of healing noted with DAT-based foams in *db/db* mice, which naturally contract less, and display impaired and delayed granulation tissue synthesis compared to wild-type mice (Tkalčević et al. 2009).

The histological and biochemical analyses showed similar levels of cell infiltration, matrix production, and the same final granulation tissue diameter. However, it is important to consider the limited sample size of this study, especially in day 7 tissue for which three pigs were assessed. Consequently, the effect size required to be able to detect statistically significant differences with high power is potentially larger than what might be biologically significant. Although few statistically significant differences were noted between treatment groups and the control group, some of these measurements warrant

further exploration in future studies. One such parameter of importance is the immune cell infiltrate. A significant increase in CD68⁺CD163⁺ double-labelled macrophages was noted in the DAT treatment group at 7 days post wounding, and a trend towards increased CD163⁺ cell infiltration was noted in all treatment groups at day 7, including those treated with ASCs, compared to the untreated controls. CD163 itself is a scavenger receptor with affinity for hemoglobin-haptoglobin complexes and both gram-positive and gram-negative bacteria (Buechler et al. 2000; Fabrick et al. 2011). In previous reports, CD163⁺ macrophages have been shown to accumulate at tissue-biomaterial interfaces and were associated with a reduction in total inflammation over time following biomaterial implantation in a rat model (Badylak et al. 2008; Bullers et al. 2014). Generally, CD163 is associated with an M2 phenotype due to its positive regulation by IL-6 and IL-10, and negative regulation by pro-inflammatory stimuli including LPS, TNF α , and IFN γ (Buechler et al. 2000). However, it is well established that macrophage phenotypes represent a large spectrum, and therefore single markers are insufficient to describe their function (Mosser and Edwards 2008). The results provided here, suggest a potentially more regenerative phenotype in all biomaterial treated wounds, supporting the need for a more complete assessment in future studies.

The findings in this study support that the tested biomaterials are promising carriers for cell therapy. Although limited by the small sample size, this preliminary study found that allogeneic porcine ASCs could be delivered into the viable granulation tissue via scaffold seeding. Early clinical trials using MSCs suggest that they are safe (Lalu et al. 2012), and that they are potentially beneficial as a chronic wound therapy, with roles in immunomodulation postulated to be a major influencing factor (Falanga et al. 2007;

Nuschke 2014; Otero-Viñas and Falanga 2016). Additionally, MSCs have previously been genetically modified to produce and deliver bioactive factors, including antibodies and signaling proteins, in animal models (Loebinger et al. 2009; Braid et al. 2016), opening up a range of possibilities for this technology by combining their innate immunomodulatory and angiogenic functionality with an engineering approach to tissue repair. Such a system could even be used to modify the scaffold production as performed here, by inducing cells to produce the matricellular proteins investigated, or by providing alternative biological cues.

Compared to rodent skin, porcine skin is anatomically more similar to that of humans and is a more translationally relevant model of wound closure (Sullivan et al. 2001; Seaton et al. 2015). Regardless, how well the findings in an acute wound model will translate to an impaired model is difficult to assess. In fact, strategies that would be beneficial for acute wounds, such as reducing matrix deposition, would be detrimental for chronic wounds (Levinson 2013). Similarly, approaches that would be favorable for chronic wounds, such as enhancing fibroblast function or inducing angiogenesis, could have negative consequences during acute wound healing. While enhanced fibroblast function is associated with fibrotic repair, evidence supports that excessive angiogenesis plays a supporting role in this process (DiPietro 2016). Importantly, an investigation of five approved acellular dermal substitutes in a porcine full thickness model reported similar findings to those here (Philandrianos et al. 2012). More specifically, reduced contraction at 21 days post-wounding was noted for three of the five dermal substitutes relative to an untreated control, and no differences in clinical wound parameters, including wound contraction, were detected at 2- and 6-month endpoints. Thus, while pig skin is more

similar to that of humans as compared to rodent skin (Sullivan et al. 2001), it is apparent that beyond an assessment of basic parameters such as cell infiltration and matrix degradation, an acute model in young, healthy animals is likely not an appropriate pre-clinical model of human chronic wounds as they do not recapitulate the underlying pathophysiology.

Impaired healing models in pigs are more complex than in rodents. However, such models are capable of reproducing some aspects of human chronic wounds (Seaton et al. 2015). Bipedicle flaps, which disconnect the skin from the underlying vascular supply, have been used to recreate chronic ischemia, leading to impaired rates of closure, and histological parameters mimicking those of ischemic wounds in humans (Roy et al. 2009). Additionally, streptozotocin induced type I diabetes has been used as a model for diabetic wounds, with pigs displaying impaired re-epithelialization, and reduced TGF β and insulin-like growth factor-1 (IGF-1) expression (Velandar et al. 2008). However, in our hands, a pilot study to explore the use of streptozotocin-induced diabetes resulted in the mortality of one of two pigs directly following the initial streptozotocin injection, which precluded continuation of this approach. Such discrepancy could be due to the animal background and breeding practices, or a dosing consideration. Streptozotocin has a low circulating half-life of 5-15 minutes (Eleazu et al. 2013), and thus the rate at which it is administered can greatly affect its efficacy and toxicity. Nevertheless, these models of impaired wound healing could represent important pre-clinical models of human chronic wounds and constitute a critical next step in testing the efficacy of these foam biomaterials.

4.6 Conclusions

Periostin and CCN2 containing type I collagen foam biomaterials and DAT foam biomaterials were assessed in a porcine model of acute wound repair in healthy juvenile pigs. Treatment with the biomaterials resulted in a delay in wound closure during early repair, related to delayed contraction. Other wound healing parameters explored were similar between treatment groups at both 7 and 28 days. The biomaterial strategy utilized in this study offers a straightforward and customizable method to synthesize foam biomaterials that are easy to handle and integrate into the wound. Moreover, these biomaterials offer a platform for delivering therapeutic cell populations, supporting allogeneic ASC integration within the granulation tissue at 7 days. Further investigation in a clinically-relevant impaired wound healing model is warranted to more fully assess the potential of these scaffold-based approaches for the treatment of chronic wounds.

4.7 Acknowledgements

I would like to thank Fang He for statistical support regarding the regression analysis performed on wound size measurements.

4.8 References

- Armstrong DG, Lavery LA, Harkless LB (1998) Validation of a diabetic wound classification system: The contribution of depth, infection, and ischemia to risk of amputation. *Diabetes Care* 21:855–859. doi: 10.2337/diacare.21.5.855
- Badylak SF, Valentin JE, Ravindra AK, et al (2008) Macrophage Phenotype as a Determinant of Biologic Scaffold Remodeling. *Tissue Eng Part A* 14:1835–1842. doi: 10.1089/ten.tea.2007.0264
- Baltzis D, Eleftheriadou I, Veves A (2014) Pathogenesis and Treatment of Impaired Wound Healing in Diabetes Mellitus: New Insights. *Adv Ther* 31:817–836. doi: 10.1007/s12325-014-0140-x

- Bateman ME, Strong AL, Gimble JM, Bunnell BA (2018) Concise Review: Using Fat to Fight Disease: A Systematic Review of Nonhomologous Adipose-Derived Stromal/Stem Cell Therapies. *Stem Cells* 1311–1328. doi: 10.1002/stem.2847
- Braid LR, Hu W-G, Davies JE, Nagata LP (2016) Engineered Mesenchymal Cells Improve Passive Immune Protection Against Lethal Venezuelan Equine Encephalitis Virus Exposure. *Stem Cells Transl Med* 5:1026–1035
- Buechler C, Ritter M, Orsó E, et al (2000) Regulation of scavenger receptor CD163 expression in human monocytes and macrophages by pro- and antiinflammatory stimuli. *J Leukoc Biol* 67:97–103. doi: 10.1002/jlb.67.1.97
- Bullers SJ, Baker SC, Ingham E, Southgate J (2014) The Human Tissue–Biomaterial Interface: A Role for PPAR γ -Dependent Glucocorticoid Receptor Activation in Regulating the CD163⁺ M2 Macrophage Phenotype. *Tissue Eng Part A* 20:2390–2401. doi: 10.1089/ten.tea.2013.0628
- Crisan M, Yap S, Casteilla L, et al (2008) A Perivascular Origin for Mesenchymal Stem Cells in Multiple Human Organs. *Cell Stem Cell* 3:301–313. doi: 10.1016/j.stem.2008.07.003
- Demidova-Rice TN, Durham JT, Herman IM (2012a) Wound Healing Angiogenesis: Innovations and Challenges in Acute and Chronic Wound Healing. *Adv Wound Care* 1:17–22. doi: 10.1089/wound.2011.0308
- Demidova-Rice TN, Hamblin MR, Herman IM (2012b) Chronic Wounds: Biology, Causes, and Approaches to Care. *Wound Rep Reg* 25:304–314. doi: 10.1097/01.ASW.0000416006.55218.d0.Acute
- DiPietro LA (2016) Angiogenesis and wound repair: when enough is enough. *J Leukoc Biol* 100:979–984. doi: 10.1189/jlb.4MR0316-102R
- Driskell RR, Lichtenberger BM, Hoste E, et al (2013) Distinct fibroblast lineages determine dermal architecture in skin development and repair. *Nature* 504:277–281. doi: 10.1038/nature12783
- El Agha E, Moiseenko A, Kheirollahi V, et al (2017) Two-Way Conversion between Lipogenic and Myogenic Fibroblastic Phenotypes Marks the Progression and Resolution of Lung Fibrosis (*Cell Stem Cell* (2017) 20(2) (261–273) (S1934590916303447) (10.1016/j.stem.2016.10.004)). *Cell Stem Cell* 20:571. doi: 10.1016/j.stem.2017.03.011
- Eleazu CO, Eleazu KC, Chukwuma S, Essien UN (2013) Review of the mechanism of cell death resulting from streptozotocin challenge in experimental animals, its practical use and potential risk to humans. *J Diabetes Metab Disord* 12:60. doi: 10.1186/2251-6581-12-60
- Elliott CG, Forbes TL, Leask A, Hamilton DW (2015) Inflammatory microenvironment and tumor necrosis factor alpha as modulators of Periostin and CCN2 expression in human non-healing skin wounds and dermal fibroblasts. *Matrix Biol* 43:71–84. doi: 10.1016/j.matbio.2015.03.003
- Elliott CG, Wang J, Guo X, et al (2012) Periostin modulates myofibroblast differentiation

- during full-thickness cutaneous wound repair. *J Cell Sci* 125:121–132. doi: 10.1242/jcs.087841
- Elliott CG, Wang J, Walker JT, et al (2018) Periostin and CCN2 Scaffolds Promote the Wound Healing Response in the Skin of Diabetic Mice. *Tissue Eng Part A* 2018–0268.:Under review
- Fabriek BO, Bruggen R Van, Deng DM, et al (2011) The macrophage scavenger receptor CD163 functions as an innate immune sensor for bacteria. *113:887–892*. doi: 10.1182/blood-2008-07-167064
- Falanga V, Iwamoto S, Chartier M, et al (2007) Autologous Bone Marrow–Derived Cultured Mesenchymal Stem Cells Delivered in a Fibrin Spray Accelerate Healing in Murine and Human Cutaneous Wounds. *Tissue Eng* 13:1299–1312. doi: 10.1089/ten.2006.0278
- Flynn LE (2010) The use of decellularized adipose tissue to provide an inductive microenvironment for the adipogenic differentiation of human adipose-derived stem cells. *Biomaterials* 31:4715–4724. doi: 10.1016/j.biomaterials.2010.02.046
- Fox J, Weisberg S (2011) *An {R} Companion to Applied Regression* No Title, Second. Sage, Thousand Oaks CA
- Frykberg RG, Banks J (2015) Challenges in the Treatment of Chronic Wounds. *Adv Wound Care* 4:560–582. doi: 10.1089/wound.2015.0635
- Gottfried E, Kunz-Schughart LA, Weber A, et al (2008) Expression of CD68 in non-myeloid cell types. *Scand J Immunol* 67:453–463. doi: 10.1111/j.1365-3083.2008.02091.x
- Hall-Glenn F, Lyons KM (2011) Roles for CCN2 in normal physiological processes. *Cell Mol Life Sci* 68:3209–3217. doi: 10.1007/s00018-011-0782-7
- Hauner H, Skurk T, Wabitsch M (2001) Cultures of Human Adipose Precursor Cells. In: Ailhaud G (ed) *Adipose Tissue Protocols*. Springer New York, Totowa, NJ, pp 239–247
- Hesketh M, Sahin KB, West ZE, Murray RZ (2017) Macrophage phenotypes regulate scar formation and chronic wound healing. *Int J Mol Sci* 18:1–10. doi: 10.3390/ijms18071545
- Hopkins RB, Burke N, Harlock J, et al (2015) Economic burden of illness associated with diabetic foot ulcers in Canada. *BMC Health Serv Res* 15:13. doi: 10.1186/s12913-015-0687-5
- Hothorn T, Bretz F, Westfall P (2008) Simultaneous inference in general parametric models. *Biometrical J* 50:346–363. doi: 10.1002/bimj.200810425
- Kramann R, Schneider RK, Dirocco DP, et al (2015) Perivascular Gli1+ progenitors are key contributors to injury-induced organ fibrosis. *Cell Stem Cell* 16:51–66. doi: 10.1016/j.stem.2014.11.004
- Kuljanin M, Brown CFC, Raleigh MJ, et al (2017) Collagenase treatment enhances proteomic coverage of low-abundance proteins in decellularized matrix bioscaffolds.

- Biomaterials 144:130–143. doi: 10.1016/j.biomaterials.2017.08.012
- Lalu MM, McIntyre L, Pugliese C, et al (2012) Safety of Cell Therapy with Mesenchymal Stromal Cells (SafeCell): A Systematic Review and Meta-Analysis of Clinical Trials. *PLoS One* 7:. doi: 10.1371/journal.pone.0047559
- Levinson H (2013) A Paradigm of Fibroblast Activation and Dermal Wound Contraction to Guide the Development of Therapies for Chronic Wounds and Pathologic Scars. *Adv Wound Care* 2:149–159. doi: 10.1089/wound.2012.0389
- Li Q, Yu Y, Bischoff J, et al (2003) Differential expression of CD146 in tissues and endothelial cells derived from infantile haemangioma and normal human skin. *J Pathol* 201:296–302. doi: 10.1002/path.1443
- Li WW, Carter MJ, Mashiach E, Guthrie SD (2017) Vascular assessment of wound healing: a clinical review. *Int Wound J* 14:460–469. doi: 10.1111/iwj.12622
- Loebinger MR, Eddaoudi A, Davies D, Janes SM (2009) Mesenchymal stem cell delivery of TRAIL can eliminate metastatic cancer. *Cancer Res* 69:4134–4142. doi: 10.1158/0008-5472.CAN-08-4698
- Marangoni RG, Korman BD, Wei J, et al (2015) Myofibroblasts in murine cutaneous fibrosis originate from adiponectin-positive intradermal progenitors. *Arthritis Rheumatol* 67:1062–1073. doi: 10.1002/art.38990
- Mosser DM, Edwards JP (2008) Exploring the full spectrum of macrophage activation. *Nat Rev Immunol* 8:958–969. doi: 10.1038/nri2448
- Mustoe TA, O’Shaughnessy K, Kloeters O (2006) Chronic wound: Pathogenesis and current treatments: A Unifying Hypothesis. *Plast Reconstr Surg* 117:35S–41S. doi: 10.1097/01.prs.0000225431.63010.1b
- Nuschke A (2014) Activity of mesenchymal stem cells in therapies for chronic skin wound healing. *Organogenesis* 10:29–37. doi: 10.4161/org.27405
- Otero-Viñas M, Falanga V (2016) Mesenchymal Stem Cells in Chronic Wounds: The Spectrum from Basic to Advanced Therapy. *Adv Wound Care* 5:149–163. doi: 10.1089/wound.2015.0627
- Philandrianos C, Andrac-Meyer L, Mordon S, et al (2012) Comparison of five dermal substitutes in full-thickness skin wound healing in a porcine model. *Burns* 38:820–829. doi: 10.1016/j.burns.2012.02.008
- Pinheiro J, Bates D, R-core (2014) Linear and Nonlinear Mixed Effects Models
- Powers JG, Higham C, Broussard K, Phillips TJ (2016) Wound healing and treating wounds Chronic wound care and management. *J Am Acad Dermatol* 74:607–625. doi: 10.1016/j.jaad.2015.08.070
- R core team (2017) R: A language and environment for statistical computing. R Found. Stat. Comput. Vienna, Austria.
- Ramsay J, Wickham H, Graves S, Hooker G (2017) Functional Data Analysis in R
- Roy S, Biswas S, Khanna S, et al (2009) Characterization of a preclinical model of chronic ischemic wound. *Physiol Genomics* 37:211–224. doi:

- 10.1152/physiolgenomics.90362.2008.
- Schneider CA, Rasband WS, Eliceiri KW (2012) NIH Image to ImageJ: 25 years of image analysis. *Nat Methods* 9:671–675. doi: 10.1038/nmeth.2089
- Schneider RK, Mullally A, Dugourd A, et al (2017) Gli1+Mesenchymal Stromal Cells Are a Key Driver of Bone Marrow Fibrosis and an Important Cellular Therapeutic Target. *Cell Stem Cell* 20:785–800.e8. doi: 10.1016/j.stem.2017.03.008
- Seaton M, Hocking A, Gibran NS (2015) Porcine models of cutaneous wound healing. *ILAR J* 56:127–138. doi: 10.1093/ilar/ilv016
- Sen CK, Gordillo GM, Roy S, et al (2009) Human skin wounds: A major and snowballing threat to public health and the economy: PERSPECTIVE ARTICLE. *Wound Repair Regen* 17:763–771. doi: 10.1111/j.1524-475X.2009.00543.x
- Sullivan TP, Eaglstein WH, Davis SC, Mertz P (2001) The pig as a model for human wound healing. *Wound Repair Regen* 9:66–76. doi: 10.1046/j.1524-475x.2001.00066.x
- Tkalčević VI, Čužić S, Parnham MJ, et al (2009) Differential evaluation of excisional non-occluded wound healing in *db/db* mice. *Toxicol Pathol* 37:183–192. doi: 10.1177/0192623308329280
- Valencia IC, Falabella A, Kirsner RS, Eaglstein WH (2001) Chronic venous insufficiency and venous leg ulceration. *J Am Acad Dermatol* 44:401–424. doi: 10.1067/mjd.2001.111633
- Valencia WM, Florez H (2017) How to prevent the microvascular complications of type 2 diabetes beyond glucose control. *BMJ* 356:1–17. doi: 10.1136/bmj.i6505
- Velander P, Theopold C, Hirsch T, et al (2008) Impaired wound healing in an acute diabetic pig model and the effects of local hyperglycemia. *Wound Repair Regen* 16:288–293. doi: 10.1111/j.1524-475X.2008.00367.x
- Walker JT, McLeod K, Kim S, et al (2016) Periostin as a multifunctional modulator of the wound healing response. *Cell Tissue Res* 365:453–465. doi: 10.1007/s00441-016-2426-6
- Williams KJ, Godke RA, Bondioli KR (2011) Adipose-Derived Stem Cells. *702:77–86*. doi: 10.1007/978-1-61737-960-4
- Wong VW, Sorkin M, Glotzbach JP, et al (2011) Surgical Approaches to Create Murine Models of Human Wound Healing. *J Biomed Biotechnol* 2011:1–8. doi: 10.1155/2011/969618
- Yu C, Bianco J, Brown C, et al (2013) Porous decellularized adipose tissue foams for soft tissue regeneration. *Biomaterials* 34:3290–3302. doi: 10.1016/j.biomaterials.2013.01.056
- Zomer HD, Trentin AG (2018) Skin wound healing in humans and mice: Challenges in translational research. *J Dermatol Sci* 90:3–12. doi: 10.1016/j.jdermsci.2017.12.009

Chapter 5: Discussion

5.1 General Discussion

In this thesis, research into cell-intrinsic and cell-extrinsic factors that regulate wound repair was presented with the goal of guiding future therapeutic development. To this end, progress was made in 1) developing a better understanding of the basic biology of key cell populations and extracellular matrix (ECM) constituents involved in wound repair, and 2) initial analysis of the wound healing response to novel ECM-derived biomaterials in a porcine model.

5.1.1 Lineage tracing of Foxd1-expressing embryonic progenitors to assess the role of divergent embryonic lineages on adult dermal fibroblast function

The first aim of this thesis focused on examining fibroblast lineage as a determinant of cell function during skin homeostasis and in wound repair. Based on previous lineage tracing studies in kidney (Humphreys et al. 2010) and lung (Hung et al. 2013) fibrosis, the *Foxd1*-lineage as a marker of myofibroblast progenitors was investigated in the dorsal dermis through lineage tracing. Embryonic *Foxd1*-expressing progenitors migrated into the dorsal skin during development and contributed to *Foxd1* lineage-positive populations in adult tissue, including a subset of dermal fibroblasts. Furthermore, the *Foxd1* lineage was a source of myofibroblast during cutaneous wound repair. Notably, the binary expression of *Foxd1* during development correlated with differential fibrosis-related gene expression patterns in the fibroblast progeny in adult tissue. Specifically, during wound repair, the lineage-positive fibroblast population maintained higher levels of expression for matrix synthesis associated genes, including type III collagen, and decorin, whereas

the lineage-negative population maintained higher gene expression of several integrins, and signaling proteins including PDGF-A, PDGF-B, TNF α , and Endothelin-1. These findings support a level of functional heterogeneity between these two fibroblast populations.

While the findings of this work are not immediately applicable to biomaterials development, there are several directions in which a contribution to therapeutic design are potentially foreseeable. An exceptional study by Rinkevich *et al.* utilized a relatively broad lineage tracing strategy in dermal fibroblasts to focus in on a specific, druggable target, Dpp4 (CD26), which could be inhibited to reduce scarring during acute wound repair in mice (Rinkevich *et al.* 2015). Whether a similar strategy could be used to identify targets to promote ECM synthesis and skin repair in a model of impaired healing, is unknown. The work presented in this thesis contributes to a growing understanding of fibroblast heterogeneity and provides insight into how divergent populations might cooperate during wound repair.

Whereas most organs undergo fibrotic repair following acute or chronic injury, chronic wounds represent a unique challenge in that they are characterized by impaired ECM synthesis (Hinz 2016). Accordingly, it is natural that studies investigating fibroblast lineages outside of the skin focus on strategies to reduce matrix production. Even within the skin, much of the work to date has focused on inhibition of fibrosis and scarring. This emphasis on fibrosis may be related to the translational interests of the broader myofibroblast progenitor community, or that fibrotic repair is the natural end-point of cutaneous wound healing in healthy wild-type mice, making it a simpler initial point of study. Several studies, including those by Dulauroy *et al.*, Rinkevich *et al.*, and

Marangoni *et al.*, have identified specific populations of myofibroblast progenitors with fibrogenic potential (Dulauroy *et al.* 2012; Marangoni *et al.* 2015; Rinkevich *et al.* 2015). An investigation by Driskell *et al.* highlighted two spatially distinct lineages that contributed either to granulation tissue synthesis or hair follicle formation during wound repair (Driskell *et al.* 2013). Interestingly, interaction between activated myofibroblasts and hair follicles has been observed to induce myofibroblast differentiation into adipocytes during wound resolution, a mechanism which could be exploited to reduce scarring (Plikus *et al.* 2017). It is evident that within the last 7 years, an immense amount of knowledge regarding skin fibroblast functional heterogeneity has been established, but whether this work can be translated into models of impaired healing remains unknown. Potential strategies to explore in models of impaired healing could include cell delivery by enriching for fibroblast subsets with the greatest fibrogenic potential, or targeting the molecular mechanisms involved in fibroblast subset-specific activation and deactivation. Jiang *et al.* (2018) performed cell transplantation studies in immune deficient *Rag2* knockout recipient mice, which resulted in fibrotic repair when wounds were enriched with the more fibrogenic *Engrailed-1* lineage and more regenerative when enriched with their less fibrogenic lineage-negative counterparts (Jiang *et al.* 2018). Such findings could have important implications for cell therapy. However, testing in models of impaired healing would be required to fully assess their potential effects.

A further question of interest that warrants more in-depth investigation is what the roles are of fibroblast populations that contribute less to matrix synthesis during wound repair. The presence of these populations in such an evolutionarily-conserved process suggests that they may have alternative functional roles, which have not yet been fully elucidated.

Jiang *et al.* highlighted that lesser fibrogenic *Engrailed-1* lineage-negative fibroblasts are involved in fibronectin deposition during development (Jiang *et al.* 2018), and it is perceivable that they may maintain this functionality during healing in adult mice. Furthermore, fibroblast populations that do not contribute to early granulation tissue formation can play an influential role in hair follicle regeneration (Driskell *et al.* 2013). However, in this thesis, *Foxd1* lineage-negative fibroblasts (PDGFR α ⁺/ Vimentin⁺/ *Foxd1* lineage-negative) were observed within the wound at 3 days post wounding, suggesting that there are fibroblasts with lesser fibrotic potential present even during early stages of skin repair. Further, the work presented in this thesis identified that a number of integrins, cell receptors, and growth factors were enriched in the *Foxd1* lineage-negative population during wound repair, while type III collagen mRNA was relatively under-expressed compared to the *Foxd1* lineage-positive fibroblasts. At the present time, the consequences of these differential expression patterns are difficult to predict, but it is hypothesized that this cell population may play a more supportive role during skin repair, influencing matrix deposition by the more fibrogenic *Foxd1* lineage-positive fibroblast population.

5.1.2 The role of Galectin-3 in cell recruitment and differentiation during wound healing

In the second aim of this thesis, the matricellular protein Galectin-3 was investigated as a potential extrinsic mediator of cell behavior in wound repair. Matricellular proteins are temporally regulated throughout the wound repair process, and their expression has been linked to a range of important functional outcomes, including the regulation of

inflammation, angiogenesis, and fibrogenesis (Walker et al. 2015). This, in combination with their extracellular localization, makes them potential candidates for incorporation into ECM-mimetic biomaterials. Galectin-3 is considered a member of the matricellular protein family, but does not act exclusively in the ECM (Midwood et al. 2004). In fact, its role within keratinocytes during dermal wound repair is associated with intracellular protein trafficking after receptor-ligand binding (Liu et al. 2012). However, Galectin-3 can also modify receptor activation and trafficking extracellularly. Receptor clustering resulting from the binding of Galectin-3 homopentamers to cell surface receptors has been shown to activate focal adhesion kinase (FAK) through $\alpha V\beta 3$ integrin clustering, prevent endocytosis of vascular endothelial growth factor receptor 2 (VEGFR2) and transforming growth factor receptor 2 (TGFR2), and can activate regenerative macrophage polarization through binding and activation of CD98 (MacKinnon et al. 2008, 2012, Markowska et al. 2010, 2011).

Recognizing these extracellular roles that result in enhanced signaling in pro-regenerative pathways motivated the investigation of Galectin-3 in wound healing. Surprisingly, genetic deletion of Galectin-3 in a murine model resulted in no major defects during acute wound repair. Specifically, in relation to fibroblast activation, Galectin-3 knockout mice did not display impairments within the skin as has been observed in other organs (Henderson et al. 2006, 2008; Jiang et al. 2012; MacKinnon et al. 2012). Further, characterization of primary dermal fibroblasts *in vitro* supported intrinsic differences compared to primary pulmonary fibroblasts studied by MacKinnon *et al.* (2012). Whereas Galectin-3 knockout pulmonary fibroblasts displayed impaired fibroblast activation *in vitro*, Galectin-3 knockout dermal fibroblasts were similar to wild-type.

Although both sources of fibroblast are responsible for fibrotic repair, it is evident that there might be subtle differences in the mechanisms that result in an activated state in order to do so.

The findings in this chapter do not imply that treatment with exogenous Galectin-3 would not be beneficial in an impaired wound model. In this thesis, it was shown that Galectin-3 gene expression is highest in the wound one day post excisional wounding in a mouse model, corresponding with inflammatory cell infiltration. However, human chronic wounds, which are characterized by an unresolved inflammatory phase (Demidova-Rice et al. 2012; Frykberg and Banks 2015), have a significantly decreased level of Galectin-3 in the tissue at the wound edge. Whether this decrease contributes to the pathophysiology of chronic wounds or is protective is not currently known. This question should be assessed in models of impaired wound healing through exploration of its expression profile and through treatment with exogenous protein.

5.1.3 Profibrotic and pro-angiogenic biomaterials to induce cell recruitment and differentiation during skin healing

The final aim of this thesis was to investigate the effects of ECM-based biomaterials in a porcine wound model. Although a specific role for Galectin-3 in acute dermal wound repair was not determined, previous work from the Hamilton laboratory identified a key role of the matricellular protein periostin in myofibroblast differentiation (Elliott et al. 2012). Continuation of this work identified the therapeutic potential of exogenous periostin through an improved rate of wound closure in a *db/db* model of impaired wound healing when delivered in an electrospun type I collagen scaffold (Elliott et al. 2018). Similarly, exploration of the pro-fibrotic matricellular protein CCN2, which shares a

similar expression profile with periostin during acute wound repair, identified a positive effect on the rate of closure in *db/db* mice (Elliott et al. 2018). Micro-array analysis of gene expression in whole wound tissue following treatment with either exogenous periostin or CCN2 resulted in distinct expression patterns, suggesting that these matricellular proteins function through different pathways (Elliott et al. 2018). Moreover, treatment with both periostin and CCN2 resulted in novel genes being regulated compared to each individually. Overall, in this work, the rate of healing was improved in all matricellular protein treated groups, but granulation tissue thickness was significantly greater in the combined group, and thus, this approach was chosen for future investigation. These promising findings using periostin and CCN2 served as the rationale to explore their delivery further in the porcine wound model.

To continue this work in the present thesis, a combination treatment including both periostin and CCN2 was applied using an alternative foam biomaterial format, and acute healing was assessed in 3-month-old healthy pigs. Switching to a foam design offered several benefits over the electrospinning process including greater uniformity, ease of synthesis and customization, scaffold stability without chemical cross-linking, and larger scaffold pore sizes to enhance cell infiltration. Furthermore, healing was assessed in a porcine wound model, which has greater anatomical similarity to human skin as compared to rodents and has been suggested to be a more appropriate model for translation of wound therapeutics (Sullivan et al. 2001).

In addition to the modifications made to the previous research design investigating matricellular protein-based therapies, similar foam scaffolds derived from human decellularized adipose tissue (DAT) were explored as a novel wound healing therapeutic.

The exploration of the DAT foams provides insight relevant to future scaffold design, not only in terms of applying these materials as stand-alone biological dermal substitutes, but also as a potential platform for further modification with other pro-regenerative factors such as matricellular proteins. Numerous components of the ECM are suggested to be beneficial for skin repair including structural proteins, glycoproteins, glycosaminoglycans, proteoglycans, and matricellular proteins (Turner and Badylak 2015), all of which are present in DAT (Kuljanin et al. 2017). The DAT foam biomaterials were not excluded from the wounds during repair and were assumed to integrate into the granulation tissue and to be remodeled by the cellular infiltrate in an acute wound setting.

Lastly, the application of the foams as delivery platforms for allogeneic adipose-derived stem/stromal cells (ASCs) was explored. While the studies performed were preliminary in nature, it is promising that the ASCs delivered on the various scaffolding platforms could be visualized within the viable granulation tissue in all treated wounds at 7 days post wounding. Adding a cellular component to the therapeutic design opens a range of possibilities for future exploration. While the innate immunomodulatory properties of mesenchymal stem/stromal cells (MSCs) are promising independently (Falanga et al. 2007; Nuschke 2014; Otero-Viñas and Falanga 2016), previous work has shown that MSCs can also be genetically modified to deliver proteins of interest upon *in vivo* implantation (Braid et al. 2016). This approach could be investigated in the future as an alternative strategy to deliver matricellular proteins. In conclusion, previous work from our research groups was combined and modified to make progress towards improving biomaterial design and assessing therapeutic efficacy for wound healing applications. The

findings of this work demonstrate the need to explore models of impaired healing in future studies to bridge the gap between bench and bedside.

5.1.4 Conclusion

Work in this thesis has contributed to the present state of knowledge in diverse areas of wound healing research. Contributions have been made to the broader wound healing field to better understand the cell-intrinsic and -extrinsic properties that regulate wound repair. Moreover, within our laboratories new techniques have been introduced and pre-existing techniques have been advanced to expand upon the expertise available. Specifically, lineage tracing studies have been introduced into our lab, and fibroblast isolation through fluorescence activated cell sorting has been explored; expertise in a splinted murine wound model has been established; scaffold synthesis has been adapted for better infiltration and easier handling; an acute porcine wound model has been established; isolation and characterization of porcine ASCs has been performed, and an effective method for allogeneic transplantation of ASCs was developed. An exploration of future directions for near-term continuation of this work will be provided below.

5.2 Future directions

5.2.1 Investigating the functional relevance of divergent gene expression in Foxd1 lineage-positive fibroblasts

Foxd1 lineage-positive and lineage-negative dermal fibroblasts were identified to have divergent gene expression patterns. Future studies should focus on further probing how these genetic differences impact cell function. Most importantly, the differential expression of surface markers, including those identified in the PCR array such as integrins $\alpha 2$, $\alpha 3$, $\beta 6$, and $\beta 8$ as well as dermal fibroblast markers characterized in previous lineage studies including CD90, PDGFR α , and PDGFR β (Rinkevich et al. 2015; Philippeos et al. 2018), should be assessed through flow cytometry. Determining markers to stratify the different lineages is an important step towards translation away from the lineage tracing model, making these findings more relevant to the broader research community. Proteins expressed on the cell surface are critical mediators of cellular interactions with their immediate environment, and thus, differential expression of these surface markers can give clues towards the mechanisms driving divergent expression patterns and overall cell phenotypes. Furthermore, differential surface marker expression could be useful in identifying these distinct fibroblast sub-populations in human skin. Such findings could be helpful in understanding the etiology of human chronic wounds. Specifically, identification of fibroblast sub-populations in human chronic wounds would help to determine the relationship between cell-intrinsic and -extrinsic factors in determining wound chronicity. Theoretically, if sub-populations exist in skin, depletion of certain populations could result in an inability to heal, leading to wound chronicity.

Moving forward, functional differences between lineages should be assessed *in vitro* and *in vivo*. An effective strategy to assess cell function *in vivo* is through transplantation studies using FACS-sorted populations. Using this strategy, Driskell *et al.* identified a role of papillary fibroblasts in hair follicle formation (Driskell *et al.* 2013). Additionally, Rinkevich *et al.* and Jiang *et al.* provided evidence of scarring potential in the *engrailed-1* lineage of fibroblasts over the lineage-negative population using transplantation studies (Rinkevich *et al.* 2015; Jiang *et al.* 2018). However, with cell transplantation studies, the lineages are not assessed in isolation of each other due to the contribution of cells endogenous to the recipient. Regardless, these experiments can provide important information on cell function. Another method that allows for the assessment of specific lineages *in vivo* is cell ablation using a *diphtheria* toxin (DT)/ DT receptor (DTR) approach (Dulauroy *et al.* 2012; Rinkevich *et al.* 2015). This method results in the selective ablation of cells, controlled by Cre/Lox recombination or cell-specific promoters, inducing cell death through inhibition of protein synthesis (Saito *et al.* 2001). However, because the *Foxd1* lineage is not specific to the fibroblast population, using this approach could have severe health consequences for the animal if not controlled by additional cell-type specific promoters, or localized DT delivery. Another ablation method, Herpes simplex virus thymidine kinase (HSV-TK)/ ganciclovir, is toxic primarily to replicating cells by inhibiting DNA elongation (Heyman *et al.* 1989; Tieng *et al.* 2016), and thus may be more appropriate for targeting wound fibroblasts more selectively. However, ablation strategies have been used to target only the fibroblast population tracked through lineage tracing, but not the reciprocal non-lineage fibroblasts (Dulauroy *et al.* 2012; Rinkevich *et al.* 2015). Thus, the effects of ablation could simply

be due to a loss in total fibroblast number and not specifically the cells of interest. While the reciprocal experiment is theoretically possible (potentially a *Col1a1* or *PDGFR α* promoter controlling loxP-DTR-loxP/ loxP-HSV-TK-loxP), how well this would work in practice is uncertain. To my knowledge, such an approach has not been explored. Overall, with the current state of available methods, cell transplantation studies offer a more robust model for *in vivo* exploration of functional differences between fibroblast lineages.

In vitro approaches to investigate cell function are required to allow greater control over experimental parameters, but normal cell culture conditions alter cell phenotype. Few studies to date have explored different fibroblast lineages in culture. Similar to our findings in collagen gels, Philippeos *et al.* reported altered expression in a selection of markers explored after culturing human dermal fibroblasts sorted into papillary and reticular populations. Specifically, the human papillary dermal fibroblast specific markers CD39 and *Col6A5* were lost upon culturing. However, the other markers monitored, CD36, *Lumican*, and CD90, were expressed at similar levels in the freshly isolated and cultured populations (Philippeos et al. 2018). The group also found that FACS-enriched papillary or reticular human dermal fibroblasts maintained important functional differences *in vitro* on tissue culture plastic. More specifically, expression differences were maintained in culture for genes relating to ECM synthesis, and differences in their responsiveness to interferon γ (IFN γ) were noted. However, while papillary dermal fibroblasts displayed upregulated Wnt signaling genes *in vivo*, some of these were higher in the reticular population *in vitro*, including *Wnt5a* and *Lef1* (Philippeos et al. 2018).

Overall, these findings suggest that specific properties of disparate fibroblast populations are retained on tissue culture plastic while others are not.

More promising for the development of relevant *in vitro* models to assess dermal fibroblast function, Philippeos *et al.* found that cultured human papillary and reticular dermal fibroblasts maintained functional differences when transplanted into an organotypic culture model that consisted of human decellularized dermal tissue and a seeded keratinocyte layer (Philippeos *et al.* 2018). The papillary fibroblasts integrated with the epidermis, while increased epidermal thickness and formation of rete ridges were evident. In contrast, implanted reticular fibroblasts were more evenly spread throughout the tissue and negatively affected epidermal thickness. Using this human decellularized dermis model, the fibroblasts entered a state of quiescence with minimal cell proliferation similar to native tissue. However, the fibroblasts were shown to become activated upon localized injection of collagenase as a model for tissue injury, supporting the utility of this system for exploration of diverse tissue states (Rognoni *et al.* 2018). These findings highlight the relevance of this organotypic model, which could potentially be utilized to assess functional differences in the *Foxd1* lineage. However, it is unknown whether murine fibroblasts will behave similarly on human-derived decellularized dermis or whether murine sources would be required. Nevertheless, use of a compositionally-relevant organotypic culture model could be a useful tool to provide valuable insight into the functional diversity of fibroblast populations.

To conclude, further characterization of protein expression in the *Foxd1* lineage should be performed to verify changes in gene expression and assist in the translation of this work. Further exploration of functional differences could help to identify underlying cell-

intrinsic mechanisms that regulate skin repair. Moreover, a better understanding of how diverse fibroblast populations interact, and the major mechanisms coordinating their interactions could potentially identify important targets for future investigation in the context of cutaneous wound healing.

5.2.2 Galectin-3 as a therapeutic for impaired wound healing

Galectin-3 is a matricellular protein with diverse roles in processes involved in wound repair. Our group recently published a review article discussing these roles with a focus on the potential use of exogenous Galectin-3 in a chronic wound setting (McLeod et al. 2018). Overall, Galectin-3 has roles in both pro- and anti- inflammatory processes, fibrosis, angiogenesis, and wound re-epithelialization, all of which could be beneficial when applied to chronic wounds (McLeod et al. 2018). However, a distinct pathophysiological feature associated with human chronic wounds, advanced glycation end-products (AGEs), could affect translation of Galectin-3 research from culture systems and animal models into human chronic wounds. This will be discussed in more detail below.

Like all lectins, Galectin-3 recognizes specific sugar moieties through its carbohydrate recognition domain based on a tightly controlled glycosylation state. This “sugar code” is normally tightly regulated by post-translational modification by enzymatic means (Murphy et al. 2013). One of these enzymes, Mgat5, modifies proteins with β 1,6-GlcNAc-branched N-glycans, which are high affinity ligands of Galectin-3 (Lagana et al. 2006; Markowska et al. 2011). However, in diabetic patients, glycosylation begins to occur randomly, through non-enzymatic means in the presence of excessive amounts of reducing sugars over prolonged periods of time (Singh et al. 2014). Notably, the resultant

AGE modifications are particularly apparent at sites of diabetic complications, including within chronic wounds (Pepe et al. 2014), and have been reported to have roles in diabetic pathology, including altered immune function and impaired vascular function (Stirban et al. 2014). Importantly, AGE modifications have been reported to be ligands for the carbohydrate recognition domain of Galectin-3 (Vlassara et al. 1995), with Galectin-3 itself acting in a larger AGE-receptor complex (Pricci et al. 2000). Ligand binding with the AGE-receptor complex results in endocytosis and degradation of AGE-modified proteins, and has also been shown to be protective against oxidative stress, counteracting the pro-inflammatory effects of the other major AGE receptor, receptor for advanced glycation end-products (RAGE) (Torreggiani et al. 2009; Ott et al. 2014). Although the role of endogenous Galectin-3 is protective against AGE accumulation, further investigation is required to assess the effect of the exogenous protein delivered as a therapeutic agent in impaired healings environments.

Unfortunately, there is no standard animal model for AGE accumulation, with combinations of time, high AGE diets, diabetes, and/or delivery of AGE-modified compounds or precursors being used experimentally (Peppia et al. 2003; Sandu et al. 2005; Berlanga et al. 2005; Liao et al. 2009), and are rarely assessed for the extent of glycation. However, one exemplary study investigated AGE accumulation in wild-type and diabetic (*db/db*) mice fed a high- or low-AGE diet (Peppia et al. 2003). The diets were controlled for protein, fat, carbohydrate, and caloric content, differing only in AGE content. Importantly, *db/db* mouse skin on its own did not show increased AGE content, but this was increased when combined with a high AGE diet for three months. Thus, to

assess the effect of exogenous Galectin-3 in a translational model, a *db/db* mouse combined with a high-AGE diet should be considered.

5.2.3 Assessment of biomaterial scaffolds in a porcine model of impaired wound healing

As highlighted previously in this thesis, a logical continuation of the work on the developed foam biomaterials would be to assess their effects on healing using a relevant impaired wound model. It is important to note that no animal model will recapitulate every aspect of a human disease state, and thus it is necessary to select a subset of parameters that can be mimicked to provide a more representative and translational model system.

Chronic wound pathophysiology includes excessive inflammation, chronic infection, and an impaired response of resident populations to injury (Demidova-Rice et al. 2012; Frykberg and Banks 2015). Moreover, chronic wounds of vascular or diabetic ulcer etiology are associated with vascular insufficiency leading to tissue ischemia. As such, several different models of impaired wound healing have been developed, each replicating some of these aspects (Seaton et al. 2015). Unfortunately, there is no gold-standard porcine model used to quantitatively assess diverse therapeutics for specific indications. In fact, even clinically, the selection of therapeutics for chronic wounds from wound dressings to skin substitutes is not strongly based on evidence (Snyder et al. 2012; Frykberg and Banks 2015; Santema et al. 2016; Norman et al. 2017). Although the use of approved therapies leads to better outcomes than standard care alone, the level of evidence to choose one therapeutic over another for a specific indication is poor (Snyder et al. 2012; Santema et al. 2016; Norman et al. 2017).

More robust and standardized pre-clinical models of impaired healing are critically needed to allow for better assessment of outcomes of novel materials in a highly controlled environment, as well as to validate and compare current therapeutics. A similar approach to the one undertaken in this thesis using an acute porcine wound model showed no benefit of currently approved dermal substitutes over untreated controls (Philandrianos et al. 2012). However, an acute porcine wound model, while useful for assessing integration and the host tissue response to implanted biomaterials, does not reproduce any of the pathophysiological features of human chronic wounds.

Induced-diabetic porcine models have been explored, but the overall level of impairment in terms of the rate of closure is small compared to closure in non-diabetic pigs (Velandar et al. 2008; O'Brien et al. 2014). This is consistent with the fact that in humans, diabetic complications, including micro- and macro-vascular complications and all-cause mortality, are positively associated with both age and duration of disease (Zoungas et al. 2014). Even in pigs, increasing the duration of induced-diabetes and resultant hyperglycemia from 20 to 90 days prior to wounding, was shown to negatively impact the rate of healing (O'Brien et al. 2014). In our hands, a pilot investigation exploring the induction of diabetes via administration of streptozotocin resulted in mortality for one of two pigs tested (unpublished data). Still, others have reported much lower mortality associated with streptozotocin (Velandar et al. 2008; O'Brien et al. 2014), suggesting that further in-house optimization may be sufficient to overcome this hurdle. However, it is important to note that in our pilot investigation, while the surviving pig maintained a hyperglycemic state over three weeks, the wounds that were inflicted one-week post streptozotocin administration healed similarly to those in a non-diabetic control pig over

a two-week period of assessment. These findings further support that short-term induction of diabetes may not be sufficient to impair wound closure. Overall, due to the cost, time, ethical considerations, and limited impairment associated with this model, it is not recommended for future investigation.

Another porcine model that has been shown to have a more drastic effect on the rate of closure relies on surgically-induced ischemia (Roy et al. 2009). In this model, a bipedicle flap was created in the dorsal skin, and a silicone sheet placed below and sutured into place. With this approach, the flap was disconnected from the underlying circulation and the overlying skin became ischemic, as measured by laser Doppler imaging, and the level of tissue oxygen content via spectroscopic techniques. Importantly, by 3 weeks, ischemic wounds only closed to ~80% of their initial size, whereas those in non-ischemic tissue were fully closed. These findings were further supported with histological analyses showing delayed macrophage recruitment into the wound, and fewer von Willebrand Factor (vWF)-positive endothelial cells within the granulation tissue. Whether outcomes in this porcine ischemic wound model accurately reflect those in human chronic wound patients would require further testing. However, due to the extent of impairment displayed, this model system is intriguing and warrants further investigation. One potential concern is how well this model can be replicated. During study optimization in a single pig, a recent study using this approach cited problems with fluid build-up and dehiscence along the incision associated with the underlying silicone sheet (Patil et al. 2017). To remedy this, the flap was disconnected from the underlying tissue, without placement of the silicone sheet for the remaining three pigs tested. The study reported equivalent blood flow within the ischemic and non-ischemic wounds based on laser

Doppler imaging by 8 days. Unfortunately, no wound size or oxygenation measurements were reported, and untreated control wounds within the ischemic tissue were not performed, making it difficult to assess the level of impairment. Regardless, potential problems associated with this surgical model should not be discounted, and whether it can be reproduced would require further exploration. Moreover, whether the ischemic model with the adaptations made by Patil *et al.* is sufficient to impair wound closure in a reproducible manner, would require investigation.

Overall, it is evident that there is a need to develop and test relevant animal models of impaired wound healing. There is already a vast array of skin substitutes approved for use, with few randomized controlled trials systematically comparing their efficacy (Snyder *et al.* 2012). Moreover, meta-analyses to compare wound therapeutics are hindered by a lack of quality clinical data (Santema *et al.* 2016; Norman *et al.* 2017). Consequently, the current approach to selection of wound therapeutics is not evidence-based, and patient outcomes may be compromised. No animal model will replace the need for high quality clinical trials, however, standardized, predictive, and reproducible pre-clinical models would be extremely valuable for screening and comparing therapeutic options.

5.2.4 Exploring the interplay between cell-intrinsic and -extrinsic properties governing wound repair

As a longer-term goal of this work it would be interesting to explore the interplay between cell lineage and the microenvironment. A key finding from the lineage tracing of *Foxd1* lineage-positive and lineage-negative fibroblasts was the dichotomy in their expression profiles. Specifically, lineage-negative populations expressed higher levels of

genes associated with cell signaling, including integrins which act as cellular receptors for numerous ECM components (Koivisto et al. 2014). Using the biomaterial foams explored in this thesis as a culture substrate, the response of lineage-positive and lineage-negative fibroblasts to diverse ECM components including the matricellular proteins periostin, CCN2, and galectin-3 could be explored systematically. Findings from such an experiment would provide further insight into the functional differences in fibroblast sub-populations. Furthermore, differences in the fibroblast response to specific ECM components have not previously been linked to specific fibroblast lineages or populations. Such findings would point to novel mechanisms of tissue level control over the response to specific stimuli. If fibroblast subsets respond differently to external cues, then differences in their distribution between regions of the skin could be a useful predictor of how each region will respond following tissue injury.

As mentioned above, transplantation studies offer a potential strategy to investigate functional differences between fibroblast subsets. Alternatively, in models of impaired healing such as db/db mice or impaired porcine wound models, it would be valuable to explore how divergent fibroblast subsets modify the healing response. The expression data collected from *Foxd1* lineage-positive and lineage-negative fibroblasts suggested that while the lineage-positive cells may be more synthetic, the lineage-negative population may be more modulatory in nature. However, it is unknown how delivery of these populations into an impaired wound would affect the healing outcome. Again, this would provide valuable information regarding the interplay between cell lineage and external cues which would be useful for the development of novel cell-based therapies for wound healing applications.

Continuation of the studies provided in this thesis will offer a wide range of opportunities to further explore the relationship between cells and their environment. In addition to enhancing the understanding of the fundamental mechanisms involved in wound repair and tissue homeostasis, future exploration in this direction would be impactful for regenerative medicine applications.

5.3 Summary

The overall focus of this thesis was to expand upon the understanding of fundamental mechanisms involved in wound repair, with the goal of applying the findings to future therapeutics for chronic wounds. First, a cell lineage tracing strategy previously used to identify profibrotic populations in the kidney and lung was determined to label a fibroblast population with similar potential within the skin. Next, the matricellular protein Galectin-3 was determined to be dispensable during acute wound repair, however further investigation into impaired models is warranted. Finally, progress was made in developing a flexible platform to deliver functionally relevant proteins and cells into a wound, using a porcine model. Through these diverse studies, insights into functional heterogeneity of fibroblasts and effects of the ECM microenvironment in the context of cutaneous repair have been made that could be exploited in the future to develop innovative strategies for the treatment of chronic wounds.

5.4 References

Berlanga J, Cibrian D, Guillen I, et al (2005) Methylglyoxal administration induces diabetes-like microvascular changes and perturbs the healing process of cutaneous wounds. *Clin Sci* 109:83–95. doi: 10.1042/CS20050026

- Braid LR, Hu W-G, Davies JE, Nagata LP (2016) Engineered Mesenchymal Cells Improve Passive Immune Protection Against Lethal Venezuelan Equine Encephalitis Virus Exposure. *Stem Cells Transl Med* 5:1026–1035
- Demidova-Rice TN, Hamblin MR, Herman IM (2012) nd Chronic Wounds: Biology, Causes, and Approaches to Care. 25:304–314. doi: 10.1097/01.ASW.0000416006.55218.d0.Acute
- Driskell RR, Lichtenberger BM, Hoste E, et al (2013) Distinct fibroblast lineages determine dermal architecture in skin development and repair. *Nature* 504:277–281. doi: 10.1038/nature12783
- Dulauroy S, Di Carlo SE, Langa F, et al (2012) Lineage tracing and genetic ablation of ADAM12 + perivascular cells identify a major source of profibrotic cells during acute tissue injury. *Nat Med* 18:1262–1270. doi: 10.1038/nm.2848
- Elliott CG, Wang J, Guo X, et al (2012) Periostin modulates myofibroblast differentiation during full-thickness cutaneous wound repair. *J Cell Sci* 125:121–132. doi: 10.1242/jcs.087841
- Elliott CG, Wang J, Walker JT, et al (2018) Periostin and CCN2 Scaffolds Promote the Wound Healing Response in the Skin of Diabetic Mice. *Tissue Eng Part A* 2018–0268.:Under review
- Falanga V, Iwamoto S, Chartier M, et al (2007) Autologous Bone Marrow–Derived Cultured Mesenchymal Stem Cells Delivered in a Fibrin Spray Accelerate Healing in Murine and Human Cutaneous Wounds. *Tissue Eng* 13:1299–1312. doi: 10.1089/ten.2006.0278
- Frykberg RG, Banks J (2015) Challenges in the Treatment of Chronic Wounds. *Adv Wound Care* 4:560–582. doi: 10.1089/wound.2015.0635
- Henderson NC, Mackinnon AC, Farnworth SL, et al (2006) Galectin-3 regulates myofibroblast activation and hepatic fibrosis. *Proc Natl Acad Sci* 103:5060–5065. doi: 10.1073/pnas.0511167103
- Henderson NC, Mackinnon AC, Farnworth SL, et al (2008) Galectin-3 expression and secretion links macrophages to the promotion of renal fibrosis. *Am J Pathol* 172:288–298. doi: 10.2353/ajpath.2008.070726
- Heyman R a, Borrelli E, Lesley J, et al (1989) Thymidine kinase obliteration: creation of transgenic mice with controlled immune deficiency. *Proc Natl Acad Sci* 86:2698–2702. doi: 10.1073/pnas.86.8.2698
- Hinz B (2016) The role of myofibroblasts in wound healing. *Curr Res Transl Med* 64:171–177. doi: 10.1016/j.retram.2016.09.003
- Humphreys BD, Lin SL, Kobayashi A, et al (2010) Fate tracing reveals the pericyte and not epithelial origin of myofibroblasts in kidney fibrosis. *Am J Pathol* 176:85–97. doi: 10.2353/ajpath.2010.090517
- Hung C, Linn G, Chow YH, et al (2013) Role of lung Pericytes and resident fibroblasts in the pathogenesis of pulmonary fibrosis. *Am J Respir Crit Care Med* 188:820–830. doi: 10.1164/rccm.201212-2297OC

- Jiang D, Correa-Gallegos D, Christ S, et al (2018) Two succeeding fibroblastic lineages drive dermal development and the transition from regeneration to scarring. *Nat Cell Biol* 20:422–431. doi: 10.1038/s41556-018-0073-8
- Jiang JX, Chen X, Hsu DK, et al (2012) Galectin-3 modulates phagocytosis-induced stellate cell activation and liver fibrosis in vivo. *AJP Gastrointest Liver Physiol* 302:G439–G446. doi: 10.1152/ajpgi.00257.2011
- Koivisto L, Heino J, Häkkinen L, Larjava H (2014) Integrins in Wound Healing. *Adv Wound Care* 3:762–783. doi: 10.1089/wound.2013.0436
- Kuljanin M, Brown CFC, Raleigh MJ, et al (2017) Collagenase treatment enhances proteomic coverage of low-abundance proteins in decellularized matrix bioscaffolds. *Biomaterials* 144:130–143. doi: 10.1016/j.biomaterials.2017.08.012
- Lagana A, Goetz JG, Cheung P, et al (2006) Galectin Binding to Mgat5-Modified N-Glycans Regulates Fibronectin Matrix Remodeling in Tumor Cells Galectin Binding to Mgat5-Modified N-Glycans Regulates Fibronectin Matrix Remodeling in Tumor Cells. 26:3181–3193. doi: 10.1128/MCB.26.8.3181
- Liao H, Zakhaleva J, Chen W (2009) Cells and tissue interactions with glycated collagen and their relevance to delayed diabetic wound healing. *Biomaterials* 30:1689–1696. doi: 10.1016/j.biomaterials.2008.11.038
- Liu W, Hsu DK, Chen HY, et al (2012) Galectin-3 regulates intracellular trafficking of EGFR through alix and promotes keratinocyte migration. *J Invest Dermatol* 132:2828–2837. doi: 10.1038/jid.2012.211
- MacKinnon AC, Farnworth SL, Hodgkinson PS, et al (2008) Regulation of Alternative Macrophage Activation by Galectin-3. *J Immunol* 180:2650–2658. doi: 10.4049/jimmunol.180.4.2650
- MacKinnon AC, Gibbons MA, Farnworth SL, et al (2012) Regulation of transforming growth factor- β 1-driven lung fibrosis by galectin-3. *Am J Respir Crit Care Med* 185:537–546. doi: 10.1164/rccm.201106-0965OC
- Marangoni RG, Korman BD, Wei J, et al (2015) Myofibroblasts in murine cutaneous fibrosis originate from adiponectin-positive intradermal progenitors. *Arthritis Rheumatol* 67:1062–1073. doi: 10.1002/art.38990
- Markowska AI, Jefferies KC, Panjwani N (2011) Galectin-3 protein modulates cell surface expression and activation of vascular endothelial Growth factor receptor 2 in human endothelial cells. *J Biol Chem* 286:29913–29921. doi: 10.1074/jbc.M111.226423
- Markowska AI, Liu F-T, Panjwani N (2010) Galectin-3 is an important mediator of VEGF- and bFGF-mediated angiogenic response. *J Exp Med* 207:1981–1993. doi: 10.1084/jem.20090121
- McLeod K, Walker JT, Hamilton DW (2018) Galectin-3 regulation of wound healing and fibrotic processes: insights for chronic skin wound therapeutics. *J Cell Commun Signal* 1–7. doi: 10.1007/s12079-018-0453-7
- Midwood KS, Williams LV, Schwarzbauer JE (2004) Tissue repair and the dynamics of

- the extracellular matrix. *Int J Biochem Cell Biol* 36:1031–1037. doi: 10.1016/j.biocel.2003.12.003
- Murphy P V., André S, Gabius HJ (2013) The third dimension of reading the sugar code by lectins: Design of glycoclusters with cyclic scaffolds as tools with the Aim to Define Correlations between spatial presentation and activity. *Molecules* 18:4026–4053. doi: 10.3390/molecules18044026
- Norman G, Westby M, Rithalia A, et al (2017) Dressings and topical agents for treating pressure ulcers (Review) Dressings and topical agents for treating pressure ulcers (Review). *Cochrane Database Syst Rev* Dr. doi: 10.1002/14651858.CD011947.pub2
- Nuschke A (2014) Activity of mesenchymal stem cells in therapies for chronic skin wound healing. *Organogenesis* 10:29–37. doi: 10.4161/org.27405
- O'Brien K, Bhatia A, Tsen F, et al (2014) Identification of the critical therapeutic entity in secreted Hsp90 α that promotes wound healing in newly re-standardized healthy and diabetic pig models. *PLoS One* 9:1–25. doi: 10.1371/journal.pone.0113956
- Otero-Viñas M, Falanga V (2016) Mesenchymal Stem Cells in Chronic Wounds: The Spectrum from Basic to Advanced Therapy. *Adv Wound Care* 5:149–163. doi: 10.1089/wound.2015.0627
- Ott C, Jacobs K, Haucke E, et al (2014) Role of advanced glycation end products in cellular signaling. *Redox Biol* 2:411–429. doi: 10.1016/j.redox.2013.12.016
- Patil P, Martin JR, Sarett SM, et al (2017) Porcine Ischemic Wound-Healing Model for Preclinical Testing of Degradable Biomaterials. *Tissue Eng Part C Methods* 23:754–762. doi: 10.1089/ten.tec.2017.0202
- Pepe D, Elliott CG, Forbes TL, Hamilton DW (2014) Detection of galectin-3 and localization of advanced glycation end products (AGE) in human chronic skin wounds. *Histol Histopathol* 29:251–258. doi: 10.14670/HH-29.251
- Peppas M, Brem H, Ehrlich P, et al (2003) Adverse Effects of Dietary Glycotoxins on Wound Healing in Genetically Diabetic Mice. *Diabetes* 52:2805–2813. doi: 10.2337/diabetes.52.11.2805
- Philandrianos C, Andrac-Meyer L, Mordon S, et al (2012) Comparison of five dermal substitutes in full-thickness skin wound healing in a porcine model. *Burns* 38:820–829. doi: 10.1016/j.burns.2012.02.008
- Philippeos C, Telerman SB, Oulès B, et al (2018) Spatial and Single-Cell Transcriptional Profiling Identifies Functionally Distinct Human Dermal Fibroblast Subpopulations. *J Invest Dermatol* 138:811–825. doi: 10.1016/j.jid.2018.01.016
- Plikus M V., Guerrero-Juarez CF, Ito M, et al (2017) Regeneration of fat cells from myofibroblasts during wound healing. *Science* (80-) 355:748–752. doi: 10.1126/science.aai8792
- Pricci F, Leto G, Amadio L, et al (2000) Role of galectin-3 as a receptor for advanced glycosylation end products. *Kidney Int* 58:S31–S39. doi: 10.1046/j.1523-1755.2000.07706.x

- Rinkevich Y, Walmsley GG, Hu MS, et al (2015) Identification and isolation of a dermal lineage with intrinsic fibrogenic potential. *Science* (80-) 348:aaa2151. doi: 10.1126/science.aaa2151
- Rognoni E, Pisco AO, Hiratsuka T, et al (2018) Fibroblast state switching orchestrates dermal maturation and wound healing. *Mol Syst Biol* 14:e8174. doi: 10.15252/msb.20178174
- Roy S, Biswas S, Khanna S, et al (2009) Characterization of a preclinical model of chronic ischemic wound. *Physiol Genomics* 37:211–224. doi: 10.1152/physiolgenomics.90362.2008.
- Saito M, Iwawaki T, Taya C, et al (2001) Diphtheria toxin receptor-mediated conditional and targeted cell ablation in transgenic mice. *Nat Biotechnol* 19:746–750. doi: 10.1038/90795
- Sandu O, Song K, Cai W, et al (2005) Insulin resistance and type 2 diabetes in high-fat-fed mice are linked to high glycotxin intake. *Diabetes* 54:2314–2319. doi: 10.2337/diabetes.54.8.2314
- Santema TB, Poyck PPC, Ubbink DT (2016) Skin grafting and tissue replacement for treating foot ulcers in people with diabetes. *Cochrane Database Syst Rev* 2016:. doi: 10.1002/14651858.CD011255.pub2
- Seaton M, Hocking A, Gibran NS (2015) Porcine models of cutaneous wound healing. *ILAR J* 56:127–138. doi: 10.1093/ilar/ilv016
- Singh VP, Bali A, Singh N, Jaggi AS (2014) Advanced glycation end products and diabetic complications. *Korean J Physiol Pharmacol* 18:1–14. doi: 10.4196/kjpp.2014.18.1.1
- Snyder DL, Sullivan N, Schoelles KM (2012) Skin Substitutes for Treating Chronic Wounds - Technology Assessment. *Agency Healthc Res Qual* 89
- Stirban A, Gawlowski T, Roden M (2014) Vascular effects of advanced glycation endproducts: Clinical effects and molecular mechanisms. *Mol Metab* 3:94–108. doi: 10.1016/j.molmet.2013.11.006
- Sullivan TP, Eaglstein WH, Davis SC, Mertz P (2001) The pig as a model for human wound healing. *Wound Repair Regen* 9:66–76. doi: 10.1046/j.1524-475x.2001.00066.x
- Tieng V, Cherpain O, Gutzwiller E, et al (2016) Elimination of proliferating cells from CNS grafts using a Ki67 promoter-driven thymidine kinase. *Mol Ther - Methods Clin Dev* 3:16069. doi: 10.1038/mtm.2016.69
- Torreggiani M, Liu H, Wu J, et al (2009) Advanced glycation end product receptor-1 transgenic mice are resistant to inflammation, oxidative stress, and post-injury intimal hyperplasia. *Am J Pathol* 175:1722–1732. doi: 10.2353/ajpath.2009.090138
- Turner NJ, Badylak SF (2015) The Use of Biologic Scaffolds in the Treatment of Chronic Nonhealing Wounds. *Adv Wound Care* 4:490–500. doi: 10.1089/wound.2014.0604

- Velander P, Theopold C, Hirsch T, et al (2008) Impaired wound healing in an acute diabetic pig model and the effects of local hyperglycemia. *Wound Repair Regen* 16:288–293. doi: 10.1111/j.1524-475X.2008.00367.x
- Vlassara H, Li YM, Imani F, et al (1995) Identification of galectin-3 as a high-affinity binding protein for advanced glycation end products (AGE): a new member of the AGE-receptor complex. *Mol Med* 1:634–46
- Walker JT, Kim SS, Michelsons S, et al (2015) Cell–matrix interactions governing skin repair: matricellular proteins as diverse modulators of cell function. *Res Reports Biochem* 5:1–16. doi: 10.2147/RRBC.S57407
- Zoungas S, Woodward M, Li Q, et al (2014) Impact of age, age at diagnosis and duration of diabetes on the risk of macrovascular and microvascular complications and death in type 2 diabetes. *Diabetologia* 57:2465–2474. doi: 10.1007/s00125-014-3369-7

Appendices:

Appendix A: Supplemental Figures and Tables

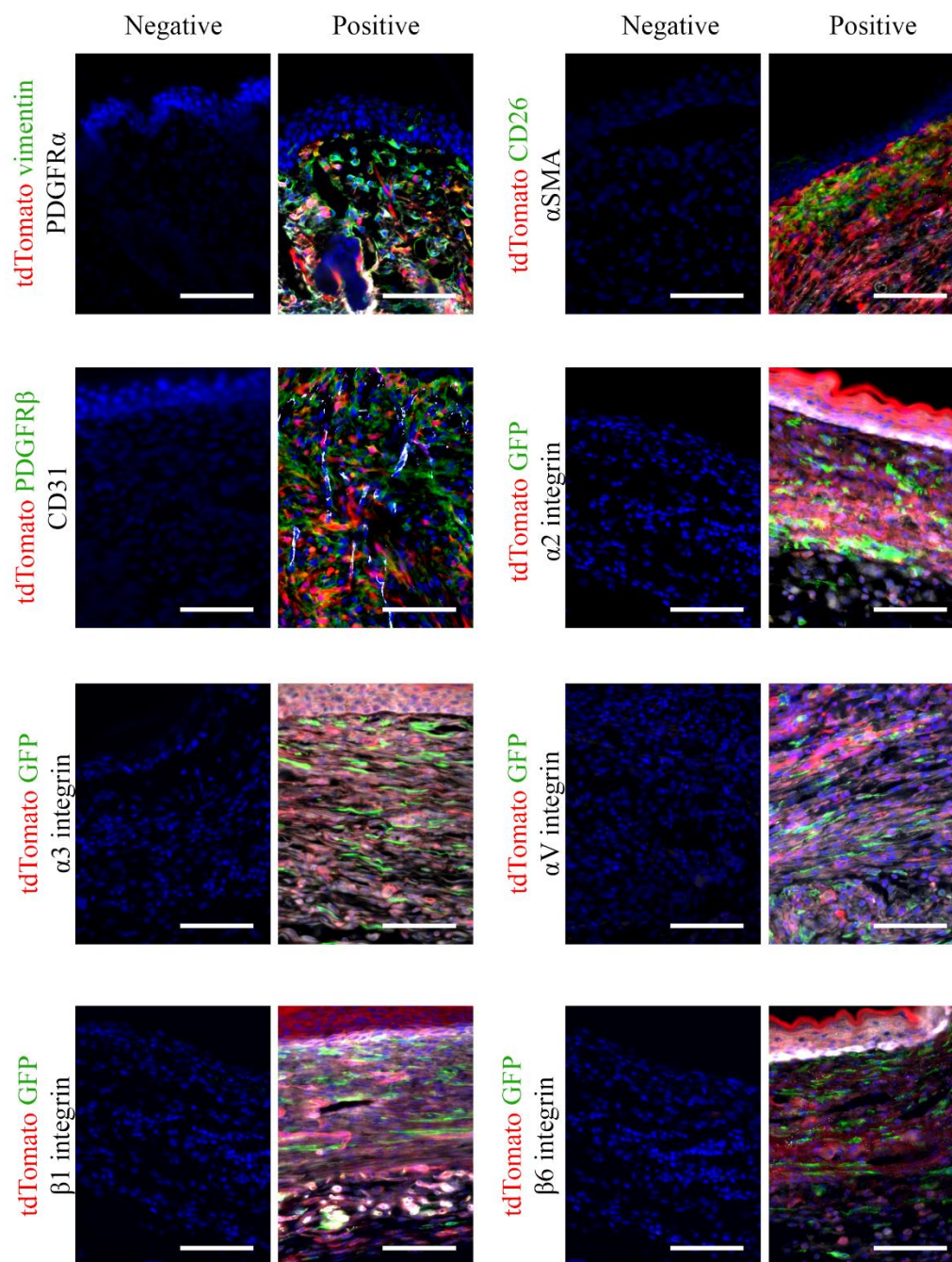


Figure A-1: Negative staining controls (no-primary controls) for staining. Nuclei are stained with DAPI in all samples. Scale bar is 100 μm . Colors are as indicated (black text is shown in white).

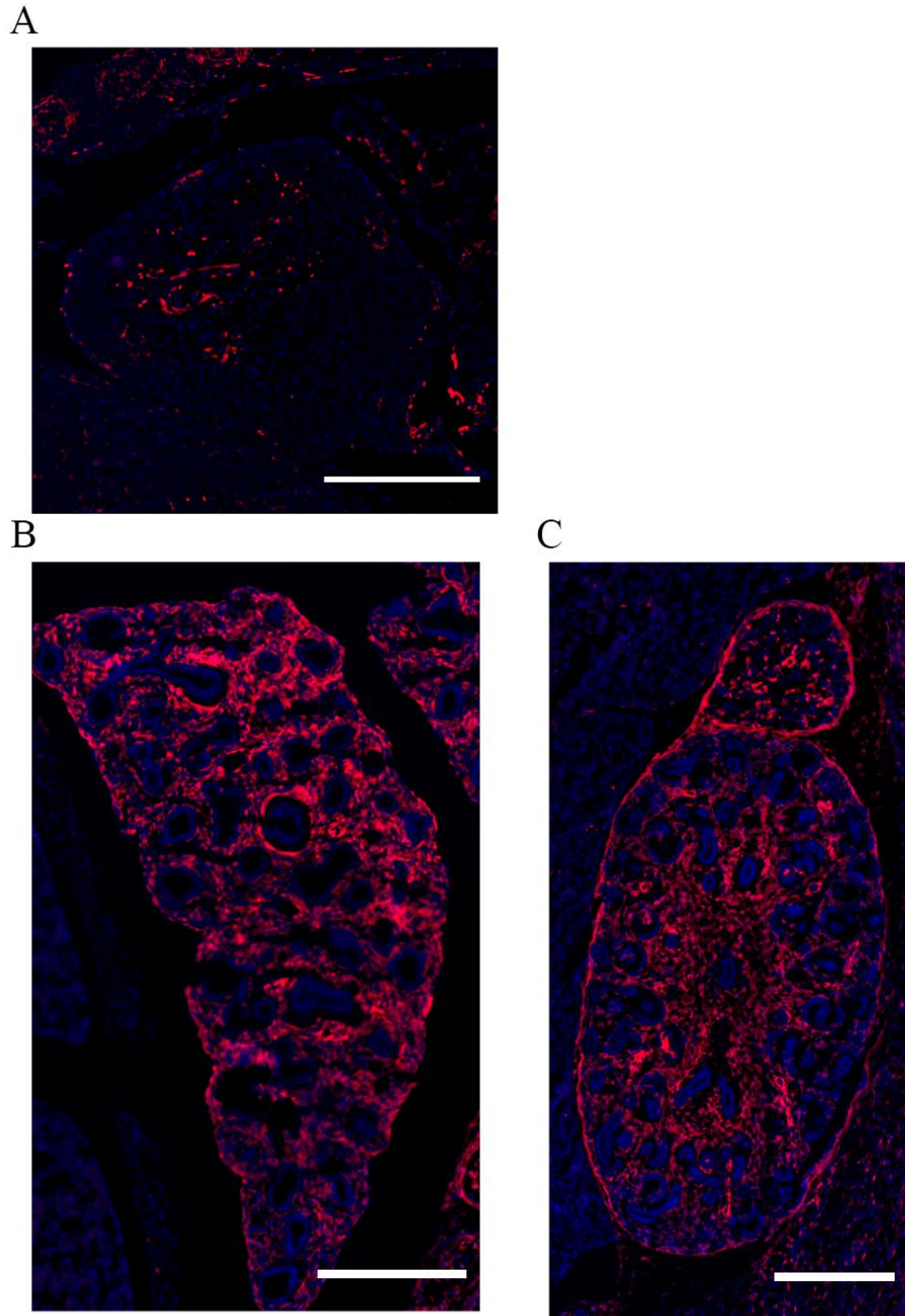


Figure A-2: FLP cells contribute to populations within the heart (A), lungs (B), and kidney (C) in mice at embryonic day 14.5. A cross between *Foxd1*^{GC} and *Ai14* mice results in tdTomato expression in FLP cells (shown in red). Cells are counterstained with DAPI. Scale bars are 500 μm.

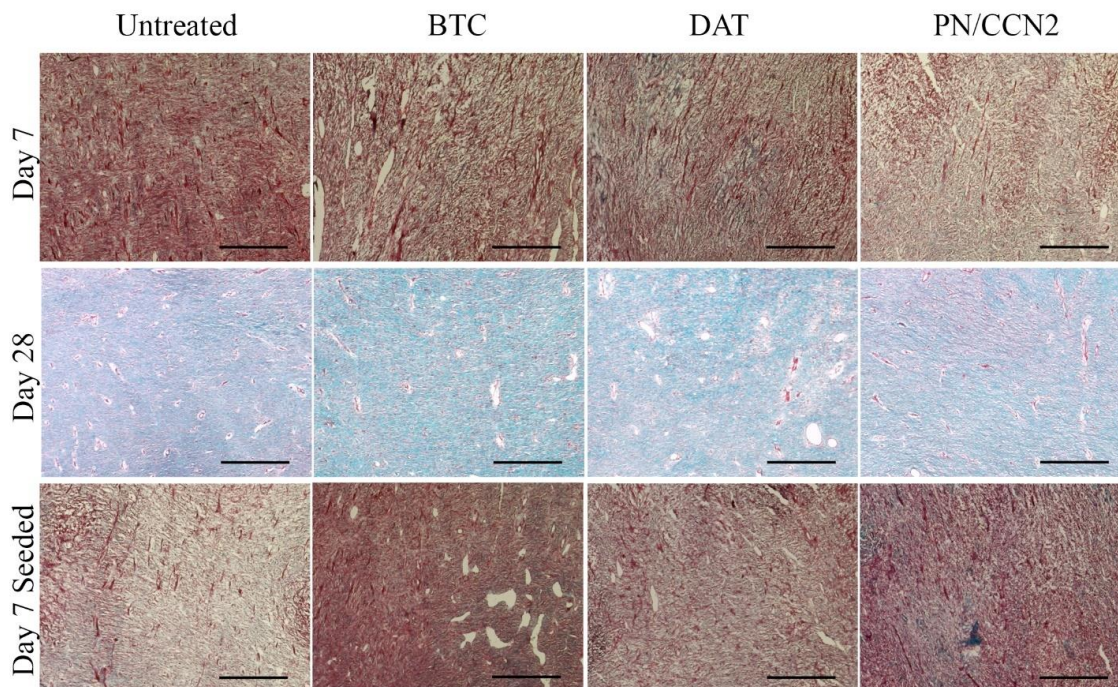


Figure A-3: High magnification images of porcine granulation tissue stained with Masson's trichrome stain. Scale bars are 500 μ m.

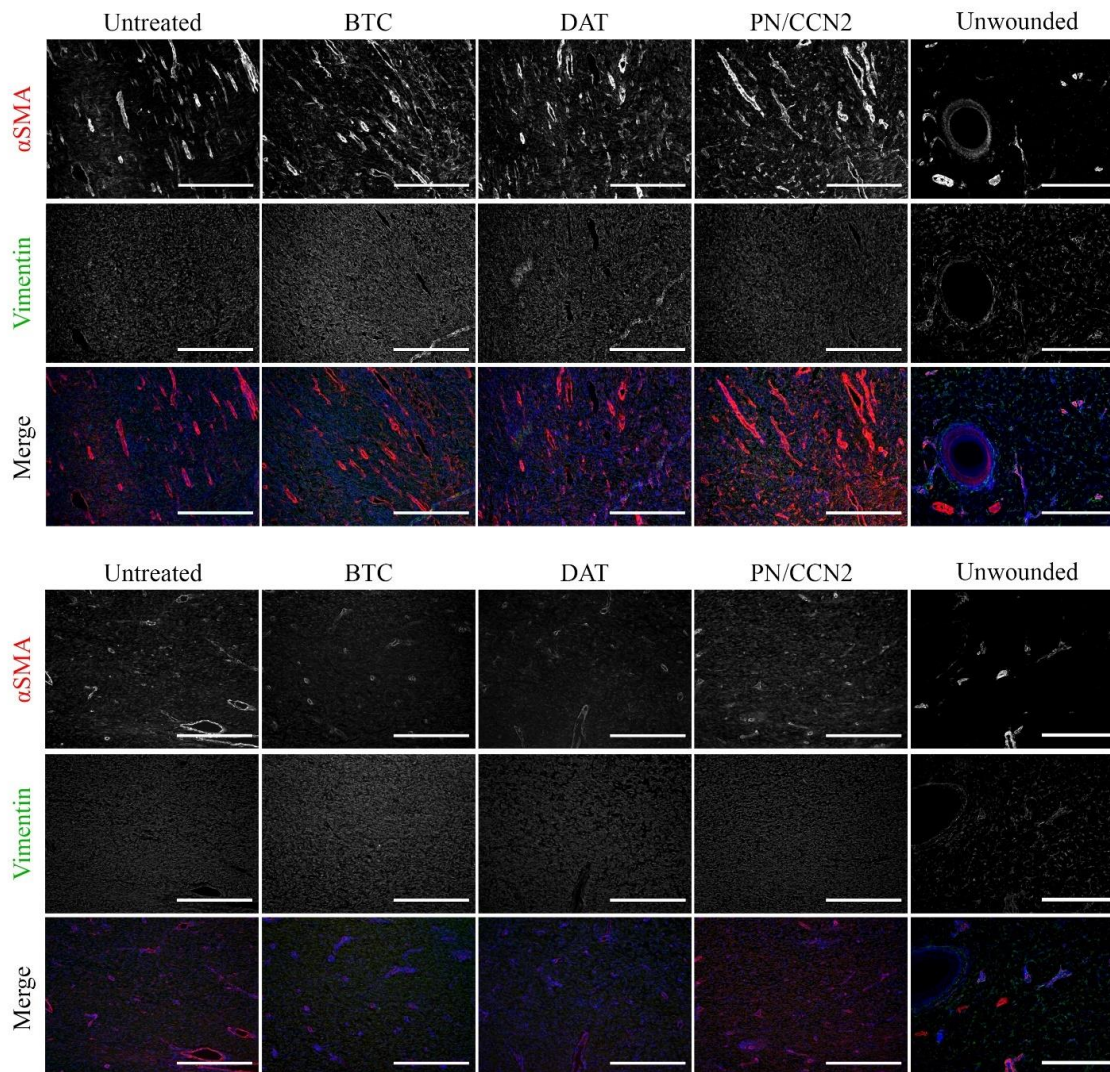


Figure A-4: High magnification images of α SMA (red) and vimentin (green) stained porcine wound tissue at Day 7 (top) and Day 28 (bottom). Nuclei are stained with DAPI (blue); scale bars are 500 μ m.

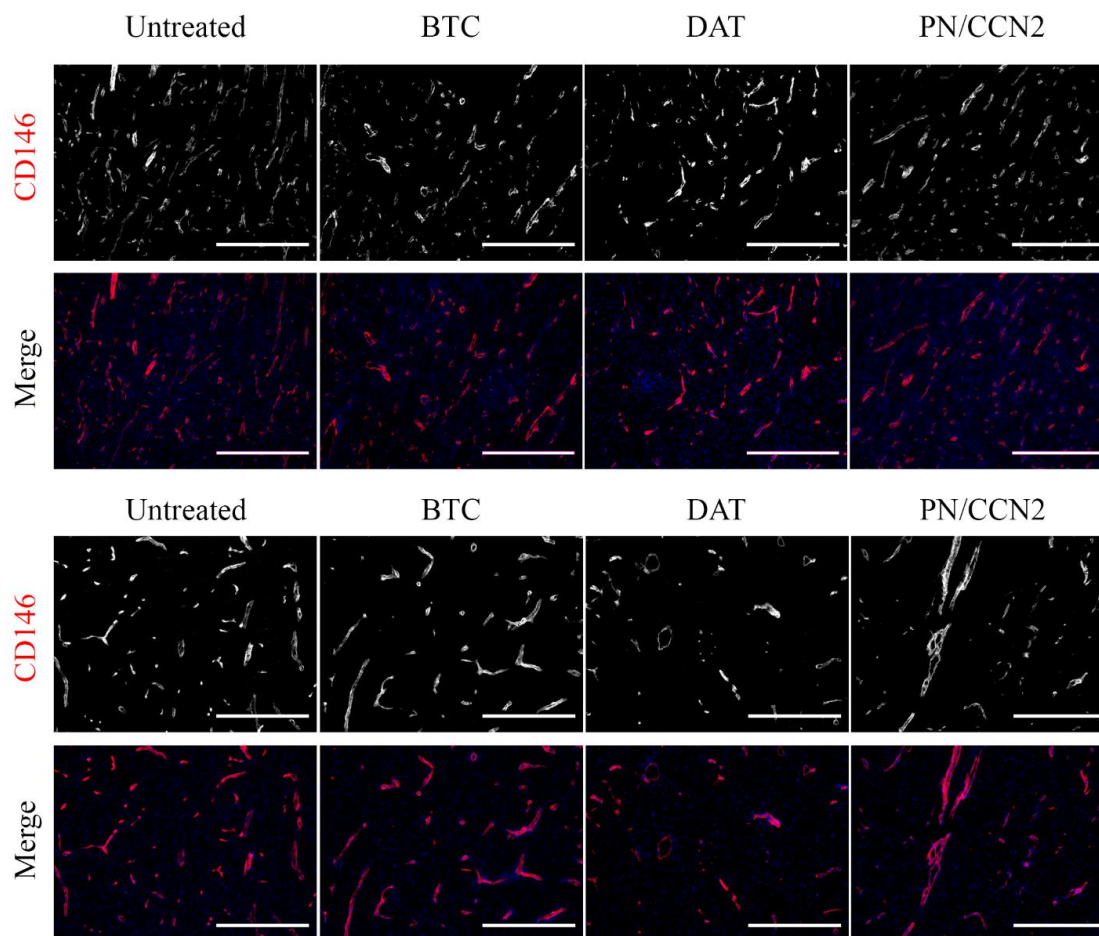


Figure A-5: High magnification images of CD146 (red) stained porcine wound tissue at Day 7 (top) and Day 28 (bottom). Nuclei are stained with DAPI (blue); scale bars are 500 μm .

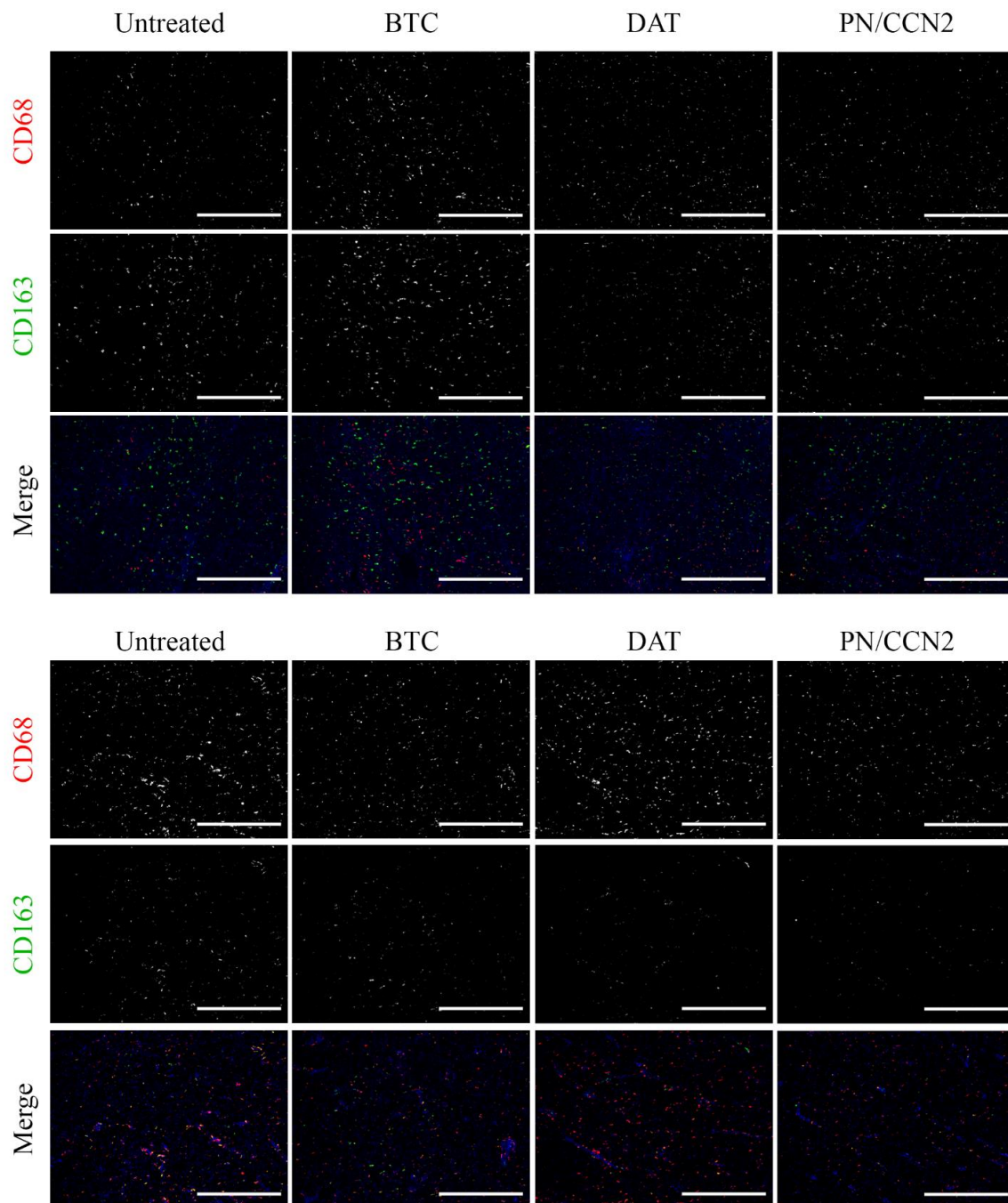


Figure A-6: High magnification images of CD68 (red) and CD163 (green) stained porcine wound tissue at Day 7 (top) and Day 28 (bottom). Nuclei are stained with DAPI (blue); scale bars are 500 μm .

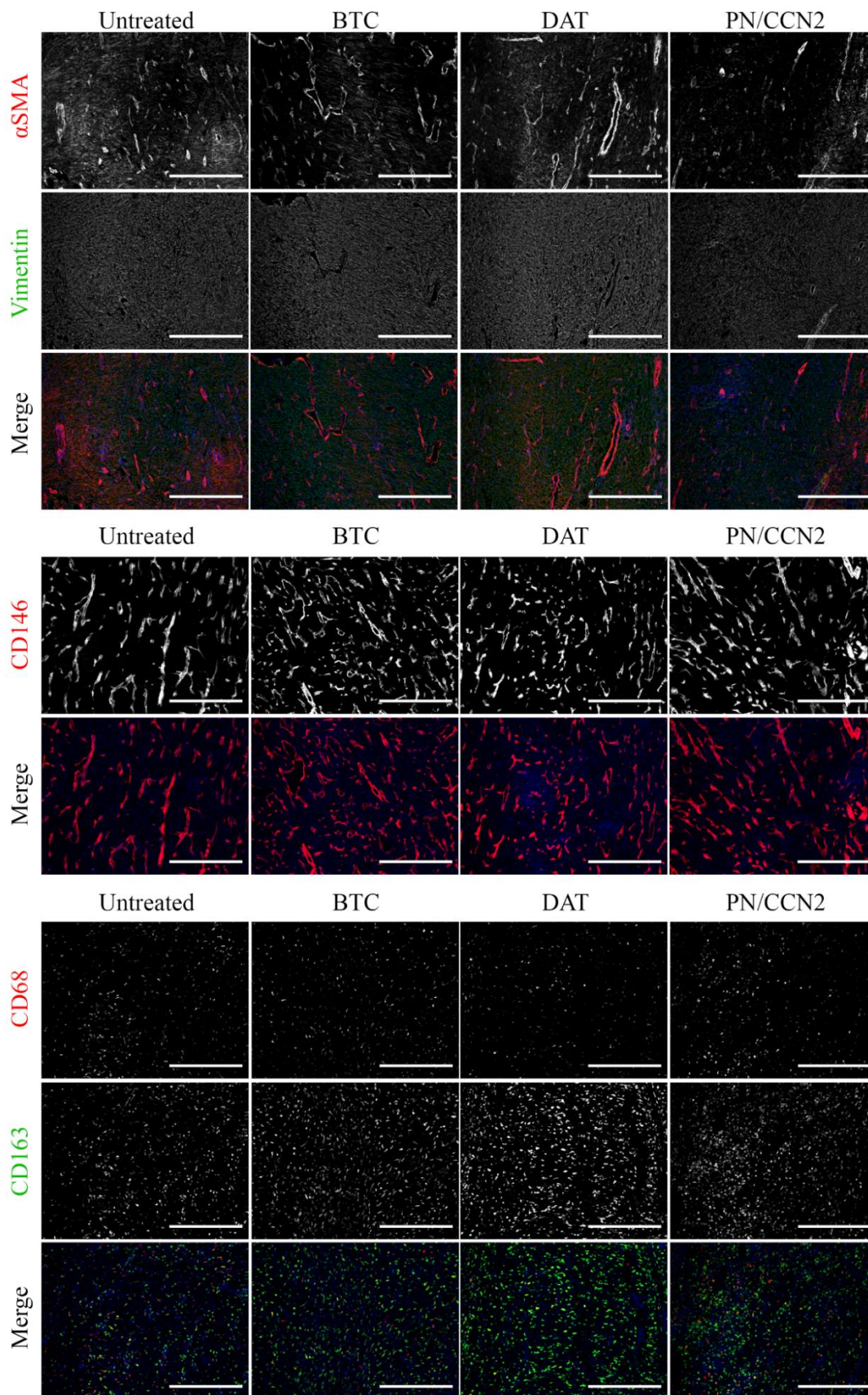


Figure A-7: High magnification images of wounds treated with ASC seeded biomaterials at 7 days. Top panel: α SMA (red); vimentin (green). Middle panel: CD146 (red). Bottom panel: CD68 (red); CD163 (green). Nuclei are stained with DAPI (blue); scale bars are 500 μ m.

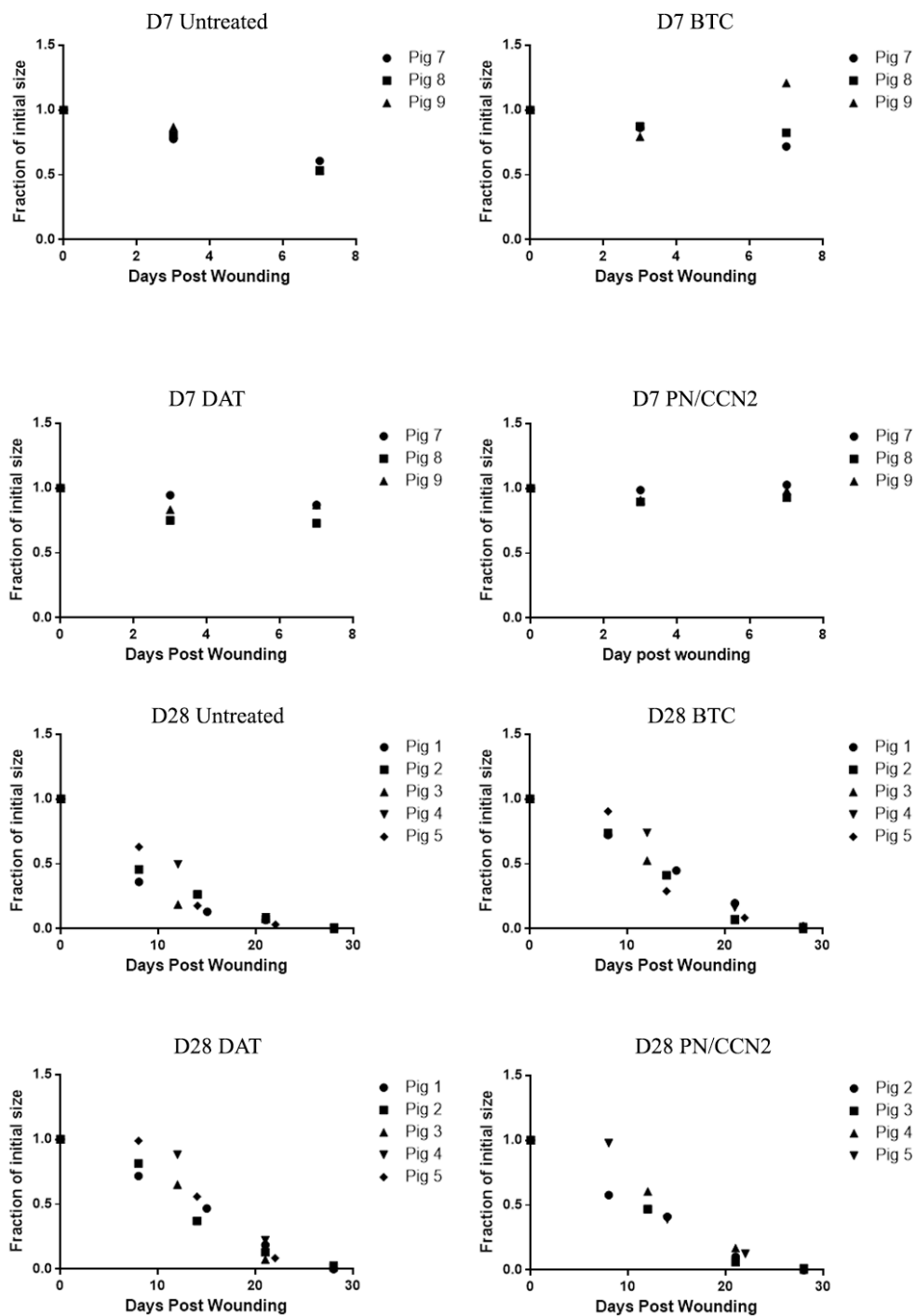


Figure A-8: Individual wound size measurements used to complete the regression analyses highlighted in Figures 3.2 and 3.3.

Table A-1: Normalized Gene expression data relative to housekeeping panel from Qiagen RT² Profiler array for fibrosis related genes; unwounded tissue comparison.

Gene	Discovery?	P value	Mean unwounded FLN	Mean unwounded FLP	Difference	SE of difference	t ratio	df
Acta2		0.634914	0.616963	0.735142	-0.118179	0.243064	0.486207	13
Agt		0.971656	0.00362571	0.003575	5.07143E-05	0.0014001	0.0362219	13
Akt1		0.0909378	0.198106	0.270086	-0.0719805	0.0394252	1.82575	13
Bcl2		0.104419	0.00410571	0.003105	0.00100071	0.000573213	1.7458	13
Bmp7		0.356914	0.107879	0.0863737	0.0215048	0.022514	0.955176	13
Cav1		0.321783	1.17691	1.47905	-0.302136	0.293329	1.03002	13
Ccl11		0.152835	0.540463	0.710196	-0.169733	0.111779	1.51847	13
Ccl3		0.0322879	0.00235571	0.00078	0.00157571	0.00065747	2.39663	13
Cebpb		0.0269476	1.67512	2.40513	-0.730015	0.289778	2.51922	12
Colla2		0.182805	83.1964	125.028	-41.8311	29.5855	1.41391	12
Col3a1		0.26553	35.3815	44.9769	-9.59532	8.24679	1.16352	13
Ctgf		0.451333	0.375689	0.451394	-0.0757052	0.0974914	0.776532	13
Cxcr4	*	0.00831787	0.00738143	0.00324375	0.00413768	0.0013313	3.10799	13
Dcn		0.52726	14.3297	16.1474	-1.81772	2.7982	0.649604	13
Edn1		0.206692	0.05198	0.0401825	0.0117975	0.00887675	1.32903	13
Egf		0.46395	0.00192857	0.00249	- 0.000561429	0.000744024	0.754584	13
Eng		0.0248758	0.188467	0.302794	-0.114327	0.0446113	2.56274	12
Grem1		0.563756	0.177119	0.20666	-0.0295414	0.0498687	0.592384	13
Hgf		0.0640165	0.0541014	0.0866513	-0.0325498	0.0160814	2.02407	13
Il10		0.775462	0.00476143	0.00519	- 0.000428571	0.00147154	0.291241	13
Il13ra2		0.355287	0.00304286	0.00244333	0.000599524	0.000621276	0.964988	11
Il1a	*	< 0.0001	0.00390714	0.000180143	0.003727	0.000605922	6.15096	12
Il1b		0.121834	0.00267286	0.00106125	0.00161161	0.000973727	1.65509	13
Ilk		0.167775	0.259764	0.354564	-0.0947995	0.0648889	1.46095	13
Itga1		0.919285	0.0566343	0.0578725	-0.00123821	0.0119841	0.103322	13
Itga2	*	0.00159188	0.0375957	0.0167513	0.0208445	0.00524692	3.9727	13
Itga3	*	0.0146205	0.0863186	0.0049175	0.0814011	0.0289229	2.81442	13

Itgav		0.343393	0.550541	0.68055	-0.130009	0.132213	0.983329	13
Itgb1		0.0816699	1.56866	2.1692	-0.600534	0.318224	1.88715	13
Itgb3		0.110607	0.214646	0.362486	-0.147841	0.0863487	1.71213	13
Itgb5		0.106998	0.634389	1.13882	-0.504436	0.29132	1.73155	13
Itgb6	*	< 0.0001	0.0184014	0.00266375	0.0157377	0.00281452	5.5916	13
Itgb8	*	0.00689869	0.0269571	0.0069975	0.0199596	0.00622734	3.20516	13
Jun		0.284225	1.3148	1.12377	0.19103	0.171024	1.11697	13
Lox	*	0.0033334	2.09645	3.59958	-1.50312	0.419418	3.58383	13
Ltbp1		0.134205	0.438347	0.544015	-0.105668	0.0661529	1.59733	13
Mmp13		0.161662	0.0404843	0.015715	0.0247693	0.0165087	1.50038	11
Mmp14		0.162952	1.54771	1.9581	-0.410397	0.277478	1.47903	13
Mmp1a		0.142321	0.000568571	0.0009025	- 0.000333929	0.000213798	1.56189	13
Mmp2		0.0682244	3.64687	5.99811	-2.35124	1.18239	1.98854	13
Mmp3	*	0.00924985	1.62256	2.8758	-1.25324	0.410521	3.05281	13
Mmp8		0.0935178	0.00661	0.0163625	-0.0097525	0.00538912	1.80966	13
Mmp9		0.691412	0.01167	0.00981429	0.00185571	0.00456323	0.406666	12
Myc		0.189024	0.319444	0.268455	0.0509893	0.0367854	1.38613	13
Nfkb1		0.337063	0.527876	0.408602	0.119273	0.119658	0.996782	13
Pdgfa		0.0445869	0.0386833	0.024515	0.0141683	0.00631778	2.24261	12
Pdgfb		0.0166271	0.03108	0.0077225	0.0233575	0.00850235	2.74718	13
Plat		0.752836	1.04266	1.08533	-0.0426684	0.132657	0.321644	13
Plau		0.0393458	0.465539	0.345875	0.119664	0.0522434	2.2905	13
Serpine1		0.0742413	0.938399	1.36976	-0.43136	0.222225	1.9411	13
Serpinh1	*	0.00471221	2.65042	4.95482	-2.3044	0.677104	3.40332	13
Smad2		0.159925	0.197391	0.277326	-0.0799348	0.0536257	1.49061	13
Smad3		0.291228	0.124423	0.1757	-0.0512771	0.0466098	1.10014	13
Smad4		0.0375703	0.132441	0.0986275	0.0338139	0.014604	2.31538	13
Smad6		0.305899	0.0710129	0.0976725	-0.0266596	0.0250132	1.06582	13
Smad7		0.190027	0.05723	0.068545	-0.011315	0.00818283	1.38277	13
Snai1		0.170862	0.0115429	0.0176667	-0.00612381	0.00417956	1.46518	11
Sp1		0.280726	0.268163	0.375519	-0.107356	0.0953848	1.1255	13
Stat1		0.114802	0.127681	0.177174	-0.0494923	0.0292811	1.69025	13
Stat6		0.345663	0.00200286	0.00120833	0.000794524	0.000806394	0.98528	11

Tgfb1		0.244665	0.357791	0.44903	-0.0912386	0.0748743	1.21856	13
Tgfb2		0.368076	0.0491729	0.0546562	-0.00548339	0.00588033	0.932498	13
Tgfb3		0.38087	0.0245386	0.0266925	-0.00215393	0.00237457	0.907082	13
Tgfb1		0.110569	0.129563	0.167615	-0.0380521	0.0222224	1.71233	13
Tgfb2		0.760386	0.35422	0.371194	-0.0169738	0.0544965	0.311465	13
Tgif1	*	0.000309042	0.0142457	0.0072325	0.00701321	0.00144171	4.86451	13
Thbs1		0.135883	3.80892	5.9654	-2.15648	1.3564	1.58985	13
Thbs2		0.251963	1.30932	1.6862	-0.376875	0.314349	1.19891	13
Timp1		0.108444	0.266021	0.474925	-0.208904	0.121195	1.7237	13
Timp2		0.151351	2.39077	3.34708	-0.956306	0.627316	1.52444	13
Timp3		0.23345	1.35835	1.95398	-0.59563	0.476629	1.24967	13
Timp4		0.0559856	0.00242143	0.0011025	0.00131893	0.000628572	2.09829	13
Tnf	*	0.00367252	0.00431667	0.0008525	0.00346417	0.000963329	3.59604	12
Vegfa		0.201713	0.638917	0.88731	-0.248393	0.184719	1.34471	13

Table A-2: Normalized Gene expression data relative to housekeeping panel from Qiagen RT² Profiler array for fibrosis related genes; wounded tissue comparison.

Gene	Discovery?	P value	Mean wounded FLN	Mean wounded FLP	Difference	SE of difference	t ratio	df
Acta2		0.0737829	1.55205	0.857998	0.694052	0.356914	1.94459	13
Agt		0.278323	0.00132286	0.0018675	-0.000544643	0.000481385	1.13141	13
Akt1		0.467398	0.198116	0.212149	-0.014033	0.0187445	0.74865	13
Bcl2		0.603073	0.00192857	0.00221875	-0.000290179	0.000544496	0.53293	13
Bmp7	*	0.0121957	0.148619	0.0403487	0.10827	0.0372191	2.90899	13
Cav1		0.057228	1.67892	0.886535	0.792388	0.379825	2.08619	13
Ccl11		0.484319	0.627933	0.548415	0.0795179	0.110454	0.719917	13
Ccl3		0.0422429	0.0235633	0.001885	0.0216783	0.00953921	2.27255	12
Cebpb		0.0513599	2.07708	1.17703	0.90005	0.419471	2.14568	13
Colla2		0.736434	97.8863	87.3718	10.5145	30.5759	0.343882	13
Col3a1	*	0.0050077	31.3666	62.3805	-31.014	9.19841	3.37167	13
Ctgf	*	0.00411083	0.160476	0.354964	-0.194488	0.055977	3.47443	13

Cxcr4		0.224537	0.00730571	0.004675	0.00263071	0.00206289	1.27526	13
Dcn	*	0.00124996	7.23182	13.2328	-6.00101	1.46318	4.10136	13
Edn1	*	0.0035927	0.0847214	0.0158325	0.0688889	0.0194343	3.5447	13
Egf		0.149429	0.00148429	0.00078375	0.000700536	0.000457194	1.53225	13
Eng		0.447562	0.174737	0.153231	0.0215059	0.0274602	0.783167	13
Grem1		0.055317	0.0521657	0.105287	-0.0531218	0.025237	2.10491	13
Hgf		0.920767	0.0699157	0.0726537	-0.00273804	0.0269979	0.101417	13
Il10		0.064421	0.0107086	0.00584375	0.00486482	0.00240766	2.02056	13
Il13ra2		0.730462	0.0108157	0.00946375	0.00135196	0.00384055	0.352023	13
Il1a	*	0.00122348	0.00491	0.00127375	0.00363625	0.000864979	4.20386	12
Il1b		0.0448307	0.0304243	0.0011275	0.0292968	0.0131976	2.21986	13
Ilk		0.0521942	0.294146	0.230043	0.0641032	0.029999	2.13685	13
Itga1		0.0485497	0.201064	0.084105	0.116959	0.0537385	2.17645	13
Itga2	*	0.00473543	0.0723686	0.0171275	0.0552411	0.0162438	3.40076	13
Itga3	*	0.000317166	0.07782	0.003265	0.074555	0.0149558	4.98503	12
Itgav		0.0545087	0.973169	0.512201	0.460967	0.218156	2.11301	13
Itgb1		0.176021	2.47284	1.82993	0.642912	0.449266	1.43103	13
Itgb3		0.0828145	0.307753	0.1863	0.121453	0.064629	1.87923	13
Itgb5		0.854017	0.749311	0.719936	0.0293752	0.156509	0.18769	13
Itgb6	*	< 0.0001	0.0239486	0.0031575	0.0207911	0.00326654	6.36486	13
Itgb8	*	0.00621946	0.0720033	0.0135	0.0585033	0.0176724	3.31043	12
Jun		0.076934	0.643719	1.08833	-0.444615	0.23145	1.921	13
Lox		0.466655	3.24312	3.85222	-0.609097	0.81221	0.749926	13
Ltbp1		0.417644	0.26	0.29501	-0.03501	0.0418215	0.83713	13
Mmp13		0.24039	0.174983	0.239025	-0.0640421	0.0520548	1.23028	13
Mmp14	*	0.00943269	1.24578	2.02525	-0.779463	0.25618	3.04264	13
Mmp1a		0.0782242	0.00170714	0.00082625	0.000880893	0.000460816	1.91159	13
Mmp2		0.780116	5.26942	4.91861	0.350807	1.2308	0.285024	13
Mmp3		0.320594	3.54759	4.69702	-1.14943	1.10941	1.03608	12
Mmp8		0.0639558	0.00832833	0.0321	-0.0237717	0.0115442	2.05918	11
Mmp9		0.9492	0.0792629	0.0810262	-0.00176339	0.0271491	0.0649521	13
Myc	*	0.00396502	0.24814	0.398999	-0.150859	0.0431857	3.49325	13
Nfkb1		0.347686	0.72009	0.597936	0.122154	0.125375	0.974306	13
Pdgfa	*	0.0225694	0.12113	0.04529	0.07584	0.0293195	2.58667	13

Pdgb	*	0.0198367	0.0610757	0.00817625	0.0528995	0.0199273	2.65462	13
Plat		0.490702	1.74946	1.51876	0.230696	0.325273	0.709237	13
Plau	*	0.00724158	0.853203	0.389811	0.463392	0.145722	3.17997	13
Serpine1		0.214839	1.41411	1.71148	-0.29737	0.228038	1.30404	13
Serpinh1		0.454056	3.01872	3.52037	-0.501647	0.650002	0.771763	13
Smad2		0.0464625	0.358286	0.174952	0.183333	0.0833178	2.20041	13
Smad3		0.0360272	0.138274	0.0870188	0.0512555	0.0219235	2.33793	13
Smad4		0.161781	0.0985243	0.113199	-0.0146745	0.00989189	1.48348	13
Smad6	*	0.0278754	0.0782729	0.0302075	0.0480654	0.019421	2.47492	13
Smad7		0.126746	0.0434771	0.0519112	-0.00843411	0.00516933	1.63157	13
Snai1	*	0.0022331	0.00495	0.00960375	-0.00465375	0.00122664	3.79389	13
Sp1	*	0.0193868	0.383954	0.163284	0.220671	0.0827513	2.66667	13
Stat1	*	0.0192642	0.195503	0.111524	0.0839791	0.0314528	2.67	13
Stat6		0.560539	0.00129857	0.00114375	0.000154821	0.000259183	0.597343	13
Tgfb1		0.126836	0.530799	0.337012	0.193786	0.118804	1.63115	13
Tgfb2	*	0.0038915	0.03945	0.0709912	-0.0315413	0.00900404	3.50301	13
Tgfb3	*	0.000329841	0.0155671	0.037375	-0.0218079	0.0045169	4.82806	13
Tgfb1		0.0939911	0.17235	0.120681	0.0516688	0.0285975	1.80676	13
Tgfb2	*	0.0102387	0.194876	0.357994	-0.163118	0.0543725	3.00001	13
Tgif1		0.479628	0.0109886	0.0124037	-0.00141518	0.0019444	0.727821	13
Thbs1		0.726903	3.46332	3.69149	-0.228177	0.638198	0.357532	12
Thbs2	*	<0.0001	1.1126	2.29054	-1.17795	0.211382	5.57261	13
Timp1		0.951707	0.732224	0.719904	0.0123205	0.199549	0.061742	13
Timp2		0.132944	1.85864	2.46326	-0.604612	0.377176	1.603	13
Timp3	*	0.0229377	2.07066	0.955054	1.1156	0.432717	2.57813	13
Timp4		0.055868	0.00106429	0.000618	0.000446286	0.000212572	2.09945	13
Tnf	*	0.0208898	0.00780286	0.0012875	0.00651536	0.00247976	2.62741	13
Vegfa		0.144233	1.00906	0.611171	0.397887	0.256075	1.55379	13

Table A-3: Normalized Gene expression data relative to housekeeping panel from Qiagen RT² Profiler array for fibrosis related genes; FLN lineage comparison.

Gene	Discovery?	P value	Mean unwounded FLN	Mean wounded FLN	Difference	SE of difference	t ratio	df
Acta2		0.0229857	0.616963	1.55205	-0.935086	0.35887	2.60564	12
Agt		0.0399098	0.00362571	0.00132286	0.00230286	0.000999518	2.30397	12
Akt1		0.999707	0.198106	0.198116	-1.00008E-05	0.0266856	0.00037476	12
Bcl2		0.0145119	0.00410571	0.00192857	0.00217714	0.000762812	2.8541	12
Bmp7		0.362094	0.107879	0.148619	-0.04074	0.0429991	0.947461	12
Cav1		0.253405	1.17691	1.67892	-0.50201	0.418444	1.19971	12
Ccl11		0.489743	0.540463	0.627933	-0.08747	0.122755	0.712559	12
Ccl3		0.0626594	0.00235571	0.0235633	-0.0212076	0.01024	2.07105	11
Cebpb		0.413279	1.67512	2.07708	-0.40196	0.472723	0.850309	11
Colla2		0.699921	83.1964	97.8863	-14.6899	37.2089	0.394795	12
Col3a1		0.595047	35.3815	31.3666	4.01499	7.35298	0.546036	12
Ctgf	*	0.00321674	0.375689	0.160476	0.215213	0.0586677	3.66834	12
Cxcr4		0.973288	0.00738143	0.00730571	7.57145E-05	0.00221452	0.0341899	12
Dcn	*	0.00356825	14.3297	7.23182	7.09787	1.96522	3.61173	12
Edn1		0.159278	0.05198	0.0847214	-0.0327414	0.0218174	1.5007	12
Egf		0.472273	0.00192857	0.00148429	0.000444286	0.000598646	0.74215	12
Eng		0.635456	0.188467	0.174737	0.0137295	0.0281616	0.487527	11
Grem1	*	0.00878206	0.177119	0.0521657	0.124953	0.0399921	3.12444	12
Hgf		0.523854	0.0541014	0.0699157	-0.0158143	0.0240865	0.656563	12
Il10		0.0361815	0.00476143	0.0107086	-0.00594714	0.00252209	2.35802	12
Il13ra2		0.0142448	0.00304286	0.0108157	-0.00777286	0.00271389	2.86411	12
Il1a		0.374625	0.00390714	0.00491	-0.00100286	0.00108373	0.925377	11
Il1b		0.0745538	0.00267286	0.0304243	-0.0277514	0.0142106	1.95287	12
Ilk		0.423366	0.259764	0.294146	-0.0343814	0.0414805	0.828857	12
Itga1		0.0250286	0.0566343	0.201064	-0.14443	0.0564309	2.55941	12
Itga2		0.0749278	0.0375957	0.0723686	-0.0347729	0.0178322	1.95	12
Itga3		0.824353	0.0863186	0.07782	0.00849857	0.0373877	0.227309	11
Itgav		0.0944573	0.550541	0.973169	-0.422627	0.232753	1.81577	12
Itgb1		0.0726774	1.56866	2.47284	-0.904179	0.459562	1.96748	12

Itgb3		0.244939	0.214646	0.307753	-0.0931071	0.076153	1.22263	12
Itgb5		0.520412	0.634389	0.749311	-0.114923	0.17357	0.662113	12
Itgb6		0.246049	0.0184014	0.0239486	-0.00554714	0.00454836	1.21959	12
Itgb8		0.0461313	0.0269571	0.0720033	-0.0450462	0.0200472	2.24701	11
Jun	*	0.000718908	1.3148	0.643719	0.67108	0.148925	4.50616	12
Lox		0.136153	2.09645	3.24312	-1.14667	0.717821	1.59743	12
Ltbp1		0.0167216	0.438347	0.26	0.178347	0.0642068	2.7777	12
Mmp13	*	0.00219976	0.0404843	0.174983	-0.134499	0.0346913	3.87701	12
Mmp14		0.231362	1.54771	1.24578	0.301923	0.239479	1.26075	12
Mmp1a		0.0360844	0.000568571	0.00170714	-0.00113857	0.000482549	2.3595	12
Mmp2		0.255766	3.64687	5.26942	-1.62255	1.35958	1.19342	12
Mmp3		0.0534178	1.62256	3.54759	-1.92502	0.889948	2.16307	11
Mmp8		0.564482	0.00661	0.00832833	-0.00171833	0.00289247	0.594071	11
Mmp9	*	0.00236377	0.01167	0.0792629	-0.0675929	0.0176144	3.83736	12
Myc		0.0650901	0.319444	0.24814	0.0713043	0.0351195	2.03033	12
Nfkb1		0.190004	0.527876	0.72009	-0.192214	0.138361	1.38923	12
Pdgfa		0.032526	0.0386833	0.12113	-0.0824467	0.0337188	2.44512	11
Pdgfb		0.219393	0.03108	0.0610757	-0.0299957	0.0231473	1.29586	12
Plat		0.0204154	1.04266	1.74946	-0.706794	0.264729	2.66988	12
Plau		0.0205235	0.465539	0.853203	-0.387664	0.145355	2.66702	12
Serpine1		0.0547285	0.938399	1.41411	-0.475714	0.223527	2.12822	12
Serpinh1		0.593875	2.65042	3.01872	-0.3683	0.672331	0.547796	12
Smad2		0.0958676	0.197391	0.358286	-0.160894	0.0890351	1.80709	12
Smad3		0.623617	0.124423	0.138274	-0.0138514	0.0275014	0.503662	12
Smad4		0.0570055	0.132441	0.0985243	0.0339171	0.0161103	2.1053	12
Smad6		0.769308	0.0710129	0.0782729	-0.00726	0.0241997	0.300004	12
Smad7		0.113668	0.05723	0.0434771	0.0137529	0.00805989	1.70633	12
Snai1		0.112265	0.0115429	0.00495	0.00659286	0.00384705	1.71375	12
Sp1		0.244814	0.268163	0.383954	-0.115791	0.09468	1.22298	12
Stat1		0.0741897	0.127681	0.195503	-0.0678214	0.0346792	1.95568	12
Stat6		0.376754	0.00200286	0.00129857	0.000704286	0.000767284	0.917895	12
Tgfb1		0.196637	0.357791	0.530799	-0.173007	0.126544	1.36717	12
Tgfb2		0.109447	0.0491729	0.03945	0.00972286	0.0056238	1.72888	12
Tgfb3	*	0.00293544	0.0245386	0.0155671	0.00897143	0.00241271	3.7184	12

Tgfb1		0.187628	0.129563	0.17235	-0.0427871	0.0306217	1.39728	12
Tgfb2		0.0368598	0.35422	0.194876	0.159344	0.0678697	2.3478	12
Tgif1		0.0726173	0.0142457	0.0109886	0.00325714	0.00165509	1.96795	12
Thbs1		0.635934	3.80892	3.46332	0.345602	0.709903	0.48683	11
Thbs2		0.320503	1.30932	1.1126	0.196721	0.189834	1.03628	12
Timp1		0.0270113	0.266021	0.732224	-0.466203	0.185153	2.51794	12
Timp2		0.339169	2.39077	1.85864	0.53213	0.534564	0.995446	12
Timp3		0.145134	1.35835	2.07066	-0.712309	0.457109	1.55829	12
Timp4		0.0546326	0.00242143	0.00106429	0.00135714	0.000637395	2.1292	12
Tnf		0.277412	0.00431667	0.00780286	-0.00348619	0.00305075	1.14273	11
Vegfa		0.215573	0.638917	1.00906	-0.370141	0.283113	1.3074	12

Table A-4: Normalized Gene expression data relative to housekeeping panel from Qiagen RT² Profiler array for fibrosis related genes; FLP lineage comparison.

Gene	Discovery?	P value	Mean wounded FLP	Mean unwounded FLP	Difference	SE of difference	t ratio	df
Acta2		0.637374	0.857998	0.735142	0.122856	0.254979	0.481826	14
Agt		0.133722	0.0018675	0.003575	-0.0017075	0.0010726	1.59193	14
Akt1		0.10503	0.212149	0.270086	-0.0579375	0.0334293	1.73314	14
Bcl2	*	0.0162345	0.00221875	0.003105	-0.00088625	0.000324497	2.73115	14
Bmp7	*	0.0118122	0.0403487	0.0863737	-0.046025	0.015911	2.89266	14
Cav1		0.0397179	0.886535	1.47905	-0.592514	0.261304	2.26753	14
Ccl11		0.129764	0.548415	0.710196	-0.161781	0.100501	1.60974	14
Ccl3		0.202964	0.001885	0.00078	0.001105	0.000827296	1.33568	14
Cebpb	*	0.00044084	1.17703	2.40513	-1.22811	0.269022	4.56507	14
Colla2		0.114109	87.3718	125.028	-37.6557	22.2313	1.69381	13
Col3a1		0.090647	62.3805	44.9769	17.4037	9.57712	1.81721	14
Ctgf		0.309767	0.354964	0.451394	-0.09643	0.0914959	1.05393	14
Cxcr4		0.268985	0.004675	0.00324375	0.00143125	0.00124341	1.15107	14
Dcn		0.244086	13.2328	16.1474	-2.91457	2.39683	1.21601	14
Edn1	*	0.00154609	0.0158325	0.0401825	-0.02435	0.00621494	3.91798	14

Egf	*	0.0164401	0.00078375	0.00249	-0.00170625	0.000626207	2.72474	14
Eng	*	0.002264	0.153231	0.302794	-0.149563	0.0401545	3.72468	14
Grem1	*	0.0205459	0.105287	0.20666	-0.101372	0.03883	2.61067	14
Hgf		0.506103	0.0726537	0.0866513	-0.0139975	0.0205113	0.682429	14
Il10		0.661041	0.00584375	0.00519	0.00065375	0.00145942	0.447953	14
Il13ra2		0.0484265	0.00946375	0.00244333	0.00702042	0.00319596	2.19666	12
Il1a	*	0.00319474	0.00127375	0.000180143	0.00109361	0.000303271	3.60604	13
Il1b		0.908365	0.0011275	0.00106125	0.00006625	0.000565266	0.117201	14
Ilk		0.0432222	0.230043	0.354564	-0.124521	0.0560235	2.22266	14
Itga1		0.111777	0.084105	0.0578725	0.0262325	0.0154568	1.69715	14
Itga2		0.921457	0.0171275	0.0167513	0.00037625	0.00374784	0.100391	14
Itga3		0.287907	0.003265	0.0049175	-0.0016525	0.00149586	1.10472	14
Itgav		0.201344	0.512201	0.68055	-0.168349	0.125561	1.34078	14
Itgb1		0.311267	1.82993	2.1692	-0.339268	0.322946	1.05054	14
Itgb3		0.0354821	0.1863	0.362486	-0.176186	0.0757132	2.32702	14
Itgb5		0.141288	0.719936	1.13882	-0.418889	0.268674	1.55909	14
Itgb6		0.533186	0.0031575	0.00266375	0.00049375	0.000772782	0.638925	14
Itgb8		0.0376227	0.0135	0.0069975	0.0065025	0.00283189	2.29617	14
Jun		0.882207	1.08833	1.12377	-0.035435	0.234823	0.150901	14
Lox		0.670385	3.85222	3.59958	0.252642	0.581149	0.434729	14
Ltbp1	*	0.000114472	0.29501	0.544015	-0.249005	0.0470815	5.28881	14
Mmp13	*	0.000466178	0.239025	0.015715	0.22331	0.0469394	4.75741	12
Mmp14		0.816459	2.02525	1.9581	0.0671438	0.283889	0.236514	14
Mmp1a		0.735652	0.00082625	0.0009025	-7.625E-05	0.000221389	0.344416	14
Mmp2		0.32878	4.91861	5.99811	-1.0795	1.06686	1.01185	14
Mmp3	*	0.0274615	4.69702	2.8758	1.82121	0.74006	2.4609	14
Mmp8		0.17529	0.0321	0.0163625	0.0157375	0.0109774	1.43363	13
Mmp9	*	0.00659856	0.0810262	0.00981429	0.071212	0.0220589	3.22827	13
Myc	*	0.00911454	0.398999	0.268455	0.130544	0.0431747	3.02362	14
Nfkb1		0.101583	0.597936	0.408602	0.189334	0.108048	1.75231	14
Pdgfa	*	0.0126286	0.04529	0.024515	0.020775	0.00726701	2.85881	14
Pdgfb		0.841424	0.00817625	0.0077225	0.00045375	0.00222619	0.203824	14
Plat		0.0842404	1.51876	1.08533	0.43343	0.233208	1.85855	14
Plau		0.541266	0.389811	0.345875	0.0439362	0.0701644	0.62619	14

Serpine1		0.150209	1.71148	1.36976	0.341724	0.224485	1.52225	14
Serpinh1		0.0449587	3.52037	4.95482	-1.43445	0.651527	2.20168	14
Smad2		0.0627051	0.174952	0.277326	-0.102374	0.0506273	2.0221	14
Smad3		0.0513175	0.0870188	0.1757	-0.0886813	0.0416187	2.1308	14
Smad4		0.114593	0.113199	0.0986275	0.0145712	0.00865946	1.6827	14
Smad6	*	0.00576878	0.0302075	0.0976725	-0.067465	0.0207341	3.25381	14
Smad7	*	0.0112093	0.0519112	0.068545	-0.0166338	0.00569812	2.91916	14
Snai1	*	< 0.0001	0.00960375	0.0176667	-0.00806292	0.00132515	6.08454	12
Sp1	*	0.0245312	0.163284	0.375519	-0.212235	0.0842418	2.51936	14
Stat1	*	0.0262614	0.111524	0.177174	-0.06565	0.0264283	2.48408	14
Stat6		0.752153	0.00114375	0.00120833	-6.45833E-05	0.000199864	0.323137	12
Tgfb1		0.138391	0.337012	0.44903	-0.112018	0.0712813	1.57148	14
Tgfb2		0.0829096	0.0709912	0.0546562	0.016335	0.00874702	1.86749	14
Tgfb3	*	0.0252797	0.037375	0.0266925	0.0106825	0.00426649	2.50381	14
Tgfbr1		0.040731	0.120681	0.167615	-0.0469337	0.0208207	2.25419	14
Tgfbr2		0.752272	0.357994	0.371194	-0.0132	0.0410043	0.321917	14
Tgif1	*	0.0100566	0.0124037	0.0072325	0.00517125	0.00173882	2.97399	14
Thbs1		0.0914036	3.69149	5.9654	-2.2739	1.25456	1.8125	14
Thbs2		0.0731793	2.29054	1.6862	0.60435	0.311989	1.93709	14
Timp1		0.117194	0.719904	0.474925	0.244979	0.146728	1.66961	14
Timp2		0.0989167	2.46326	3.34708	-0.883824	0.50003	1.76754	14
Timp3		0.0434315	0.955054	1.95398	-0.998924	0.449947	2.22009	14
Timp4		0.102459	0.000618	0.0011025	-0.0004845	0.000277272	1.74738	14
Tnf		0.200243	0.0012875	0.0008525	0.000435	0.000323599	1.34426	14
Vegfa		0.110631	0.611171	0.88731	-0.276139	0.162136	1.70313	14

Table A-5: Information on patient cells examined in vitro.

Sex	Age	Diabetic (Type 1, Type 2, No)	Wound Site
M	60	No	Toe
F	64	No	Toe
F	87	2	Toe
M	88	2	Heel

Table A-6: Information on patients used for histological analysis.

Sex	Age	Diabetic (Type 1, Type 2, No)	Wound Site
F	46	2	Toe
F	64	No	Toe
F	79	No	Foot
F	87	2	Toe
M	56	2	Forefoot
M	60	No	Toe
M	70	2	Toe
M	74	No	Heel
M	88	2	Heel

Table A-7: Information on patients included in direct RNA analysis.

Sex	Age	Diabetic (Type 1, Type 2, No)	Wound site
M	34	1	Heel
F	46	2	Toe
M	47	2	Plantar flap
M	55	2	Not available
M	56	2	Forefoot
M	58	2	Toe
M	65	2	Not available
M	66	2	Toe
M	70	2	Toe
M	73	2	Heel and plantar region
M	78	2	Non-healing wound from previous foot amputation
F	79	No	Not available
M	79	2	Toe
F	83	2	Toe
M	86	2	Foot

Appendix B: Human Ethics Approval



Date: 25 June 2018

To: Douglas Hamilton

Project ID: 6311

Study Title: Role of periostin in the repair of skin - 16245E

Application Type: Continuing Ethics Review (CER) Form

Review Type: Delegated

REB Meeting Date: 03/Jul/2018

Date Approval Issued: 25/Jun/2018

REB Approval Expiry Date: 24/Jun/2019

Dear Douglas Hamilton,

The Western University Research Ethics Board has reviewed the application. This study, including all currently approved documents, has been re-approved until the expiry date noted above.

REB members involved in the research project do not participate in the review, discussion or decision.

Western University REB operates in compliance with, and is constituted in accordance with, the requirements of the TriCouncil Policy Statement: Ethical Conduct for Research Involving Humans (TCPS 2); the International Conference on Harmonisation Good Clinical Practice Consolidated Guideline (ICH GCP); Part C, Division 5 of the Food and Drug Regulations; Part 4 of the Natural Health Products Regulations; Part 3 of the Medical Devices Regulations and the provisions of the Ontario Personal Health Information Protection Act (PHIPA 2004) and its applicable regulations. The REB is registered with the U.S. Department of Health & Human Services under the IRB registration number IRB 00000940.

Please do not hesitate to contact us if you have any questions.

Sincerely,

Daniel Wyzniski, Research Ethics Coordinator, on behalf of Dr. Joseph Gilbert, HSREB Chair

Note: This correspondence includes an electronic signature (validation and approval via an online system that is compliant with all regulations).



Western
Research

Research Ethics

Western University Health Science Research Ethics Board
HSREB Delegated Initial Approval Notice

Principal Investigator: Dr. Lauren Flynn

Department & Institution: Schulich School of Medicine and Dentistry\Anatomy & Cell Biology, Western University

HSREB File Number: 105426

Study Title: Tissue Engineering with Adipose-derived Stem Cells

Sponsor: Canadian Institutes of Health Research

HSREB Initial Approval Date: August 13, 2014

HSREB Expiry Date: August 31, 2019

Documents Approved and/or Received for Information:

Document Name	Comments	Version Date
Other	Letter for OR and Clinic Staff to Introduce the Study (received June 2/14)	
Western University Protocol		2014/07/23
Letter of Information & Consent		2014/07/23

The Western University Health Science Research Ethics Board (HSREB) has reviewed and approved the above named study, as of the HSREB Initial Approval Date noted above.

HSREB approval for this study remains valid until the HSREB Expiry Date noted above, conditional to timely submission and acceptance of HSREB Continuing Ethics Review. If an Updated Approval Notice is required prior to the HSREB Expiry Date, the Principal Investigator is responsible for completing and submitting an HSREB Updated Approval Form in a timely fashion.

The Western University HSREB operates in compliance with the Tri-Council Policy Statement Ethical Conduct for Research Involving Humans (TCPS2), the International Conference on Harmonization of Technical Requirements for Registration of Pharmaceuticals for Human Use Guideline for Good Clinical Practice Practices (ICH E6 R1), the Ontario Personal Health Information Protection Act (PHIPA, 2004), Part 4 of the Natural Health Product Regulations, Health Canada Medical Device Regulations and Part C, Division 5, of the Food and Drug Regulations of Health Canada.

Members of the HSREB who are named as Investigators in research studies do not participate in discussions related to, nor vote on such studies when they are presented to the REB.

The HSREB is registered with the U.S. Department of Health & Human Services under the IRB registration number IRB 00000940.

Ethics Officer to Contact for Further Information

Erika Basile ebasile@uwo.ca	Grace Kelly grace.kelly@uwo.ca	Mina Mekhail mmekhail@uwo.ca	Vikki Tran vikki.tran@uwo.ca
--------------------------------	-----------------------------------	---------------------------------	---------------------------------

This is an official document. Please retain the original in your files.

Appendix C: Animal Ethics Approval



2016-085:3:

AUP Number: 2016-085

AUP Title: Influence of biomaterials and material physiochemical properties on cell behaviour in vitro and in vivo.

Yearly Renewal Date: 01/01/2019

The YEARLY RENEWAL to Animal Use Protocol (AUP) 2016-085 has been approved by the Animal Care Committee (ACC), and will be approved through to the above review date.

Please at this time review your AUP with your research team to ensure full understanding by everyone listed within this AUP.

As per your declaration within this approved AUP, you are obligated to ensure that:

- 1) Animals used in this research project will be cared for in alignment with:
 - a) Western's Senate MAPPs 7.12, 7.10, and 7.15
http://www.uwo.ca/univsec/policies_procedures/research.html
 - b) University Council on Animal Care Policies and related Animal Care Committee procedures
http://uwo.ca/research/services/animalethics/animal_care_and_use_policies.html
- 2) As per UCAC's Animal Use Protocols Policy,
 - a) this AUP accurately represents intended animal use;
 - b) external approvals associated with this AUP, including permits and scientific/departmental peer approvals, are complete and accurate;
 - c) any divergence from this AUP will not be undertaken until the related Protocol Modification is approved by the ACC; and
 - d) AUP form submissions - Annual Protocol Renewals and Full AUP Renewals - will be submitted and attended to within timeframes outlined by the ACC. http://uwo.ca/research/services/animalethics/animal_use_protocols.html
- 3) As per MAPP 7.10 all individuals listed within this AUP as having any hands-on animal contact will
 - a) be made familiar with and have direct access to this AUP;
 - b) complete all required CCAC mandatory training (training@uwo.ca); and
 - c) be overseen by me to ensure appropriate care and use of animals.
- 4) As per MAPP 7.15,
 - a) Practice will align with approved AUP elements;
 - b) Unrestricted access to all animal areas will be given to ACVS Veterinarians and ACC Leaders;
 - c) UCAC policies and related ACC procedures will be followed, including but not limited to:
 - i) Research Animal Procurement
 - ii) Animal Care and Use Records
 - iii) Sick Animal Response
 - iv) Continuing Care Visits
- 5) As per institutional OH&S policies, all individuals listed within this AUP who will be using or potentially exposed to hazardous materials will have completed in advance the appropriate institutional OH&S training, facility-level training, and reviewed

Submitted by: Copeman, Laura
on behalf of the Animal Care Committee
University Council on Animal Care

The University of Western Ontario
Animal Care Committee / University Council on Animal Care
London, Ontario Canada N6A 5C1
519-661-2111 x 88792 Fax 519-661-2028
auspc@uwo.ca <http://www.uwo.ca/research/services/animalethics/index.html>



AUP Number: 2017-082
PI Name: Hamilton, Doug
AUP Title: Novel Biomaterial Scaffolds for Skin Repair in Pigs
Approval Date: 04/01/2018

Official Notice of Animal Care Committee (ACC) Approval:

Your new Animal Use Protocol (AUP) 2017-082:1: entitled " Novel Biomaterial Scaffolds for Skin Repair in Pigs" has been APPROVED by the Animal Care Committee of the University Council on Animal Care. This approval, although valid for up to four years, is sub

Prior to commencing animal work, please review your AUP with your research team to ensure full understanding by everyone listed within this AUP.

As per your declaration within this approved AUP, you are obligated to ensure that:

- 1) Animals used in this research project will be cared for in alignment with:
 - a) Western's Senate MAPPs 7.12, 7.10, and 7.15
http://www.uwo.ca/univsec/policies_procedures/research.html
 - b) University Council on Animal Care Policies and related Animal Care Committee procedures
http://uwo.ca/research/services/animalethics/animal_care_and_use_policies.htm
- 2) As per UCAC's Animal Use Protocols Policy,
 - a) this AUP accurately represents intended animal use;
 - b) external approvals associated with this AUP, including permits and scientific/departmental peer approvals, are complete and accurate;
 - c) any divergence from this AUP will not be undertaken until the related Protocol Modification is approved by the ACC; and
 - d) AUP form submissions - Annual Protocol Renewals and Full AUP Renewals - will be submitted and attended to within timeframes on
 - e) http://uwo.ca/research/services/animalethics/animal_use_protocols.html
- 3) As per MAPP 7.10 all individuals listed within this AUP as having any hands-on animal contact will
 - a) be made familiar with and have direct access to this AUP;
 - b) complete all required CCAC mandatory training (training@uwo.ca); and
 - c) be overseen by me to ensure appropriate care and use of animals.
- 4) As per MAPP 7.15,
 - a) Practice will align with approved AUP elements;
 - b) Unrestricted access to all animal areas will be given to ACVS Veterinarians and ACC Leaders;
 - c) UCAC policies and related ACC procedures will be followed, including but not limited to:
 - i) Research Animal Procurement
 - ii) Animal Care and Use Records
 - iii) Sick Animal Response
 - iv) Continuing Care Visits
- 5) As per institutional OH&S policies, all individuals listed within this AUP who will be using or potentially exposed to hazardous materials will have completed in advance the appropriate institutional OH&S training, facility-level training, and reviewed related (M)S
<http://www.uwo.ca/hr/learning/required/index.html>

Submitted by: Copeman, Laura
 on behalf of the Animal Care Committee
 University Council on Animal Care

Dr. Timothy Regnault,
 Animal Care Committee Chair

The University of Western Ontario
 Animal Care Committee / University Council on Animal Care
 London, Ontario Canada N6A 5C1
 519-661-2111 x 88792 Fax 519-661-2028
auspc@uwo.ca ♦ <http://www.uwo.ca/research/services/animalethics/index.html>

Curriculum Vitae

John T. Walker

Education:

Bachelor of Health Sciences (Honours) (2008-2012)

Major in biomedical sciences; Minor in Nanoscience

University of Calgary, Calgary, AB

Ph.D. Candidate (2012-Present)

Department of Anatomy and Cell Biology

Western University, London, ON

Honours and Awards:

1. NSERC Canada Graduate Scholarship – Master’s, CGSM (2012-2013)
2. Western Graduate Research Scholarship (2012-2018)
3. Ontario Graduate Scholarship (declined; 2014-2015)
4. NSERC Alexander Graham Bell Canada Graduate Scholarship – Doctoral, CGSD (2014-2018)
5. Western University Doctoral Excellence Research Award (2016-2017)
6. European Tissue Repair Society Young Investigator Award, 2nd place (2017)

Related Work Experience:

Teaching Assistantships

1. Medical Sciences 4900F/G – Medical Sciences Laboratory (2013-2017)
2. Medical Sciences 3900F/G – Medical Sciences Laboratory (2017-2018)

Internships

1. Tissue Regeneration Therapeutics, Toronto, ON (May 2015- August 2015)
2. Tissue Regeneration Therapeutics, Toronto, ON (May 2016- August 2016)

Publications:

1. McLeod K, **Walker JT**, Hamilton DW. Galectin-3 regulation of wound healing and fibrotic processes: insights for chronic skin wound therapeutics. *J Cell Commun Signal*. 2018; 12(1):281-287
2. Davies JE, **Walker JT**, Keating AK. Wharton's jelly: the rich, but enigmatic, source of MSCs. *Stem Cells Transl Med*. 2017;6:1620-1630
3. **Walker JT**, Keating AK, Davies JE. Stem Cells: Umbilical Cord/Wharton's Jelly Derived. In: *Tissue Engineering and Regeneration: Cell Engineering and Regeneration*. Springer; In Press.
4. **Walker JT**, Elliott CG, Forbes TL, Hamilton DW. Genetic Deletion of Galectin-3 Does Not Impair Full-Thickness Excisional Skin Healing. *J Invest Dermatol*. 2016;136(5):1042–50
5. **Walker JT**, McLeod K, Kim S, Conway SJ, Hamilton DW. Periostin as a multifunctional modulator of the wound healing response. *Cell Tissue Res. Cell and Tissue Research*; 2016; 1-13
6. **Walker JT**, Kim S, Michelsons S, Creber K, Elliott C, Leask A, et al. Cell–matrix interactions governing skin repair: matricellular proteins as diverse modulators of cell function. *Res Reports Biochem*. 2015;5:73
7. Arnold CR, Lamont RE, **Walker JT**, Spice PJ, Chan C, Ho C, et al. Comparative analysis of genes regulated by Dzip1/iguana and hedgehog in zebrafish. *Dev Dyn*. 2015;211–23.
8. Yaehne K, Tekrony A, Clancy A, Gregoriou Y, **Walker JT**, Dean K, et al. Nanoparticle accumulation in angiogenic tissues: Towards predictable pharmacokinetics. *Small*. 2013;9(18):3118–27.
9. Hoegh-Petersen M, Goodyear D, Geddes MN, Liu S, Ugarte-Torres A, Liu Y, **Walker JT**, et al. High incidence of post transplant lymphoproliferative disorder after antithymocyte globulin-based conditioning and ineffective prediction by day 28 EBV-specific T lymphocyte counts. *Bone Marrow Transplant*. 2011;46(8):1104–12

Presentations

1. **Walker JT**, Flynn LE, Hamilton DW; FoxD1 lineage derived fibroblasts as contributors to skin development, homeostasis, and wound healing (Poster); Canadian Connective Tissue Conference (2018); Toronto, Canada
2. **Walker JT**, Flynn LE, Hamilton DW; FoxD1 lineage derived fibroblasts as contributors to skin development and wound healing (Oral); European Tissue Repair Society (2017); Brussels, Belgium
3. **Walker JT**, Flynn LE, Hamilton DW; Biomaterials for Cell Recruitment and Differentiation in Wound Repair (Poster); Toronto Fibrosis Conference (2017); Toronto, Canada
4. **Walker JT**, Elliott CG, Li X, Dunmore-Buyze J, Drangova M, Forbes T, Guan J, Leask A, Hamilton D; 2014; Granulation-Tissue Biomimetic Scaffolds Induce the Proliferative/Profibrotic Phase of Skin healing (Oral); Canadian Biomaterials Society.